

UC San Diego

UC San Diego Electronic Theses and Dissertations

Title

Mesoionic Carbenes in Single Electron Transfer Reactions

Permalink

<https://escholarship.org/uc/item/31p0x7nk>

Author

Vianna, Adam

Publication Date

2022

Peer reviewed|Thesis/dissertation

UNIVERSITY OF CALIFORNIA SAN DIEGO

Mesoionic Carbenes in Single Electron Transfer Reactions

A Dissertation submitted in partial satisfaction of the requirements
for the degree Doctor of Philosophy

in

Chemistry

by

Adam Vianna

Committee in charge:

Professor Guy Bertrand, Chair
Professor Prabhakar Bandaru
Professor Joseph O'Connor
Professor Jeffrey Rinehart

2022

Copyright

Adam Vianna, 2022

All rights reserved.

The Dissertation of Adam Vianna is approved, and it is acceptable in quality and form for publication on microfilm and electronically.

University of California San Diego

2022

DEDICATION

This dissertation is dedicated to my grandfather, Gerard G. Lown PhD (1921-2012). You inspired me to focus on my studies and I wish you could be here to read this paper.

TABLE OF CONTENTS

DISSERTATION APPROVAL PAGE	iii
DEDICATION	iv
TABLE OF CONTENTS	v
LIST OF FIGURES	vii
LIST OF SCHEMES	x
LIST OF TABLES	xii
LIST OF ABBREVIATIONS	xv
ACKNOWLEDGEMENTS	xviii
VITA	xxi
ABSTRACT OF THE DISSERTATION	xxii
CHAPTER 1: GENERAL INTRODUCTION	1
1.1: TWO- AND ONE-ELECTRON CHEMISTRY	2
1.2: STABLE CARBENES AND DEVELOPMENT OF MESOIONIC CARBENES	3
1.3: ORGANIC ELECTRON DONORS	9
1.4: BRESLOW INTERMEDIATES: TWO- AND ONE-ELECTRON CHEMISTRY	14
1.5: CARBENE REACTIVITY WITH CARBON MONOXIDE AND ISOCYANIDES	20
1.6: CHAPTER 1 REFERENCES	24
CHAPTER 2: MESOIONIC CARBENE-BRESLOW INTERMEDIATES AS SUPER ELECTRON DONORS: APPLICATION TO THE METAL-FREE ARYLACYLATION OF ALKENES	32
2.1: SUMMARY	33
2.2: THE BIGGER PICTURE	33
2.3: INTRODUCTION	33
2.4: RESULTS AND DISCUSSION	36
2.5: CONCLUSIONS	46
2.6: ACKNOWLEDGEMENTS	47
2.7: REFERENCES AND NOTES	47
2.8: SUPPLEMENTAL EXPERIMENTAL PROCEDURES	52
2.8.1: General Considerations	52
2.8.1.1: Synthetic Procedures	52
2.8.1.2: NMR Spectroscopy	52
2.8.1.3: Mass Spectrometry	53

2.8.1.4: Electrochemical Analysis	53
2.8.1.5: Computational Details	53
2.8.1.6: Crystal Structure Determination	54
2.8.2: Synthetic Procedures for MIC-Catalyzed Arylacylation of Alkenes.....	54
2.8.2.1: Preparation of Catalyst 1g.....	54
2.8.2.2: Preparation of 4a ⁺ and 4a ⁻	55
2.8.3: Radical Clock Reaction	82
2.8.4: DFT Calculations details of Breslow Intermediates and 4a ⁻	84
2.8.5: X-ray Crystallographic Data.....	94
2.8.6: Supplemental Reference Lists	99
2.8.7: Supplemental Figures	102
2.8.7.1: Electrochemical Measurements	102
2.8.7.2: Computational Analysis.....	104
CHAPTER 3: INVESTIGATIONS OF MESOIONIC CARBENE-ISOCYANIDE ADDUCTS	106
3.1: INTRODUCTION TO CARBENE-ISOCYANIDE ADDUCTS	107
3.2: RESULTS AND DISCUSSION.....	108
3.3: CONCLUSIONS.....	126
3.4: ACKNOWLEDGEMENTS.....	127
3.5: EXPERIMENTAL PROCEDURES AND DATA	127
3.5.1: Materials	127
3.5.2: General Methods, Instrumentation, and Measurements	127
3.5.3: Synthetic and Reaction Procedures.....	129
3.5.4: EPR Fitting Data.....	147
3.5.5: Electrochemical Data.....	150
3.5.6: Computational Details	150
3.5.7: X-ray Crystallographic Data.....	151
3.6: CHAPTER 3 REFERENCES.....	194
CHAPTER 4: SINGLE ELECTRON TRANSFER REACTIONS OF FREE MESOIONIC CARBENES	197
4.1: INTRODUCTION	198
4.2: RESULTS AND DISCUSSION.....	198
4.3: CONCLUSION.....	213
4.4: ACKNOWLEDGEMENTS.....	213
4.5: EXPERIMENTAL PROCEDURES	213
4.5.1: Materials	213
4.5.2: General Methods, Instrumentation, and Measurements	214
4.5.3: Synthetic and Reaction Procedures.....	215
4.5.4: EPR Fitting Data.....	227
4.5.5: Electrochemical Data.....	228
4.5.6: X-ray Crystallographic Data.....	229
4.6: CHAPTER 4 REFERENCES.....	255

LIST OF FIGURES

Figure 1.1: <i>Left:</i> the principal two-electron processes underpinning the majority of the undergraduate organic chemistry curriculum. <i>Right:</i> specific one-electron reactions covered in the same curriculum.....	2
Figure 1.2: Several stable carbenes of varying substitution patterns.....	4
Figure 1.3: Imidazol-5-ylidene (aNHC) and 1,2,3-triazol-5-ylidene (MIC) with mesoionic resonance emphasized.....	5
Figure 1.4: Tetrakis(dimethylamino)ethylene undergoes two successive one-electron oxidations, with the cationic products stabilized by resonance.....	9
Figure 1.5: Bis(benzimidazolylidene)s and bis(imidazolylidene)s are readily oxidized and contain aromatic resonance in the cationic forms.....	10
Figure 1.6: Fukuzumi's Breslow enolate (<i>left</i>) with neutral radical (<i>right</i>).....	17
Figure 1.7: Several ketenes from the reaction of carbenes with CO. <i>From left to right:</i> methylene (parent ketene), acyclic (alkyl)(amino)carbene, CAAC, BiCAAC, diamidocarbene.....	20
Figure 1.8: Several ketenimines resulting from the reaction of tert-butyl isocyanide with electrophilic carbenes (<i>top</i>) and 3-azabutadiene derivatives resulting from the reaction of cyclohexyl isocyanide with classical NHCs (<i>bottom</i>).	24
Figure 2.1: Breslow Intermediates (BIs) for Single Electron Transfer Reactions.....	35
Figure 2.2: Synthesis and Characterization of 3a and 4a'	37
Figure 2.3: Optimization of the MIC-Catalyzed Arylacylation.....	41
Figure 2.4: Substrate Scope of the MIC-catalyzed Arylacylation of Alkenes.....	43
Figure 2.5: Substrate Scope of the MIC-Catalyzed Annulation and Cascade Acylation	45
Figure 2.6: Cyclic voltammograms of 3a (1 mM) vs Fc/Fc ⁺ in THF (0.1 M nBu ₄ NPF ₆) at room temperature (scan rate: 100 mV/s). $E_{1/2}^* = -1.98$ V.	102
Figure 2.7: Cyclic voltammograms of 4a' (1 mM) vs Fc/Fc ⁺ in THF (0.1 M nBu ₄ NPF ₆) at room temperature (scan rate: 100 mV/s). Cyclovoltammograms of 4a' solutions feature the reversible peak of the [4a'/4a ⁺] couple at $E_{1/2} = -1.53$ V, $E_{1/2}^* = -2.02$ V.	102
Figure 2.8: Cyclic voltammograms of 4a ⁺ (0.1 mM) vs Fc/Fc ⁺ in THF (0.1 M nBu ₄ NPF ₆) at room temperature (scan rate: 100 mV/s). Cyclovoltammograms of 4a ⁺ solutions feature the reversible peak of the [4a'/4a ⁺] couple at $E_{1/2} = -1.50$ V, $E_{1/2}^* = -1.98$ V.	103

Figure 2.9: Cyclic voltammograms of 1a (0.1 mM) vs Fc/Fc ⁺ in THF (0.1 M nBu ₄ NPF ₆) at room temperature (scan rate: 100 mV/s). Cyclovoltammograms of 1a solutions feature the reversible peak at $E_{1/2} = -1.98$ V.....	103
Figure 2.10: The optimized structure and HOMO and LUMO orbitals with their energy (in eV). Isovalue = 0.05.....	104
Figure 2.11: The representation of SOMO (Isovalue = 0.06) and spin density of 4a [•] (Isovalue = 0.002).	105
Figure 3.1: Solid state structure of 2a	109
Figure 3.2: EPR spectra of 3a (<i>left</i>) and 3b (<i>right</i>) in benzene. Experimental data (<i>top</i>) is in blue with the simulation fit (<i>bottom</i>) in red.	111
Figure 3.3: Solid state structure of 3aHBF₄ , with hydrogen atoms omitted for clarity. The tetrafluoroborate anion (background) is disordered in orientation.	116
Figure 3.4: Solid state structure of 3aPQ with hydrogen atoms omitted for clarity. One molecule of THF co-crystallized in the unit cell.	119
Figure 3.5: EPR spectra of 3aPQ (<i>left</i>) and 3bPQ (<i>right</i>) in benzene. Experimental data (<i>top</i>) is in blue with the simulation fit (<i>bottom</i>) in red.	120
Figure 3.6: Solid state structure of 3aAl	123
Figure 3.7: EPR spectrum of 3bH [•] in benzene. Experimental data (<i>top</i>) is in blue with the simulation fit (<i>bottom</i>) in red.	126
Figure 3.8: ¹³ C NMR (126 MHz, C ₆ D ₆) of the reaction of 3a with 2x excess diphenylphosphine oxide after sitting overnight. The highlighted signal was characteristic for the product ($J_{C-P} = 59.9$ Hz). The unphased signal at ~154 ppm is an unresolved artifact from the NMR instrument.	143
Figure 3.9: ³¹ P NMR (121 MHz, THF) of carbene 1 -catalyzed bisphosphonation of 2,6-diisopropylphenyl isocyanide after overnight at room temperature.	144
Figure 3.9: Cyclic voltammogram of 3bHPF₆ in THF (0.1 M nBu ₄ NPF ₆) at room temperature (scan rate: 100 mV/s). The 3bHPF₆ / 3bH [•] couple is at $E_{1/2} = -1.69$ V.....	150
Figure 4.1: Solid state structure of 1HPQ [•]	199
Figure 4.2: EPR spectrum of 1HPQ [•] with experimental data in blue (<i>top</i>) and simulated fit in red (<i>bottom</i>).....	200
Figure 4.3: Solid state structure of 1HAQ [•]	208
Figure 4.4: EPR spectrum of 1HAQ [•] with experimental data in blue (<i>top</i>) and simulated fit in red (<i>bottom</i>).....	209

Figure 4.5: 1 tritBF ₄ and 1 HBF ₄ product mixture with characteristic isopropyl C-H highlighted.	217
Figure 4.6: 2 tritBF ₄ and 2 HBF ₄ product mixture with characteristic isopropyl C-H highlighted.	219
Figure 4.7: Expanded view of ¹³ C NMR (125 MHz, CDCl ₃) of the catalytic reduction of phenanthrenequinone after quenching with acid. Signals matching phenanthrenequinhydrone are circled.	222
Figure 4.8: ¹ H NMR (400 MHz, DMSO-d ₆) of the catalytic reduction of anthraquinone after overnight heating. Signals for reduced anthracene are highlighted.	224
Figure 4.8: Cyclic Voltammogram of carbene 1 in THF (0.1 M nBu ₄ NPF ₆) at room temperature (scan rate: 100 mV/s). The redox couple is at $E_{1/2} = -1.86$ V.	228
Figure 4.9: Cyclic voltammogram of 1 HPF ₆ in THF (0.1 M nBu ₄ NPF ₆) at room temperature (scan rate: 100 mV/s). The redox couple is at $E_{1/2} = -1.86$ V.	228

LIST OF SCHEMES

Scheme 1.1: MICs with a small N-substituent (methyl), degrade in solution to the C-5 methylated triazole or the protonated neutral triazole.	6
Scheme 1.2: Several synthetic approaches to 1,2,3-triazolium MIC precursors and subsequent deprotonation to the free carbene.....	8
Scheme 1.3: Reductive cleavage of sulfones and sulfonamides via SET	11
Scheme 1.4: Catalytic cycle of a benzimidazole-derived super electron donor (<i>above</i>) with transformation of a representative substrate (<i>below</i>). C ₁₂ H ₂₃ SH is used as a polarity reversal catalyst to facilitate the hydrogen atom transfer from the nucleophilic dihydrobenzimidazole to the nucleophilic aryl radical.....	12
Scheme 1.5: Catalytic cycle of a diazaphosphine-derived electron donor (<i>above</i>) with transformation of a representative substrate (<i>below</i>).....	13
Scheme 1.6: Formation of a Breslow intermediate using a classical thiazolium NHC, with umpolung shown, and schematic examples of the benzoin condensation and Stetter reactions. ..	14
Scheme 1.7: Formation of the Breslow Intermediate homoenolate equivalent, original reports of lactone formation via homoenolate equivalent, generalized mechanism with alcohol substituting acyl azolium ion.....	16
Scheme 1.8: Successive oxidations of a Breslow intermediate by TEMPO leads to a TEMPO ester with regeneration of the carbene.	17
Scheme 1.9: Mechanistic cycle of Ohmiya's carbene-catalyzed decarboxylative alkylation of aldehydes (<i>top</i>) with alkylation resulting from interception of the alkyl radical by an alkene (<i>below</i>).	19
Scheme 1.10: Metal-free carbonylation of a quinone via CAAC organocatalysis.	22
Scheme 1.11: Some C-1 functionalization reactions of isocyanides.	23
Scheme 2.1: Proposed Reaction Pathway for the MIC-Catalyzed Arylacylation of Alkenes	39
Scheme 2.2: Radical Clock Reaction	46
Scheme 3.1: Reactivity of MIC 1 with carbon monoxide, cyclohexyl isocyanide, and n-butyl isocyanide.	109
Scheme 3.2: Reactivity of MIC 1 with quaternary isocyanides DippNC and tBuNC	111
Scheme 3.3: Attempts to obtain crystalline adduct 3 by use of different isocyanides.	113
Scheme 3.4: Attempted derivatization of 3a with electrophilic reagents.	114

Scheme 3.5: Formation of 3a proceeds in the presence of known radical traps.	115
Scheme 3.6: Synthesis of 3aH from 3a with postulated radical cation intermediate.	116
Scheme 3.7: Reaction of phenanthrenequinone with 3a and 3b , giving adducts 3aPQ and 3bPQ , respectively.	118
Scheme 3.8: 3aPQ does not give the dioxol-2-imine on heating, even with a trapping agent. ...	120
Scheme 3.9: Bisphosphonation of Dipp isocyanide stoichiometrically from 3a (<i>top</i>) and catalytically with respect to MIC 1 (<i>bottom</i>).	121
Scheme 3.10: Synthesis of 3aAl with possible mechanism.	123
Scheme 3.11: Synthesis of 3bHPF₆ by cyclization of the corresponding alkyne, followed by reaction with base and reductants.	125
Scheme 4.1: Reduction of phenanthrenequinone by free MIC 1	199
Scheme 4.2: General reactions of triazolium/MICs under cyclic voltammetry (<i>top</i>) and the formation of carbene 1 by reduction of 1HPF₆ with KC ₈ (<i>bottom</i>).	201
Scheme 4.3: Reactions of carbenes 1 and 2 with trityl cation.	203
Scheme 4.4: MIC radical cation trapping experiments with TEMPO and deuterated acetonitrile. PQ = phenanthrenequinone.	205
Scheme 4.5: General hypothetical catalytic cycle for the MIC as a reducing agent. X ⁻ could be the reduced substrate, or a fragmentation product thereof, in addition to the counterion of the carbene precursor.	206
Scheme 4.6: Catalytic reduction of phenanthrenequinone by 1HPF₆ with quenching to phenanthrenequinhydrone dimer.	207
Scheme 4.7: Stoichiometric reduction of anthraquinone with carbene 1	208
Scheme 4.8: Catalytic reduction of anthraquinone by 1HPF₆ in DMSO-d ₆ (<i>above</i>) with the semiquinone equilibrium (<i>below</i>).	210
Scheme 4.9: Reduction of 2-tert-butylanthraquinone followed by ethylation gives 2-(tert-butyl)-9,10-diethoxyanthracene with or without carbene catalyst.	211
Scheme 4.10: Catalytic reduction of 2-bromoacetophenone with MIC gives acetophenone rather than the diketone.	212
Scheme 4.11: Catalytic reduction of N-tosylindole (Ts = 4-toluenesulfonyl) by MIC to indole.	213

LIST OF TABLES

Table 2.1: Crystal data and structure refinement for 4a (CCDC: 2047374).	94
Table 2.2: Crystal data and structure refinement for 11ah (CCDC: 2043281).	96
Table 3.1: Full EPR fitting parameters for 3a	147
Table 3.2: Full EPR fitting parameters for 3b	148
Table 3.3: Full EPR fitting parameters for 3aPQ	148
Table 3.4: Full EPR fitting parameters for 3bPQ	149
Table 3.5: Full EPR fitting parameters for 3bH	149
Table 3.6: calculated singlet-triplet gaps for 3a , 3b , and 3aPQ at three different levels of theory.	150
Table 3.7: Crystal Data and Structure Refinement for 2a	151
Table 3.8: Fractional atomic coordinates ($\times 10^4$) and Equivalent Isotropic Displacement Parameters ($\text{\AA}^2 \times 10^3$) for 2a . U_{eq} is defined as 1/3 of the trace of the orthogonalized U_{ij} tensor.	152
Table 3.9: Anisotropic Displacement Parameters ($\text{\AA}^2 \times 10^3$) for 2a . The anisotropic displacement factor exponent takes the form: $-2\pi^2[h^2a^{*2}U_{11}+2hka^*b^*U_{12}+\dots]$	155
Table 3.10: Bond Lengths for 2a	157
Table 3.11: Bond Angles for 2a	159
Table 3.12: Hydrogen Atom Coordinates ($\text{\AA} \times 10^4$) and Isotropic Displacement Parameters ($\text{\AA}^2 \times 10^3$) for 2a	161
Table 3.13: Crystal Data and Structure Refinement for 3aHBF₄	164
Table 3.14: Fractional atomic coordinates ($\times 10^4$) and Equivalent Isotropic Displacement Parameters ($\text{\AA}^2 \times 10^3$) for 3aHBF₄ . U_{eq} is defined as 1/3 of the trace of the orthogonalized U_{ij} tensor.	165
Table 3.15: Anisotropic Displacement Parameters ($\text{\AA}^2 \times 10^3$) for 3aHBF₄ . The anisotropic displacement factor exponent takes the form: $-2\pi^2[h^2a^{*2}U_{11}+2hka^*b^*U_{12}+\dots]$	167
Table 3.16: Bond Lengths for 3aHBF₄	169
Table 3.17: Bond Angles for 3aHBF₄	170

Table 3.18: Hydrogen Atom Coordinates ($\text{\AA} \times 10^4$) and Isotropic Displacement Parameters ($\text{\AA}^2 \times 10^3$) for 3aHBF₄	171
Table 3.19: Atomic Occupancy for 3aHBF₄	173
Table 3.20: Crystal Data and Structure Refinement for 3aPQ	174
Table 3.21: Fractional atomic coordinates ($\times 10^4$) and Equivalent Isotropic Displacement Parameters ($\text{\AA}^2 \times 10^3$) for 3aPQ . U_{eq} is defined as 1/3 of the trace of the orthogonalized U_{IJ} tensor.	175
Table 3.22: Anisotropic Displacement Parameters ($\text{\AA}^2 \times 10^3$) for 3aPQ . The anisotropic displacement factor exponent takes the form: $-2\pi^2[h^2a^{*2}U_{11}+2hka^*b^*U_{12}+\dots]$	177
Table 3.23: Bond Lengths for 3aPQ	179
Table 3.24: Bond Angles for 3aPQ	181
Table 3.25: Hydrogen Atom Coordinates ($\text{\AA} \times 10^4$) and Isotropic Displacement Parameters ($\text{\AA}^2 \times 10^3$) for 3aPQ	182
Table 3.26: Crystal Data and Structure Refinement for 3aAl	185
Table 3.27: Fractional atomic coordinates ($\times 10^4$) and Equivalent Isotropic Displacement Parameters ($\text{\AA}^2 \times 10^3$) for 3aAl . U_{eq} is defined as 1/3 of the trace of the orthogonalized U_{IJ} tensor.	186
Table 3.28: Anisotropic Displacement Parameters ($\text{\AA}^2 \times 10^3$) for 3aAl . The anisotropic displacement factor exponent takes the form: $-2\pi^2[h^2a^{*2}U_{11}+2hka^*b^*U_{12}+\dots]$	188
Table 3.29: Bond Lengths for 3aAl	190
Table 3.30: Bond Angles for 3aAl	191
Table 3.31: Hydrogen Atom Coordinates ($\text{\AA} \times 10^4$) and Isotropic Displacement Parameters ($\text{\AA}^2 \times 10^3$) for 3aAl	192
Table 4.1: Full EPR fitting parameters for 1HPQ	227
Table 4.2: Full EPR fitting parameters for 1HAQ	227
Table 4.3: Crystal Data and Structure Refinement for 1HPQ	229
Table 4.4: Fractional atomic coordinates ($\times 10^4$) and Equivalent Isotropic Displacement Parameters ($\text{\AA}^2 \times 10^3$) for 1HPQ . U_{eq} is defined as 1/3 of the trace of the orthogonalized U_{IJ} tensor.....	230
Table 4.5: Anisotropic Displacement Parameters ($\text{\AA}^2 \times 10^3$) for 1HPQ . The anisotropic displacement factor exponent takes the form: $-2\pi^2[h^2a^{*2}U_{11}+2hka^*b^*U_{12}+\dots]$	234

Table 4.6: Bond Lengths for 1HPQ	238
Table 4.7: Bond Angles for 1HPQ	240
Table 4.8: Hydrogen Atom Coordinates ($\text{\AA} \times 10^4$) and Isotropic Displacement Parameters ($\text{\AA}^2 \times 10^3$) for 1HPQ	242
Table 4.9: Atomic Occupancy for 1HPQ	246
Table 4.10: Crystal Data and Structure Refinement for 1HAQ	247
Table 4.11: Fractional atomic coordinates ($\times 10^4$) and Equivalent Isotropic Displacement Parameters ($\text{\AA}^2 \times 10^3$) for 1HAQ . U_{eq} is defined as 1/3 of the trace of the orthogonalized U_{ij} tensor.....	248
Table 4.12: Anisotropic Displacement Parameters ($\text{\AA}^2 \times 10^3$) for 1HAQ . The anisotropic displacement factor exponent takes the form: $-2\pi^2[h^2a^{*2}U_{11}+2hka^*b^*U_{12}+\dots]$	250
Table 4.13: Bond Lengths for 1HAQ	251
Table 4.14: Bond Angles for 1HAQ	252
Table 4.15: Hydrogen Atom Coordinates ($\text{\AA} \times 10^4$) and Isotropic Displacement Parameters ($\text{\AA}^2 \times 10^3$) for 1HAQ	254

LIST OF ABBREVIATIONS

Ac	Acetyl
Ad	Adamantyl
AIBN	Azobisisobutyronitrile
aNHC	abnormal N-Heterocyclic Carbene
AQ	Anthraquinone
AQH ₂	Dihydroxyanthracene
Ar	Aryl
BHT	Butylated hydroxytoluene
BI	Breslow Intermediate
BiCAAC	Bicyclic (Alkyl)(Amino)Carbene
BIMIC	Mesoionic Carbene Breslow Intermediate
BOC	tert-Butyloxy carbonyl
Bpin	Pinacolborate
Bu	Butyl
CAAC	Cyclic (Alkyl)(Amino)Carbene
CO	Carbon monoxide
CV	Cyclic Voltammetry
Cy	Cyclohexyl
DAC	Diamidocarbene
DBU	1,8-Diazabicyclo[5.4.0]undec-7-ene
DCM	Dichloromethane
DFT	Density Functional Theory

DIAD	Diisopropyl azodicarboxylate
Dipp	2,6-diisopropylphenyl
E	Electrophile or Element
EPR	Electron Paramagnetic Resonance (spectroscopy)
ESI	Electron Spray Ionization
Et	Ethyl
Fc	Ferrocene
Fc ⁺	Ferrocenium
HMDS	Hexamethyldisilazide ($((\text{CH}_3)_3\text{Si})_2\text{N}^-$)
HOMO	Highest Occupied Molecular Orbital
HRMS	High Resolution Mass Spectroscopy
iAm	isoamyl (isopentyl)
IMes	1,3-bis(2,4,6-trimethylphenyl)imidazolylidene
iPr	isopropyl
IR	Infrared (spectroscopy)
LG	Leaving Group
LRMS	Low Resolution Mass Spectroscopy
M	Molar
Me	Methyl
Mes	2,4,6-trimethylphenyl
MIC	Mesoionic Carbene (generally referring to 1,2,3-triazolylidenes)
mM	milimolar
mmol	milimole

mol	mole
nBu	n-Butyl
NHC	N-Heterocyclic Carbene
NMR	Nuclear Magnetic Resonance (spectroscopy)
Nu	Nucleophile
PE	Petroleum Ether
Ph	Phenyl
PQ	Phenanthrenequinone
SCE	Saturated Calomel Electrode
SET	Single Electron Transfer
SIMes	1,3-bis(2,4,6-trimethylphenyl)imidazolidinylidene
SOMO	Singly Occupied Molecular Orbital
tBu	tert-butyl
TDAE	Tetrakis(dimethylamino)ethylene
TEMPO	(2,2,6,6-Tetramethylpiperidin-1-yl)oxyl radical
Tf	Triflyl
THF	Tetrahydrofuran
TMS	Trimethylsilyl or Tetramethylsilane
Ts	4-toluenesulfonyl
UV	Ultraviolet (spectroscopy)
X	Halogen
XRD	X-ray Diffraction
ZPE	Zero Point Energy

ACKNOWLEDGEMENTS

Firstly, I would like to thank my advisor, Professor Guy Bertrand, for his guidance throughout my time in the PhD program. You set up a lab where we can do all of this wonderful chemistry. I learned much in my time here, from you specifically and from the many talented people you brought into the lab.

I would also like to thank the other members of my committee: professors Prabhakar Bandaru, Seth Cohen, Joseph O'Connor, and Jeffrey Rinehart. Your comments over my exams and evaluations have helped guide my progress in the program.

Michele, you have taught me so much about laboratory operations. Thank you for all the trust you have shown me in bringing me into the fold on operations and procurement decisions. I believe my experiences working with you as the consumables inventory manager will serve me well in my future career.

Glen, when I joined the lab back in 2016, you had already started your summer rotation and were already familiar with the lab through the STARS program. I still remember how welcoming you were and I'm glad that we officially started the program in the same year. I always appreciated your enthusiasm anytime I went over to your side of the lab, whether we were talking about chemistry or something else entirely. I'm not good at keeping in touch with people I don't see regularly, but I hope we remain in contact as we continue careers.

Francois, this guy! Congratulations on defending! You were always a friendly face around from the time we were working directly across from each other to when you moved to your final fume hood. You are a master of organic synthesis who knows how to relax when it is rightfully time to take a break. I'll miss having you around as we move into the workforce in (likely) different industries but I hope you won't be a stranger.

Melinda, I think we might be the only people who stayed in room 5118 for our entire PhD's, or at least as long as my time has gone. I remember first meeting you and my first impression was that you were not particularly affable (which might have something to do with my introverted nature) ... I quickly realized that you were a wonderful labmate with a work ethic stronger than mine, and I don't just mean your working hours. With a little bit of luck, I will be staying in SD for a while, and I look forward to seeing you defend next year.

To all the other members of the lab, past and present; Mo, Rudy, Ying Kai, Sonia, Victor, Joseph, Alexis, Patrick, Hao, Ryo, Max, Eder, Lilja, Cory, Erik, Daniel, Jesse, Sima, Jan, Delphine, Luana, Florian, Joseph, Andre, Armand, Vojtech, Nahal, Sebastian, thank you for making the lab and, by extension, my PhD, what it is today.

More importantly, I would like to thank my family for all the support they've given over the years. Particularly, Mom and Dad, thank you for pushing me excel and supporting me when I missed the mark. Neither of you finished your respective PhD programs for reasons which I now understand very well, but I still hope I've made you proud. Thank you for letting me go to the opposite side of the country when you'd rather I stayed closer to home.

Finally, Amy, I don't know how I would have completed graduate school without you here. In all honesty, I probably wouldn't have. I love you so much and I'm still excited I married you. You've supported me when I had doubts about the PhD program and always encouraged me to do my best and be happy. I can't thank you enough, but I know I'll have plenty of time to think about how to do so. With this dissertation and my thesis defense, we will have both finished our education, and I hope they will signal a new chapter in our lives more fulfilling and more fun than the past 10 years.

Chapter 2 is adapted, with slight modifications, from Liu, W.; Vianna, A.; Zhang, Z.; Huang, S.; Huang, L.; Melaimi, M.; Bertrand, G.; Yan, X. Mesoionic Carbene-Breslow Intermediates as Super Electron Donors: Application to the Metal-Free Arylacylation of Alkenes. *Chem Catalysis* **2021**, *1* (1), 196–206. The dissertation author was the second author of this paper.

Chapter 3 contains material currently being prepared for submission for publication. Vianna, A.; Melaimi, M.; Mulks, F. F.; Bertrand, G. Investigations of Mesoionic Carbene-Isocyanide Adducts. The dissertation author was the primary researcher and first author of this material.

Chapter 4 contains material currently being prepared for submission for publication. Vianna, A.; Melaimi, M.; Bertrand, G. Single-Electron Transfer Reactions of Free Mesoionic Carbenes. The dissertation author was the primary researcher and first author of this material.

VITA

- 2016 Bachelor of Science in Chemistry, Case Western Reserve University
Advisor: Professor Anna Samia
- 2018 Master of Science in Chemistry, University of California San Diego
- 2022 Doctor of Philosophy in Chemistry, University of California San Diego
Advisor: Professor Guy Bertrand

PUBLICATIONS

- (1) Popa, A.; Abenojar, E. C.; Vianna, A.; Buenviaje, C. Y. A.; Yang, J.; Pascual, C. B.; Samia, A. C. S. Fabrication of Metal Nanoparticle-Modified Screen Printed Carbon Electrodes for the Evaluation of Hydrogen Peroxide Content in Teeth Whitening Strips. *J. Chem. Educ.* **2015**, 92 (11), 1913–1917. <https://doi.org/10.1021/acs.jchemed.5b00096>.
- (2) Liu, W.; Vianna, A.; Zhang, Z.; Huang, S.; Huang, L.; Melaimi, M.; Bertrand, G.; Yan, X. Mesoionic Carbene-Breslow Intermediates as Super Electron Donors: Application to the Metal-Free Arylacylation of Alkenes. *Chem Catalysis* **2021**, 1 (1), 196–206. <https://doi.org/10.1016/J.CHECAT.2021.03.004/ATTACHMENT/030A406B-3A14-4D13-A30A-396E00D289F5/MMC1.PDF>.

FIELD OF STUDY

Small molecule reactivity of mesoionic carbenes and single-electron transfer resulting thereof.

ABSTRACT OF THE DISSERTATION

Mesoionic Carbenes in Single Electron Transfer Reactions

by

Adam Vianna

Doctor of Philosophy in Chemistry

University of California San Diego, 2022

Professor Guy Bertrand, Chair

Much of classical organic chemistry is focused on two-electron reactions. Indeed, it is common to teach sophomore organic chemistry with only the bare minimum of radical chemistry, such as free radical halogenation of alkanes. However, there is a wide world of single-electron chemistry to explore if we look beyond classical organic reactivity.

This dissertation will explore some of this hidden single electron chemistry, specifically as it pertains to stable mesoionic carbenes (MICs). MICs are so differentiated from other carbenes by the inability to draw a fully neutral resonance form without assigning formal charges. In practical terms, this results in a carbene that does not have the usual propensity of carbenes to dimerize and is nucleophilic but not electrophilic. Another property is that they are good leaving groups (weak bases) and so are adept at organocatalytic reactions just as N-heterocyclic carbenes (NHCs) are.

While the polar two electron chemistry of MICs has been well explored, single electron transfer reactions are not considered part of their repertoire. This dissertation will detail new single electron reactivity of MICs through super electron donating Breslow Intermediates, MIC-isocyanide adducts, and the free carbenes themselves. In this way, we find that the 1,2,3-triazolium framework of these carbenes is supportive of a range of single electron transfer reactions.

CHAPTER 1: GENERAL INTRODUCTION

1.1: Two- and One-Electron Chemistry

The focus of this dissertation will be on the application of stable carbenes, specifically mesoionic carbenes, to single electron transfer (SET) reactions. As carbenes are fully organic compounds, this type of reactivity is relatively unusual. Indeed, SET is not a commonly used reaction type in organic chemistry, and even then, it is usually considered to be the domain of metallic elements

The dissertation author has taught many undergraduate courses as a teaching assistant over the course of the doctoral program. Except for two laboratory courses, all of these were from the three-quarter second-year organic chemistry lecture series. The textbook currently used for these courses is the eighth edition of *Organic Chemistry: Structure and Function* by Vollhardt and Schore.¹

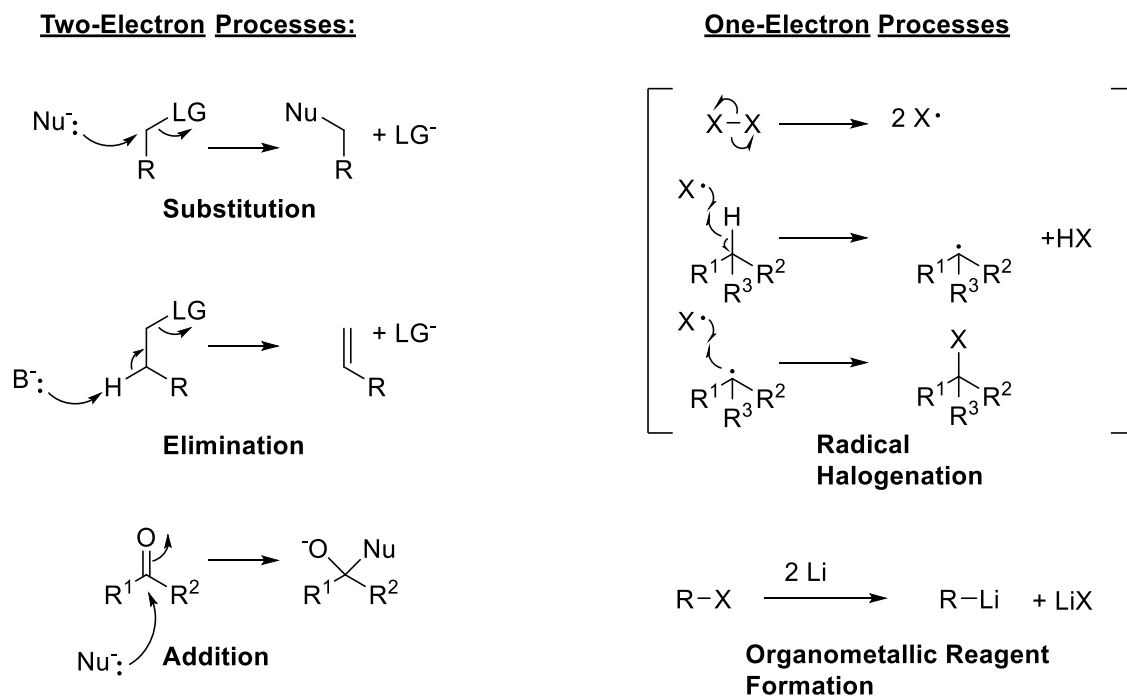


Figure 1.1: *Left:* the principal two-electron processes underpinning the majority of the undergraduate organic chemistry curriculum. *Right:* specific one-electron reactions covered in the same curriculum.

When introducing chemical reactions in chapter 3, the book teaches students both double-headed arrow (two-electron) and single-headed arrow (one-electron) notation. Subsequently, students learn free radical halogenation of alkanes as their first organic reaction. However, it is generally noted that this reaction has limited synthetic utility due to the difficulty of controlling the number of substitutions and poor regiochemical control. The remainder of the textbook primarily covers examples of two-electron reactions of substitution, elimination, and addition types (see **Figure 1.1**). Indeed, this is representative of how many undergraduate students learn organic chemistry; two-electron reactivity is most important.

Even in the undergraduate discussion of single-electron chemistry, electron transfer is barely mentioned. To be fair, students do learn about the formation of organometallic reagents by reduction of carbon-halogen bonds. This is reflective of the classical school of thought in that electron transfer is done by metals such as lithium or magnesium. However, it is possible for organic molecules to act as electron donors², and this is the focus of the dissertation.

1.2: Stable Carbenes and Development of Mesoionic Carbenes

A carbene is classically a molecule containing a carbon atom with two bonds and two electrons, generally in the form of a lone pair and a vacant p-orbital. Lacking a full octet, they are highly reactive species which, until relatively recently, could not be isolated. This changed with the first stable carbene, the phosphino-silyl carbene reported by Bertrand and co-workers in 1988.³ The breakthrough was to recognize that the substituents flanking the carbene carbon had to stabilize the reactive center by π -donation and π -acceptance, also known as the push-pull effect.⁴ A few years later, in 1991, Arduengo reported the first crystalline N-Heterocyclic Carbene (NHC) using an imidazole framework.⁵ In this case, the carbene was stabilized by π -donation from both flanking amino substituents (the push-push effect).⁴

Since these early discoveries, a wide range of carbene classes have been developed, including 1,2,4-triazolylidenes⁶, cyclic alkyl amino carbenes (CAACs)^{7,8}, the cyclopropenylidene⁹, and diamidocarbenes.^{10,11} All of these carbenes have varied electronic properties, resulting in a range of applications.¹² However, the focus of this dissertation is on mesoionic carbenes, an class of carbenes which is unusual due to their charged structures.

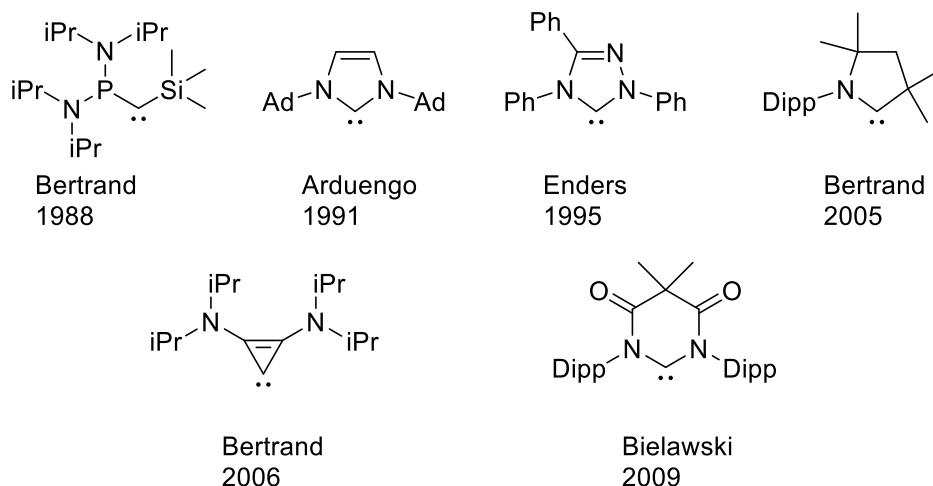


Figure 1.2: Several stable carbenes of varying substitution patterns.

IUPAC defines the term “mesoionic” as referring to a heterocyclic compound that is overall neutral but which cannot be drawn with a completely covalent structure without formal charges.¹³ The first isolable example of a mesoionic carbene was reported in 2009 by Bertrand in the form of the imidazole-5-ylidene, or abnormal NHC (aNHC).¹⁴ This compound was termed “abnormal” as the C-2 position, which would normally be deprotonated to form an Arduengo-type NHC, was blocked by a phenyl substituent. As a result, deprotonation occurs at the C-5 position, giving the molecule its mesoionic character. The synthesis of aNHCs is not straightforward and has steps which can be very sensitive to the duration and temperature, so another class of MIC was developed.

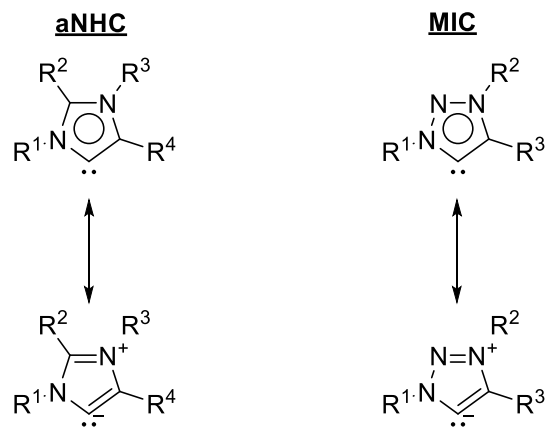
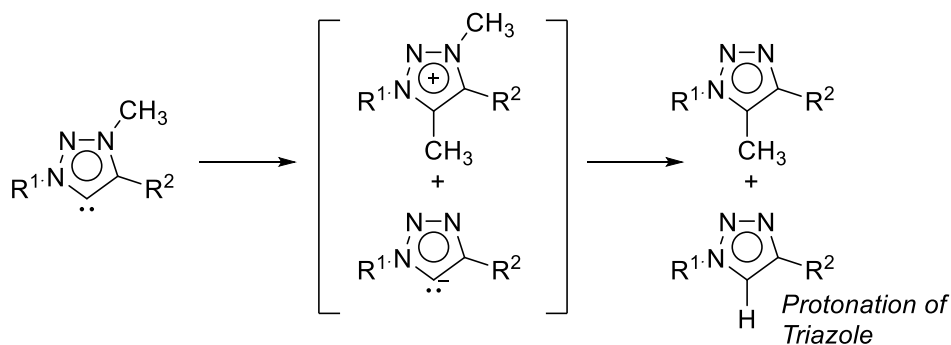


Figure 1.3: Imidzaol-5-ylidene (aNHC) and 1,2,3-triazol-5-ylidene (MIC) with mesoionic resonance emphasized.

Whereas the Arduengo NHC requires the C-2 position of an imidazolium salt to be deprotonated, the lack of such necessity in a mesoionic carbene means that it is not necessary to have a carbon atom there. For example, it may be replaced by a nitrogen to give a 1,2,3-triazolium framework. Curiously, the deprotonation of 1,3-disubstituted triazoliums, with subsequent reactions with electrophiles such as sulfur and halocarbons, was reported by Begtrup as early as 1975.^{15,16} However, these early reports used small N-substituents, such as methyl, leading to an unstable carbene, which had to be functionalized *in-situ* at low temperature. Bertrand and co-workers developed this chemistry to make stable mesoionic carbenes derived from the 1,2,3-triazolium framework.^{17,18} The key development was to use at least one N-aryl substituent. This framework is generalizable, as evidenced by the subsequent synthesis of a bidentate bis(MIC).¹⁹ Collectively, the aNHCs and triazolium mesoionic carbenes have found applications in a number of organocatalytic and transition-metal applications.^{20,21}

Triazolium mesoionic carbenes, which will be referred to simply as MICs going forward, are tempting substrates due to their versatility. They are strong nucleophiles, and their aromatic character makes them less electrophilic than many other stable carbenes. Furthermore, they lack

any propensity to dimerize, and the free carbene can be isolated even with a hydrogen adjacent to the carbene carbon.²² Their synthetic procedure is generalizable and allows for a variety of substituents. In the original preparation¹⁷, a one-pot conversion of an aniline to the corresponding azide followed by Huisgen cycloaddition with an alkyne gives a triazole. This triazole is then alkylated with either methyl or isopropyl triflate to give a triazolium, which is then deprotonated to give the free carbene. It was found that carbenes with a methyl group on the N-3 position were susceptible to substitution of the methyl by another equivalent of carbene, although this decomposition could be mitigated by using a bulkier isopropyl substituent.



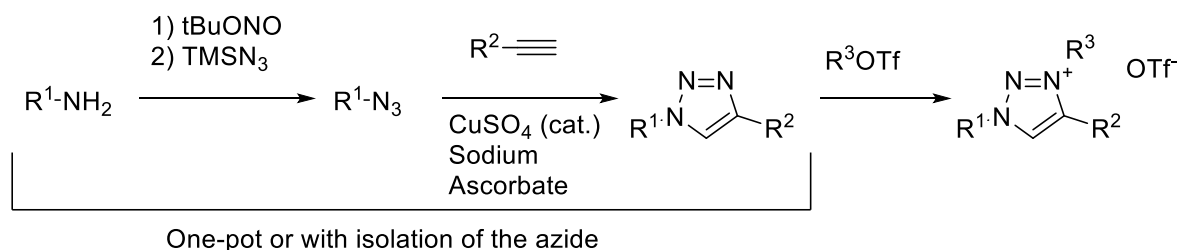
Scheme 1.1: MICs with a small N-substituent (methyl), degrade in solution to the C-5 methylated triazole or the protonated neutral triazole.

A subsequent preparation¹⁸ overcame the limitations of alkyl substituents by first generating a diaryl triazene via either coupling of an aniline with isoamyl nitrite or reaction of an aryl Grignard reagent with an aryl azide (see **Scheme 1.2**). Oxidation of the triazene with tert-butyl hypochlorite in the presence of potassium hexafluorophosphate gives a strongly electrophilic triazenium cation, which undergoes cycloaddition with alkynes and vinyl halides to directly give the 1,3-diaryl triazolium salts. This latter approach is tolerant of a number of functional groups on the alkyne, such as alkenes, alcohols, esters, and ketones.^{18,23} However,

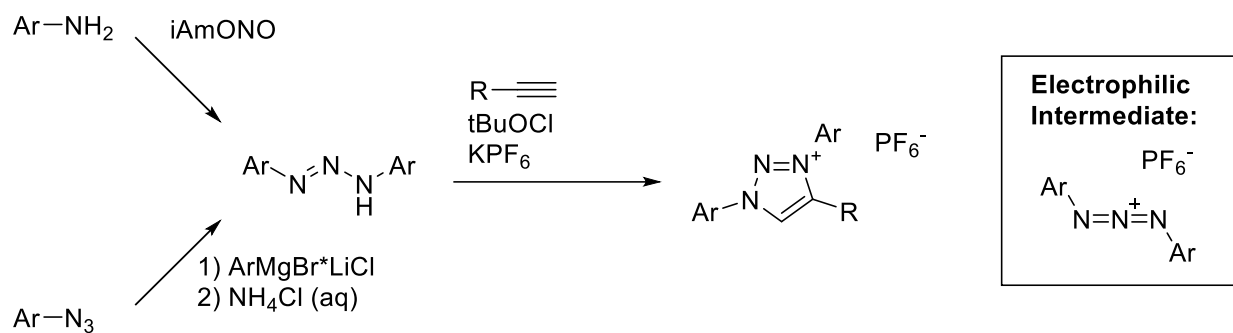
tert-butyl hypochlorite is a strong oxidant and so any reducing function groups (i.e. phosphines) are incompatible with this procedure.

Even if the desired substituent cannot be incorporated into an alkyne, or such a substituent is incompatible with the cycloaddition reaction, there is an alternative. The free H-substituted MIC can be reacted with electrophiles by substitution to give a new triazolium salt which, in turn, can be deprotonated again. This approach has been used to synthesize MICs with iodo²⁴ and phosphino²⁵ substituents at the 4- position.

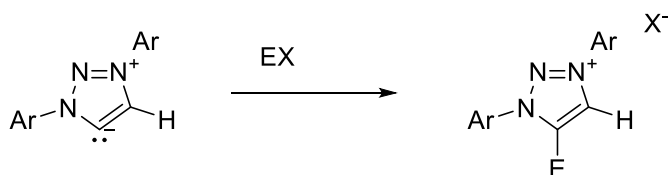
Azide Method



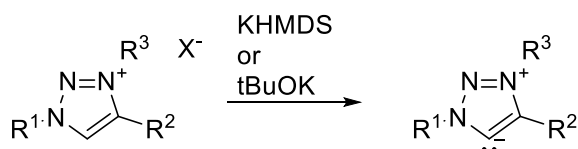
Triazene Method



Substitution Method



Carbene Formation



Scheme 1.2: Several synthetic approaches to 1,2,3-triazolium MIC precursors and subsequent deprotonation to the free carbene

In summary, mesoionic carbenes can be readily synthesized with a variety of substitution patterns. The steric environment around the carbene can be easily adjusted by the C-4 substituent, ranging from a small hydrogen atom to a bulky tert-butyl. Alternatively, the electronics of the carbene center can be modulated by the introduction of function groups such as

esters, halogens, phosphines, etc. This versatility allows the MIC to adapt to a variety of roles and is of particular benefit to catalysis as the carbene can be easily tailored to the exact needs of the reaction.

1.3: Organic Electron Donors

The main theme of this dissertation is single electron transfer (SET) from MIC-derived species. As such it is necessary to give a quick background on this process and other organic compounds which are known to effect this transformation. First of all, SET is defined as the transfer of one electron from one chemical species to another.²⁶ Perhaps the first such example a chemistry student learns is transfer to/from an electrode in an electrochemical process. Another commonly taught example would be alkali metals, such as lithium and sodium, donating an electron as a reductant.

Organic molecules have also been known to act as electron donors. A well-known example is tetrakis(dimethylamino)ethylene, originally reported in 1950.²⁷ In this molecule, we can see some general features of many organic electron donors. TDAE is an electron-rich alkene, with each of two successive oxidation products (redox potentials of -0.78 V and -0.61 V vs. SCE in acetonitrile)²⁸ stabilized by resonance. This resonance stabilization is a common feature of strongly reducing organic electron donors.

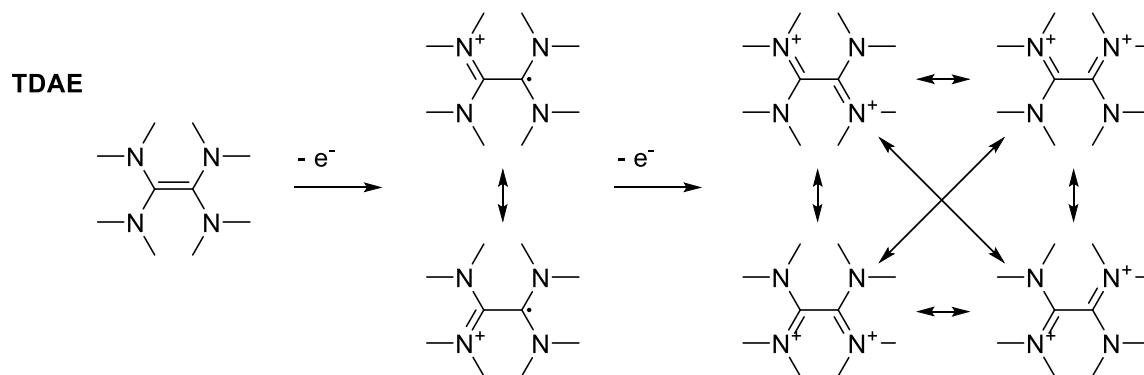
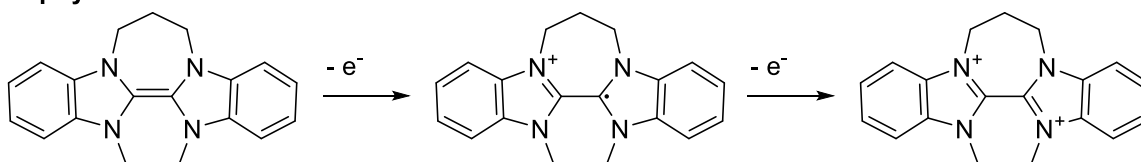


Figure 1.4: Tetrakis(dimethylamino)ethylene undergoes two successive one-electron oxidations, with the cationic products stabilized by resonance.

Additional reducing power can be gained by using molecules which become aromatic upon oxidation. Such is the case with tetraazafulvalenes derived from imidazole²⁹⁻³² and benzimidazole^{30,33} frameworks. These are sufficiently reactive as to reduce aryl iodides to the corresponding radical, which in turn can add to alkenes in an intramolecular fashion to form cyclic products. Similar reactions of aryl radicals will feature in chapter 2, albeit in an intermolecular fashion. It should also be noted that these tetraazafulvalenes are formally dimers of Arduengo-type NHCs, highlighting the versatility of carbene frameworks.

Murphy 2005



Murphy and Tuttle 2007

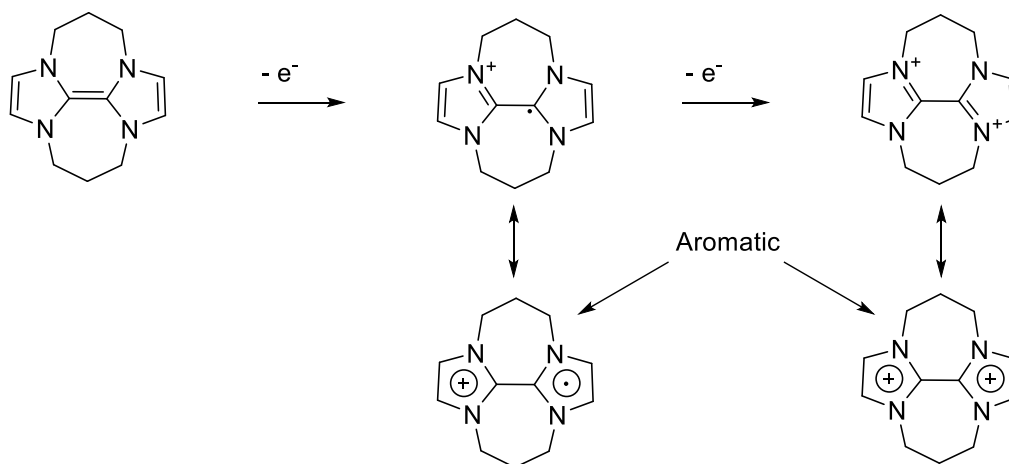
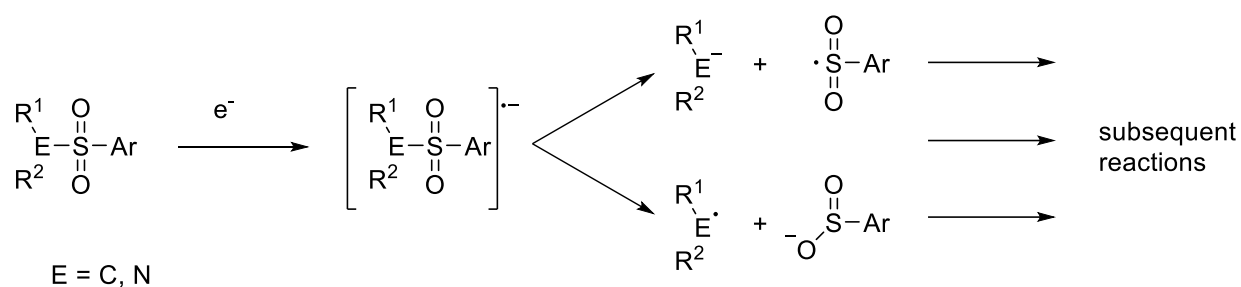


Figure 1.5: Bis(benzimidazolylidene)s and bis(imidazolylidene)s are readily oxidized and contain aromatic resonance in the cationic forms.

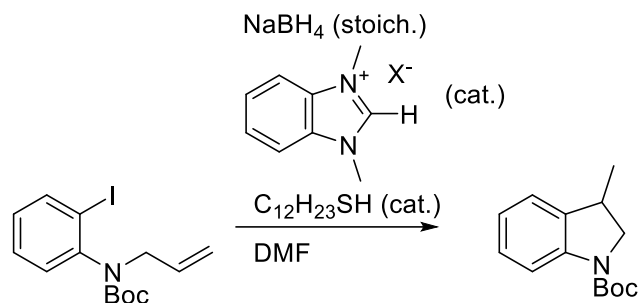
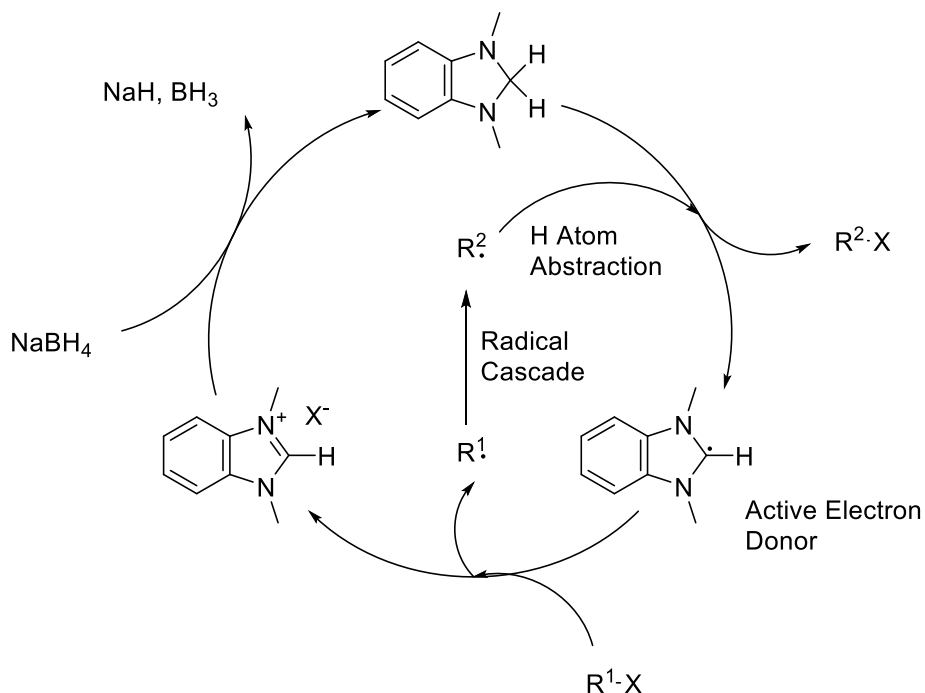
Of particular note for this dissertation is that strong electron donors can reductively cleave the C-S and N-S bonds in sulfones and sulfonamides, respectively.^{34,35} The tetraazafulvalenes used for this transformation are two-electron donors, but the process is single-

electron in nature. Reduction to the radical anion is followed rapidly by a fragmentation to an anion and a neutral radical which is, in turn reduced by another SET process.^{2,34} This implies that such reductive cleavage could occur via a one-electron donor, provided some method of trapping the neutral radical is available.



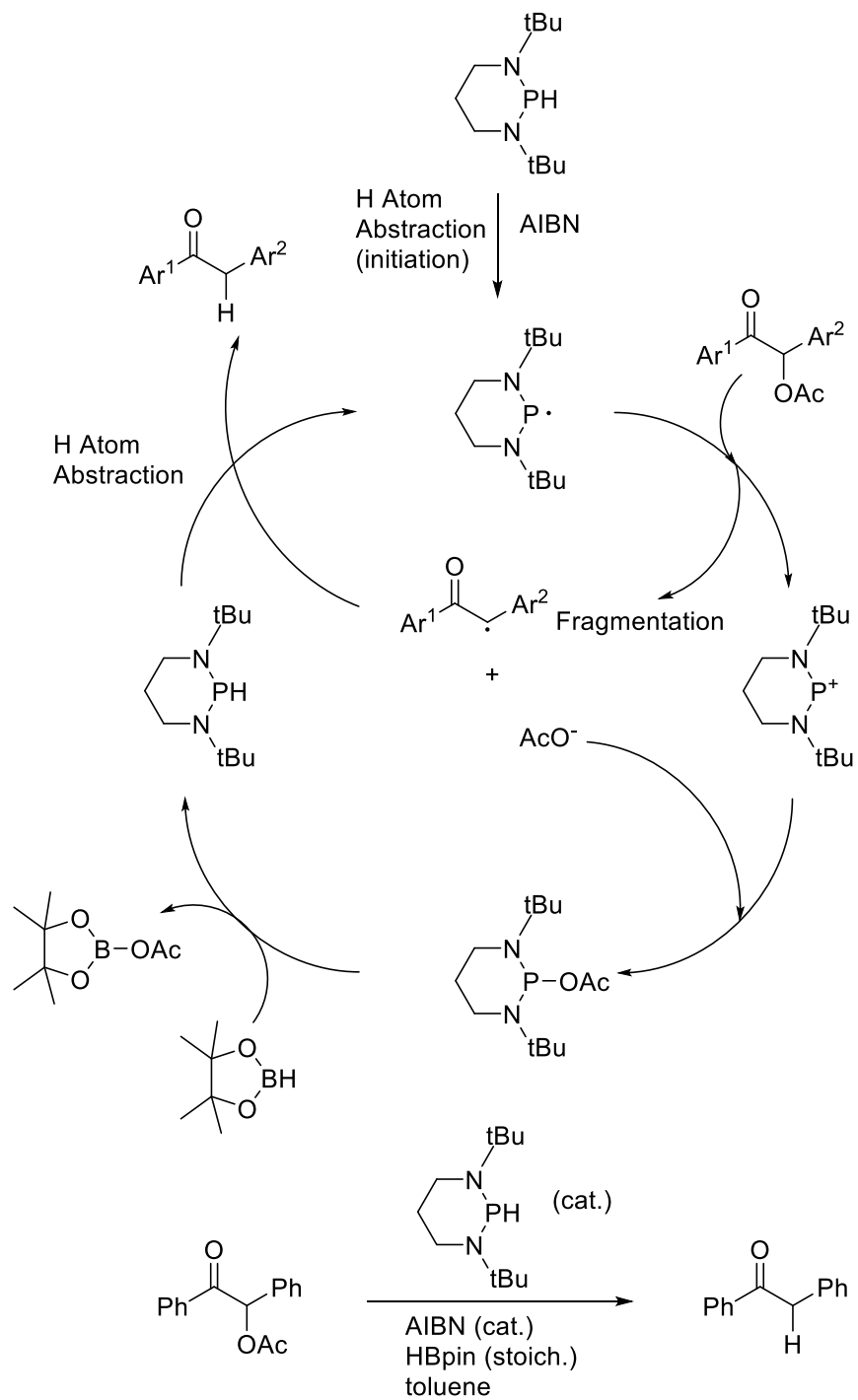
Scheme 1.3: Reductive cleavage of sulfones and sulfonamides via SET

In all the previous examples, the electron donor was utilized in a stoichiometric fashion with respect to the substrate. Indeed, when we look at TDAE or tetraazafulvalenes, the only way to regenerate the neutral, electron-donating olefin would be to reduce them again by SET processes. The development of catalytic electron donors is more recent, starting with Tuttle and Murphy's report of a super electron donor acting in a catalytic fashion.³⁶ The dihydrobenzimidazole is activated by hydrogen atom abstraction and subsequent reduction by the resulting radical gives a benzimidazolium salt. The key step was the addition of stoichiometric sodium borohydride to reduce the benzimidazolium back to the dihydrobenzimidazole.



Scheme 1.4: Catalytic cycle of a benzimidazole-derived super electron donor (*above*) with transformation of a representative substrate (*below*). C₁₂H₂₃SH is used as a polarity reversal catalyst to facilitate the hydrogen atom transfer from the nucleophilic dihydrobenzimidazole to the nucleophilic aryl radical.

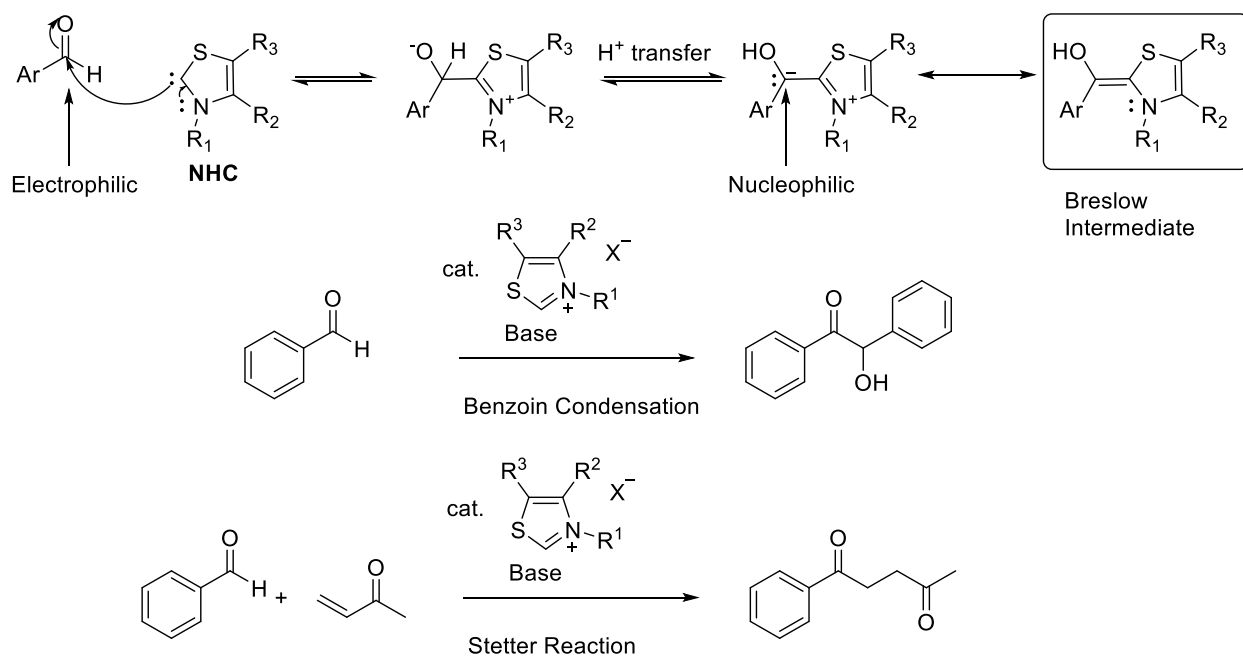
A diazaphosphine was subsequently reported by Yang and Cheng as a catalyst for the reductive cleavage of α -carboxy ketones using stoichiometric pinacol borane.³⁷ Boranes and borohydrides are widely considered to be polar (two-electron) reducing agents, but it would be interesting if a catalytic cycle could be driven by reagents not classically thought of as reducing.



Scheme 1.5: Catalytic cycle of a diazaphosphine-derived electron donor (*above*) with transformation of a representative substrate (*below*).

1.4: Breslow Intermediates: Two- and One-Electron Chemistry

In 1958, Ronald Breslow reported on thiamine-catalyzed transformations via the formation of a thiazolium ylide.³⁸ In particular, the thiazolium ylide could catalyze acyloin condensation via the formation of an enol-type structure on reaction with an aldehyde. This is what became known as the Breslow intermediate, and it is a classic example of umpolung (polarity reversal) chemistry. The nucleophilicity of the Breslow intermediate becomes clear upon inspection of its resonance structure, as the previously electrophilic aldehyde carbon now holds a partial negative charge.

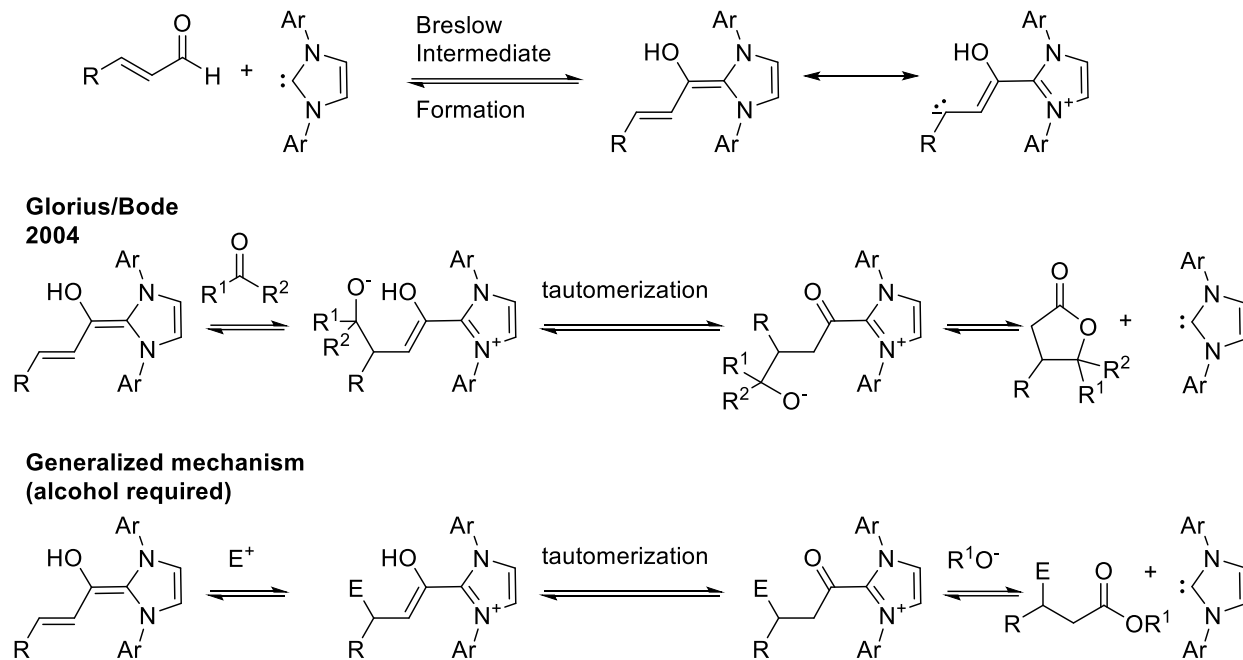


Scheme 1.6: Formation of a Breslow intermediate using a classical thiazolium NHC, with umpolung shown, and schematic examples of the benzoin condensation and Stetter reactions.

What Breslow did not recognize at the time is that drawing the thiazolium ylide with a fully neutral resonance structure gives a free carbene. Indeed, many stable NHCs can form Breslow intermediates^{39–42}, and therefore are catalysts for a many transformations of aldehydes. There is, of course, the aforementioned acyloin/benzoin condensation of two aldehydes.^{43–45} This reaction was originally reported in 1832⁴⁶ using a cyanide catalyst, but the current NHC catalysts

are, of course, significantly less toxic. Furthermore, NHCs can catalyze the condensation of aliphatic aldehydes whereas cyanide is only effective for aryl aldehydes. Another well-known NHC-catalyzed reaction that proceeds via a Breslow intermediate is the Stetter reaction, originally reported in 1976.⁴⁷ In this case, the Breslow intermediate acts as a soft nucleophile in the 1,4-addition to a Michael acceptor (generally an α - β unsaturated aldehyde/ketone).

In both the acyloin/benzoin condensations and the Stetter reaction, the Breslow intermediate is acting as a 1,2-nucleophile with respect to the starting aldehyde. If the aldehyde used has an α - β unsaturation pattern, a homoenolate equivalent is formed upon reaction with NHC.^{48,49} It should be noted that a nucleophile is necessary at the end of any carbene-catalyzed homoenolate-forming reaction as the NHC is now attached to a ketone. In the original reports, the carbene was released by nucleophilic acyl substitution by the γ -alkoxide. An alternative is to provide an alcohol which, upon deprotonation with in-situ base, can substitute off the ketone and regenerate the carbene.⁵⁰



Scheme 1.7: Formation of the Breslow Intermediate homoenolate equivalent, original reports of lactone formation via homoenolate equivalent, generalized mechanism with alcohol substituting acyl azolium ion.

Redox-type processes of Breslow Intermediates are a more recent development. Chapter 2 of this dissertation, which is taken from a publication of which the dissertation author was a co-author²³, does reference earlier reports, but not in detail. As such, a more in-depth introduction will be presented here.

The first reports on the oxidation of Breslow intermediates were published by Fukuzumi in 1997.^{51,52} They reacted a several thiazole-derived NHCs with 2-methylbenzaldehyde in the presence of excess base (DBU) to generate the enolate (deprotonated Breslow intermediate) and examined the redox process by cyclic voltammetry. The neutral radical formed by partial electrolysis of the enolate was also examined by electron paramagnetic resonance spectroscopy (EPR). With reported redox potentials of around -0.96 V vs. SCE for the enolate to radical

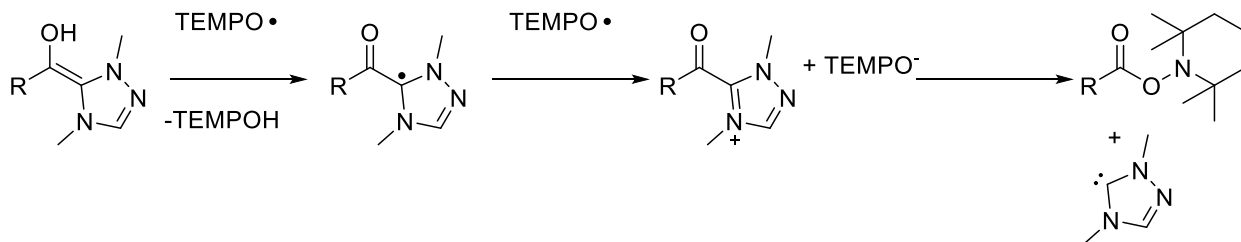
process and around -0.52 V vs. SCE for the subsequent oxidation to the cation, these are not quite as reducing as the organic electron donors discussed earlier in this chapter.



Figure 1.6: Fukuzumi's Breslow enolate (*left*) with neutral radical (*right*).

It should be noted that Fukuzumi's measurements were taken in reaction solution and with a large excess of aldehyde, which would make it difficult to ascertain the redox potential of one component of the solution. A very recent report by Martin sought to rectify this uncertainty by generating the pure acyl azolium salts and examining their cyclic voltammograms.⁵³ Their results showed that Fukuzumi's system has a significantly more reducing redox potential than originally reported of -1.41 V vs. SCE for the enolate to radical process.

The first report of a catalytic process proceeding via redox of a Breslow intermediate was the oxidation of aldehydes with TEMPO.⁵⁴ This transformation is done by two successive oxidations of the Breslow intermediate with an intermediate deprotonation by TEMPO⁻ to give the cationic acyl azolium intermediate. The acyl group is then extruded from the carbene catalyst by substitution with the second equivalent of TEMPO⁻.

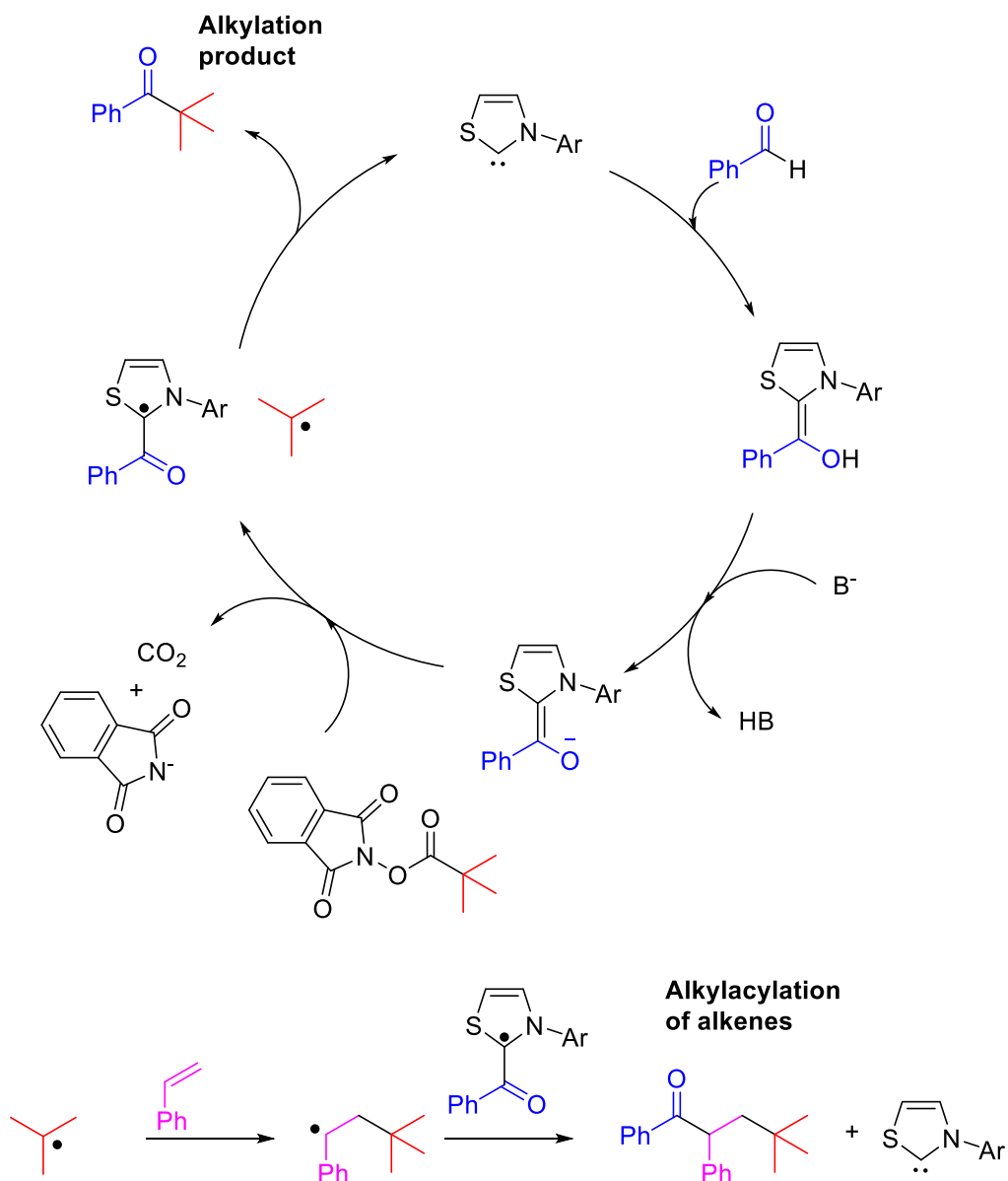


Scheme 1.8: Successive oxidations of a Breslow intermediate by TEMPO leads to a TEMPO ester with regeneration of the carbene.

It is also possible to oxidize homoenolate equivalents at the β position. This was demonstrated by Rovis in 2014 with the NHC-catalyzed oxidation of enals with nitroarenes to

form β -hydroxy esters.⁵⁵ As for previous two-electron reactions of homoenolate Breslow intermediates, an alcohol component (methanol in this case) was necessary to release the final β -hydroxy ester from the catalyst. Similarly, CBr_4 or CBrCl_3 can be used as oxidants to convert enals bearing a γ -carbonate leaving group to the corresponding γ -dihalomethylene esters, after substitution of the acyl azolium by methanol.⁵⁶

Of all types of chemical reactions, carbon-carbon bond formation is generally the most exciting for organic chemists. This is why the recent work by Ohmiya and co-workers was of particular influence for the work presented in chapter 2 of this dissertation. In 2019,⁵⁷ they published the carbene-catalyzed decarboxylative alkylation of aldehydes via use of a redox-active phthalimide ester. Phthalimide esters, which are readily synthesized by esterification of *n*-hydroxy phthalimide, are known to fragment upon single-electron reduction into phthalimide anion, carbon dioxide, and the alkyl radical corresponding to the ester substituent.⁵⁸ Ohmiya leveraged this reaction by generating a deprotonated Breslow intermediate of the type Fukuzumi had reported^{51,52} in situ and using that as the reductant for the fragmentation of the phthalimide ester. The resulting oxidized Breslow intermediate radical and the alkyl radical recombine with extrusion of the carbene catalyst to give the corresponding ketone. While originally reported for aromatic aldehydes, this reaction was later demonstrated to be effective for alkyl aldehydes as well.⁵⁹



Scheme 1.9: Mechanistic cycle of Ohmiya's carbene-catalyzed decarboxylative alkylation of aldehydes (*top*) with alkylacylation resulting from interception of the alkyl radical by an alkene (*below*).

Shortly after the first 2019 report, Ohmiya also showed that the Breslow intermediate-phthalimide ester combination could be adapted to a radical relay reaction.⁶⁰ The alkyl radical can be intercepted by a resonance-stabilized alkene (a styrene, for example) to give a new radical. This can then recombine with the oxidized Breslow intermediate to give an alkylacylation product of the alkene and regenerate the carbene catalyst as shown previously.

1.5: Carbene Reactivity with Carbon Monoxide and Isocyanides

C-1 feedstocks are a tempting target for functionalization due to their abundance and the synthetic flexibility of adding carbon atoms one at a time. One of the simplest such molecules is carbon monoxide (CO), and its functionalization by the Fischer-Tropsch process to is a classic example of C-1 chemistry.⁶¹ However, the Fischer-Tropsch process requires high temperatures and pressures of CO and hydrogen gas, as well as transition metal catalysts, which are constraining in a resource-limited world. Furthermore, it is difficult to apply CO as a C-1 feedstock for the synthesis of fine chemicals due to the product distribution of many CO reactions.

One of the classical reactions of carbenes is the formation of ketenes in the presence of CO.⁶² In this way, carbenes can be thought of as transition metal-mimics. For unstable transient carbenes, this requires a low-temperature matrix where the products are determined by spectroscopic methods such as IR, UV, and EPR. This reactivity was of particular interest as it may allow for CO functionalization without the use of transition metals.

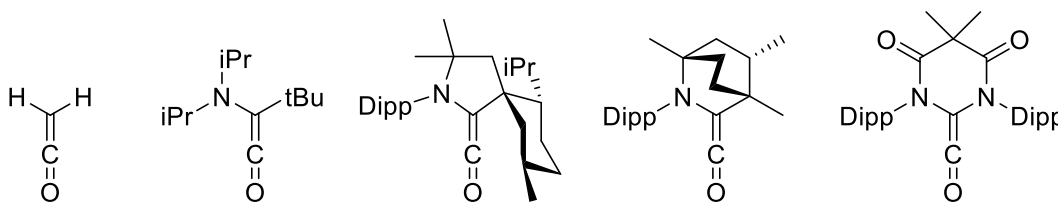
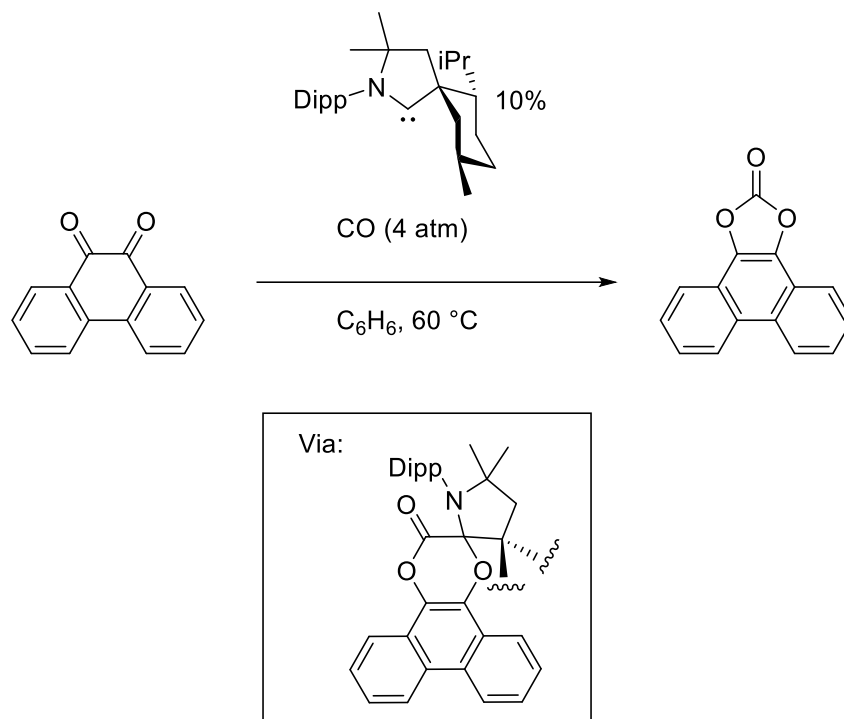


Figure 1.7: Several ketenes from the reaction of carbenes with CO. *From left to right:* methylene (parent ketene), acyclic (alkyl)(amino)carbene, CAAC, BiCAAC, diamidocarbene.

The fixation of CO by stable carbenes was not readily accessible. Despite an early report of an Arduengo-type NHC forming a diaminoketene on exposure to CO⁶³, this report was later refuted by computations and follow-up experiments indicating the formation of only weak Van-Deer-Waals interactions between the carbene and CO.^{64,65} Generally speaking, for carbenes to react with CO, they must be sufficiently electrophilic. In an NHC, the two π -donating

substituents quench the electrophilicity of the carbene p-orbital. Indeed, it was later reported by Bertrand in 2006 that the more electrophilic alkyl-amino carbenes are reactive towards CO to give the corresponding aminoketene.⁶⁶ This reaction proceeded for both cyclic and acyclic carbene frameworks and the products were reported to be stable upon storage without loss of CO. Since then, several other stable carbenes, such as the bicyclic (alkyl)(amino)carbene (BiCAAC)⁶⁷ and the diamidocarbene¹⁰ have been demonstrated to exhibit this reactivity. In the case of the diamidocarbene, fixation of CO is reversible, which hints to its intermediate electrophilicity in comparison to classical NHCs and CAACs.

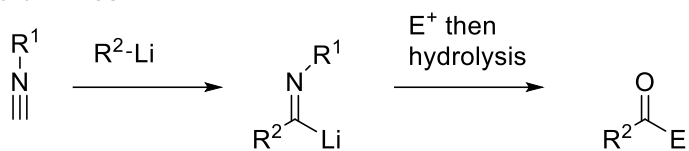
For the moment, the study of ketenes derived from the carbonylation of stable carbenes is mostly limited to their isolation and characterization of their structural and spectroscopic properties. There is one example in 2020 by Bertrand of their application.⁶⁷ It was found that aminoketenes derived from CAAC and BiCAAC could undergo a [4+2] cycloaddition with a quinone to give the corresponding lactone. Upon heating under several atmospheres of CO, the corresponding carbonate was formed along with, in the case of the CAAC, another aminoketene. Thus, the CAAC was used as a catalyst for the metal-free carbonylation of quinones by CO. These results were also the inspiration for the initial investigations shown in both chapters 3 and 4 of this dissertation.



Scheme 1.10: Metal-free carbonylation of a quinone via CAAC organocatalysis.

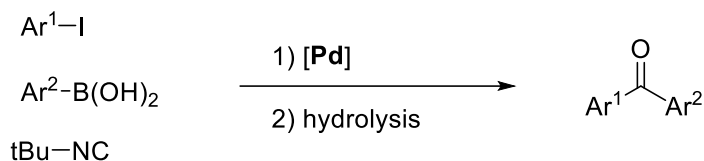
CO is a difficult reagent to use, and this is due not only to its famous toxicity but also its gaseous nature. It can therefore be useful to study similar species such as isocyanides, which are isoelectronic to CO.⁶⁸ When comparing based on metal-ligand properties, isocyanides are slightly more σ -donating and less π -accepting than CO, but are still used as stand-ins for the latter. Isocyanides can also be used much like a C-1 feedstock, as evidenced by their reactions with organolithiums to form lithium aldimines (acyl anion equivalents)^{69,70} and their palladium-catalyzed insertions into C-X bonds.⁷¹ Hydrolysis of the thus-produced imine gives ketones analogous to the similar functionalization of CO. However, these reactions use either strong, pyrophoric nucleophiles or transition metal catalysis, so more straightforward C-1 transformations of isocyanides are in demand.

lithium aldimines:



E = H, alkyl, R₃Si, CH(OH)Ar, CO₂R, etc.

Palladium-Catalyzed Insertions:



Scheme 1.11: Some C-1 functionalization reactions of isocyanides.

Another advantage of isocyanides over CO for reactivity studies is that they are easier to handle. Even the simplest example, methyl isocyanide, is a liquid at room temperature. Furthermore, the use of larger substituents can give solid isocyanides. The most significant impediment to using isocyanides is their terrible smell, but even this can be avoided by using non-volatile examples.

Many stable carbenes which are reactive with CO similarly form ketenimines on reaction with isocyanides. This has been reported for a number of carbenes, ranging from the first phosphino-silyl carbene to other acyclic carbenes, CAACs, and diamidocarbenes.⁷²⁻⁷⁴ However, the ketenimines thus formed have not yet been applied to a synthetic transformation as the CAAC-derived ketenes have been.

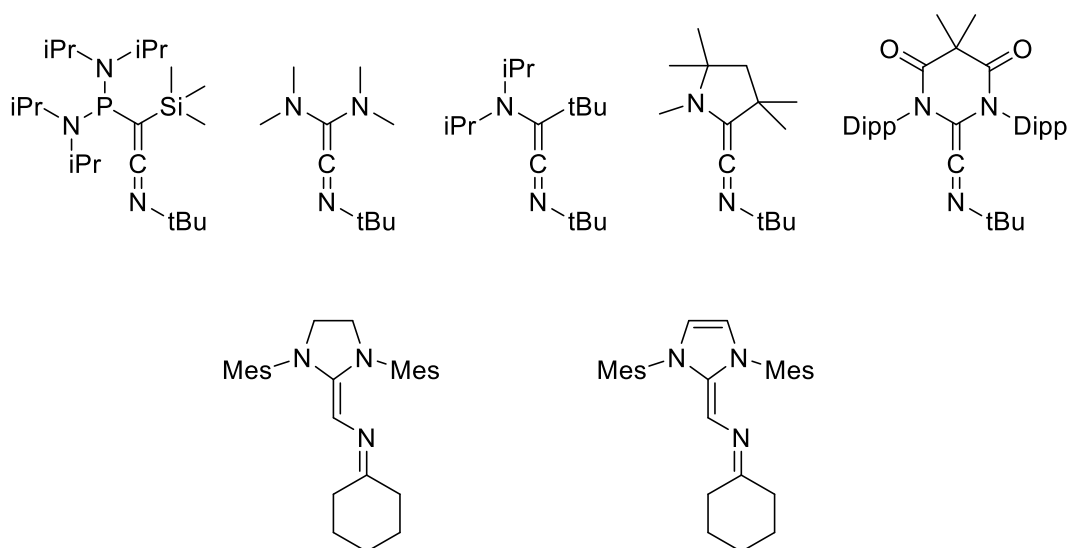


Figure 1.8: Several ketenimines resulting from the reaction of tert-butyl isocyanide with electrophilic carbenes (*top*) and 3-azabutadiene derivatives resulting from the reaction of cyclohexyl isocyanide with classical NHCs (*bottom*).

Just as in the case of CO, isocyanides were thought to be unreactive with classical NHCs due to the carbene's insufficient electrophilicity. Indeed, this was reported to be the case by Bertrand and co-workers in 2014 using a dimesityl imidazolium-derived NHC.⁷⁴ However, in 2019, Stephan and co-workers reported that the same NHC did react with cyclohexyl isocyanide, with the main difference being that the reaction was run overnight at room temperature rather than at $-78\text{ }^{\circ}\text{C}$ as in the 2014 report.⁷⁵ More interestingly, the result of this reaction was not a ketenimine as would be expected but rather a 3-azabutadiene resulting from the apparent tautomerization of the ketenimine. This product was also found to exhibit some nucleophilic reactivity and could be oxidized by triphenylmethyl cation.

1.6: Chapter 1 References

- (1) Vollhardt, P.; Schore, N. *Organic Chemistry: Structure and Function*, 8th ed.; W. H. Freeman, 2018.
- (2) Broggi, J.; Terme, T.; Vanelle, P. Organic Electron Donors as Powerful Single-Electron Reducing Agents in Organic Synthesis. *Angew. Chem. Int. Ed.* **2014**, *53* (2), 384–413. <https://doi.org/10.1002/anie.201209060>.

- (3) Igau, A.; Grutzmacher, H.; Baceiredo, A.; Bertrand, G. Analogous α,α' -Bis-Carbenoid Triply Bonded Species: Synthesis of a Stable Λ^3 -Phosphinocarbene- Λ^5 -Phosphaacetylene. *Journal of the American Chemical Society* **1988**, *110* (19), 6463–6466. <https://doi.org/10.1021/ja00227a028>.
- (4) Soleilhavoup, M.; Bertrand, G. Stable Carbenes, Nitrenes, Phosphinidenes, and Borylenes: Past and Future. *Chem* **2020**, *6* (6), 1275–1282. <https://doi.org/10.1016/j.chempr.2020.04.015>.
- (5) Arduengo, A. J.; Harlow, R. L.; Kline, M. A Stable Crystalline Carbene. *Journal of the American Chemical Society* **1991**, *113* (1), 361–363. <https://doi.org/10.1021/ja00001a054>.
- (6) Enders, D.; Breuer, K.; Raabe, G.; Runsink, J.; Teles, J. H.; Melder, J.-P.; Ebel, K.; Brode, S. Preparation, Structure, and Reactivity of 1,3,4-Triphenyl-4,5-Dihydro-1H-1,2,4-Triazol-5-Ylidene, a New Stable Carbene. *Angewandte Chemie International Edition in English* **1995**, *34* (9), 1021–1023. <https://doi.org/10.1002/anie.199510211>.
- (7) Lavallo, V.; Canac, Y.; Präsang, C.; Donnadiou, B.; Bertrand, G. Stable Cyclic (Alkyl)(Amino)Carbenes as Rigid or Flexible, Bulky, Electron-Rich Ligands for Transition-Metal Catalysts: A Quaternary Carbon Atom Makes the Difference. *Angewandte Chemie - International Edition* **2005**, *44* (35), 5705–5709. <https://doi.org/10.1002/anie.200501841>.
- (8) Lavallo, V.; Canac, Y.; DeHope, A.; Donnadiou, B.; Bertrand, G. A Rigid Cyclic (Alkyl)(Amino)Carbene Ligand Leads to Isolation of Low-Coordinate Transition-Metal Complexes. *Angewandte Chemie International Edition* **2005**, *44* (44), 7236–7239. <https://doi.org/10.1002/anie.200502566>.
- (9) Lavallo, V.; Canac, Y.; Donnadiou, B.; Schoeller, W. W.; Bertrand, G. Cyclopropenylidenes: From Interstellar Space to an Isolated Derivative in the Laboratory. *Science* **2006**, *312* (5774), 722–724. <https://doi.org/10.1126/science.1126675>.
- (10) Hudnall, T. W.; Bielawski, C. W. An N,N'-Diamidocarbene: Studies in C–H Insertion, Reversible Carbonylation, and Transition-Metal Coordination Chemistry. *J. Am. Chem. Soc.* **2009**, *131* (44), 16039–16041. <https://doi.org/10.1021/ja907481w>.
- (11) Hudnall, T. W.; Moerdyk, J. P.; Bielawski, C. W. Ammonia N–H Activation by a N,N'-Diamidocarbene. *Chem. Commun.* **2010**, *46* (24), 4288–4290. <https://doi.org/10.1039/C0CC00638F>.
- (12) Bellotti, P.; Koy, M.; Hopkinson, M. N.; Glorius, F. Recent Advances in the Chemistry and Applications of N-Heterocyclic Carbenes. *Nat Rev Chem* **2021**, *5* (10), 711–725. <https://doi.org/10.1038/s41570-021-00321-1>.
- (13) Chemistry (IUPAC), T. I. U. of P. and A. *IUPAC - mesoionic compounds (M03842)*. <https://goldbook.iupac.org/terms/view/M03842> (accessed 2022-04-14). <https://doi.org/10.1351/goldbook.M03842>.

- (14) Aldeco-Perez, E.; Rosenthal, A. J.; Donnadiou, B.; Pattiyil, P.; Frenking, G.; Bertrand, G.; Guisado-Barrios, G.; Bouffard, J.; Donnadiou, B.; Bertrand, G. Isolation of a C5-Deprotonate Imidazolium, a Crystalline “Abnormal” N-Heterocyclic Carbene. *Science* **2009**, *326*, 556–559. <https://doi.org/10.1002/ejoc.201501626>.
- (15) Begtrup, M. Reactions between Azolium Anions and Electrophilic Reagents. I. Direct Thiation of 1,3-Disubstituted 1,2,3-Triazolium Anions with Sulfur. *Acta Chemica Scandinavica* **1975**, *29B*, 141–144.
- (16) Begtrup, M. Azolium Anions and Their Reaction with Electrophilic Reagents. *Journal of the Chemical Society, Chemical Communications* **1975**, No. 9, 334–335. <https://doi.org/10.1039/C39750000334>.
- (17) Guisado-Barrios, G.; Bouffard, J.; Donnadiou, B.; Bertrand, G. Crystalline 1H-1,2,3-Triazol-5-Ylidenes: New Stable Mesoionic Carbenes (MICs). *Angewandte Chemie - International Edition* **2010**, *49* (28), 4759–4762. <https://doi.org/10.1002/anie.201001864>.
- (18) Bouffard, J.; Keitz, B. K.; Tonner, R.; Guisado-Barrios, G.; Frenking, G.; Grubbs, R. H.; Bertrand, G. Synthesis of Highly Stable 1,3-Diaryl-1 H -1,2,3-Triazol-5-Ylidenes and Their Applications in Ruthenium-Catalyzed Olefin Metathesis. *Organometallics* **2011**, *30* (9), 2617–2627. <https://doi.org/10.1021/om200272m>.
- (19) Guisado-Barrios, G.; Bouffard, J.; Donnadiou, B.; Bertrand, G. Bis(1,2,3-Triazol-5-Ylidenes)(i-Bitz) as Stable 1,4-Bidentate Ligands Based on Mesoionic Carbenes (MICs). *Organometallics* **2011**, *30* (21), 6017–6021. <https://doi.org/10.1021/om200844b>.
- (20) Sau, S. C.; Hota, P. K.; Mandal, S. K.; Soleilhavoup, M.; Bertrand, G. Stable Abnormal N-Heterocyclic Carbenes and Their Applications. *Chem. Soc. Rev.* **2020**, *49* (4), 1233–1252. <https://doi.org/10.1039/C9CS00866G>.
- (21) Guisado-Barrios, G.; Soleilhavoup, M.; Bertrand, G. 1H-1,2,3-Triazol-5-Ylidenes: Readily Available Mesoionic Carbenes. *Acc. Chem. Res.* **2018**, *51* (12), 3236–3244. <https://doi.org/10.1021/acs.accounts.8b00480>.
- (22) Keitz, B. K.; Bouffard, J.; Bertrand, G.; Grubbs, R. H. Protonolysis of a Ruthenium–Carbene Bond and Applications in Olefin Metathesis. *J. Am. Chem. Soc.* **2011**, *133* (22), 8498–8501. <https://doi.org/10.1021/ja203070r>.
- (23) Liu, W.; Vianna, A.; Zhang, Z.; Huang, S.; Huang, L.; Melaimi, M.; Bertrand, G.; Yan, X. Mesoionic Carbene-Breslow Intermediates as Super Electron Donors: Application to the Metal-Free Arylacylation of Alkenes. *Chem Catalysis* **2021**, *1* (1), 196–206. <https://doi.org/10.1016/J.CHECAT.2021.03.004/ATTACHMENT/030A406B-3A14-4D13-A30A-396E00D289F5/MMC1.PDF>.
- (24) Xu, X.; Zhang, Z.; Huang, S.; Cao, L.; Liu, W.; Yan, X. 4-Halo-1,2,3-Triazolylidenes: Stable Carbenes Featuring Halogen Bonding. *Dalton Trans.* **2019**, *48* (20), 6931–6941. <https://doi.org/10.1039/C9DT01018A>.

- (25) Cao, L.; Huang, S.; Liu, W.; Yan, X. 4-Phosphino-1,2,3-Triazol-5-Ylidenes: Stable Bridging Ligands for Coinage Metal Complexes. *Organometallics* **2018**, *37* (13), 2010–2013. <https://doi.org/10.1021/acs.organomet.8b00305>.
- (26) Zhang, N.; Samanta, S. R.; Rosen, B. M.; Percec, V. Single Electron Transfer in Radical Ion and Radical-Mediated Organic, Materials and Polymer Synthesis. *Chem. Rev.* **2014**, *114* (11), 5848–5958. <https://doi.org/10.1021/cr400689s>.
- (27) Pruett, R. L.; Barr, J. T.; Rapp, K. E.; Bahner, C. T.; Gibson, J. D.; Lafferty, R. H. Reactions of Polyfluoro Olefins. II.1 Reactions with Primary and Secondary Amines. *J. Am. Chem. Soc.* **1950**, *72* (8), 3646–3650. <https://doi.org/10.1021/ja01164a090>.
- (28) Burkholder, C.; Dolbier, W. R.; Médebielle, M. Tetrakis(Dimethylamino)Ethylene as a Useful Reductant of Some Bromodifluoromethyl Heterocycles. Application to the Synthesis of New *Gem* -Difluorinated Heteroarylated Compounds. *J. Org. Chem.* **1998**, *63* (16), 5385–5394. <https://doi.org/10.1021/jo980201+>.
- (29) Murphy, J. A.; Zhou, S.; Thomson, D. W.; Schoenebeck, F.; Mahesh, M.; Park, S. R.; Tuttle, T.; Berlouis, L. E. A. The Generation of Aryl Anions by Double Electron Transfer to Aryl Iodides from a Neutral Ground-State Organic Super-Electron Donor. *Angewandte Chemie International Edition* **2007**, *46* (27), 5178–5183. <https://doi.org/10.1002/anie.200700554>.
- (30) Ames, J. R.; Houghtaling, M. A.; Terrian, D. L.; Mitchell, T. P. Annulated Derivatives of 2,2'-Biimidazole, 2-(2'-Imidazolyl)Benzimidazole, and 2,2'-Bibenzimidazole. *Can. J. Chem.* **1997**, *75* (1), 28–36. <https://doi.org/10.1139/v97-004>.
- (31) Thummel, R. P.; Gouille, V.; Chen, B. Bridged Derivatives of 2,2'-Biimidazole. *J. Org. Chem.* **1989**, *54* (13), 3057–3061. <https://doi.org/10.1021/jo00274a019>.
- (32) Taton, T. A.; Chen, P. A Stable Tetraazafulvalene. *Angewandte Chemie International Edition in English* **1996**, *35* (9), 1011–1013. <https://doi.org/10.1002/anie.199610111>.
- (33) Murphy, J. A.; Khan, T. A.; Zhou, S.; Thomson, D. W.; Mahesh, M. Highly Efficient Reduction of Unactivated Aryl and Alkyl Iodides by a Ground-State Neutral Organic Electron Donor. *Angew. Chem. Int. Ed.* **2005**, *44* (9), 1356–1360. <https://doi.org/10.1002/anie.200462038>.
- (34) Schoenebeck, F.; Murphy, J. A.; Zhou, S.; Uenoyama, Y.; Miclo, Y.; Tuttle, T. Reductive Cleavage of Sulfones and Sulfonamides by a Neutral Organic Super-Electron-Donor (S.E.D.) Reagent. *J. Am. Chem. Soc.* **2007**, *129* (44), 13368–13369. <https://doi.org/10.1021/ja074417h>.
- (35) Hanson, S. S.; Doni, E.; Traboulsee, K. T.; Coulthard, G.; Murphy, J. A.; Dyker, C. A. Pushing the Limits of Neutral Organic Electron Donors: A Tetra(Iminophosphorano)-Substituted Bipyridinylidene. *Angewandte Chemie International Edition* **2015**, *54* (38), 11236–11239. <https://doi.org/10.1002/anie.201505378>.

- (36) Rohrbach, S.; Shah, R. S.; Tuttle, T.; Murphy, J. A. Neutral Organic Super Electron Donors Made Catalytic. *Angewandte Chemie International Edition* **2019**, *58* (33), 11454–11458. <https://doi.org/10.1002/anie.201905814>.
- (37) Zhang, J.; Yang, J.-D.; Cheng, J.-P. Diazaphosphinyl Radical-Catalyzed Deoxygenation of α -Carboxy Ketones: A New Protocol for Chemo-Selective C–O Bond Scission via Mechanism Regulation. *Chem. Sci.* **2020**, *11* (32), 8476–8481. <https://doi.org/10.1039/D0SC03220D>.
- (38) Breslow, R. On the Mechanism of Thiamine Action. IV. ¹ Evidence from Studies on Model Systems. *J. Am. Chem. Soc.* **1958**, *80* (14), 3719–3726. <https://doi.org/10.1021/ja01547a064>.
- (39) Berkessel, A.; Elfert, S.; Yatham, V. R.; Neudörfl, J.-M.; Schlörer, N. E.; Teles, J. H. Umpolung by N-Heterocyclic Carbenes: Generation and Reactivity of the Elusive 2,2-Diamino Enols (Breslow Intermediates). *Angew. Chem. Int. Ed.* **2012**, *51* (49), 12370–12374. <https://doi.org/10.1002/anie.201205878>.
- (40) Paul, M.; Sudkaow, P.; Wessels, A.; Schlörer, N. E.; Neudörfl, J.; Berkessel, A. Breslow Intermediates from Aromatic N-Heterocyclic Carbenes (Benzimidazolin-2-ylidenes, Thiazolin-2-ylidenes). *Angew. Chem. Int. Ed.* **2018**, *57* (27), 8310–8315. <https://doi.org/10.1002/anie.201801676>.
- (41) Paul, M.; Neudörfl, J.; Berkessel, A. Breslow Intermediates from a Thiazolin-2-ylidene and Fluorinated Aldehydes: XRD and Solution-Phase NMR Spectroscopic Characterization. *Angew. Chem. Int. Ed.* **2019**, *58* (31), 10596–10600. <https://doi.org/10.1002/anie.201904308>.
- (42) Liu, W.; Zhao, L. L.; Melaimi, M.; Cao, L.; Xu, X.; Bouffard, J.; Bertrand, G.; Yan, X. Mesoionic Carbene (MIC)-Catalyzed H/D Exchange at Formyl Groups. *Chem* **2019**, *5* (9), 2484–2494. <https://doi.org/10.1016/J.CHEMPR.2019.08.011/ATTACHMENT/4AF280FC-0A48-4C9B-A9B7-5327459FC5E1/MMC1.PDF>.
- (43) Pareek, M.; Reddi, Y.; Sunoj, R. B. Tale of the Breslow Intermediate, a Central Player in N-Heterocyclic Carbene Organocatalysis: Then and Now. *Chemical Science* **2021**, *12* (23), 7973–7992. <https://doi.org/10.1039/D1SC01910D>.
- (44) Hopkinson, M. N.; Richter, C.; Schedler, M.; Glorius, F. An Overview of N-Heterocyclic Carbenes. *Nature* **2014**, *510* (7506), 485–496. <https://doi.org/10.1038/nature13384>.
- (45) Menon, R. S.; Biju, A. T.; Nair, V. Recent Advances in N-Heterocyclic Carbene (NHC)-Catalysed Benzoin Reactions. *Beilstein Journal of Organic Chemistry* **2016**, *12* (1), 444–461. <https://doi.org/10.3762/bjoc.12.47>.
- (46) Wöhler; Liebig. Untersuchungen Über Das Radikal Der Benzoessäure. *Annalen der Pharmacie* **1832**, *3* (3), 249–282. <https://doi.org/10.1002/jlac.18320030302>.

- (47) Stetter, H. Catalyzed Addition of Aldehydes to Activated Double Bonds—A New Synthetic Approach. *Angewandte Chemie International Edition in English* **1976**, *15* (11), 639–647. <https://doi.org/10.1002/anie.197606391>.
- (48) Sohn, S. S.; Rosen, E. L.; Bode, J. W. N-Heterocyclic Carbene-Catalyzed Generation of Homo-enolates: γ -Butyrolactones by Direct Annulations of Enals and Aldehydes. *J. Am. Chem. Soc.* **2004**, *126* (44), 14370–14371. <https://doi.org/10.1021/ja044714b>.
- (49) Burstein, C.; Glorius, F. Organocatalyzed Conjugate Umpolung of α,β -Unsaturated Aldehydes for the Synthesis of γ -Butyrolactones. *Angewandte Chemie International Edition* **2004**, *43* (45), 6205–6208. <https://doi.org/10.1002/anie.200461572>.
- (50) Sohn, S. S.; Bode, J. W. Catalytic Generation of Activated Carboxylates from Enals: A Product-Determining Role for the Base. *Org. Lett.* **2005**, *7* (18), 3873–3876. <https://doi.org/10.1021/ol051269w>.
- (51) Nakanishi, I.; Itoh, S.; Suenobu, T.; Fukuzumi, S. Electron Transfer Properties of Active Aldehydes Derived from Thiamin Coenzyme Analogues. *Chemical Communications* **1997**, No. 19, 1927–1928. <https://doi.org/10.1039/A704559J>.
- (52) Nakanishi, I.; Itoh, S.; Suenobu, T.; Inoue, H.; Fukuzumi, S. Redox Behavior of Active Aldehydes Derived from Thiamin Coenzyme Analogues. *Chem. Lett.* **1997**, *26* (8), 707–708. <https://doi.org/10.1246/cl.1997.707>.
- (53) Delfau, L.; Nichilo, S.; Molton, F.; Broggi, J.; Tomás-Mendivil, E.; Martin, D. Critical Assessment of the Reducing Ability of Breslow-Type Derivatives and Implications for Carbene-Catalyzed Radical Reactions**. *Angewandte Chemie International Edition* **2021**, *60* (51), 26783–26789. <https://doi.org/10.1002/ANIE.202111988>.
- (54) Guin, J.; De Sarkar, S.; Grimme, S.; Studer, A. Biomimetic Carbene-Catalyzed Oxidations of Aldehydes Using TEMPO. *Angew. Chem. Int. Ed.* **2008**, *47* (45), 8727–8730. <https://doi.org/10.1002/anie.200802735>.
- (55) White, N. A.; Rovis, T. Enantioselective N-Heterocyclic Carbene-Catalyzed β -Hydroxylation of Enals Using Nitroarenes: An Atom Transfer Reaction That Proceeds via Single Electron Transfer. *J. Am. Chem. Soc.* **2014**, *136* (42), 14674–14677. <https://doi.org/10.1021/ja5080739>.
- (56) Yang, W.; Hu, W.; Dong, X.; Li, X.; Sun, J. N-Heterocyclic Carbene Catalyzed γ -Dihalomethylenation of Enals by Single-Electron Transfer. *Angew. Chem. Int. Ed.* **2016**, *55* (51), 15783–15786. <https://doi.org/10.1002/anie.201608371>.
- (57) Ishii, T.; Kakeno, Y.; Nagao, K.; Ohmiya, H. N-Heterocyclic Carbene-Catalyzed Decarboxylative Alkylation of Aldehydes. *Journal of the American Chemical Society* **2019**, *141* (9), 3854–3858. https://doi.org/10.1021/JACS.9B00880/SUPPL_FILE/JA9B00880_SI_001.PDF.

- (58) Murarka, S. N-(Acyloxy)Phthalimides as Redox-Active Esters in Cross-Coupling Reactions. *Advanced Synthesis & Catalysis* **2018**, *360* (9), 1735–1753. <https://doi.org/10.1002/adsc.201701615>.
- (59) Kakeno, Y.; Kusakabe, M.; Nagao, K.; Ohmiya, H. Direct Synthesis of Dialkyl Ketones from Aliphatic Aldehydes through Radical N-Heterocyclic Carbene Catalysis. *ACS Catalysis* **2020**, *10* (15), 8524–8529. https://doi.org/10.1021/ACSCATAL.0C02849/SUPPL_FILE/CS0C02849_SI_001.PDF.
- (60) Ishii, T.; Ota, K.; Nagao, K.; Ohmiya, H. N-Heterocyclic Carbene-Catalyzed Radical Relay Enabling Vicinal Alkylacylation of Alkenes. *Journal of the American Chemical Society* **2019**, *141* (36), 14073–14077. https://doi.org/10.1021/JACS.9B07194/SUPPL_FILE/JA9B07194_SI_001.PDF.
- (61) Mahmoudi, H.; Mahmoudi, M.; Doustdar, O.; Jahangiri, H.; Tsolakis, A.; Gu, S.; LechWyszynski, M. A Review of Fischer Tropsch Synthesis Process, Mechanism, Surface Chemistry and Catalyst Formulation. *Biofuels Engineering* **2017**, *2* (1), 11–31. <https://doi.org/10.1515/bfuel-2017-0002>.
- (62) Sander, Wolfram.; Bucher, Goetz.; Wierlacher, Stefan. Carbenes in Matrixes: Spectroscopy, Structure, and Reactivity. *Chem. Rev.* **1993**, *93* (4), 1583–1621. <https://doi.org/10.1021/cr00020a009>.
- (63) Lyashchuk, S. N.; Skrypnik, Yuri. G. Synthesis of 1,3-Di-1-Adamantylimidazol-2-Carbonyl from 1,3-Di-1-Adamantylimidazol-2-Ylidene. *Tetrahedron Letters* **1994**, *35* (29), 5271–5274. [https://doi.org/10.1016/S0040-4039\(00\)77082-1](https://doi.org/10.1016/S0040-4039(00)77082-1).
- (64) Dixon, D. A.; Arduengo, A. J.; Dobbs, K. D.; Khasnis, D. V. On the Proposed Existence of a Ketene Derived from Carbon Monoxide and 1,3-Di-1-Adamantylimidazol-2-Ylidene. *Tetrahedron Letters* **1995**, *36* (5), 645–648. [https://doi.org/10.1016/0040-4039\(94\)02341-8](https://doi.org/10.1016/0040-4039(94)02341-8).
- (65) Denk, M. K.; Rodezno, J. M.; Gupta, S.; Lough, A. J. Synthesis and Reactivity of Subvalent Compounds: Part 11. Oxidation, Hydrogenation and Hydrolysis of Stable Diamino Carbenes. *Journal of Organometallic Chemistry* **2001**, *617–618*, 242–253. [https://doi.org/10.1016/S0022-328X\(00\)00551-9](https://doi.org/10.1016/S0022-328X(00)00551-9).
- (66) Lavallo, V.; Canac, Y.; Donnadiu, B.; Schoeller, W. W.; Bertrand, G. CO Fixation to Stable Acyclic and Cyclic Alkyl Amino Carbenes: Stable Amino Ketenes with a Small HOMO–LUMO Gap. *Angewandte Chemie International Edition* **2006**, *45* (21), 3488–3491. <https://doi.org/10.1002/anie.200600987>.
- (67) Peltier, J. L.; Tomás-Mendivil, E.; Tolentino, D. R.; Hansmann, M. M.; Jazzar, R.; Bertrand, G. Realizing Metal-Free Carbene-Catalyzed Carbonylation Reactions with CO. *J. Am. Chem. Soc.* **2020**, *142* (43), 18336–18340. <https://doi.org/10.1021/jacs.0c09938>.

- (68) Massarotti, A.; Brunelli, F.; Aprile, S.; Giustiniano, M.; Tron, G. C. Medicinal Chemistry of Isocyanides. *Chem. Rev.* **2021**, *121* (17), 10742–10788. <https://doi.org/10.1021/acs.chemrev.1c00143>.
- (69) Walborsky, H. M.; Niznik, G. E. Lithium Aldimines. A New Synthetic Intermediate. *J. Am. Chem. Soc.* **1969**, *91* (27), 7778–7778. <https://doi.org/10.1021/ja50001a064>.
- (70) Niznik, G. E.; Morrison, W. H.; Walborsky, H. M. Metallo Aldimines. Masked Acyl Carbanion. *J. Org. Chem.* **1974**, *39* (5), 600–604. <https://doi.org/10.1021/jo00919a004>.
- (71) Collet, J. W.; Roose, T. R.; Weijers, B.; Maes, B. U. W.; Ruijter, E.; Orru, R. V. A. Recent Advances in Palladium-Catalyzed Isocyanide Insertions. *Molecules* **2020**, *25* (21), 4906. <https://doi.org/10.3390/molecules25214906>.
- (72) Hudnall, T. W.; Moorhead, E. J.; Gusev, D. G.; Bielawski, C. W. N,N'-Diamidoketenimines via Coupling of Isocyanides to an N-Heterocyclic Carbene. *J. Org. Chem.* **2010**, *75* (8), 2763–2766. <https://doi.org/10.1021/jo100427g>.
- (73) Igau, A.; Baceiredo, A.; Trinquier, G.; Bertrand, G. [Bis(Diisopropylamino)Phosphino]Trimethylsilylcarbene: A Stable Nucleophilic Carbene. *Angewandte Chemie International Edition in English* **1989**, *28* (5), 621–622. <https://doi.org/10.1002/anie.198906211>.
- (74) Martin, D.; Canac, Y.; Lavallo, V.; Bertrand, G. Comparative Reactivity of Different Types of Stable Cyclic and Acyclic Mono- and Diamino Carbenes with Simple Organic Substrates. *J. Am. Chem. Soc.* **2014**, *136* (13), 5023–5030. <https://doi.org/10.1021/ja412981x>.
- (75) Kim, Y.; Liu, L. L.; Stephan, D. W. N-Heterocyclic Carbene Derived 3-Azabutadiene as a Π -Base in Classic and Frustrated Lewis Pair Chemistry. *Chem. Eur. J.* **2019**, *25* (29), 7110–7113. <https://doi.org/10.1002/chem.201901609>.

CHAPTER 2: MESOIONIC
CARBENE-BRESLOW
INTERMEDIATES AS SUPER
ELECTRON DONORS:
APPLICATION TO THE
METAL-FREE
ARYLACYLATION OF
ALKENES

2.1: Summary

Classical N-heterocyclic carbenes (NHCs), such as thiazolylienes, 1,2,4-triazolylienes and imidazol(in)-2-ylidenes, are powerful organocatalysts for aldehyde transformations, through the so-called Breslow intermediates (BIs). The reactions usually occur via electron-pair-transfer processes. In contrast, the use of BIs in single electron transfer (SET) pathways is still in its infancy, and the scope is limited by the moderate reduction potential of BIs derived from classical NHCs (ca -1.0 V vs SCE). Here we report that BIs from 1,2,3-triazolylienes, a type of mesoionic carbenes (MICs), have a reduction potential as negative as -1.93 V vs SCE, and thus are among the most potent organic reducing agents reported to date. They are reductive enough to undergo SET with iodoarenes, which allows the highly efficient inter- and intra-molecular MIC-catalyzed arylation of styrenes and alkenes, respectively.

2.2: The Bigger Picture

N-heterocyclic carbenes (NHCs) have been demonstrated to be powerful organocatalysts for carbonyl transformations via the so-called Breslow Intermediates (BIs). Recently, NHC-catalyzed reactions via single electron transfer (SET) pathways have been developed but still suffer from the limitation of moderate reduction potential of BIs. In this paper, taking advantage of highly reductive MIC-derived BIs, we describe the three-component coupling reaction of iodoarenes, alkenes and aldehydes catalyzed by mesoionic carbenes (MICs). This reaction affords various substituted ketones and even polycyclic ketones with readily available substrates.

2.3: Introduction

Over the past decades, N-heterocyclic carbenes (NHCs) have been demonstrated to be powerful organocatalysts for aldehyde transformations.¹⁻⁶ The umpolung of aldehydes by NHCs⁷ through the formation of nucleophilic Breslow intermediates (BIs) was later extended to provide

other reactive intermediates, such as acyl azoliums, enolates and homoenolates.⁸⁻¹² These intermediates react with diverse electrophilic / nucleophilic coupling partners via electron-pair-transfer processes. In contrast, NHC-catalyzed reactions via single electron transfer (SET) pathways are still in their infancy.¹³⁻¹⁵ In 2008, Studer and co-workers reported the NHC-catalyzed oxidation of aldehydes by TEMPO via a SET process (Figure 1).¹⁶ Other oxidants, such as nitroarenes, nitroalkenes, CX₄, C₂Cl₆, and sulfonic carbamate, were also employed to achieve oxidative reactions of aldehydes.¹⁷⁻²¹ Recently, an important breakthrough has been reported by Ohmiya, Nagao and co-workers who showed that redox-active esters could be employed as both SET oxidants and alkylating reagents.^{22,23} The same group also described a three-component alkylacylation reaction of alkenes via a radical relay strategy,²⁴ and the Li group achieved the NHC-catalyzed radical acylfluoroalkylation of olefins with the Togni reagent or polyfluoroalkyl halides.²⁵ Ye and co-workers described γ - and ε - alkylation with alkyl radicals, in which an activated alkyl halide was employed as SET oxidant and alkylating reagent.²⁶ Hong and co-worker reported the NHC-catalyzed radical coupling of aldehydes and Katritzky pyridinium salts.²⁷ However, due to the moderate reduction potential of BIs derived from classical NHCs (ca -1.0 V vs SCE),²⁸⁻³⁰ these SET catalyzed reactions required a relatively strong oxidant to ensure the electron-transfer process, which dramatically limits the scope of the reactions. For much less oxidative substrates, BIs with more negative reduction potentials are needed. Recently, we reported the formation of BIs derived from mesoionic carbenes (BIMICs), and their application to the catalytic H/D exchange of aldehydes.³¹ This class of BIs was found to be far more electron-rich than any others previously known and should thus be much more reductive. Herein, we describe the electrochemistry of BIMICs, which have a reduction potential as negative as -2.49 V vs Fc/Fc⁺ (calculated as -1.93 V vs SCE). The oxidation product, namely

the radical form of a deprotonated BIMIC, was unambiguously characterized by a single crystal X-ray diffraction study. This type of BIs can be classified as new organic super electron donors,^{32,33} and are reductive enough to undergo SET with iodoarenes. This is demonstrated by the highly efficient MIC-catalyzed aryacylation of alkenes.

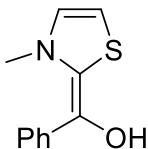
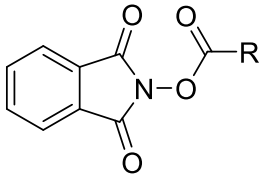
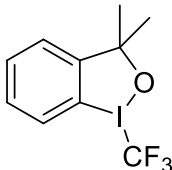
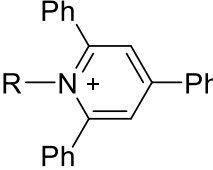
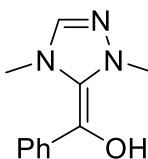
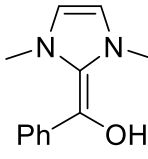
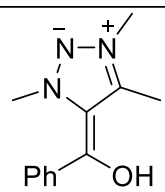
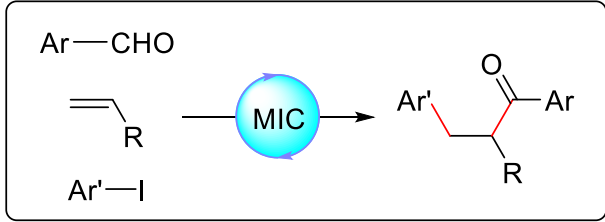
(A) Breslow intermediate	HOMO (eV)	E_{ox} (V vs SCE)	SET partners
	-4.38	-0.97 (ref. 30)	TEMPO, R-NO ₂ , CX ₄ , C ₂ Cl ₆ ArSO ₃ -NR ₂  I-C _n F _{2n+1} X-EWG  
	-4.27	-	
	-3.90	-	
(B) 	-3.56	-1.93	Ar-I <i>this work</i>
(C)			

Figure 2.1: Breslow Intermediates (BIs) for Single Electron Transfer Reactions

(A) Reduction potential of known Bis and their SET partners

(B) Mesoionic carbene Breslow Intermediates (BIMIC)

(C) Three component MIC-catalyzed aryacylation of alkenes

2.4: Results and Discussion

Initially, we investigated the electrochemistry of BIMIC **3a**, which was prepared by addition of benzaldehyde to MIC **2a**,³⁴⁻³⁷ generated by deprotonation of **1a** (Figure 2A). The cyclic voltammogram of **3a** shows an irreversible redox process between **3a** and **4a**[•] with an anodic peak potential $E_{pa} = -2.49$ V and a corresponding cathodic peak potential $E_{pc} = -2.59$ V (Figure 2F). This is in agreement with an EC process³⁸ in which the oxidation of **3a** is immediately followed by the easy deprotonation of **3a** to generate **4a**[•].²⁹ To confirm this redox process, the radical form **4a**[•] was prepared by reduction of the deprotonated BIMIC **4a**⁺ with KC_8 in THF (Figure 2B). The structure of **4a**[•] was unambiguously characterized by X-ray diffraction analysis (Figure 2C) and EPR (Figure 2D). Compared with other acyl-carbene radicals derived from NHCs and CAACs,³⁹⁻⁴¹ the C(carbene)-C(acyl) bond is slightly longer, while the dihedral angle between the carbene ring and the acyl moiety is larger. We performed DFT calculations at the B3LYP-D3(BJ)/6-311G** level of theory to gain more insight into the electronic structure of **4a**[•]. The SOMO of **4a**[•] is mainly located on the π^* orbital of the triazole ring and carbonyl group (See Supporting Information), while the spin density is mainly located on N1 and N2 with some contribution on C2, C4 and O1 (Figure 2E). As expected, EPR spectra of **4a**[•] in benzene solution featured a strong signal centered at $g = 2.003$ with hyperfine coupling with two nitrogen nuclei ($a_{iso} = 6.68$ G). In agreement with DFT calculations, the small hyperfine coupling constants indicate a strong delocalization of the unpaired electron. The cyclic voltammogram of **4a**[•] also shows two irreversible peaks with one oxidation peak at -2.46 V and one reduction peak at -2.63 V, which affords further evidence of the process between **3a** and **4a**[•] (Figure 2G). In addition, one set of reversible peaks at $E_{1/2} = -1.53$ V was observed, corresponding to the reversible process **4a**[•]/**4a**⁺. To further confirm our hypothesis, a cyclic voltammogram of **4a**⁺ was also carried out, and it shows two irreversible peaks and one set of reversible peaks (Figure 2H).

It is noteworthy that the reversible process $4a/4a^+$ was not observed in Figure 2F, which is due to the instability of $4a^+$ in the presence of excess of highly reductive $3a$.²⁹

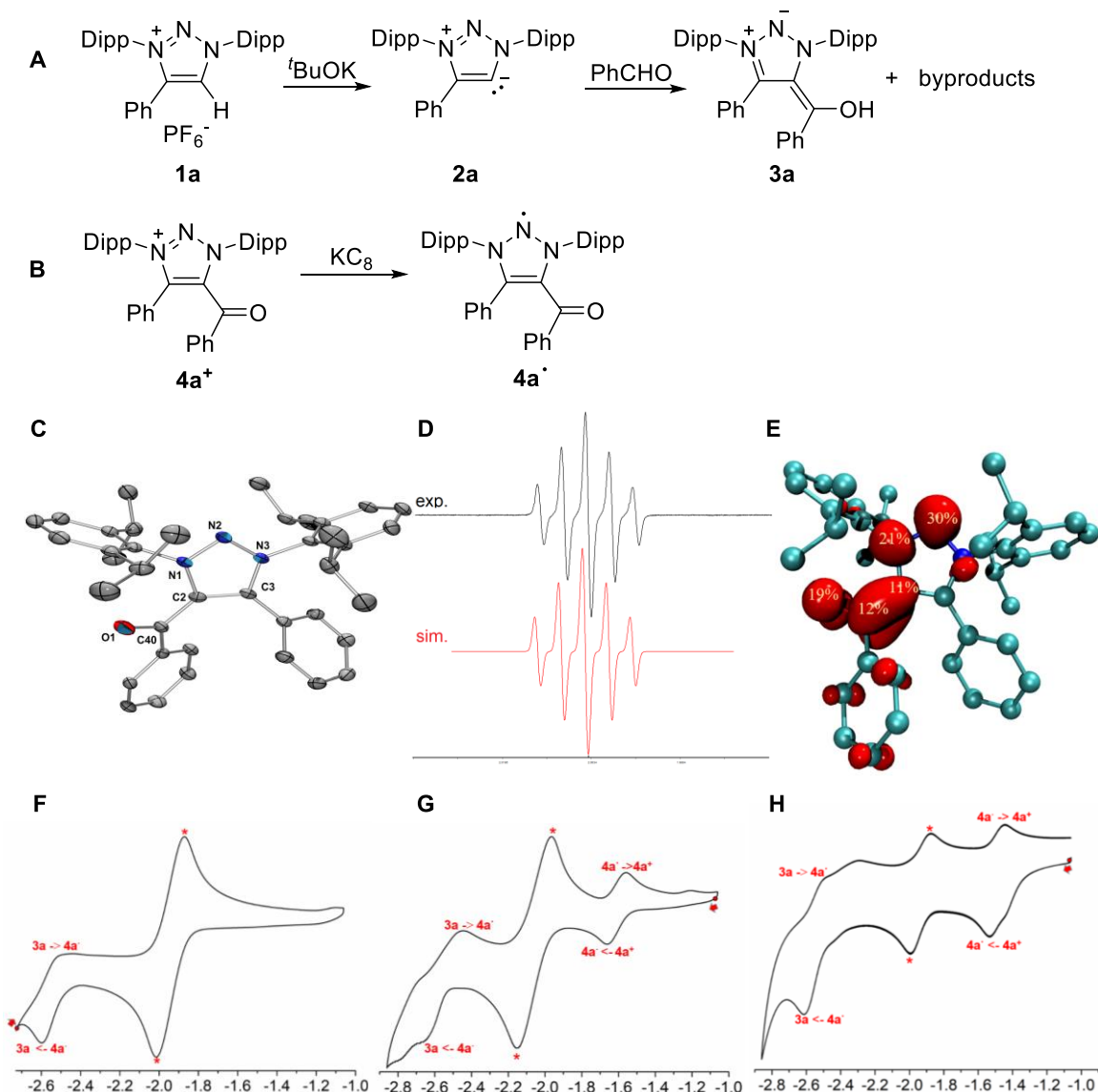
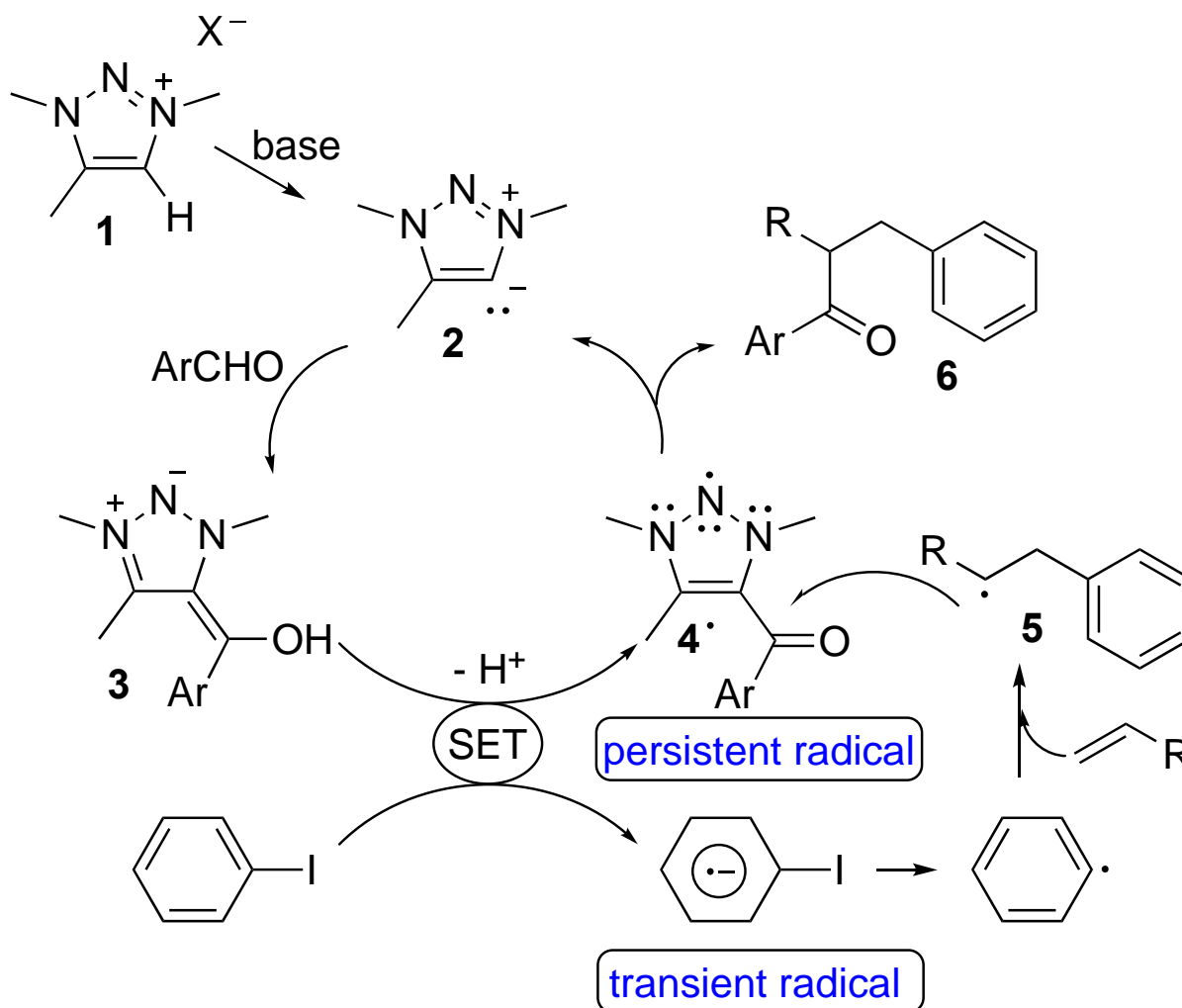


Figure 2.2: Synthesis and Characterization of $3a$ and $4a^{\bullet}$
 (A) Synthesis of $3a$. (B) Synthesis of $4a^{\bullet}$. (C) Solid-state structure of $4a^{\bullet}$. (D) EPR of $4a^{\bullet}$, top (experimental) and bottom (simulated). (E) Electron spin density of $4a^{\bullet}$. (F) Cyclic voltammograms of $3a$ in THF (+ $(nBu)_4NPF_6$ 0.1 mol/L). (G) Cyclic voltammograms of $4a^{\bullet}$ in THF (+ $(nBu)_4NPF_6$ 0.1 mol/L). (H) Cyclic voltammograms of $4a^+$ in THF (+ $(nBu)_4NPF_6$ 0.1 mol/L). *refer to the redox of in situ generated impurity $1a$. (Scan rate: 100 mV/s; E vs Fc/Fc^+).

From these results it can be concluded that **3a** is the most reductive Breslow intermediate known so far and is among the most potent organic reducing agents (in the ground state).⁴² Thus, we hypothesized that this type of BI derived from MICs should be able to reduce haloarenes under mild conditions. To prove it, a catalytic radical reaction was designed, namely the three-component arylacylation of alkenes with a MIC as catalyst (Figure 3). MICs **2**, generated in-situ by deprotonation of triazoliums**1**, should react with an aldehyde to give the BIMIC **3**, which should be deprotonated to its enolate form, and then undergo a SET process with an aryl iodide, giving a persistent radical **4** and a transient aryl radical.⁴³ The latter should add to the alkene to yield a very reactive alkyl radical **5**, which could attack **4**, regenerating the MIC catalyst, and affording the arylacylated alkene **6**.



Scheme 2.1: Proposed Reaction Pathway for the MIC-Catalyzed Arylacylation of Alkenes

To check this hypothesis, a mixture of 4-methoxybenzaldehyde **7a**, iodobenzene **8a**, and styrene **9a** was treated in $t\text{BuOMe}$ with a catalytic amount of different triazolium salts (**1a-1g**) in the presence of $t\text{BuOK}$ as a base (Figure 4, entries 1-7). When triazolium salt **1a** was used, the arylacylation product **6aaa** was formed in 13% yield. 4-Unsubstituted triazolium salts **1b** and **1c** gave better yields (41% and 51%, respectively). Low yields were observed for 4-substituted triazolium **1d** and **1e**. Surprisingly, 4-ester substituted triazolium with Dipp substituents (**1f**) gave an 85% yield while the Mes analogue **1g** only afford a rather low yield. Solvent screening showed $t\text{BuOMe}$ to be the best choice (entries 8-11). Using $t\text{BuONa}$ instead of $t\text{BuOK}$ led to much lower yields (entry 12). Temperature variation also lowered the yields (entries 13 and 14).

Importantly, other types of NHC precursors, such as imidazolium**1h**, thiazolium**1i**, 1,2,4-triazolium **1j**, were ineffective for this reaction (entries 15-17). The control experiment performed in the presence of *t*BuOK, but in the absence of the MIC catalyst **1f**, was also carried out, and no reaction was observed (entry 18). This result ruled out the hypothesis that *t*BuOK acted as a catalyst or radical initiator in this reaction.^{44,45} In addition, the reaction was not influenced by light. Either in the presence of light (day light, blue light, green light), or in the absence of light, similar yields were obtained.

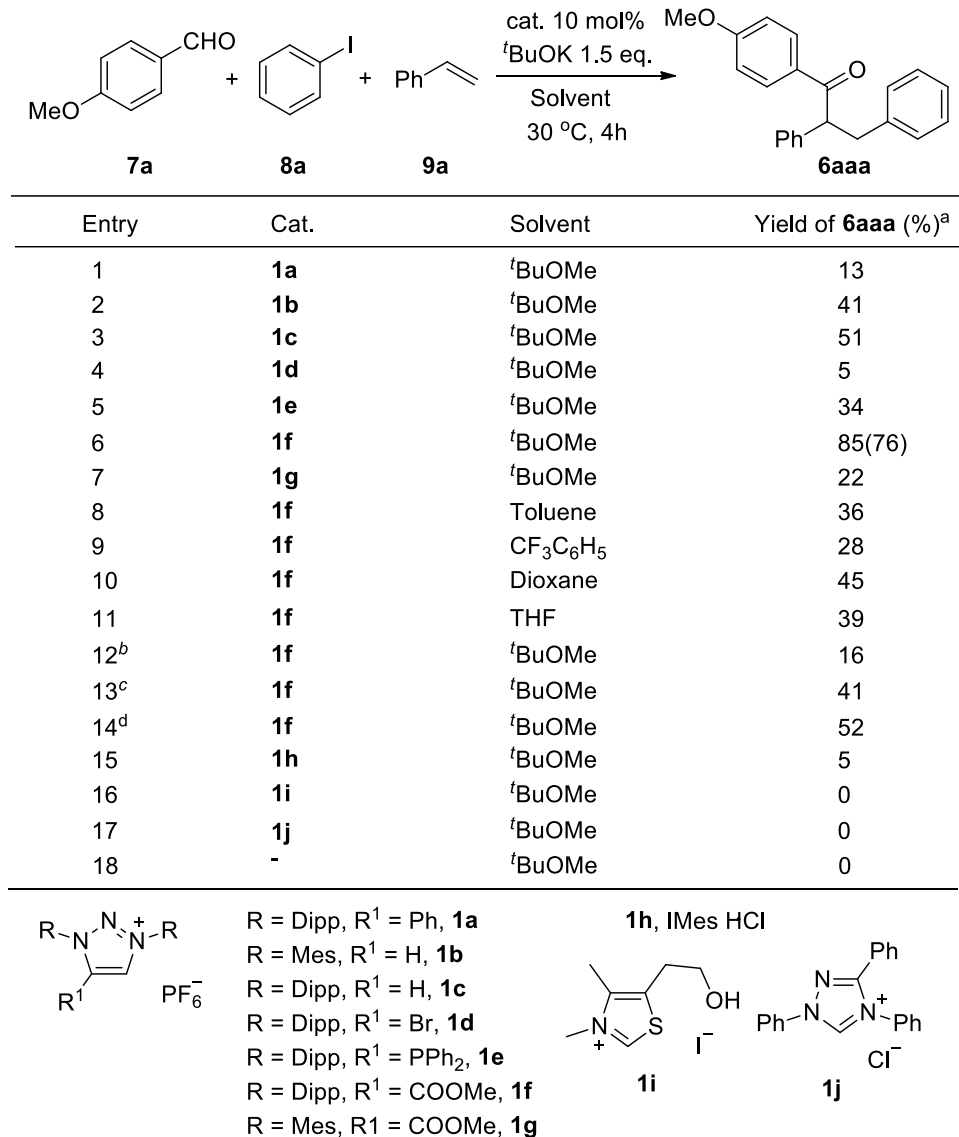


Figure 2.3: Optimization of the MIC-Catalyzed Arylacylation

Mes, 2,4,6-trimethylphenyl; Dipp, 2,6-diisopropylphenyl; IMes, 1,3-bis(2,4,6-trimethylphenyl)imidazolynilidene. Reaction conditions: **7** (0.9 mmol), **8** (0.9 mmol), **9** (0.5 mmol), **1** (0.05 mmol), base (0.75 mmol), and anhydrous *t*BuOMe (1.5 mL) for 4 h at 30 °C. The reactions were carried out in a 25 mL Schlenk tube.

^aNMR yields, isolated yields are given in parentheses.

^b*t*BuONa instead of *t*BuOK.

^cThe mixture was stirred at 0 °C.

^dThe mixture was stirred at 50 °C.

The scope of the MIC-catalyzed three-component arylacylation reaction was investigated under the optimized conditions as shown in Figure 5. Aromatic aldehydes with electron-donating

groups afforded the arylacylation products in high yields (**6aaa–6daa**), while an electron-deficient aromatic aldehyde led to a lower yield (**6eaa**). *Meta*- and *ortho*-substituted aldehydes afforded the corresponding products in 51% and 42% yield, respectively (**6faa** and **6gaa**), which shows that the steric hindrance has a significant influence on the reaction. Heterocyclic aryl aldehydes gave **6haa–6kaa** in 30%-61% yields. A variety of electron-donating and electron-withdrawing groups were tolerated on aryl iodides (**6aba–6aga**). 2-Iodonaphthalene afforded the desired product in 45% yield (**6aha**). For heteroaromatic iodides, such as N-methyl-5-iodoindole, 2-iodopyridine and 3-iodopyridine, the MIC-catalyzed reactions were accomplished in 43%-65% isolated yields (**6aia–6aka**). Substituted styrenes, such as 4-methoxystyrene, 4-methylstyrene, 3-methylstyrene, 4-bromostyrene and 2-vinylnaphthalene, were tolerated under the reaction conditions (**6aab–6aaf**). When using 1-phenyl-1,3-butadiene instead of styrene, both 1,2-addition and 1,4-addition products were formed in 2:1 ratio. Interestingly, when 2,3-dimethyl-1,3-butadiene was employed, only the 1,4-addition product was observed in high yield, while some base-induced isomerization occurred. In all cases, some amount of diarylethanes, benzyl alcohols and esters were formed as side-products. The former came from H-abstraction of **5**, while the latter resulted from reduction of aldehydes by BIMIC. Consequently, much lower yields were obtained with bulky substrates and easily reducible substrates; additionally, the process is not efficient with aliphatic aldehydes and alkenes.

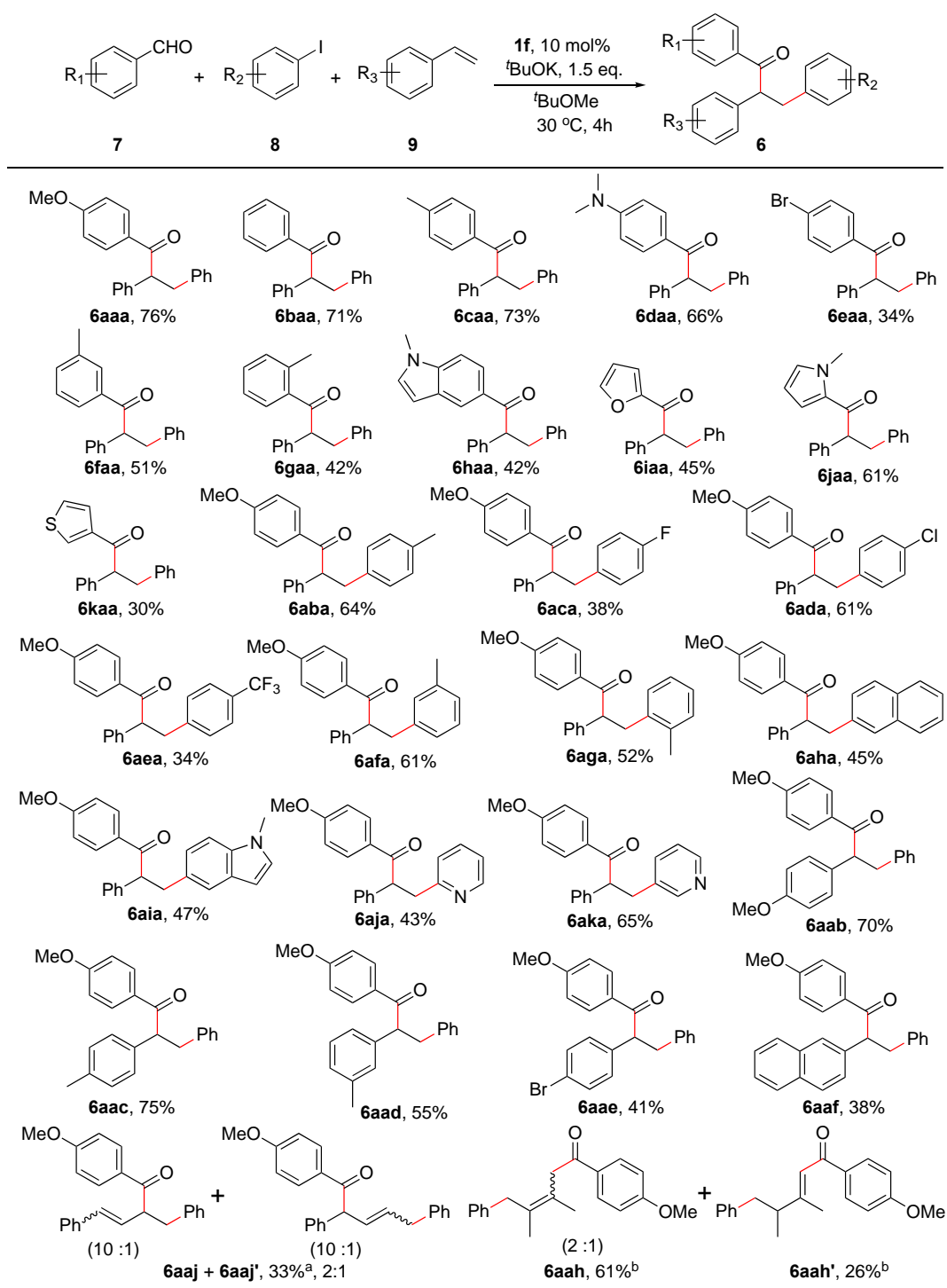


Figure 2.4: Substrate Scope of the MIC-catalyzed Arylacylation of Alkenes

Reaction conditions: aldehyde **7** (0.9 mmol), aryl iodide **8** (0.9 mmol), alkene **9** (0.5 mmol), **1f** (0.05 mmol) and ^tBuOK (0.75 mmol) in anhydrous ^tBuOMe (1.5 mL) at 30 °C for 4 h. Isolated yields are given based on alkenes.

^a4-phenyl-1,3-butadiene was employed, and the isomer ratio is given in parenthesis.

^b2,3-dimethyl-1,3-butadiene was employed, and the isomer ratio is given in parenthesis.

To further extend this reaction, compounds **10** featuring a tethered aryl iodide and an alkene were considered. In all cases, high yields were observed for the intramolecular arylacylation reaction (Figure 6). 1-Allyloxy-2-iodobenzene **10a** reacted with different aldehydes affording the corresponding products in 65%-84% isolated yields (**11aa-11ca** and **11ja**). Other substrates with different tether atoms and substituents were also compatible in the cyclization reaction. 1-(Methylallyloxy)-2-iodobenzene **10b** gave the **11ab** in 72% yield. Nitrogen-tethered aryl iodides and alkene moieties (**10c-10e**) afforded the products **11ac-11ae** in 65-76% yields. It is noteworthy that allenes can be employed in this reaction. 2-Iodophenyl allenyl ether gave benzofuran **11af** in 78% yield. 2-Iodophenyl homoallyl ether **10g** gave the six-membered chromane derivative **11ag** in 79% yield. This reaction can be further expanded to construct polycyclic compounds. The annulation of 2-iodophenyl-cyclohex-3-enyl ether led to tricyclic ketone **11ah** as a single diastereomer, the structure of which was further confirmed by X-ray diffraction analysis. The annulation of 2-iodobenzyl-cyclohex-3-enyl ether **10i** gave **11ai** in 61% yield as two diastereomers in a 1:1 ratio. Interestingly, the reaction of 2-iodophenyl-cyclohexen-1-ylmethyl ether **10j** gave spirocyclohexane **11aj** in 21% yield as a single diastereomer.

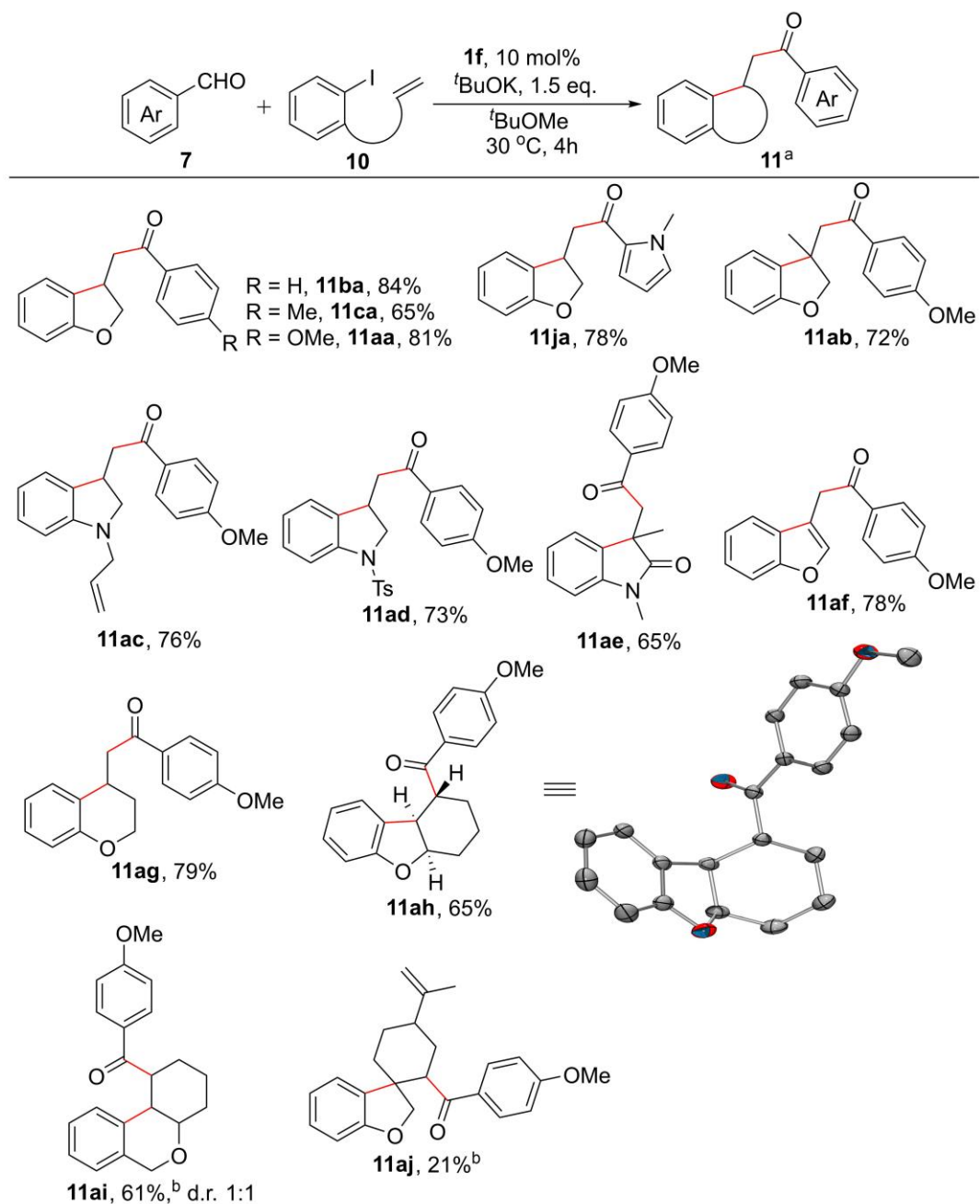
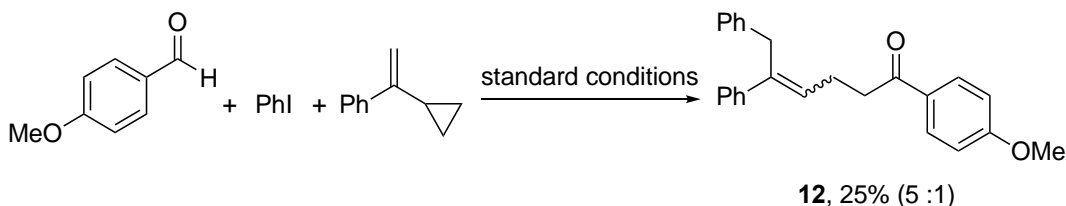


Figure 2.5: Substrate Scope of the MIC-Catalyzed Annulation and Cascade Acylation
 Reaction conditions: aldehyde **7** (0.9 mmol), *o*-iodophenyl alkene **10** (0.5 mmol), **1f** (0.05 mmol) and ^tBuOK (0.75 mmol) in anhydrous ^tBuOMe (1.5 mL) at 30 °C for 4h.

^aIsolated yields are given based on alkenes.

^bSingle isomer, the stereochemistry was not defined.

Lastly, a radical clock reaction was performed under the standard reaction conditions by using cyclopropylstyrene as the substrate. The reaction gave the cyclopropyl ring-opening adduct **12** in 25% yield, which confirmed the radical mechanism of the MIC-catalyzed arylacylation (Figure 7)



Scheme 2.2: Radical Clock Reaction

2.5: Conclusions

It was known that haloarenes could stoichiometrically be activated by super electron donors, but their functionalization was rarely reported under metal-free conditions.^{42,46,47} Intramolecular arylacylation reactions have only been achieved using Pd and Ni catalysts.⁴⁸⁻⁵¹ In this paper, we have shown that Breslow intermediates derived from mesoionic carbenes (BIMICs) are among the most potent organic reducing agents reported to date in the ground state (-2.49 V vs Fc/Fc⁺). This allows BIMICs to activate iodoarenes under mild conditions, and to promote the catalytic inter- and intra-molecular arylacylation of alkenes, which affords a number of substituted ketones and even polycyclic ketones. Importantly, triazolium salts of type **1**, as well as the ensuing MICs, are readily available in large quantities with a variety of N- and C-substituents allowing for a fine-tuning of their reduction potential and steric environment.^{34,35} The strong reduction potential of BIMICs should allow for the activation of more challenging bonds than classical NHCs such as thiazolylienes, 1,2,4-triazolyliene and imidazol(in)ylidenes can do. Other types of mesoionic carbenes are either already known, such as the so-called

abnormal NHCs,^{52,53} or can certainly be prepared, and thus are interesting targets for SET processes.

2.6: Acknowledgements

This work is supported by the National Natural Science Foundation of China (21602249), the Fundamental Research Funds for the Central Universities and the Research Funds of Renmin University of China (Program 20XNLG20), the U.S. Department of Energy, Office of Science, Basic Energy Sciences, Catalysis Science Program, under Award # DE-SC0009376, and the American Chemical Society Petroleum Research Fund (60776-ND1).

Chapter 2 is adapted, with slight modifications, from Liu, W.; Vianna, A.; Zhang, Z.; Huang, S.; Huang, L.; Melaimi, M.; Bertrand, G.; Yan, X. Mesoionic Carbene-Breslow Intermediates as Super Electron Donors: Application to the Metal-Free Arylacylation of Alkenes. *Chem Catalysis* **2021**, *1* (1), 196–206. The dissertation author was the second author of this paper.

2.7: References and Notes

- (1) Hopkinson, M. N.; Richter, C.; Schedler, M.; Glorius, F. An overview of N-heterocyclic carbenes. *Nature*. **2014**, *510*, 485–496.
- (2) Flanigan, D. M.; Romanov-Michailidis, F.; White, N. A.; Rovis, T. Organocatalytic Reactions Enabled by N-Heterocyclic Carbenes. *Chem. Rev.* **2015**, *115*, 9307–9387.
- (3) Wang, M. H.; Scheidt, K. A. Cooperative Catalysis and Activation with N-Heterocyclic Carbenes. *Angew. Chem. Int. Ed.* **2016**, *55*, 14912–14922.
- (4) Biju, A. T. N-Heterocyclic Carbenes in Organocatalysis. Wiley-VCH Verlag GmbH & Co. KGaA Weinheim, Germany. 2019.
- (5) Chen, X.-Y.; Gao, Z.-H.; Ye, S. Bifunctional N-Heterocyclic Carbenes Derived from L-Pyroglutamic Acid and Their Applications in Enantioselective Organocatalysis. *Acc. Chem. Res.* **2020**, *53*, 690–702.

- (6) Ghosh, A.; Biju, A. T. Revealing the Similarities of α,β -Unsaturated Iminiums and Acylazoliums in Organocatalysis. *Angew. Chem. Int. Ed.* **2021**. DOI: 10.1002/anie.202012581.
- (7) Bugaut, X.; Glorius, F. Organocatalytic Umpolung: N-Heterocyclic Carbenes and Beyond. *Chem. Soc. Rev.* **2012**, *41*, 3511–3522.
- (8) Breslow, R. On the Mechanism of Thiamine Action. IV. Evidence from Studies on Model Systems. *J. Am. Chem. Soc.* **1958**, *80*, 3719–3726.
- (9) Berkessel, A.; Elfert, S.; Yatham, V. R.; Neudörfl, J.-M.; Schlörer, N. E.; Teles, J.H. Umpolung by N-Heterocyclic Carbenes: Generation and Reactivity of the Elusive 2,2-Diamino Enols (Breslow Intermediates). *Angew. Chem. Int. Ed.* **2012**, *51*, 12370–12374.
- (10) Paul, M.; Neudörfl, J. M.; Berkessel, A. Breslow intermediates from a thiazolin-2-ylidene and fluorinated aldehydes: XRD and solution-phase NMR spectroscopic characterization. *Angew. Chem. Int. Ed.* **2019**, *58*, 10596–10600.
- (11) Berkessel, A.; Yatham, V. R.; Elfert, S.; Neudörfl, J.-M. Characterization of the Key Intermediates of Carbene-Catalyzed Umpolung by NMR Spectroscopy and X-Ray Diffraction: Breslow Intermediates, Homo-enolates, and Azolium Enolates. *Angew. Chem. Int. Ed.* **2013**, *52*, 11158–11162.
- (12) Paul, M.; Sudkaow, P.; Wessels, A.; Schlörer, N. E.; Neudörfl, J. M.; Berkessel, A. Breslow intermediates from aromatic N-heterocyclic carbenes (benzimidazo-2-ylidenes, thiazolin-2-ylidenes). *Angew. Chem. Int. Ed.* **2018**, *57*, 8310–8315.
- (13) Zhao, K.; Enders, D. Merging N-Heterocyclic Carbene Catalysis and Single Electron Transfer: A New Strategy for Asymmetric Transformations. *Angew. Chem. Int. Ed.* **2017**, *56*, 3754–3756.
- (14) Song, R.; Chi, Y. R. N-Heterocyclic Carbene Catalyzed Radical Coupling of Aldehydes with Redox-Active Esters. *Angew. Chem. Int. Ed.* **2019**, *58*, 8628–8630.
- (15) Ishii, T.; Nagao, K.; Ohmiya, H. Recent advances in N-heterocyclic carbene-based radical catalysis. *Chem. Sci.* **2020**, *11*, 5630–5636.
- (16) Guin, J.; De Sarkar, S.; Grimme, S.; Studer, A. Biomimetic Carbene-Catalyzed Oxidations of Aldehydes Using TEMPO. *Angew. Chem. Int. Ed.* **2008**, *47*, 8727–8730.
- (17) White, N. A.; Rovis, T. Enantioselective N-Heterocyclic Carbene-Catalyzed β -Hydroxylation of Enals Using Nitroarenes: An Atom Transfer Reaction That Proceeds via Single Electron Transfer. *J. Am. Chem. Soc.* **2014**, *136*, 14674–14677.

- (18) White, N. A.; Rovis, T. Oxidatively Initiated NHC-Catalyzed Enantioselective Synthesis of 3,4-Disubstituted Cyclopentanones from Enals. *J. Am. Chem. Soc.* **2015**, *137*, 10112–10115.
- (19) Zhang, Y.; Du, Y.; Huang, Z.; Xu, J.; Wu, X.; Wang, Y.; Wang, M.; Yang, S.; Webster, R. D.; Chi, Y. R. N-Heterocyclic Carbene-Catalyzed Radical Reactions for Highly Enantioselective β -Hydroxylation of Enals. *J. Am. Chem. Soc.* **2015**, *137*, 2416–2419.
- (20) Yang, W.; Hu, W.; Dong, X.; Li, X.; Sun, J. N-Heterocyclic Carbene Catalyzed γ -Dihalomethylenation of Enals by Single-Electron Transfer. *Angew. Chem. Int. Ed.* **2016**, *55*, 15783–15786.
- (21) Wu, X.; Zhang, Y.; Wang, Y.; Ke, J.; Jeret, M.; Reddi, R. N.; Yang, S.; Song, B.-A.; Chi, Y. R. Polyhalides as Efficient and Mild Oxidants for Oxidative Carbene Organocatalysis by Radical Processes. *Angew. Chem. Int. Ed.* **2017**, *56*, 2942–2946.
- (22) Ishii, T.; Kakeno, Y.; Nagao, K.; Ohmiya, H. N-Heterocyclic Carbene-Catalyzed Decarboxylative Alkylation of Aldehydes. *J. Am. Chem. Soc.* **2019**, *141*, 3854–3858.
- (23) Kakeno, Y.; Kusakabe, M.; Nagao, K.; Ohmiya, H. Direct Synthesis of Dialkyl Ketones from Aliphatic Aldehydes through Radical N-Heterocyclic Carbene Catalysis. *ACS Catal.* **2020**, *10*, 8524–8529.
- (24) Ishii, T.; Ota, K.; Nagao, K.; Ohmiya, H. N-Heterocyclic Carbene-Catalyzed Radical Relay Enabling Vicinal Alkylacylation of Alkenes. *J. Am. Chem. Soc.* **2019**, *141*, 14073–14077.
- (25) Li, J.-L.; Liu, Y.-Q.; Zou, W.-L.; Zeng, R.; Zhang, X.; Liu, Y.; Han, B.; Leng, H.-J.; Li, Q.-Z. Radical Acylfluoroalkylation of Olefins through N-Heterocyclic Carbene Organocatalysis. *Angew. Chem. Int. Ed.* **2020**, *59*, 1863–1870.
- (26) Dai, L.; Xia, Z.-H.; Gao, Y.-Y.; Gao, Z.-H.; Ye, S. Visible-Light-Driven N-Heterocyclic Carbene Catalyzed γ - and ϵ -Alkylation with Alkyl Radicals. *Angew. Chem. Int. Ed.* **2019**, *58*, 18124–18130.
- (27) Kim, I.; Im, H.; Lee, H.; Hong, S. N-Heterocyclic carbene-catalyzed deaminative cross-coupling of aldehydes with Katritzky pyridinium salts. *Chem. Sci.* **2020**, *11*, 3192–3197.
- (28) Nakanishi, I.; Itoh, S.; Suenobu, T.; Fukuzumi, S. Direct Observation of Radical Intermediates While Investigating the Redox Behavior of Thiamin Coenzyme Models. *Angew. Chem. Int. Ed.* **1998**, *37*, 992–994.
- (29) Regnier, V.; Romero, E. A.; Molton, F.; Jazzar, R.; Bertrand, G.; Martin, D. What Are the Radical Intermediates in Oxidative N-Heterocyclic Carbene Organocatalysis?. *J. Am. Chem. Soc.* **2019**, *141*, 1109–1117.

- (30) Nakanishi, I.; Itoh, S.; Fukuzumi, S. Electron-Transfer Properties of Active Aldehydes of Thiamin Coenzyme Models, and Mechanism of Formation of the Reactive Intermediates. *Chem. Eur. J.* **1999**, *5*, 2810–2818.
- (31) Liu, W.; Zhao, L.-L.; Melaimi, M.; Cao, L.; Xu, X.; Bouffard, J.; Bertrand, G.; Yan, X. Mesoionic Carbene (MIC)-Catalyzed H/D Exchange at Formyl Groups. *Chem.* **2019**, 2484–2494.
- (32) Broggi, J.; Terme, T.; Vanelle, P. Organic Electron Donors as Powerful Single-Electron Reducing Agents in Organic Synthesis. *Angew. Chem. Int. Ed.* **2014**, *53*, 384–413.
- (33) Murphy, J. A. Discovery and Development of Organic Super-Electron-Donors. *J. Org. Chem.* **2014**, *79*, 3731–3746.
- (34) Guisado-Barrios, G.; Bouffard, J.; Donnadiou, B.; Bertrand, G. Crystalline 1*H*-1,2,3-Triazol-5-ylidenes: New Stable Mesoionic Carbenes (MICs). *Angew. Chem. Int. Ed.* **2010**, *49*, 4759–4762.
- (35) Guisado-Barrios, G.; Soleilhavoup, M.; Bertrand, G. 1*H*-1,2,3-Triazol-5-ylidenes: Readily Available Mesoionic Carbenes. *Acc. Chem. Res.* **2018**, *51*, 3236–3244.
- (36) Donnelly, K. F.; Petronilho, A.; Albrecht, M. Application of 1,2,3-triazolyliidenes as versatile NHC-type ligands: synthesis, properties, and application in catalysis and beyond. *Chem. Commun.* **2013**, *49*, 1145–1159.
- (37) Huang, D.; Zhao, P.; Astruc, D. Catalysis by 1,2,3-triazole- and related transition-metal complexes. *Coord. Chem. Rev.* **2014**, *272*, 145–165.
- (38) EC refers to an electron transfer step (E), immediately followed by a chemical reaction step (C). For more detail, see: Bard, A.J. & Faulkner, L.R. *Electrochemical methods: fundamentals and applications*, 2nd edition (Wiley). 2008
- (39) Mahoney, J. K.; Martin, D.; Moore, C. E.; Rheingold, A. L.; Bertrand, G. Bottleable (Amino)(Carboxy) Radicals Derived from Cyclic (Alkyl)(Amino) Carbenes. *J. Am. Chem. Soc.* **2013**, *135*, 18766–18769.
- (40) Mahoney, J. K.; Martin, D.; Thomas, F.; Moore, C. E.; Rheingold, A. L.; Bertrand, G. Air-Persistent Monomeric (Amino)(carboxy) Radicals Derived from Cyclic (Alkyl)(Amino) Carbenes. *J. Am. Chem. Soc.* **2015**, *137*, 7519–7525.
- (41) Deardorff, C. L.; Sikma, R. E.; Rhodes, C. P.; Hudnall, T. W. Carbene-derived α -acyl formamidiniumcations: organic molecules with readily tunable multiple redox processes. *Chem. Commun.* **2016**, *52*, 9024–9027.
- (42) Rohrbachm, S.; Shah, R. S.; Tuttle, T.; Murphy, J. A. Neutral Organic Super Electron Donors Made Catalytic. *Angew. Chem. Int. Ed.* **2019**, *58*, 11454–11458.

- (43) Leifert, D.; Studer, A. The Persistent Radical Effect in Organic Synthesis. *Angew. Chem. Int. Ed.* **2020**, *59*, 74–108.
- (44) Nocera, G.; Young, A.; Palumbo, F.; Emery, K. J.; Coulthard, G.; McGuire, T.; Tuttle, T.; Murphy, J. A. Electron Transfer Reactions: KOtBu (but not NaOtBu) Photoreduces Benzophenone under Activation by Visible Light. *J. Am. Chem. Soc.* **2018**, *140*, 9751–9757.
- (45) Nocera, G.; Murphy, J. A. Ground State Cross-Coupling of Haloarenes with Arenes Initiated by Organic Electron Donors, Formed in situ: An Overview. *Synthesis.* **2020**, *52*, 327–336.
- (46) Li, M.; Berritt, S.; Matuszewski, L.; Deng, G.; Pascual-Escudero, A.; Panetti, G. B.; Poznik, M.; Yang, X.; Chruma, J. J.; Walsh, P. Transition-Metal-Free Radical C(sp³)-C(sp²) and C(sp³)-C(sp³) Coupling Enabled by 2-Azaallyls as Super-Electron-Donors and Coupling-Partners. *J. Am. Chem. Soc.* **2017**, *139*, 16327–16333.
- (47) Zhang, L.; Jiao, L. Pyridine-Catalyzed Radical Borylation of Aryl Halides. *J. Am. Chem. Soc.* **2017**, *139*, 607–610.
- (48) Seashore-Ludlow, B.; Somfai, P. Domino Carbopalladation-Carbonylation: Generating Quaternary Stereocenters while Controlling β -Hydride Elimination. *Org. Lett.* **2010**, *12*, 3732–3735.
- (49) Xu, S.; Wang, K.; Kong, W. Ni-Catalyzed Reductive Arylacylation of Alkenes toward Carbonyl-Containing Oxindoles. *Org. Lett.* **2019**, *21*, 7498–7503.
- (50) Hu, H.; Teng, F.; Liu, J.; Hu, W.; Luo, S.; Zhu, Q. Enantioselective Synthesis of 2-Oxindole Spiro-fused Lactones and Lactams by Heck/Carbonylative Cyclization Sequences: Method Development and Applications. *Angew. Chem. Int. Ed.* **2019**, *58*, 9225–9229.
- (51) Yuan, Z.; Zeng, Y.; Feng, Z.; Guan, Z.; Lin, A.; Yao, H. Constructing chiral bicyclo[3.2.1]octanes via palladium-catalyzed asymmetric tandem Heck/carbonylation desymmetrization of cyclopentenes. *Nat. Commun.* **2020**, *11*, 2544–2552.
- (52) Aldeco-Perez, E.; Rosenthal, A. J.; Donnadiu, B.; Parameswaran, P.; Frenking, G.; Bertrand, G. Isolation of a C-5-Deprotonated Imidazolium, a Crystalline “Abnormal” N-Heterocyclic Carbene. *Science.* **2009**, *326*, 556–559.
- (53) Sau, S. C.; Hota, P. K.; Mandal, S. K.; Soleilhavoup, M.; Bertrand, G. Stable abnormal N-heterocyclic carbenes and their applications. *Chem. Soc. Rev.* **2020**, *49*, 1233–1252.

2.8: Supplemental Experimental Procedures

2.8.1: General Considerations

2.8.1.1: Synthetic Procedures

Unless stated otherwise, all manipulations were conducted in Schlenk tubes under Ar or N₂ atmosphere. All solvents were received from commercial sources without further purification, except for the preparation of radical **4a** for which the solvent was dried and degassed using standard procedures. Flash column chromatography was performed over silica gel 200-300 mesh. All chemical reagents and deuterated solvents were purchased from Alfa, Acros, Aldrich, or J&K and used without further purification, unless otherwise stated. All bases used were anhydrous. The following compounds were prepared according to published procedures: **1a-1c**, **1f** and **2a**,¹ **1d**,² **1e**,³ **1h**,⁴ **1i**,⁵ **1j**,⁶ **3a**,⁷ **8i**,⁸ **10a**,⁹ **10b**,¹⁰ **10c**,¹¹ **10d**,¹² **10e**,¹³ **10f**,¹⁴ **10g**,¹⁵ and **10h**¹⁶.

2.8.1.2: NMR Spectroscopy

¹H and ¹³C NMR spectra were recorded on Bruker 400 MHz and 600 MHz spectrometers. Proton and carbon chemical shifts are reported relative to the solvent used as an internal reference (CDCl₃: δ H = 7.26 ppm; δ C = 77.16 ppm). The peak patterns are indicated as follows: s, singlet; d, doublet; dd, doublet of doublet; t, triplet; m, multiplet; q, quartet. The coupling constants, *J*, are reported in Hertz (Hz).

2.8.1.3: Mass Spectrometry

High resolution mass spectra (HRMS) were recorded on an APEX II (Bruker Inc.) spectrometer with Electron Spray Ionization (ESI) resource. EPR spectra were recorded on a Bruker EMX spectrometer.

2.8.1.4: Electrochemical Analysis

Cyclic voltammetry of the compounds was carried out with Shanghai Zhenhua CHI 600D electrochemical workstation. Samples were measured under inert atmosphere in an Ar atmosphere glovebox at room temperature in dry THF solution containing tetrabutylammonium hexafluorophosphate (0.1 M). The measurement was operated with a three-electrode setup containing a glassy carbon as working electrode, a platinum wire as a counter electrode, and an organic silver electrode as reference electrode. Unless otherwise stated, all CVs were run at a scan rate of 100 mV/s. Potentials were measured in THF with respect to Fc/Fc⁺ ion pair (as external standard). Potentials vs SCE were calculated according to the reference²¹: E (vs SCE) = E (vs Fc/Fc⁺) + 0.56 V.

2.8.1.5: Computational Details

Computational studies were performed utilizing Gaussian 16²² (Reversion A.03) using density functional theory (DFT) with hybrid functional B3LYP²³. Geometry optimizations were carried out at B3LYP-D3(BJ)/6-311G**²⁴ level in the gas phase without symmetry constrains. Frequency calculations were run for all structures at the same level of theory to make sure that minimum (zero imaginary modes) was located and to reach zero-point energy (ZPE) correction and thermodynamic properties. Kohn–Sham orbitals were viewed and taken from Gaussview 6.0.16.²⁵ Spin population analysis of radical **4a**· was conducted with Multiwfn 3.8 (dev)²⁶ using

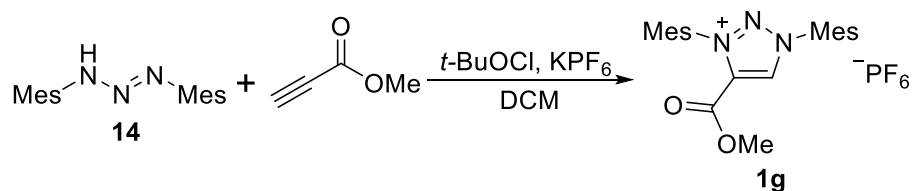
Becke atomic space and the visualization of spin density and SOMO were produced by VMD version 1.9.3.²⁷

2.8.1.6: Crystal Structure Determination

Data collections for X-ray diffraction experiments were performed on a 'Bruker APEX-II CCD' diffractometer, using graphite-monochromated Mo K α radiation ($\lambda = 0.71073 \text{ \AA}$). Using Olex2,¹⁷ the structures were solved with the ShelXT¹⁸ structure solution program using Intrinsic Phasing and refined with the ShelXL¹⁹ refinement package using Least Squares minimization. Refinement was performed on F^2 anisotropically for all the non-hydrogen atoms by the full-matrix least-squares method. The hydrogen atoms were placed at the calculated positions and were included in the structure calculation without further refinement of the parameters.

2.8.2: Synthetic Procedures for MIC-Catalyzed Arylacylation of Alkenes

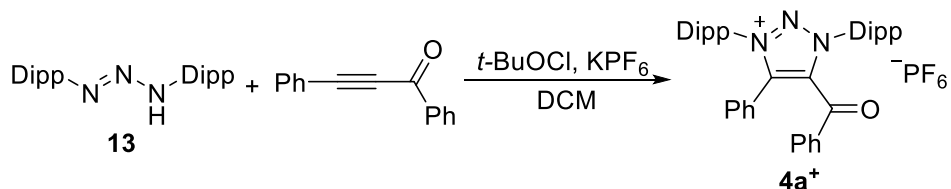
2.8.2.1: Preparation of Catalyst **1g**



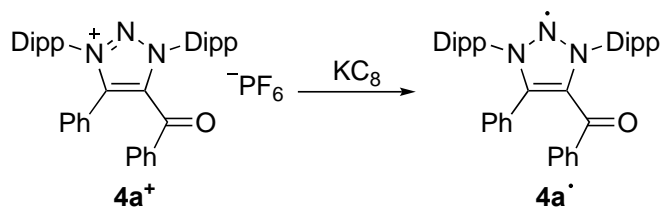
A mixture of triazene **14**¹ (2.8 g, 10.0 mmol) and anhydrous potassium hexafluorophosphate (2.2 g, 12.0 mmol) were mixed in a dry sealed tube. Under an argon atmosphere, dry dichloromethane (30 mL) was added at -78 °C. *tert*-Butyl hypochlorite (1.2 mL, 10.0 mmol) and methyl propiolate (0.9 mL, 10.0 mmol) was then added. The reaction was allowed to slowly warm to room temperature for 12 h. The mixture was then filtered, and the solid residue was washed with dichloromethane. The filtrate was collected and evaporated under reduced pressure. The crude solid was washed with diethyl ether and recrystallized by vapor diffusion of diethyl ether into dichloromethane solution of the crude triazolium salt. **1g** was obtained as a white solid (3.1 g, 61%). ¹H NMR (400 MHz, CDCl₃) δ 9.06 (s, 1H), 7.10 (s, 2H),

7.10 (s, 2H), 3.93 (s, 3H), 2.40 (s, 3H), 2.38 (s, 3H), 2.14 (s, 6H), 2.04 (s, 6H). ^{13}C NMR (100 MHz, CDCl_3) δ 154.0, 143.5, 143.1, 136.3, 135.0, 134.2, 134.1, 130.9, 130.5, 130.2, 129.9, 54.4, 21.3, 21.3, 17.1, 17.0. HRMS (ESI) m/z Calcd for $\text{C}_{22}\text{H}_{26}\text{N}_3\text{O}_2^+$ $[\text{M}]^+$ 364.2020, found 364.2015.

2.8.2.2: Preparation of 4a^+ and 4a^-

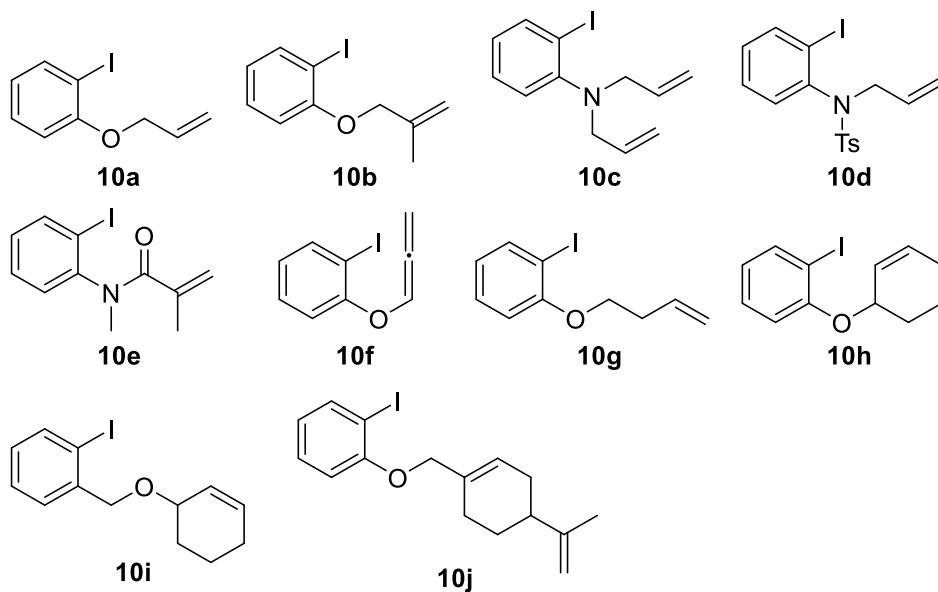


To a stirred suspension of triazene **13**²⁰ (3.3 g, 9.0 mmol) and anhydrous potassium hexafluorophosphate (2.0 g, 10.8 mmol) in dry dichloromethane (30 mL) at $-78\text{ }^\circ\text{C}$ was added *tert*-butyl hypochlorite (1.0 mL, 9.0 mmol) and diphenylpropynone (1.9 g, 9.0 mmol) under a N_2 atmosphere. The mixture was allowed to slowly warm to room temperature for 12 h. The mixture was then filtered, and the solid residue was washed with dichloromethane. The filtrate was collected, and evaporated under reduced pressure. The crude solid was washed with diethyl ether, and recrystallized by vapor diffusion of diethyl ether into dichloromethane solution of the crude triazolium salt. 4a^+ was obtained as a white solid (4.3 g, 67%). ^1H NMR (400 MHz, CDCl_3) δ 7.77 (d, $J = 7.3$ Hz, 2H), 7.64 (t, $J = 7.9$ Hz, 2H), 7.49 (t, $J = 7.4$ Hz, 1H), 7.44 – 7.31 (m, 7H), 7.24 (d, $J = 7.8$ Hz, 2H), 7.20 (d, $J = 7.3$ Hz, 2H), 2.45 (sept, $J = 6.5$ Hz, 4H), 1.24 (d, $J = 4.0$ Hz, 6H), 1.23 (d, $J = 3.9$ Hz, 6H), 1.20 (d, $J = 6.8$ Hz, 6H), 1.12 (d, $J = 6.7$ Hz, 6H). ^{13}C NMR (100 MHz, CDCl_3) δ 180.7, 145.9, 145.7, 145.2, 137.9, 136.5, 133.6, 133.3, 132.7, 132.4, 130.4, 130.0, 129.9, 129.7, 129.4, 128.7, 125.4, 124.9, 120.1, 30.0, 29.9, 25.7, 25.3, 22.9, 22.4. HRMS (ESI) m/z Calcd for $\text{C}_{39}\text{H}_{44}\text{N}_3\text{O}^+$ $[\text{M}]^+$ 570.3479, found 570.3473.

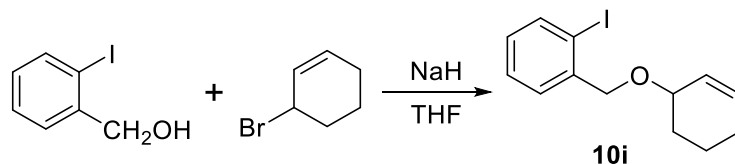


In a glovebox, a mixture of triazolium salt **4a⁺** (71.5 mg, 0.1 mmol), KC_8 (13.5 mg, 0.1 mmol) was placed in a Schlenk tube. THF (15 mL) was added and the mixture was stirred at r.t. for 2 h to afford a deep green mixture. Volatiles were removed in vacuo, and the residue was washed with toluene. The filtrate was collected and evaporated under reduced pressure to give **4a[·]** as a deep green solid (38.2 mg, 67%). The radical was characterized by EPR spectroscopy in benzene solution. An X-ray quality crystal of **4a[·]** was grown by chilling a saturated diethyl ether solution to $-40\text{ }^\circ\text{C}$ in a glovebox.

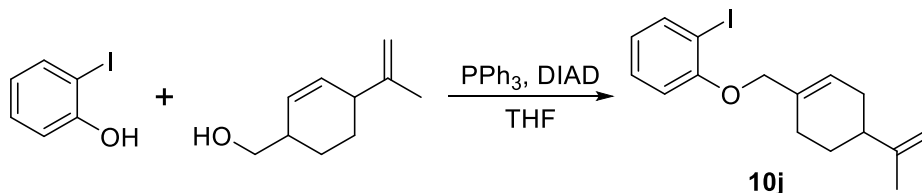
2.8.2.3: Detailed Structure of Substrates 10



2.8.2.4: Preparation of Substrates 10i and 10j



To a suspension of 2-iodobenzyl alcohol (1.12 g, 4.8 mmol) in dry THF (20 mL), sodium hydride (60% dispersion in mineral oil, 240 mg) was added at 0 °C. After stirring for 30 min, 3-bromocyclohexene (4.60 mL, 4 mmol) was added dropwise. The mixture was warmed to r.t. and then heated to 60 °C under nitrogen atmosphere for 8 h. The reaction mixture was filtered and washed with AcOEt, then concentrated in vacuo to remove volatiles. Further purification was performed by silica gel column chromatography: PE/AcOEt \rightarrow 300/1 to give **10i** as colorless liquid (817 mg, 65%). ^1H NMR (400 MHz, CDCl_3) δ 7.80 (dd, $J = 7.9, 0.9$ Hz, 1H), 7.49 (dd, $J = 7.6, 1.1$ Hz, 1H), 7.33 (td, $J = 7.6, 0.9$ Hz, 1H), 6.96 (td, $J = 7.6, 1.6$ Hz, 1H), 5.96 – 5.78 (m, 2H), 4.54 (q, $J = 12.8$ Hz, 2H), 4.15 – 3.97 (m, 1H), 2.14 – 2.03 (m, 1H), 2.02 – 1.76 (m, 4H), 1.64 – 1.53 (m, 1H). ^{13}C NMR (100 MHz, CDCl_3) δ 141.2, 139.1, 131.2, 129.0, 128.9, 128.2, 127.6, 97.8, 74.1, 73.0, 28.4, 25.3, 19.3. HRMS (ESI) m/z Calcd for $\text{C}_{13}\text{H}_{15}\text{IO}$ $[\text{M}+\text{Na}]^+$ 337.0060, found 337.0057.



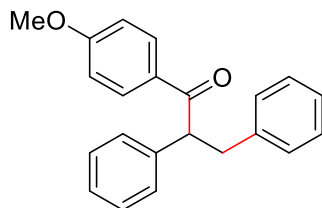
According to modified procedures of literature.²⁸ A reaction tube was charged with *o*-iodophenol (1.10 g, 5 mmol), perillyl alcohol (0.76 g, 5 mmol) and PPh_3 (1.70 g, 6.5 mmol). Then contents were then added THF (20 mL) under Ar atmosphere and stirred 30 min. DIAD (1.31 g, 6.5 mmol) was added dropwise at 0 °C and the mixture was warmed to 50 °C for 12 h.

The reaction was quenched with water (20 mL) and extracted with ethyl acetate. The organic layers were combined, dried over Na₂SO₄, filtered, and concentrated in vacuo. Further purification was performed by silica gel column chromatography: PE to give **10j** as a faint yellow liquid (1.52 g, 86%). ¹H NMR (400 MHz, CDCl₃) δ 7.77 (dd, *J* = 7.8, 1.6 Hz, 1H), 7.27 (td, *J* = 8.4, 1.5 Hz, 1H), 6.81 (dd, *J* = 8.2, 1.1 Hz, 1H), 6.70 (td, *J* = 7.6, 1.3 Hz, 1H), 5.94 – 5.84 (m, 1H), 4.74 (s, 2H), 4.44 (s, 2H), 2.32 – 2.14 (m, 4H), 2.09 – 1.95 (m, 1H), 1.94 – 1.96 (m, 1H), 1.76 (s, 3H), 1.61 – 1.48 (m, 1H). ¹³C NMR (100 MHz, CDCl₃) δ 157.5, 149.7, 139.4, 133.0, 129.4, 124.9, 122.5, 112.5, 108.8, 86.8, 73.2, 41.0, 30.5, 27.4, 26.3, 20.9. HRMS (ESI) *m/z* Calcd for C₁₆H₁₉IO [M+Na]⁺ 377.0373, found 377.0370.

2.8.2.5: General Procedure for Arylacylation of Alkenes

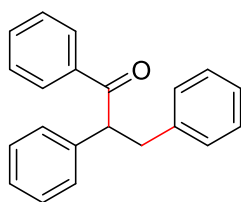
In glove box, a Schlenk tube was charged with aldehyde **7** (0.9 mmol), **1f** (29.7 mg, 0.05 mmol), *t*-BuOK (84.2 mg, 0.75 mmol) and anhydrous *t*-BuOMe (1.5 mL) under a N₂ atmosphere. When the mixture was stirred at 30 °C for 15 min, aryl iodide **8** (0.9 mmol) and alkene **9** (0.5 mmol) were added. The solution was reacted for 4 h. The reaction was then quenched with water (2 mL) and extracted with ethyl acetate. The organic layers were combined, dried over Na₂SO₄, and filtered. The volatiles were removed in vacuo and the crude product was purified by silica gel chromatography: PE/AcOEt → 3/1 to 200/1, unless otherwise stated.

Isolated yields were given based on alkene.

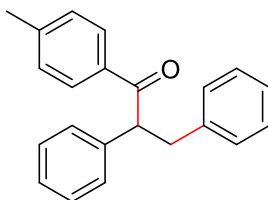


1-(4-Methoxyphenyl)-2,3-diphenylpropan-1-one (6aaa) was purified by column chromatography on silica gel (PE/AcOEt 100:1) as white solid (120.2 mg, 76% yield). ¹H NMR

(400 MHz, CDCl₃) δ 7.93 (d, $J = 9.0$ Hz, 2H), 7.27 (d, $J = 4.3$ Hz, 4H), 7.24 – 7.18 (m, 3H), 7.17 – 7.14 (m, 1H), 7.13 – 7.09 (m, 2H), 6.83 (d, $J = 9.0$ Hz, 2H), 4.80 (t, $J = 7.3$ Hz, 1H), 3.77 (s, 3H), 3.60 (dd, $J = 13.7, 7.5$ Hz, 1H), 3.09 (dd, $J = 13.7, 7.0$ Hz, 1H). ¹³C NMR (100 MHz, CDCl₃) δ 197.7, 163.3, 140.0, 139.6, 131.0, 129.7, 129.2, 128.9, 128.4, 128.3, 127.1, 126.1, 113.7, 55.6, 55.4, 40.2. HRMS (ESI) m/z Calcd for C₂₂H₂₀O₂ [M+Na]⁺ 339.1356, found 339.1354.

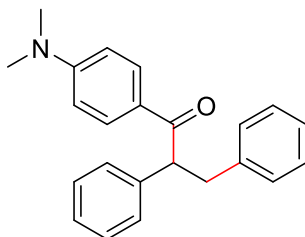


1,2,3-Triphenyl-1-propanone (6baa)²⁹ was purified by column chromatography on silica gel (PE/AcOEt 200:1) as white solid (101.6 mg, 71% yield). ¹H NMR (400 MHz, CDCl₃) δ 7.91 (d, $J = 7.2$ Hz, 2H), 7.47 – 7.42 (m, 1H), 7.34 (t, $J = 7.6$ Hz, 2H), 7.28 – 7.23 (m, 4H), 7.23 – 7.18 (m, 3H), 7.17 – 7.12 (m, 1H), 7.09 (d, $J = 6.8$ Hz, 2H), 4.82 (t, $J = 7.3$ Hz, 1H), 3.57 (dd, $J = 13.8, 7.6$ Hz, 1H), 3.07 (dd, $J = 13.7, 7.0$ Hz, 1H). ¹³C NMR (100 MHz, CDCl₃) δ 199.3, 139.8, 139.1, 136.8, 132.9, 129.2, 128.9, 128.7, 128.5, 128.3, 128.3, 127.2, 126.2, 55.9, 40.2. HRMS (ESI) m/z Calcd for C₂₁H₁₈O [M+Na]⁺ 309.1250, found 309.1247.\

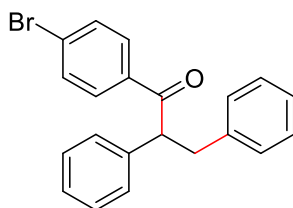


1-(4-Methylphenyl)-2,3-diphenyl-propan-1-one (6caa) was purified by column chromatography on silica gel (PE/AcOEt 200:1) as white solid (109.6 mg, 73% yield). ¹H NMR (400 MHz, CDCl₃) δ 7.83 (d, $J = 8.2$ Hz, 2H), 7.27 – 7.23 (m, 4H), 7.22 – 7.17 (m, 3H), 7.17 – 7.12 (m, 3H), 7.09 (d, $J = 7.0$ Hz, 2H), 4.81 (t, $J = 7.2$ Hz, 1H), 3.58 (dd, $J = 13.7, 7.5$ Hz, 1H),

3.07 (dd, $J = 13.7, 7.0$ Hz, 1H), 2.33 (s, 3H). ^{13}C NMR (100 MHz, CDCl_3) δ 198.8, 143.7, 139.9, 139.4, 134.2, 129.2, 129.2, 128.9, 128.9, 128.3, 128.2, 127.1, 126.1, 55.8, 40.1, 21.6. HRMS (ESI) m/z Calcd for $\text{C}_{22}\text{H}_{20}\text{O}$ $[\text{M}+\text{Na}]^+$ 323.1406, found 323.1404.



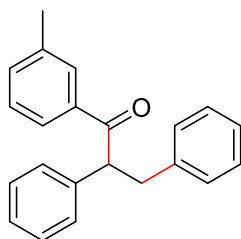
1-[4-(dimethylamino)phenyl]-2,3-diphenylpropan-1-one (6daa) was purified by column chromatography on silica gel (PE/AcOEt 30:1) as yellow solid (108.6 mg, 66% yield). ^1H NMR (400 MHz, CDCl_3) δ 7.87 (d, $J = 9.1$ Hz, 2H), 7.30 – 7.24 (m, 4H), 7.23 – 7.16 (m, 3H), 7.16 – 7.07 (m, 3H), 6.55 (d, $J = 9.1$ Hz, 2H), 4.77 (t, $J = 7.2$ Hz, 1H), 3.58 (dd, $J = 13.7, 7.5$ Hz, 1H), 3.06 (dd, $J = 13.7, 7.0$ Hz, 1H), 2.97 (s, 6H). ^{13}C NMR (100 MHz, CDCl_3) δ 197.0, 153.2, 140.4, 140.3, 130.9, 129.2, 128.7, 128.3, 128.2, 126.8, 125.9, 124.6, 110.6, 54.9, 40.2, 39.9. HRMS (ESI) m/z Calcd for $\text{C}_{23}\text{H}_{23}\text{NO}$ $[\text{M}+\text{H}]^+$ 330.1852, found 330.1848.



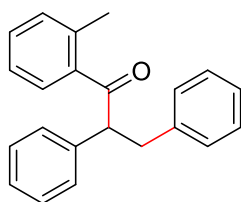
1-(4-Bromophenyl)-2,3-diphenylpropan-1-one (6eaa) was purified by column chromatography on silica gel (PE/AcOEt 200:1) as white solid (62.1 mg, 34% yield). ^1H NMR (400 MHz, CDCl_3) δ 7.74 (d, $J = 8.6$ Hz, 2H), 7.47 (d, $J = 8.6$ Hz, 2H), 7.27 – 7.23 (m, 2H), 7.22 – 7.16 (m, 5H), 7.16 – 7.11 (m, 1H), 7.06 (d, $J = 6.8$ Hz, 2H), 4.72 (t, $J = 7.2$ Hz, 1H), 3.55 (dd, $J = 13.7, 7.5$ Hz, 1H), 3.04 (dd, $J = 13.7, 7.0$ Hz, 1H). ^{13}C NMR (100 MHz, CDCl_3) δ 198.2,

139.6, 138.8, 135.4, 131.8, 130.2, 129.1, 129.0, 128.3, 128.2, 128.1, 127.3, 126.2, 56.1, 40.0.

HRMS (ESI) m/z Calcd for $C_{21}H_{17}BrO$ $[M+Na]^+$ 387.0355, found 387.0352.

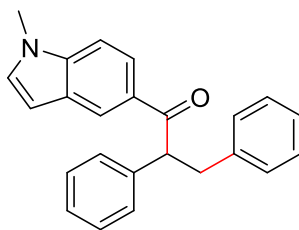


1-(3-Methylphenyl)-2,3-diphenylpropan-1-one (6faa) was purified by column chromatography on silica gel (PE/AcOEt 200:1) as colorless liquid (76.6 mg, 51% yield). 1H NMR (400 MHz, $CDCl_3$) δ 7.74 (s, 1H), 7.70 (d, $J = 7.4$ Hz, 1H), 7.30 – 7.25 (m, 6H), 7.23 – 7.18 (m, 3H), 7.16 (d, $J = 7.1$ Hz, 1H), 7.11 (d, $J = 7.3$ Hz, 2H), 4.83 (t, $J = 7.2$ Hz, 1H), 3.59 (dd, $J = 13.7, 7.6$ Hz, 1H), 3.08 (dd, $J = 13.7, 6.9$ Hz, 1H), 2.33 (s, 3H). ^{13}C NMR (100 MHz, $CDCl_3$) δ 199.5, 139.9, 139.2, 138.3, 136.8, 133.7, 129.2, 129.2, 128.9, 128.4, 128.3, 128.3, 127.1, 126.1, 125.9, 55.9, 40.2, 21.4. HRMS (ESI) m/z Calcd for $C_{22}H_{20}O$ $[M+Na]^+$ 323.1406, found 323.1406.

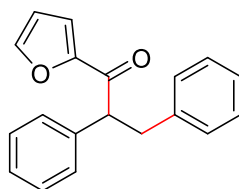


1-(2-Methylphenyl)-2,3-diphenylpropan-1-one (6gaa) was purified by column chromatography on silica gel (PE/AcOEt 200:1) as white solid (63.1 mg, 42% yield). 1H NMR (400 MHz, $CDCl_3$) δ 7.30 (d, $J = 7.7$ Hz, 1H), 7.27 – 7.20 (m, 8H), 7.15 (t, $J = 6.1$ Hz, 3H), 7.09 (t, $J = 7.4$ Hz, 2H), 4.65 (dd, $J = 8.5, 6.2$ Hz, 1H), 3.61 (dd, $J = 13.6, 8.5$ Hz, 1H), 3.05 (dd, $J = 13.6, 6.2$ Hz, 1H), 2.20 (s, 3H). ^{13}C NMR (100 MHz, $CDCl_3$) δ 203.5, 139.9, 138.9, 138.5, 137.9,

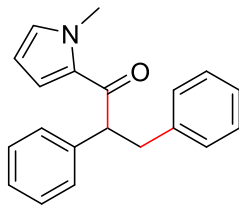
131.5, 130.8, 129.2, 128.8, 128.4, 128.3, 127.7, 127.2, 126.2, 125.4, 59.2, 39.7, 20.5. HRMS (ESI) m/z Calcd for $C_{22}H_{20}O$ $[M+Na]^+$ 323.1406, found 323.1404.



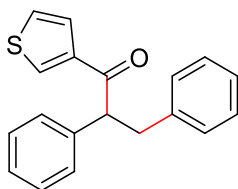
1-(1-methyl-1H-indol-5-yl)-2,3-diphenylpropan-1-one (6haa) was purified by column chromatography on silica gel (PE/AcOEt 20:1) as white solid (71.3 mg, 42% yield). 1H NMR (400 MHz, $CDCl_3$) δ 8.28 (s, 1H), 7.87 (dd, $J = 8.7, 1.4$ Hz, 1H), 7.31 (d, $J = 7.3$ Hz, 2H), 7.25 – 7.21 (m, 3H), 7.18 (t, $J = 5.8$ Hz, 3H), 7.13 (t, $J = 6.3$ Hz, 3H), 7.03 (d, $J = 3.1$ Hz, 1H), 6.52 (d, $J = 3.1$ Hz, 1H), 4.97 (t, $J = 7.2$ Hz, 1H), 3.72 (s, 3H), 3.63 (dd, $J = 13.7, 7.5$ Hz, 1H), 3.11 (dd, $J = 13.7, 7.0$ Hz, 1H). ^{13}C NMR (100 MHz, $CDCl_3$) δ 199.2, 140.2, 140.0, 139.0, 130.3, 129.2, 128.9, 128.8, 128.3, 128.2, 127.9, 126.9, 126.0, 123.5, 122.5, 109.1, 103.1, 55.5, 40.3, 33.0. HRMS (ESI) m/z Calcd for $C_{24}H_{21}NO$ $[M+Na]^+$ 362.1515, found 362.1508.



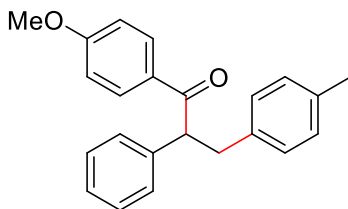
1-(2-furanyl)-2,3-diphenylpropan-1-one (6iaa) was purified by column chromatography on silica gel (PE/AcOEt 50:1) as yellow solid (62.2 mg, 45% yield). 1H NMR (400 MHz, $CDCl_3$) δ 7.48 (d, $J = 0.9$ Hz, 1H), 7.32 – 7.26 (m, 4H), 7.23 – 7.16 (m, 3H), 7.14 (d, $J = 7.0$ Hz, 1H), 7.10 (d, $J = 4.9$ Hz, 3H), 6.41 (dd, $J = 3.5, 1.6$ Hz, 1H), 4.63 (t, $J = 7.4$ Hz, 1H), 3.55 (dd, $J = 13.8, 8.0$ Hz, 1H), 3.05 (dd, $J = 13.7, 6.8$ Hz, 1H). ^{13}C NMR (100 MHz, $CDCl_3$) δ 188.2, 152.4, 146.4, 139.6, 138.8, 129.1, 128.8, 128.4, 128.3, 127.3, 126.2, 118.0, 112.2, 55.9, 39.1. HRMS (ESI) m/z Calcd for $C_{19}H_{16}O_2$ $[M+Na]^+$ 299.1043, found 299.1038.



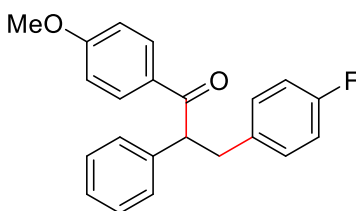
1-(1-methyl-1H-pyrrol-2-yl)-2,3-diphenylpropan-1-one (6jaa) was purified by column chromatography on silica gel (PE/AcOEt 100:1) as purple solid (88.3 mg, 61% yield). ^1H NMR (400 MHz, CDCl_3) δ 7.37 – 7.33 (m, 2H), 7.31 – 7.26 (m, 2H), 7.23 – 7.18 (m, 3H), 7.17 – 7.11 (m, 3H), 6.97 (dd, $J = 4.2, 1.6$ Hz, 1H), 6.72 (t, $J = 1.9$ Hz, 1H), 6.04 (dd, $J = 4.1, 2.5$ Hz, 1H), 4.62 (t, $J = 7.4$ Hz, 1H), 3.90 (s, 3H), 3.55 (dd, $J = 13.7, 7.8$ Hz, 1H), 3.08 (dd, $J = 13.7, 6.9$ Hz, 1H). ^{13}C NMR (100 MHz, CDCl_3) δ 190.0, 140.4, 140.1, 131.4, 130.6, 129.1, 128.7, 128.2, 128.1, 126.9, 126.1, 119.7, 108.0, 56.1, 39.7, 37.8. HRMS (ESI) m/z Calcd for $\text{C}_{20}\text{H}_{19}\text{NO}$ $[\text{M}+\text{H}]^+$ 290.1539, found 290.1536.



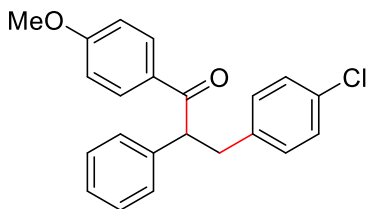
1-(3-thienyl)-2,3-diphenylpropan-1-one (6kaa) was purified by column chromatography on silica gel (PE/AcOEt 200:1) as white solid (43.9 mg, 30% yield). ^1H NMR (400 MHz, CDCl_3) δ 7.95 (dd, $J = 2.9, 1.2$ Hz, 1H), 7.47 (dd, $J = 5.1, 1.2$ Hz, 1H), 7.32 – 7.17 (m, 8H), 7.16 – 7.11 (m, 1H), 7.09 – 7.05 (m, 2H), 4.59 (t, $J = 7.3$ Hz, 1H), 3.55 (dd, $J = 13.7, 7.5$ Hz, 1H), 3.03 (dd, $J = 13.7, 7.1$ Hz, 1H). ^{13}C NMR (100 MHz, CDCl_3) δ 193.5, 141.9, 139.7, 139.2, 132.7, 129.1, 128.9, 128.3, 128.2, 127.4, 127.3, 126.2, 126.1, 57.8, 39.8. HRMS (ESI) m/z Calcd for $\text{C}_{19}\text{H}_{16}\text{OS}$ $[\text{M}+\text{Na}]^+$ 315.0814, found 315.0809.



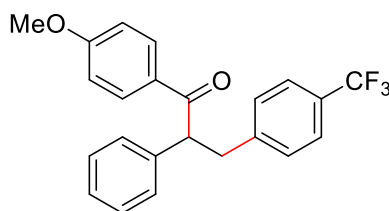
1-(4-methoxyphenyl)-2-phenyl-3-(p-tolyl)propan-1-one (6aba) was purified by column chromatography on silica gel (PE/AcOEt 100:1) as yellow liquid (105.7 mg, 64% yield). ^1H NMR (400 MHz, CDCl_3) δ 7.93 (d, $J = 8.9$ Hz, 2H), 7.28 (d, $J = 4.3$ Hz, 4H), 7.23 – 7.16 (m, 1H), 7.04 – 6.98 (m, 4H), 6.83 (d, $J = 8.9$ Hz, 2H), 4.79 (t, $J = 7.2$ Hz, 1H), 3.78 (s, 3H), 3.56 (dd, $J = 13.8, 7.6$ Hz, 1H), 3.04 (dd, $J = 13.8, 6.9$ Hz, 1H), 2.28 (s, 3H). ^{13}C NMR (100 MHz, CDCl_3) δ 197.8, 163.9, 139.7, 136.9, 135.5, 131.0, 129.8, 129.0, 128.9, 128.9, 128.3, 127.0, 113.7, 55.6, 55.4, 39.4, 21.1. HRMS (ESI) m/z Calcd for $\text{C}_{23}\text{H}_{22}\text{O}_2$ $[\text{M}+\text{Na}]^+$ 353.1512, found 353.1509.



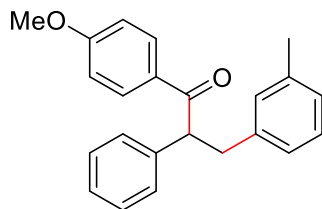
3-(4-fluorophenyl)-1-(4-methoxyphenyl)-2-phenylpropan-1-one (6aca) was purified by column chromatography on silica gel (PE/AcOEt 100:1) as yellow solid (63.5 mg, 38% yield). ^1H NMR (400 MHz, CDCl_3) δ 7.92 (d, $J = 8.9$ Hz, 2H), 7.29 – 7.22 (m, 4H), 7.22 – 7.16 (m, 1H), 7.06 – 7.01 (m, 2H), 6.88 (t, $J = 8.7$ Hz, 2H), 6.82 (d, $J = 9.0$ Hz, 2H), 4.74 (t, $J = 7.3$ Hz, 1H), 3.76 (s, 3H), 3.53 (dd, $J = 13.8, 7.5$ Hz, 1H), 3.05 (dd, $J = 13.8, 7.1$ Hz, 1H). ^{13}C NMR (100 MHz, CDCl_3) δ 197.6, 163.4, 161.4 (d, $J = 243.8$ Hz), 139.4, 135.6, 131.0, 130.6 (d, $J = 7.8$ Hz), 129.6, 129.0, 128.2, 127.2, 115.0 (d, $J = 21.1$ Hz), 113.7, 55.7, 55.4, 39.3. HRMS (ESI) m/z Calcd for $\text{C}_{22}\text{H}_{19}\text{FO}_2$ $[\text{M}+\text{H}]^+$ 335.1442, found 335.1443.



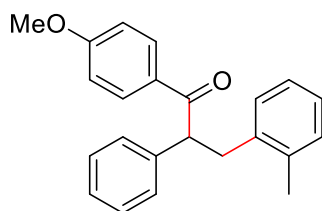
1-(4-methoxyphenyl)-3-(4-chlorophenyl)-2-phenylpropan-1-one (6ada) was purified by column chromatography on silica gel (PE/AcOEt 100:1) as white solid (107.0 mg, 61% yield). ^1H NMR (400 MHz, CDCl_3) δ 7.90 (d, $J = 8.9$ Hz, 2H), 7.29 – 7.18 (m, 5H), 7.15 (d, $J = 8.4$ Hz, 2H), 7.00 (d, $J = 8.4$ Hz, 2H), 6.82 (d, $J = 8.9$ Hz, 2H), 4.71 (t, $J = 7.3$ Hz, 1H), 3.78 (s, 3H), 3.51 (dd, $J = 13.7, 7.4$ Hz, 1H), 3.02 (dd, $J = 13.7, 7.1$ Hz, 1H). ^{13}C NMR (100 MHz, CDCl_3) δ 197.4, 163.4, 139.2, 138.4, 131.9, 131.0, 130.6, 129.5, 129.0, 128.3, 128.2, 127.2, 113.7, 55.5, 55.4, 39.5. HRMS (ESI) m/z Calcd for $\text{C}_{22}\text{H}_{19}\text{ClO}_2$ $[\text{M}+\text{H}]^+$ 351.1146, found 351.1145.



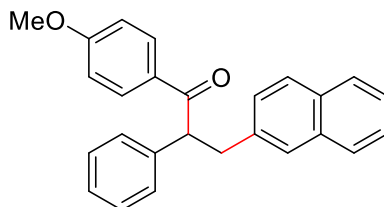
1-(4-methoxyphenyl)-2-phenyl-3-(4-(trifluoromethyl)phenyl)propan-1-one (6aea) was purified by column chromatography on silica gel (PE/AcOEt 100:1) as white solid (65.3 mg, 34% yield). ^1H NMR (400 MHz, CDCl_3) δ 7.91 (d, $J = 8.9$ Hz, 2H), 7.44 (d, $J = 8.2$ Hz, 2H), 7.31 – 7.17 (m, 7H), 6.82 (d, $J = 8.9$ Hz, 2H), 4.76 (t, $J = 7.3$ Hz, 1H), 3.78 (s, 3H), 3.60 (dd, $J = 13.8, 7.5$ Hz, 1H), 3.11 (dd, $J = 13.7, 7.0$ Hz, 1H). ^{13}C NMR (100 MHz, CDCl_3) δ 197.1, 163.4, 144.1, 139.1, 131.1, 129.5, 129.4, 129.0, 128.2, 128.2, 127.5 (q, $J = 271.8$ Hz), 127.3, 125.1 (q, $J = 3.6$ Hz), 113.8, 55.4, 55.3, 39.9. HRMS (ESI) m/z Calcd for $\text{C}_{23}\text{H}_{19}\text{F}_3\text{O}_2$ $[\text{M}+\text{H}]^+$ 385.1410, found 385.1408.



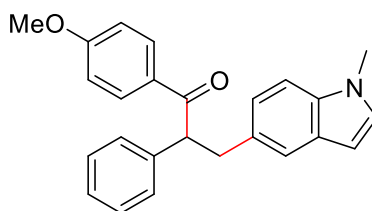
1-(4-methoxyphenyl)-2-phenyl-3-(*m*-tolyl)propan-1-one (6afa) was purified by column chromatography on silica gel (PE/AcOEt 100:1) as yellow liquid (100.8 mg, 61% yield). ^1H NMR (400 MHz, CDCl_3) δ 7.92 (d, $J = 8.9$ Hz, 2H), 7.30 – 7.24 (m, 4H), 7.23 – 7.16 (m, 1H), 7.09 (t, $J = 7.5$ Hz, 1H), 6.96 (d, $J = 7.6$ Hz, 1H), 6.93 – 6.87 (m, 2H), 6.83 (d, $J = 8.9$ Hz, 2H), 4.78 (t, $J = 7.2$ Hz, 1H), 3.78 (s, 3H), 3.55 (dd, $J = 13.7, 7.6$ Hz, 1H), 3.03 (dd, $J = 13.7, 6.8$ Hz, 1H), 2.27 (s, 3H). ^{13}C NMR (100 MHz, CDCl_3) δ 197.8, 163.3, 139.9, 139.7, 137.7, 131.0, 130.0, 129.8, 128.9, 128.3, 128.1, 127.0, 126.8, 126.1, 113.7, 55.5, 55.4, 40.1, 21.4. HRMS (ESI) m/z Calcd for $\text{C}_{23}\text{H}_{22}\text{O}_2$ $[\text{M}+\text{Na}]^+$ 353.1512, found 353.1510.



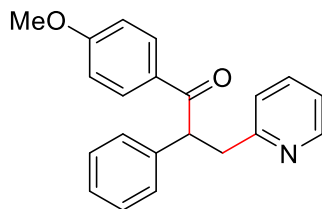
1-(4-methoxyphenyl)-2-phenyl-3-(*o*-tolyl)propan-1-one (6aga) was purified by column chromatography on silica gel (PE/AcOEt 100:1) as white solid (85.9 mg, 52% yield). ^1H NMR (400 MHz, CDCl_3) δ 7.93 (d, $J = 9.0$ Hz, 2H), 7.32 – 7.18 (m, 5H), 7.15 – 7.00 (m, 4H), 6.84 (d, $J = 9.0$ Hz, 2H), 4.81 (t, $J = 7.1$ Hz, 1H), 3.78 (s, 3H), 3.60 (dd, $J = 14.1, 7.2$ Hz, 1H), 3.10 (dd, $J = 14.1, 7.0$ Hz, 1H), 2.25 (s, 3H). ^{13}C NMR (100 MHz, CDCl_3) δ 197.8, 163.3, 139.8, 138.1, 136.4, 131.1, 130.2, 129.8, 129.7, 128.9, 128.2, 127.1, 126.3, 125.8, 113.7, 55.4, 54.20 (s), 37.2, 19.6. HRMS (ESI) m/z Calcd for $\text{C}_{23}\text{H}_{22}\text{O}_2$ $[\text{M}+\text{Na}]^+$ 353.1512, found 353.1512.



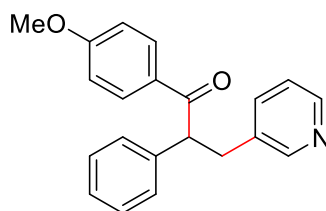
1-(4-methoxyphenyl)-3-(naphthalen-2-yl)-2-phenylpropan-1-one (6aha) was purified by column chromatography on silica gel (PE/AcOEt 100:1) as white solid (82.5 mg, 45% yield). ^1H NMR (400 MHz, CDCl_3) δ 7.93 (d, $J = 8.9$ Hz, 2H), 7.80 – 7.74 (m, 1H), 7.74 – 7.67 (m, 2H), 7.55 (s, 1H), 7.45 – 7.37 (m, 2H), 7.31 – 7.16 (m, 6H), 6.81 (d, $J = 9.0$ Hz, 2H), 4.89 (t, $J = 7.2$ Hz, 1H), 3.81 – 3.70 (m, 4H), 3.24 (dd, $J = 13.7, 7.0$ Hz, 1H). ^{13}C NMR (100 MHz, CDCl_3) δ 197.7, 163.3, 139.6, 137.6, 133.5, 132.1, 131.1, 129.7, 128.9, 128.2, 127.8, 127.7, 127.7, 127.6, 127.5, 127.1, 125.8, 125.3, 113.7, 55.6, 55.4, 40.3. HRMS (ESI) m/z . Calcd for $\text{C}_{26}\text{H}_{22}\text{O}_2$ $[\text{M}+\text{Na}]^+$ 389.1512, found 389.1507.



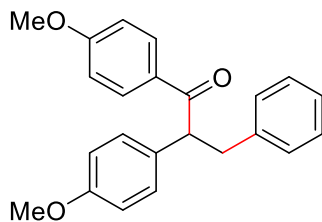
1-(4-methoxyphenyl)-3-(1-methyl-1H-indol-5-yl)-2-phenylpropan-1-one (6aia) was purified by column chromatography on silica gel (PE/AcOEt 20:1) as white solid (86.8 mg, 47% yield). ^1H NMR (400 MHz, CDCl_3) δ 7.91 (d, $J = 8.9$ Hz, 2H), 7.37 (s, 1H), 7.32 – 7.23 (m, 4H), 7.22 – 7.16 (m, 1H), 7.14 (d, $J = 8.4$ Hz, 1H), 6.99 – 6.94 (m, 2H), 6.80 (d, $J = 8.9$ Hz, 2H), 6.37 (d, $J = 2.7$ Hz, 1H), 4.85 (t, $J = 7.1$ Hz, 1H), 3.77 (s, 3H), 3.74 – 3.65 (m, 4H), 3.15 (dd, $J = 13.7, 6.7$ Hz, 1H). ^{13}C NMR (100 MHz, CDCl_3) δ 198.2, 163.2, 140.0, 135.5, 131.0, 130.8, 130.0, 128.8, 128.8, 128.5, 128.3, 126.9, 123.2, 121.0, 113.6, 108.8, 100.6, 56.3, 55.4, 40.3, 32.8. HRMS (ESI) m/z . Calcd for $\text{C}_{25}\text{H}_{23}\text{NO}_2$ $[\text{M}+\text{Na}]^+$ 392.1621, found 392.1615.



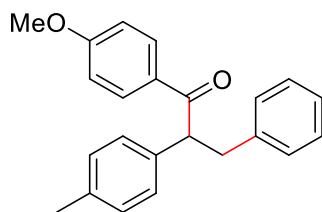
1-(4-methoxyphenyl)-2-phenyl-3-(pyridin-2-yl)propan-1-one (6aja) was purified by column chromatography on silica gel (PE/AcOEt 4:1) as yellow liquid (68.2 mg, 43% yield). ^1H NMR (400 MHz, CDCl_3) δ 8.47 (dd, $J = 5.1, 1.7$ Hz, 1H), 7.94 (d, $J = 9.0$ Hz, 2H), 7.44 (td, $J = 7.7, 1.8$ Hz, 1H), 7.31 – 7.26 (m, 2H), 7.25 – 7.20 (m, 2H), 7.17 – 7.12 (m, 1H), 7.04 – 6.99 (m, 2H), 6.80 (d, $J = 8.9$ Hz, 2H), 5.32 – 5.24 (m, 1H), 3.75 (s, 3H), 3.70 (dd, $J = 14.0, 8.4$ Hz, 1H), 3.19 (dd, $J = 14.0, 6.4$ Hz, 1H). ^{13}C NMR (100 MHz, CDCl_3) δ 197.8, 163.2, 159.6, 149.0, 139.6, 136.2, 131.1, 129.6, 128.9, 128.2, 127.0, 124.2, 121.2, 113.6, 55.4, 52.9, 42.3. HRMS (ESI) m/z Calcd for $\text{C}_{21}\text{H}_{19}\text{NO}_2$ $[\text{M}+\text{H}]^+$ 318.1489, found 318.1486.



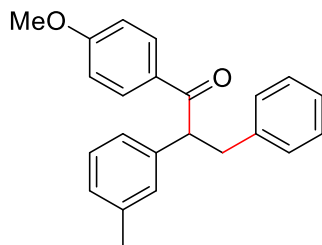
1-(4-methoxyphenyl)-2-phenyl-3-(pyridin-3-yl)propan-1-one (6aka) was purified by column chromatography on silica gel (PE/AcOEt 3:1) as white solid (103.2 mg, 65% yield). ^1H NMR (400 MHz, CDCl_3) δ 8.38 – 8.32 (m, 2H), 7.87 (d, $J = 9.0$ Hz, 2H), 7.31 (dt, $J = 7.8, 1.9$ Hz, 1H), 7.26 – 7.12 (m, 5H), 7.06 (dd, $J = 7.4, 4.8$ Hz, 1H), 6.79 (d, $J = 9.0$ Hz, 2H), 4.70 (t, $J = 7.3$ Hz, 1H), 3.74 (s, 3H), 3.49 (dd, $J = 13.9, 7.4$ Hz, 1H), 3.05 (dd, $J = 13.9, 7.3$ Hz, 1H). ^{13}C NMR (100 MHz, CDCl_3) δ 197.0, 163.4, 150.5, 147.6, 138.9, 136.8, 135.3, 131.0, 129.3, 129.1, 128.2, 127.4, 123.1, 113.7, 55.4, 55.3, 37.2. HRMS (ESI) m/z Calcd for $\text{C}_{21}\text{H}_{19}\text{NO}_2$ $[\text{M}+\text{H}]^+$ 318.1489, found 318.1488.



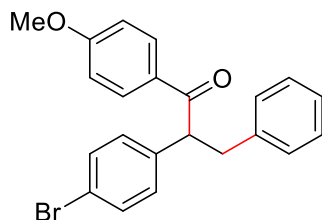
1,2-bis(4-methoxyphenyl)-3-phenylpropan-1-one (6aab)³⁰ was purified by column chromatography on silica gel (PE/AcOEt 30:1) as white solid (121.2 mg, 70% yield). ¹H NMR (400 MHz, CDCl₃) δ 7.92 (d, *J* = 9.0 Hz, 2H), 7.24 – 7.12 (m, 5H), 7.11 – 7.07 (m, 2H), 6.86 – 6.77 (m, 4H), 4.74 (t, *J* = 7.3 Hz, 1H), 3.78 (s, 3H), 3.74 (s, 3H), 3.54 (dd, *J* = 13.7, 7.3 Hz, 1H), 3.05 (dd, *J* = 13.7, 7.2 Hz, 1H). ¹³C NMR (100 MHz, CDCl₃) δ 198.0, 163.3, 158.6, 140.1, 131.6, 131.0, 129.7, 129.3, 129.2, 128.2, 126.1, 114.3, 113.7, 55.4, 55.2, 54.6, 40.2. HRMS (ESI) *m/z* Calcd for C₂₃H₂₂O₃ [M+Na]⁺ 369.1461, found 369.1457.



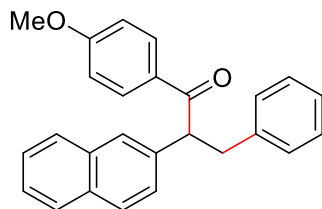
1-(4-methoxyphenyl)-2-(*p*-tolyl)-3-phenylpropan-1-one (6aac) was purified by column chromatography on silica gel (PE/AcOEt 100:1) as white solid (123.9 mg, 75% yield). ¹H NMR (400 MHz, CDCl₃) δ 7.92 (d, *J* = 8.9 Hz, 2H), 7.24 – 7.19 (m, 2H), 7.14 (dd, *J* = 11.9, 4.6 Hz, 4H), 7.09 (t, *J* = 7.5 Hz, 3H), 6.83 (d, *J* = 8.9 Hz, 2H), 4.77 (t, *J* = 7.2 Hz, 1H), 3.78 (s, 3H), 3.58 (dd, *J* = 13.7, 7.6 Hz, 1H), 3.06 (dd, *J* = 13.7, 6.9 Hz, 1H), 2.29 (s, 3H). ¹³C NMR (100 MHz, CDCl₃) δ 197.9, 163.3, 140.2, 136.7, 136.6, 131.0, 129.8, 129.6, 129.2, 128.2, 128.1, 126.1, 113.7, 55.4, 55.1, 40.2, 21.1. HRMS (ESI) *m/z* Calcd for C₂₃H₂₂O₂ [M+Na]⁺ 353.1512, found 353.1511.



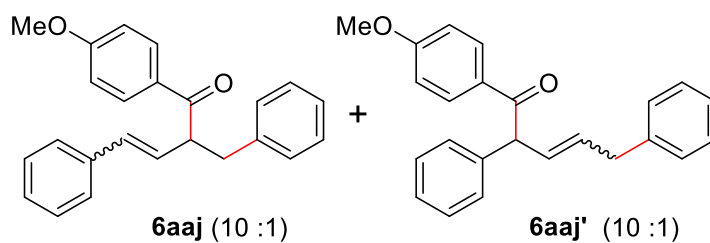
1-(4-methoxyphenyl)-2-(*m*-tolyl)-3-phenylpropan-1-one (6aad) was purified by column chromatography on silica gel (PE/AcOEt 100:1) as colorless liquid (90.9 mg, 55% yield). ^1H NMR (400 MHz, CDCl_3) δ 7.93 (d, $J = 8.9$ Hz, 2H), 7.24 – 7.18 (m, 2H), 7.17 – 7.12 (m, 3H), 7.10 (d, $J = 6.0$ Hz, 2H), 7.06 (d, $J = 7.7$ Hz, 1H), 7.02 (d, $J = 7.5$ Hz, 1H), 6.83 (d, $J = 8.9$ Hz, 2H), 4.77 (t, $J = 7.2$ Hz, 1H), 3.78 (s, 3H), 3.59 (dd, $J = 13.7, 7.9$ Hz, 1H), 3.05 (dd, $J = 13.7, 6.6$ Hz, 1H), 2.30 (s, 3H). ^{13}C NMR (100 MHz, CDCl_3) δ 197.8, 163.3, 140.2, 139.6, 138.5, 131.0, 129.8, 129.2, 128.7, 128.6, 128.2, 127.9, 126.1, 125.4, 113.7, 55.5, 55.4, 40.2, 21.5. HRMS (ESI) m/z Calcd for $\text{C}_{23}\text{H}_{22}\text{O}_2$ $[\text{M}+\text{Na}]^+$ 353.1512, found 353.1507.



1-(4-methoxyphenyl)-2-(4-bromophenyl)-3-phenylpropan-1-one (6aae) was purified by column chromatography on silica gel (PE/AcOEt 100:1) as white solid (81.0 mg, 41% yield). ^1H NMR (400 MHz, CDCl_3) δ 7.88 (d, $J = 9.0$ Hz, 2H), 7.37 (d, $J = 8.5$ Hz, 2H), 7.23 – 7.13 (m, 3H), 7.10 (d, $J = 8.4$ Hz, 2H), 7.06 (d, $J = 6.8$ Hz, 2H), 6.83 (d, $J = 9.0$ Hz, 2H), 4.73 (t, $J = 7.3$ Hz, 1H), 3.79 (s, 3H), 3.52 (dd, $J = 13.7, 7.0$ Hz, 1H), 3.03 (dd, $J = 13.7, 7.5$ Hz, 1H). ^{13}C NMR (100 MHz, CDCl_3) δ 197.3, 163.5, 139.5, 138.5, 132.0, 131.0, 130.0, 129.4, 129.1, 128.3, 126.3, 121.1, 113.8, 55.5, 54.8, 40.0. HRMS (ESI) m/z Calcd for $\text{C}_{22}\text{H}_{19}\text{BrO}_2$ $[\text{M}+\text{H}]^+$ 395.0641, found 395.0633.

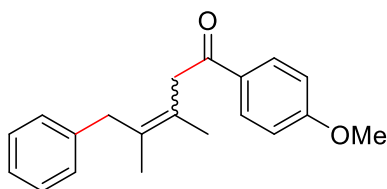


1-(4-methoxyphenyl)-2-(naphthalen-2-yl)-3-phenylpropan-1-one (6aaf) was purified by column chromatography on silica gel (PE/AcOEt 50:1) as white solid (69.6 mg, 38% yield). ^1H NMR (400 MHz, CDCl_3) δ 7.96 (d, $J = 9.0$ Hz, 2H), 7.77 (dt, $J = 6.4, 3.7$ Hz, 3H), 7.70 (s, 1H), 7.48 – 7.38 (m, 3H), 7.23 – 7.10 (m, 5H), 6.81 (d, $J = 9.0$ Hz, 2H), 4.96 (t, $J = 7.2$ Hz, 1H), 3.76 (s, 3H), 3.68 (dd, $J = 13.8, 7.4$ Hz, 1H), 3.17 (dd, $J = 13.8, 7.0$ Hz, 1H). ^{13}C NMR (100 MHz, CDCl_3) δ 197.7, 163.3, 140.0, 137.1, 133.6, 132.5, 131.1, 129.7, 129.2, 128.7, 128.3, 127.8, 127.7, 127.1, 126.4, 126.2, 126.1, 125.9, 113.7, 55.7, 55.4, 40.2. HRMS (ESI) m/z Calcd for $\text{C}_{26}\text{H}_{22}\text{O}_2$ $[\text{M}+\text{Na}]^+$ 389.1512, found 389.1506.

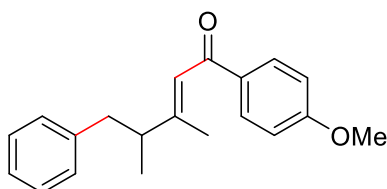


1-(4-methoxyphenyl)-2-benzyl-4-phenylbut-3-en-1-one (6aaj) and **1-(4-methoxyphenyl)-2,5-diphenylpent-3-en-1-one (6aaj')** were purified by column chromatography on silica gel (PE/AcOEt 100:1) as yellow solid (56.5 mg, 33% yield). Yield ratio of **6aaj** (E/Z isomer 10 : 1) and **6aaj'** (E/Z isomer 10 : 1) were 2:1. The following description mainly points out the spectral signals of *trans*-isomer **1a** and **2a**. ^1H NMR (400 MHz, CDCl_3) δ 8.00 – 7.93 (m, 1.88H), 7.56 (d, $J = 8.9$ Hz, 0.13H), 7.39 – 7.08 (m, 10H), 6.95 – 6.84 (m, 1.77H), 6.82 – 6.74 (m, 0.28H), 6.40 (d, $J = 16.0$ Hz, 1a PhCH), 6.32 (dd, $J = 16.0, 8.3$ Hz, 1a PhCHCH), 6.14 (dt, $J = 15.0, 6.7$ Hz, 2a PhCH₂CH), 5.69 (dd, $J = 15.2, 7.5$ Hz, 2a PhCH₂CHCH), 5.26 (d, $J = 8.0$ Hz,

2a PhCH₂CO), 4.45 (q, *J* = 7.2 Hz, 1a PhCH₂CO), 3.84 (s, 1.82H), 3.82 (s, 0.95H), 3.81 (s, 0.23H), 3.41 (d, *J* = 6.9 Hz, 2a PhCH₂), 3.35 (dd, *J* = 13.7, 7.0 Hz, 1a PhCH₂), 3.06 – 3.0 (dd, *J* = 13.7, 7.2 Hz, 1a PhCH₂). ¹³C NMR (100 MHz, CDCl₃) δ 198.7, 197.4, 163.5, 163.4, 140.2, 139.5, 139.4, 136.9, 132.9, 131.6, 131.2, 130.9, 130.7, 129.7, 129.7, 129.4, 129.3, 128.9, 128.6, 128.5, 128.4, 128.4, 128.3, 128.3, 128.1, 127.6, 127.5, 127.3, 127.0, 126.3, 126.2, 126.1, 113.8, 113.8, 113.6, 56.6, 55.5, 52.5, 39.0, 38.8. HRMS (ESI) *m/z* Calcd for C₂₄H₂₂O₂ [M+Na]⁺ 365.1512, found 365.1506.



1-(4-methoxyphenyl)-3,4-dimethyl-5-phenylpent-3-en-1-one (6aah) was purified by column chromatography on silica gel (PE/AcOEt 100:1) as colorless liquid (89.8 mg, 61% yield), E/Z isomer 2 : 1. ¹H NMR (600 MHz, CDCl₃) δ 8.05 – 7.98 (m, 2H), 7.35 – 7.28 (m, 2H), 7.28 – 7.20 (m, 3H), 7.00 – 6.92 (m, 2H), 3.91 – 3.89 (s, 3H), 3.89 – 3.82 (s, 2H), 3.56 – 3.47 (s, 2H), 1.88 – 1.84 (s, 3H), 1.75 – 1.69 (s, 3H). Major diastereoisomer: ¹³C NMR (150 MHz, CDCl₃) δ 197.1, 163.5, 140.2, 130.6, 130.4, 128.6, 128.5, 128.4, 125.9, 124.5, 113.8, 55.5, 44.5, 40.2, 19.5, 18.8. HRMS (ESI) *m/z* Calcd for C₂₀H₂₂O₂ [M+Na]⁺ 317.1512, found 317.1508.

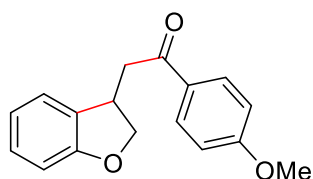


(E)-1-(4-methoxyphenyl)-3,4-dimethyl-5-phenylpent-2-en-1-one (6aah') were purified by column chromatography on silica gel (PE/AcOEt 80:1) as colorless liquid (38.3 mg, 26% yield). ¹H NMR (400 MHz, CDCl₃) δ 7.65 (d, *J* = 8.9 Hz, 2H), 7.29 (t, *J* = 7.3 Hz, 2H), 7.21 (t, *J*

= 7.3 Hz, 1H), 7.16 (t, $J = 7.9$ Hz, 2H), 6.85 (d, $J = 8.9$ Hz, 2H), 6.46 (s, 1H), 3.84 (s, 3H), 2.83 (dd, $J = 13.2, 7.5$ Hz, 1H), 2.73 – 2.58 (m, 2H), 2.10 (d, $J = 1.1$ Hz, 3H), 1.15 (d, $J = 6.7$ Hz, 3H). ^{13}C NMR (100 MHz, CDCl_3) δ 191.2, 163.0, 160.0, 140.3, 132.1, 130.5, 129.0, 128.4, 126.1, 121.4, 113.5, 55.4, 46.3, 41.5, 18.8, 16.5. HRMS (ESI) m/z Calcd for $\text{C}_{20}\text{H}_{22}\text{O}_2$ $[\text{M}+\text{Na}]^+$ 317.1512, found 317.1510.

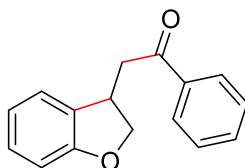
2.8.2.6: General Procedure for the MIC-Catalyzed Annulation and Cascade Acylation

In glove box, a Schlenk tube was charged with aldehyde **7** (0.9 mmol), **1f** (29.7 mg, 0.05 mmol), *t*-BuOK (84.2 mg, 0.75 mmol) and anhydrous *t*-BuOMe (1.5 mL) under a N_2 atmosphere. When the mixture was stirred at 30 °C for 15 min, *o*-iodophenyl alkene **10** (0.5 mmol) was added. The solution was reacted for 4 h. The reaction was then quenched with water (2 mL) and extracted with ethyl acetate. The organic layers were combined, dried over Na_2SO_4 , and filtered. The volatiles were removed in vacuo and the crude product was purified by silica gel chromatography: PE/AcOEt \rightarrow 4/1 to 100/1, unless otherwise stated. Isolated yields were given based on alkene.

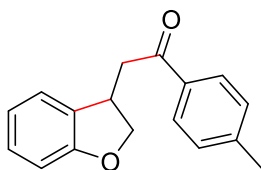


2-(2,3-dihydro-3-benzofuranyl)-1-(4-methoxyphenyl)-ethanone (11aa) was purified by column chromatography on silica gel (PE/AcOEt 50:1) as white solid (108.7 mg, 81% yield). ^1H NMR (400 MHz, CDCl_3) δ 7.94 (d, $J = 8.7$ Hz, 2H), 7.20 (d, $J = 7.3$ Hz, 1H), 7.14 (t, $J = 7.7$ Hz, 1H), 6.93 (d, $J = 8.7$ Hz, 2H), 6.87 (t, $J = 7.4$ Hz, 1H), 6.81 (d, $J = 8.0$ Hz, 1H), 4.87 (t, $J = 9.1$ Hz, 1H), 4.20 (dd, $J = 9.2, 6.3$ Hz, 1H), 4.12 – 3.99 (m, 1H), 3.86 (s, 3H), 3.47 (dd, $J = 17.9, 4.4$ Hz, 1H), 3.21 (dd, $J = 17.9, 9.6$ Hz, 1H). ^{13}C NMR (100 MHz, CDCl_3) δ 196.8, 163.8, 160.0,

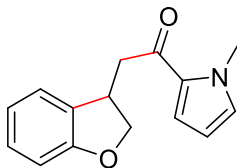
130.3, 129.9, 129.7, 128.5, 124.5, 120.5, 113.9, 109.7, 77.4, 55.5, 44.2, 37.5. HRMS (ESI) m/z Calcd for $C_{17}H_{16}O_3$ $[M+Na]^+$ 291.0992, found 291.0985.



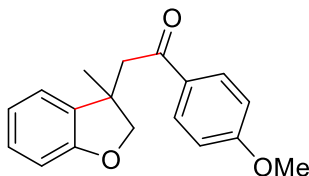
2-(2,3-dihydro-3-benzofuranyl)-1-phenylethanone (11ba)³¹ was purified by column chromatography on silica gel (PE/AcOEt 100:1) as white solid (100.1 mg, 84% yield). ¹H NMR (400 MHz, CDCl₃) δ 8.00 – 7.94 (m, 2H), 7.58 (t, $J = 7.4$ Hz, 1H), 7.47 (t, $J = 7.6$ Hz, 2H), 7.21 (d, $J = 7.4$ Hz, 1H), 7.16 (t, $J = 7.7$ Hz, 1H), 6.88 (t, $J = 7.4$ Hz, 1H), 6.82 (d, $J = 8.0$ Hz, 1H), 4.89 (t, $J = 9.1$ Hz, 1H), 4.21 (dd, $J = 9.2, 6.3$ Hz, 1H), 4.12 – 4.00 (m, 1H), 3.53 (dd, $J = 18.1, 4.5$ Hz, 1H), 3.27 (dd, $J = 18.1, 9.5$ Hz, 1H). ¹³C NMR (100 MHz, CDCl₃) δ 198.3, 160.0, 136.5, 133.5, 129.8, 128.8, 128.6, 128.1, 124.4, 120.5, 109.8, 77.3, 44.6, 37.4. HRMS (ESI) m/z Calcd for $C_{16}H_{14}O_2$ $[M+Na]^+$ 261.0886, found 261.0882.



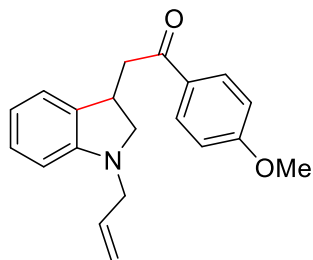
2-(2,3-dihydro-3-benzofuranyl)-1-(p-methylphenyl)-ethanone (11ca) was purified by column chromatography on silica gel (PE/AcOEt 100:1) as white solid (82.0 mg, 65% yield). ¹H NMR (400 MHz, CDCl₃) δ 7.86 (d, $J = 8.2$ Hz, 2H), 7.26 (d, $J = 8.0$ Hz, 2H), 7.20 (d, $J = 7.4$ Hz, 1H), 7.15 (t, $J = 7.7$ Hz, 1H), 6.87 (td, $J = 7.4, 0.8$ Hz, 1H), 6.82 (d, $J = 8.0$ Hz, 1H), 4.88 (t, $J = 9.1$ Hz, 1H), 4.20 (dd, $J = 9.2, 6.3$ Hz, 1H), 4.14 – 3.98 (m, 1H), 3.50 (dd, $J = 18.0, 4.5$ Hz, 1H), 3.24 (dd, $J = 18.0, 9.6$ Hz, 1H), 2.42 (s, 3H). ¹³C NMR (100 MHz, CDCl₃) δ 197.9, 160.0, 144.3, 134.1, 129.9, 129.4, 128.5, 128.2, 124.4, 120.5, 109.7, 77.4, 44.4, 37.5, 21.7. HRMS (ESI) m/z Calcd for $C_{17}H_{16}O_2$ $[M+Na]^+$ 275.1043, found 275.1036.



2-(2,3-dihydro-3-benzofuranyl)-1-(1-methyl-1H-pyrrol-2-yl)-ethanone (11ja) was purified by column chromatography on silica gel (PE/AcOEt 100:1) as yellow liquid (94.1 mg, 78% yield). ^1H NMR (400 MHz, CDCl_3) δ 7.19 (d, $J = 7.4$ Hz, 1H), 7.15 (t, $J = 7.7$ Hz, 1H), 6.94 (dd, $J = 4.1, 1.6$ Hz, 1H), 6.87 (t, $J = 7.4$ Hz, 1H), 6.82 (d, $J = 8.0$ Hz, 2H), 6.13 (dd, $J = 4.1, 2.5$ Hz, 1H), 4.83 (t, $J = 9.1$ Hz, 1H), 4.24 (dd, $J = 9.2, 6.4$ Hz, 1H), 4.08 – 3.99 (m, 1H), 3.97 (s, 3H), 3.34 (dd, $J = 16.9, 4.6$ Hz, 1H), 3.10 (dd, $J = 16.9, 9.8$ Hz, 1H). ^{13}C NMR (100 MHz, CDCl_3) δ 188.8, 159.9, 131.3, 130.5, 130.0, 128.5, 124.4, 120.5, 119.5, 109.7, 108.2, 77.3, 44.4, 37.8, 37.7. HRMS (ESI) m/z Calcd for $\text{C}_{15}\text{H}_{15}\text{NO}_2$ $[\text{M}+\text{Na}]^+$ 264.0995, found 264.0992.

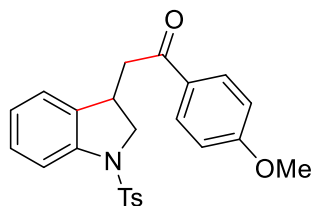


2-(2,3-dihydro-3-methyl-3-benzofuranyl)-1-(4-methoxyphenyl)-ethanone (11ab)³² was purified by column chromatography on silica gel (PE/AcOEt 100:1) as colorless liquid (101.6 mg, 72% yield). ^1H NMR (400 MHz, CDCl_3) δ 7.90 (d, $J = 8.9$ Hz, 2H), 7.19 – 7.10 (m, 2H), 6.93 – 6.86 (m, 3H), 6.82 (d, $J = 8.0$ Hz, 1H), 4.58 (d, $J = 9.3$ Hz, 1H), 4.53 (d, $J = 9.4$ Hz, 1H), 3.85 (s, 3H), 3.53 (d, $J = 17.2$ Hz, 1H), 3.17 (d, $J = 17.2$ Hz, 1H), 1.48 (s, 3H). ^{13}C NMR (100 MHz, CDCl_3) δ 196.6, 163.6, 159.1, 135.5, 130.4, 130.3, 128.4, 122.8, 120.5, 113.8, 109.9, 82.9, 55.5, 47.5, 43.9, 25.4. HRMS (ESI) m/z Calcd for $\text{C}_{18}\text{H}_{18}\text{O}_3$ $[\text{M}+\text{Na}]^+$ 305.1148, found 305.1144.



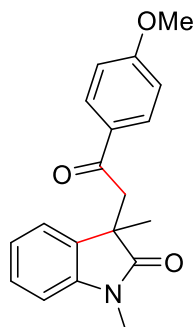
2-[2,3-dihydro-1-(2propen-1-yl)-1H-indol-3-yl]-1-(4-methoxyphenyl)-ethanone

(11ac)³² was purified by column chromatography on silica gel (PE/AcOEt 50:1) as white solid (116.8 mg, 76% yield). ¹H NMR (400 MHz, CDCl₃) δ 7.97 (d, *J* = 8.9 Hz, 2H), 7.11 (dt, *J* = 7.3, 3.7 Hz, 2H), 6.94 (d, *J* = 8.9 Hz, 2H), 6.69 (t, *J* = 7.3 Hz, 1H), 6.54 (d, *J* = 8.1 Hz, 1H), 5.98 – 5.83 (m, 1H), 5.28 (dd, *J* = 17.1, 1.5 Hz, 1H), 5.19 (dd, *J* = 10.2, 1.3 Hz, 1H), 3.93 – 3.81 (m, 4H), 3.74 – 3.66 (m, 3H), 3.40 (dd, *J* = 17.4, 4.7 Hz, 1H), 3.23 (dd, *J* = 17.4, 9.3 Hz, 1H), 3.06 (dd, *J* = 9.2, 6.3 Hz, 1H). ¹³C NMR (100 MHz, CDCl₃) δ 197.5, 163.6, 151.9, 134.0, 133.0, 130.4, 130.1, 127.9, 123.9, 117.7, 117.5, 113.8, 107.5, 59.5, 55.5, 51.7, 43.4, 36.3. HRMS (ESI) *m/z* Calcd for C₂₀H₂₁NO₂ [M+Na]⁺ 330.1465, found 330.1461.



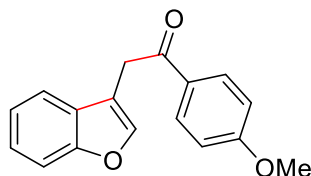
2-[2,3-dihydro-1-[(4-methylphenyl)sulfonyl]-1H-indol-3-yl]-1-(4-methoxyphenyl)-ethanone (11ad)³² was purified by column chromatography on silica gel (PE/AcOEt 7:1) as white solid (153.8 mg, 73% yield). ¹H NMR (400 MHz, CDCl₃) δ 7.77 (d, *J* = 8.9 Hz, 2H), 7.67 (d, *J* = 8.1 Hz, 1H), 7.63 (d, *J* = 8.2 Hz, 2H), 7.21 (t, *J* = 7.7 Hz, 1H), 7.15 (d, *J* = 8.1 Hz, 2H), 7.09 (d, *J* = 7.4 Hz, 1H), 6.98 (t, *J* = 7.4 Hz, 1H), 6.89 (d, *J* = 8.9 Hz, 2H), 4.17 (dd, *J* = 11.1, 8.8 Hz, 1H), 3.84 (s, 3H), 3.69 (sept, *J* = 4.6 Hz, 1H), 3.62 (dd, *J* = 11.1, 5.0 Hz, 1H), 3.09 (dd, *J* = 17.9, 4.4 Hz, 1H), 2.67 (dd, *J* = 17.9, 9.5 Hz, 1H), 2.32 (s, 3H). ¹³C NMR (100 MHz, CDCl₃) δ

196.2, 163.8, 144.1, 141.8, 134.9, 134.0, 130.3, 129.7, 129.5, 128.3, 127.3, 124.6, 124.0, 115.3, 113.8, 56.2, 55.6, 44.2, 35.7, 21.6. HRMS (ESI) m/z Calcd for $C_{24}H_{23}NO_4S$ $[M+Na]^+$ 444.1240, found 444.1233.

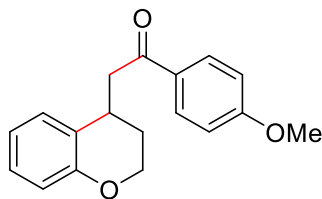


1,3-dihydro-3-[2-(4-methoxyphenyl)-2-oxoethyl]-1,3-dimethyl-2H-indol-2-one

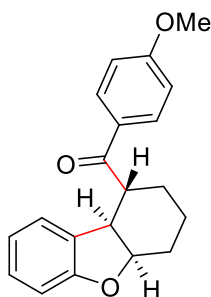
(11ae)³³ was purified by column chromatography on silica gel (PE/AcOEt 4:1) as yellow solid (100.6 mg, 65% yield). ¹H NMR (400 MHz, CDCl₃) δ 7.80 (d, *J* = 8.9 Hz, 2H), 7.21 (td, *J* = 7.7, 1.1 Hz, 1H), 7.12 (d, *J* = 7.3 Hz, 1H), 6.94 (td, *J* = 7.6, 0.8 Hz, 1H), 6.86 (d, *J* = 7.8 Hz, 1H), 6.83 (d, *J* = 8.9 Hz, 2H), 3.77 (s, 3H), 3.67 (d, *J* = 17.8 Hz, 1H), 3.57 (d, *J* = 17.7 Hz, 1H), 3.28 (s, 3H), 1.41 (s, 3H). ¹³C NMR (100 MHz, CDCl₃) δ 194.6, 180.7, 163.5, 143.9, 133.9, 130.3, 129.5, 127.8, 122.1, 121.8, 113.6, 108.1, 55.4, 45.7, 45.3, 26.5, 25.0. HRMS (ESI) *m/z* Calcd for C₁₉H₁₉NO₃ [M+Na]⁺ 332.1257, found 332.1249.



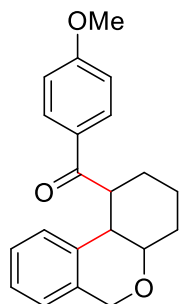
2-(3-benzofuranyl)-1-(4-methoxyphenyl)-ethanone (11af)³² was purified by column chromatography on silica gel (PE/AcOEt 50:1) as white solid (103.9 mg, 78% yield). ¹H NMR (600 MHz, CDCl₃) δ 8.07 (d, *J* = 8.1 Hz, 2H), 7.67 (s, 1H), 7.59 (d, *J* = 7.7 Hz, 1H), 7.51 (d, *J* = 8.1 Hz, 1H), 7.33 (t, *J* = 7.6 Hz, 1H), 7.28 (t, *J* = 7.4 Hz, 1H), 6.97 (d, *J* = 8.1 Hz, 2H), 4.32 (s, 2H), 3.88 (s, 3H). ¹³C NMR (150 MHz, CDCl₃) δ 194.9, 163.8, 155.2, 143.0, 130.8, 129.4, 128.0, 124.4, 122.6, 119.8, 114.0, 113.9, 111.5, 55.5, 33.5. HRMS (ESI) *m/z* Calcd for C₁₇H₁₄O₃ [M+Na]⁺ 289.0835, found 289.0830.



2-(3,4-dihydro-2H-1-benzopyran-4-yl)-1-(4-methoxyphenyl)ethanone (11ag) was purified by column chromatography on silica gel (PE/AcOEt 50:1) as yellow solid (111.5 mg, 79% yield). ^1H NMR (600 MHz, CDCl_3) δ 8.00 (d, $J = 8.2$ Hz, 2H), 7.18 (d, $J = 7.6$ Hz, 1H), 7.14 (t, $J = 7.7$ Hz, 1H), 6.98 (d, $J = 8.2$ Hz, 2H), 6.90 (t, $J = 7.4$ Hz, 1H), 6.86 (d, $J = 8.2$ Hz, 1H), 4.22 (t, $J = 4.9$ Hz, 2H), 3.90 (s, 3H), 3.70 – 3.61 (m, 1H), 3.38 (dd, $J = 16.9, 3.7$ Hz, 1H), 3.25 (dd, $J = 16.9, 9.7$ Hz, 1H), 2.29 – 2.18 (m, 1H), 1.89 – 1.82 (m, 1H). ^{13}C NMR (150 MHz, CDCl_3) δ 197.1, 163.7, 154.8, 130.4, 130.2, 128.9, 127.7, 125.6, 120.5, 117.1, 113.9, 63.5, 55.5, 45.2, 29.7, 27.7. HRMS (ESI) m/z Calcd for $\text{C}_{18}\text{H}_{18}\text{O}_3$ $[\text{M}+\text{Na}]^+$ 305.1148, found 305.1142.

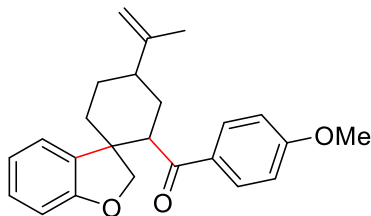


((1R,4aR,9bR)-1,2,3,4,4a,9b-hexahydrodibenzo[b,d]furan-1-yl)-(4-methoxyphenyl)methanone (11ah) was purified by column chromatography on silica gel (PE/AcOEt 100:1) as white solid (100.2 mg, 65% yield). ^1H NMR (400 MHz, CDCl_3) δ 7.78 (d, $J = 8.4$ Hz, 2H), 7.07 (t, $J = 7.4$ Hz, 1H), 6.93 (d, $J = 7.0$ Hz, 1H), 6.84 (t, $J = 9.7$ Hz, 3H), 6.68 (t, $J = 7.2$ Hz, 1H), 4.75 (s, 1H), 3.82 (s, 3H), 3.74 – 3.67 (m, 1H), 3.26 (t, $J = 9.4$ Hz, 1H), 2.33 (d, $J = 13.8$ Hz, 1H), 1.96 – 1.67 (m, 4H), 1.41 – 1.23 (m, 1H). ^{13}C NMR (100 MHz, CDCl_3) δ 200.8, 163.6, 159.1, 133.6, 130.7, 129.5, 128.1, 124.5, 120.7, 113.8, 110.0, 82.5, 55.5, 48.3, 41.5, 28.4, 27.3, 20.4. HRMS (ESI) m/z Calcd for $\text{C}_{20}\text{H}_{20}\text{O}_3$ $[\text{M}+\text{Na}]^+$ 331.1305, found 331.1302.



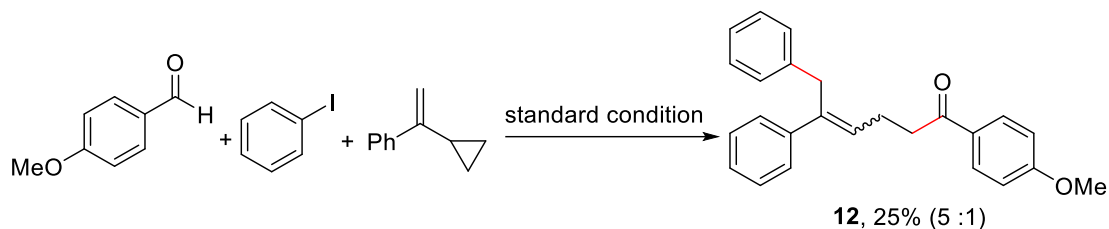
(2,3,4,4a,6,10b-hexahydro-1H-benzo[c]chromen-1-yl)(4-methoxyphenyl)methanone

(11ai) was purified by column chromatography on silica gel (PE/AcOEt 4:1) as colorless liquid (98.3 mg, 61% yield), d.r. 1:1. ^1H NMR (400 MHz, CDCl_3) δ 7.97 (d, $J = 8.8$ Hz, 1H), 7.95 (d, $J = 8.8$ Hz, 1H), 7.38 – 7.27 (m, 4H), 6.95 (d, $J = 8.9$ Hz, 1H), 6.94 (d, $J = 8.9$ Hz, 1H), 4.80 – 4.66 (m, 3H), 4.17 – 4.10 (m, 0.5H), 3.87 (s, 1.5H), 3.86 (s, 1.5H), 3.65 – 3.52 (m, 0.5H), 2.79 – 2.32 (m, 1H), 2.32 – 2.03 (m, 2H), 2.03 – 1.59 (m, 4H). ^{13}C NMR (100 MHz, CDCl_3) δ 201.0, 200.9, 163.4, 163.3, 156.7, 153.7, 137.5, 137.3, 130.8, 130.6, 129.2, 129.1, 128.4, 127.8, 127.7, 127.5, 113.8, 113.8, 94.0, 93.7, 68.8, 55.5, 42.7, 41.7, 30.4, 27.8, 26.4, 26.3, 23.2, 21.4. HRMS (ESI) m/z Calcd for $\text{C}_{21}\text{H}_{22}\text{O}_3$ $[\text{M}+\text{Na}]^+$ 345.1461, found 345.1456.



(4-methoxyphenyl)(4'-(prop-1-en-2-yl)-2H-spiro[benzofuran-3,1'-cyclohexan]-2'-yl)methanone (11aj) was purified by column chromatography on silica gel (PE/AcOEt 50:1) as colorless liquid (38.1 mg, 21% yield). ^1H NMR (400 MHz, CDCl_3) δ 7.82 (d, $J = 8.9$ Hz, 2H), 7.45 (d, $J = 7.4$ Hz, 1H), 7.19 – 7.09 (m, 1H), 6.89 – 6.81 (m, 3H), 6.78 (d, $J = 7.9$ Hz, 1H), 4.79 (d, $J = 8.1$ Hz, 2H), 4.42 (s, 2H), 3.95 (t, $J = 4.8$ Hz, 1H), 3.84 (s, 3H), 2.47 – 2.38 (m, 1H), 2.33 – 2.14 (m, 2H), 2.03 – 1.88 (m, 2H), 1.85 – 1.68 (m, 5H). ^{13}C NMR (100 MHz, CDCl_3) δ 201.3, 163.4, 159.8, 148.7, 134.8, 130.6, 129.5, 128.5, 124.7, 120.0, 113.8, 110.2, 109.6, 82.1, 55.5, 48.0, 47.2, 38.7, 33.9, 30.6, 26.4, 21.4. HRMS (ESI) m/z Calcd for $\text{C}_{24}\text{H}_{26}\text{O}_3$ $[\text{M}+\text{Na}]^+$ 385.1774, found 385.1764.

2.8.3: Radical Clock Reaction

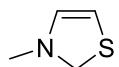


The reaction was conducted under the standard reaction condition. The mixture was purified by column chromatography on silica gel (PE/AcOEt 50:1) to give **12** as colorless liquid (44.6 mg, 25% yield), E/Z isomer 5 : 1. ^1H NMR (400 MHz, CDCl_3) δ 7.94 – 7.81 (m, 2H), 7.35 – 7.30 (m, 2H), 7.26 – 7.03 (m, 8H), 6.93 – 6.87 (m, 2H), 6.02 (t, $J = 7.3$ Hz, 0.8H), 5.54 (t, $J = 7.4$ Hz, 0.2H), 3.92 (s, 1.6H), 3.86 (d, $J = 3.7$ Hz, 3.24H), 3.77 (d, $J = 7.2$ Hz, 0.3H), 3.05 (t, $J = 7.4$ Hz, 1.67H), 2.90 (t, $J = 7.4$ Hz, 0.41H), 2.68 (q, $J = 7.4$ Hz, 1.64H), 2.38 (q, $J = 7.5$ Hz, 0.42H). Major isomer: ^{13}C NMR (100 MHz, CDCl_3) δ 198.1, 163.5, 142.8, 139.8, 138.6, 130.3,

130.0, 129.3, 129.1, 128.4, 128.2, 126.8, 126.3, 125.9, 113.8, 55.47 (s), 38.0, 35.8, 24.1. HRMS
(ESI) m/z Calcd for $C_{25}H_{24}O_2$ $[M+Na]^+$ 379.1669, found 379.1665.

2.8.4: DFT Calculations details of Breslow Intermediates and 4a

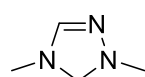
Cartesian Coordinates



Ph OH (see below Figure 2.10 A)

Sum of electronic and zero-point Energies=	-953.934379		
Sum of electronic and thermal Energies=	-953.921443		
Sum of electronic and thermal Enthalpies=	-953.920498		
Sum of electronic and thermal Free Energies=	-953.974527		
C	-0.681429000	-1.069655000	-0.117747000
S	-1.378271000	-0.100626000	-1.457101000
C	-2.325066000	-1.493639000	-1.994815000
C	-2.079226000	-2.568457000	-1.239395000
N	-1.171714000	-2.379531000	-0.204994000
C	-0.492728000	-3.521009000	0.402224000
C	0.095493000	-0.563833000	0.878515000
O	0.258910000	-1.350732000	2.023110000
C	0.654282000	0.782679000	0.942623000
C	1.034219000	1.510386000	-0.200356000
C	1.570314000	2.786842000	-0.089034000
C	1.761003000	3.371038000	1.162034000
C	1.408813000	2.656187000	2.304987000
C	0.864562000	1.382451000	2.200648000
H	-2.989618000	-1.411592000	-2.837417000

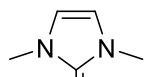
H	-2.515885000	-3.548461000	-1.361234000
H	-0.996795000	-4.428537000	0.071276000
H	0.553091000	-3.562101000	0.079230000
H	-0.519573000	-3.458236000	1.486160000
H	1.178615000	-1.271337000	2.302474000
H	0.940730000	1.061622000	-1.180383000
H	1.856444000	3.323099000	-0.986869000
H	2.181889000	4.366021000	1.244481000
H	1.548341000	3.097695000	3.285481000
H	0.566898000	0.848226000	3.094100000



Ph OH (see below Figure 2.10 B)

Sum of electronic and zero-point Energies=			-666.413522
Sum of electronic and thermal Energies=			-666.399658
Sum of electronic and thermal Enthalpies=			-666.398714
Sum of electronic and thermal Free Energies=			-666.453973
C	-0.579895000	-1.447150000	-0.040249000
N	-0.712930000	-0.944017000	-1.343976000
C	-1.385809000	-1.908958000	-2.069220000
N	-1.682330000	-2.951509000	-1.374828000
N	-1.146948000	-2.712305000	-0.120011000
C	-1.619684000	-3.512510000	0.989365000
C	0.046228000	-0.860234000	1.027451000

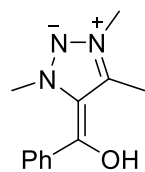
O	0.495737000	-1.731895000	2.034410000
C	0.309042000	0.555086000	1.212817000
C	-0.557827000	1.554454000	0.721114000
C	-0.305770000	2.900517000	0.951395000
C	0.798389000	3.298023000	1.705176000
C	1.643259000	2.322006000	2.233035000
C	1.406011000	0.974632000	1.995128000
C	0.130050000	0.080884000	-1.933215000
H	-1.625804000	-1.784370000	-3.112901000
H	-1.946687000	-4.466832000	0.581509000
H	-0.812283000	-3.658921000	1.702200000
H	-2.463453000	-3.027754000	1.496695000
H	0.203551000	-1.372239000	2.881076000
H	-1.456752000	1.260150000	0.192063000
H	-0.992344000	3.645187000	0.563300000
H	0.987229000	4.348464000	1.891173000
H	2.501376000	2.614580000	2.828373000
H	2.079077000	0.224966000	2.392892000
H	1.148065000	-0.022861000	-1.549214000
H	0.134388000	-0.053546000	-3.014796000
H	-0.217687000	1.086450000	-1.692761000



Ph OH (see below Figure 2.10 C)

Sum of electronic and zero-point Energies=			-650.365633
Sum of electronic and thermal Energies=			-650.351625
Sum of electronic and thermal Enthalpies=			-650.350681
Sum of electronic and thermal Free Energies=			-650.406049
C	0.119106000	-1.492421000	0.249224000
N	0.339809000	-2.843790000	0.506635000
C	-0.558949000	-3.601680000	-0.246048000
C	-1.296970000	-2.764826000	-0.994956000
N	-0.889758000	-1.454221000	-0.715798000
C	-1.069790000	-0.354182000	-1.644485000
C	0.797639000	-0.420103000	0.781839000
O	2.094789000	-0.686701000	1.261313000
C	0.324639000	0.943809000	0.882894000
C	-1.047083000	1.266037000	0.998674000
C	-1.466777000	2.580073000	1.147947000
C	-0.541120000	3.622615000	1.214962000
C	0.817922000	3.320849000	1.136781000
C	1.247307000	2.010104000	0.975121000
C	1.023609000	-3.349136000	1.682443000
H	-0.582818000	-4.674709000	-0.170367000
H	-2.067573000	-2.968213000	-1.717262000

H	-1.472888000	-0.746342000	-2.578262000
H	-1.740954000	0.413719000	-1.253063000
H	-0.102585000	0.118270000	-1.835174000
H	2.165856000	-0.286119000	2.136712000
H	-1.777699000	0.465852000	1.011134000
H	-2.526905000	2.792092000	1.238501000
H	-0.872858000	4.646471000	1.338842000
H	1.552346000	4.117362000	1.192411000
H	2.305145000	1.792992000	0.890953000
H	1.014923000	-4.438398000	1.644301000
H	2.049255000	-2.989482000	1.703886000
H	0.517784000	-3.021723000	2.598942000



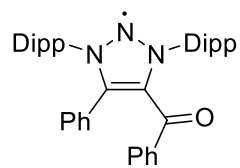
Ph OH (see below Figure 2.10 D)

Sum of electronic and zero-point Energies=	-705.678551
Sum of electronic and thermal Energies=	-705.662894
Sum of electronic and thermal Enthalpies=	-705.661950
Sum of electronic and thermal Free Energies=	-705.721169

C	-0.899346000	0.419621000	-0.038863000
C	-1.323681000	-0.930523000	-0.231574000
N	-3.182267000	0.257379000	0.221989000
N	-2.108982000	1.079885000	0.218886000
C	-2.296675000	2.451213000	0.641472000

C	0.347924000	1.008557000	-0.161796000
O	0.361057000	2.368700000	-0.540222000
C	1.616748000	0.344421000	-0.018906000
C	1.802813000	-0.764210000	0.843410000
C	3.042997000	-1.367964000	0.985514000
C	4.160919000	-0.875765000	0.308589000
C	4.008969000	0.245139000	-0.508351000
C	2.769032000	0.846938000	-0.671469000
C	-0.562915000	-2.096005000	-0.746827000
H	-3.367576000	2.622847000	0.729508000
H	-1.815889000	2.612018000	1.612211000
H	-1.850370000	3.126807000	-0.084163000
H	0.986238000	2.822094000	0.038532000
H	0.968151000	-1.112334000	1.439782000
H	3.148397000	-2.213558000	1.657540000
H	5.130541000	-1.343105000	0.431330000
H	4.867701000	0.649109000	-1.034577000
H	2.662563000	1.698367000	-1.332665000
H	0.026320000	-2.600897000	0.025522000
H	0.153480000	-1.748113000	-1.495612000
H	-1.223865000	-2.829508000	-1.212343000
C	-3.578986000	-2.046142000	-0.176197000
H	-4.561015000	-1.698778000	0.132500000

H	-3.613155000	-2.377390000	-1.214937000
H	-3.251909000	-2.867651000	0.460470000
N	-2.662303000	-0.923150000	-0.038208000



(see below Figure 2.11)

Sum of electronic and zero-point Energies=	-1751.989748
Sum of electronic and thermal Energies=	-1751.948136
Sum of electronic and thermal Enthalpies=	-1751.947192
Sum of electronic and thermal Free Energies=	-1752.065742

N	0.38099800	-1.57022900	0.34345900
N	-0.80307800	-0.93057000	0.36842400
C	-0.73534700	0.38332700	0.03659800
C	0.61887700	0.66054400	-0.18812100
N	1.25819000	-0.57892500	-0.00155100
C	-1.98005700	-1.70448700	0.64709100
C	2.62949700	-0.94463900	-0.18042900
C	-1.92429300	1.21097400	-0.20357000
C	3.56283300	-0.55541500	0.78536800
C	4.88527600	-0.96844200	0.60963200
C	5.25098700	-1.73854000	-0.48565200
C	4.30319500	-2.10064300	-1.43799100
C	2.97255100	-1.70610900	-1.30877600
C	-3.02223700	1.21133300	0.66358500

C	-4.13158800	2.00458100	0.39137200
C	-4.15997100	2.80620200	-0.74652100
C	-3.07313800	2.80526200	-1.61867300
C	-1.96598900	2.01230900	-1.35257400
C	-2.26603200	-2.05485800	1.97624400
C	-3.44986100	-2.76401500	2.19608900
C	-4.29356800	-3.11233100	1.14785100
C	-3.96354600	-2.77190900	-0.15644500
C	-2.79401300	-2.06217200	-0.43596000
C	-1.36649800	-1.79156500	3.18116600
C	-0.28513700	-2.88405000	3.29131300
C	-0.74010700	-0.39251100	3.29396600
C	1.95181800	-1.98458900	-2.39977500
C	2.00341700	-0.85210100	-3.44220600
C	2.11352700	-3.36026100	-3.05518900
C	-2.41512100	-1.74690100	-1.87363300
C	-1.96082800	-3.02790500	-2.59407900
C	-3.54893300	-1.03885300	-2.62874200
C	1.32844600	1.85044000	-0.58927200
C	0.74581400	3.18284500	-0.28112800
C	1.04325700	4.24883800	-1.14052000
C	0.52286100	5.51417700	-0.90213100
C	-0.28540700	5.74220600	0.21231700

C	-0.55495700	4.69714300	1.09397800
C	-0.03981700	3.42930700	0.85227200
O	2.43046900	1.75724200	-1.17190300
H	5.63419200	-0.68067200	1.33790400
H	6.28183900	-2.05236000	-0.60525200
H	4.60751200	-2.68424300	-2.29759500
H	-3.01287500	0.59480900	1.55048300
H	-4.97296600	1.99777700	1.07403100
H	-5.02315100	3.42787600	-0.95292000
H	-3.08598300	3.42411500	-2.50754800
H	-1.12401900	2.01094400	-2.03102100
H	-3.70648100	-3.04653000	3.21085200
H	-5.20810600	-3.65785700	1.35007000
H	-4.61743900	-3.06178300	-0.96942100
H	-2.02612100	-1.90317900	4.04814000
H	0.29069700	-2.74997800	4.21149100
H	-0.73642900	-3.87879200	3.31152800
H	0.39588700	-2.83262100	2.44109700
H	-0.33264700	-0.26842800	4.30040600
H	-1.47250600	0.40182200	3.13495800
H	0.08320000	-0.24962600	2.59658800
H	0.96387300	-1.97086400	-1.93910800
H	1.18811800	-0.95714700	-4.16496700

H	1.93755900	0.12480400	-2.96044800
H	2.95009600	-0.88337800	-3.99002100
H	1.29261200	-3.53739100	-3.75519800
H	2.10321700	-4.15845600	-2.30889800
H	3.04501000	-3.43606800	-3.62255000
H	-1.56244500	-1.06850200	-1.86442700
H	-1.63292200	-2.79502800	-3.61079100
H	-1.12880800	-3.49697200	-2.06492000
H	-2.77575500	-3.75431800	-2.65814100
H	-3.20955700	-0.74908600	-3.62647400
H	-3.86753100	-0.13735400	-2.10306500
H	-4.41812400	-1.69035400	-2.75243600
H	1.68543700	4.05506900	-1.99062600
H	0.74787300	6.32723400	-1.58328000
H	-0.69047800	6.73014500	0.39885400
H	-1.16251000	4.87214600	1.97451900
H	-0.23908600	2.62708400	1.55116800
C	3.17690600	0.30134700	1.97731200
H	2.11495200	0.53375900	1.89381400
C	3.37226900	-0.45633300	3.29934000
H	2.79587600	-1.38464200	3.30718600
H	4.42349400	-0.71182400	3.45841400
H	3.04543100	0.15830600	4.14311600

C	3.93380600	1.63914800	1.96279500
H	3.57331800	2.28825000	2.76587700
H	5.00677400	1.48746200	2.11138000
H	3.78910200	2.14784800	1.00871700

2.8.5: X-ray Crystallographic Data

Crystallographic data for **4a** and **11ah** can be obtained free of charge from www.ccdc.cam.ac.uk/structures/ with deposit numbers noted below.

Crystal data and structure refinement for 4a:

X-ray-quality crystal of **4a** was obtained by chilling a saturated diethyl ether solution to -40 °C in a glovebox. Thermal ellipsoids were at the 50% probability level. Hydrogen atoms were omitted for clarity.

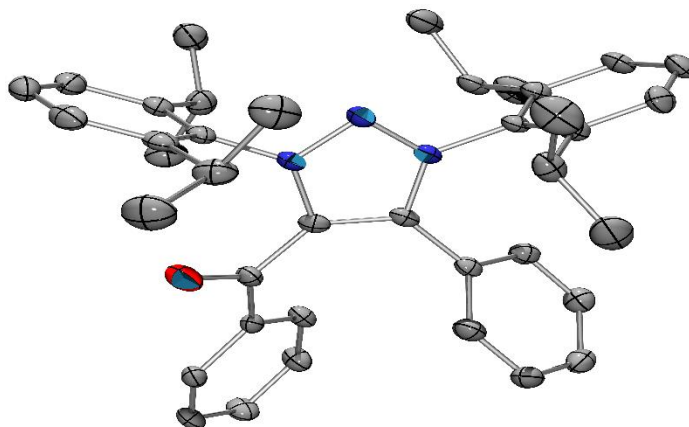


Table 2.1: Crystal data and structure refinement for **4a** (CCDC: 2047374).

Empirical formula	C ₃₉ H _{43.93} Cl _{10.07} N ₃ O
Formula weight	573.09
Temperature	100.0 K
Wavelength	0.71073 Å

Table 2.1 continued: Crystal data and structure refinement for **4a** (CCDC: 2047374).

Crystal system	Monoclinic	
Space group	P 1 21/n 1	
Unit cell dimensions	a = 11.7328(9) Å	$\alpha = 90^\circ$.
	b = 22.1476(17) Å	$\beta = 106.965(2)^\circ$.
	c = 13.4381(11) Å	$\gamma = 90^\circ$.
Volume	3340.0(5) Å ³	
Z	4	
Density (calculated)	1.140 Mg/m ³	
Absorption coefficient	0.073 mm ⁻¹	
F(000)	1232	
Crystal size	0.5 x 0.3 x 0.3 mm ³	
Crystal color, habit	yellow block	
Theta range for data collection	1.832 to 25.417°.	
Index ranges	-14 ≤ h ≤ 14, -26 ≤ k ≤ 26, -16 ≤ l ≤ 16	
Reflections collected	41124	
Independent reflections	6149 [R(int) = 0.0850, R(sigma) = 0.0668]	
Completeness to theta = 25.242°	100.0 %	
Absorption correction	Semi-empirical from equivalents	
Max. and min. transmission	0.4906 and 0.4343	
Refinement method	Full-matrix least-squares on F ²	
Data / restraints / parameters	6149 / 0 / 400	
Goodness-of-fit on F ²	1.013	

Table 2.1 continued: Crystal data and structure refinement for **4a**(CCDC: 2047374).

Final R indices [$I > 2\sigma(I)$]	R1 = 0.0502, wR2 = 0.0940
R indices (all data)	R1 = 0.0990, wR2 = 0.1111
Extinction coefficient	n/a
Largest diff. peak and hole	0.233 and -0.235 e.Å ⁻³

Crystal data and structure refinement for 11ah:

X-ray-quality crystal of **11ah** was obtained by slow evaporation of DCM from the mixture of the corresponding compound. Thermal ellipsoids were at the 50% probability level.

Hydrogen atoms were omitted for clarity.

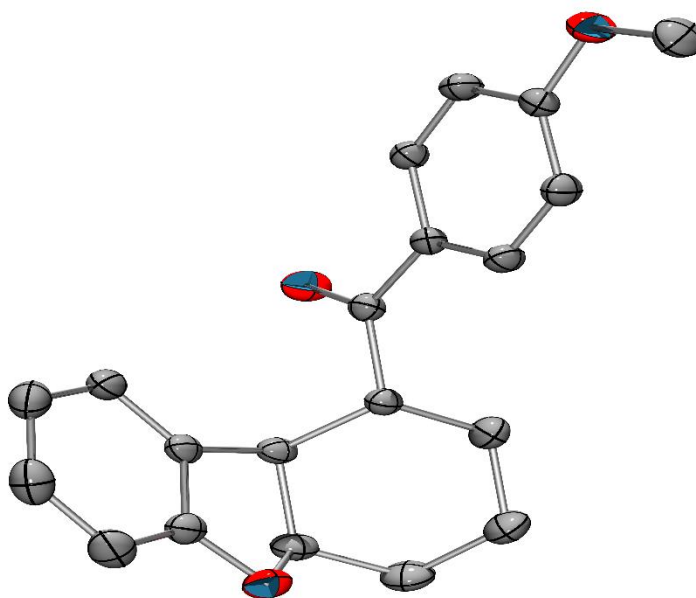


Table 2.2: Crystal data and structure refinement for **11ah**(CCDC: 2043281).

Empirical formula	C ₂₀ H ₂₀ O ₃
Formula weight	308.36
Temperature	170.00(10) K
Wavelength	0.71073 Å
Crystal system	Monoclinic

Table 2.2 continued: Crystal data and structure refinement for **4a** (CCDC: 2047374).

Space group	P 1 21/n 1
Unit cell dimensions	a = 9.8336(4) Å $\alpha = 90^\circ$. b = 16.7138(5) Å $\beta = 108.085(4)^\circ$. c = 10.3616(3) Å $\gamma = 90^\circ$.
Volume	1618.87(10) Å ³
Z	4
Density (calculated)	1.265 Mg/m ³
Absorption coefficient	0.084 mm ⁻¹
F(000)	656
Crystal size	0.38 x 0.27 x 0.03 mm ³
Crystal color, habit	clear light colourless plate
Theta range for data collection	2.400 to 31.158°.
Index ranges	-12 ≤ h ≤ 14, -20 ≤ k ≤ 24, -13 ≤ l ≤ 12
Reflections collected	13453
Independent reflections	4478 [R(int) = 0.0173, R(sigma) = 0.0196]
Completeness to theta = 25.242°	100.0 %
Absorption correction	Semi-empirical from equivalents
Max. and min. transmission	1.00000 and 0.67271
Refinement method	Full-matrix least-squares on F ²
Data / restraints / parameters	4478 / 0 / 209
Goodness-of-fit on F ²	1.030
Final R indices [I > 2σ(I)]	R1 = 0.0424, wR2 = 0.1072

Table 2.2 continued: Crystal data and structure refinement for **4a**(CCDC: 2047374).

R indices (all data) $R1 = 0.0509$, $wR2 = 0.1123$

Largest diff. peak and hole 0.351 and $-0.224 \text{ e.}\text{\AA}^{-3}$

2.8.6: Supplemental Reference Lists

- (1) Bouffard, J.; Keitz, B. K.; Tonner, R.; Guisado-Barrios, G.; Frenking, G.; Grubbs, R. H.; Bertrand, G. Synthesis of Highly Stable 1,3-Diaryl-1*H*-1,2,3-triazol-5-ylidenes and Their Applications in Ruthenium-Catalyzed Olefin Metathesis. *Organometallics* **2011**, *30*, 2617–2627.
- (2) Xu, X.; Zhang, Z.; Huang, S.; Cao, L.; Liu, W.; Yan, X. 4-Halo-1,2,3-triazolylidenes: Stable Carbenes Featuring Halogen Bonding. *Dalton Trans.* **2019**, *48*, 6931–6941.
- (3) Cao, L.; Huang, S.; Liu, W.; Yan, X. 4-Phosphino-1,2,3-triazol-5-ylidenes: Stable Bridging Ligands for Coinage Metal Complexes. *Organometallics* **2018**, *37*, 2010–2013.
- (4) Zhu, S.; Liang, R.; Jiang, H. A direct and practical approach for the synthesis of *N*-heterocyclic carbene coinage metal complexes. *Tetrahedron* **2012**, *68*, 7949–7955.
- (5) He, J.; Tang, S.; Liu, J.; Su, Y.; Pan, X.; She, X. *N*-Heterocyclic carbene catalyzed intramolecular nucleophilic addition of carbonyl anion equivalents to enol ethers. *Tetrahedron* **2008**, *64*, 8797–8800.
- (6) Beillard, A.; Bantreil, X.; Métro, T.-X.; Martinez, J.; Lamaty, F. Mechanochemistry for facilitated access to *N,N*-diaryl NHC metal complexes. *New J. Chem.* **2017**, *41*, 1057–1063.
- (7) Liu, W.; Zhao, L.-L.; Melaimi, M.; Cao, L.; Xu, X.; Bouffard, J.; Bertrand, G.; Yan, X. Mesoionic Carbene (MIC)-Catalyzed H/D Exchange at Formyl Groups. *Chem* **2019**, *5*, 2484–2494.
- (8) René, O.; Fagnou, K. Room-Temperature Direct Arylation of Polyfluorinated Arenes under Biphasic Conditions. *Org. Lett.* **2010**, *12*, 2116–2119.
- (9) Bowman, W. R.; Krintel, S. L.; Schilling, M. B. Tributylgermanium hydride as a replacement for tributyltin hydride in radical reactions. *Org. Biomol. Chem.* **2004**, *2*, 585–592.
- (10) Hu, M.; Gao, Y.; Wu, W.; Li, J.; Li, C.; Zhang, H.; Jiang, H. Efficient assembly of ynones via palladiumcatalyzed sequential carbonylation/alkynylation. *Org. Biomol. Chem.* **2018**, *16*, 7383–7392.
- (11) Yang, H.; Sun, P.; Zhu, Y.; Yan, H.; Lu, L.; Liu, D.; Rong, G.; Mao, J. Palladium-catalyzed synthesis of indoles via intramolecular Heck reaction. *Catal. Commun.* **2013**, *38*, 21–25.
- (12) Rixson, J. E.; Chaloner, T.; Heath, C. H.; Tietze, L. F.; Stewart, S. G. The Development of Domino Reactions Incorporating the Heck Reaction: The Formation of *N*-Heterocycles. *Eur. J. Org. Chem.* **2012**, *2012*, 544–558.
- (13) Liu, X.; Ma, X.; Huang, Y.; Gu, Z. Pd-Catalyzed Heck-Type Cascade Reactions with *N*-Tosyl Hydrazones: An Efficient Way to Alkenes via in Situ Generated Alkylpalladium. *Org. Lett.* **2013**, *15*, 4814–4817.

- (14) Higuchi, Y.; Mita, T.; Sato, Y. Palladium-Catalyzed Intramolecular Arylative Carboxylation of Allenes with CO₂ for the Construction of 3-Substituted Indole-2- carboxylic Acids. *Org. Lett.* **2017**, *19*, 2710–2713.
- (15) Martins, A.; Marquardt, U.; Kasravi, N.; Alberico, D.; Lautens, M. Synthesis of Substituted Benzoxacycles via a Domino *Ortho*-Alkylation/Heck Coupling Sequence. *J. Org. Chem.* **2006**, *71*, 4937–4942.
- (16) Tietze, L. F.; Düfert, A.; Lotz, F.; Sölter, L.; Oum, K.; Lenzer, T.; Beck, T.; Herbst-Irmer, R. Synthesis of Chiroptical Molecular Switches by Pd-Catalyzed Domino Reactions. *J. Am. Chem. Soc.* **2009**, *131*, 17879–17884.
- (17) Dolomanov, O. V.; Bourhis, L. J.; Gildea, R. J.; Howard, J. A. K.; Puschmann, H. OLEX2: a complete structure solution, refinement and analysis program. *J. Appl. Cryst.* **2009**, *42*, 339–341.
- (18) Sheldrick, G. M. SHELXT-Integrated space-group and crystal-structure determination. *Acta Cryst. A*, **2015**, *71*, 3–8.
- (19) Sheldrick, G. M. Crystal structure refinement with SHELXL. *Acta Cryst. C*, **2015**, *71*, 3–8.
- (20) Nimitsiriwat, N.; Gibson, V. C.; Marshall, E. L.; Takolpockdee, P.; Tomov, A. K.; White, A. J. P.; Williams, D. J.; Elsegood, M. R. J.; Dale, S. H. Mono-versus Bis-chelate Formation in Triazenide and Amidinate Complexes of Magnesium and Zinc. *Inorg. Chem.* **2007**, *46*, 9988–9997.
- (21) Connelly, N. G.; Geiger, W. E. Chemical Redox Agents for Organometallic Chemistry. *Chem. Rev.* **1996**, *96*, 877–910.
- (22) Gaussian 16, Revision A.03, M. J. Frisch, G. W. Trucks, H. B. Schlegel, G. E. Scuseria, M. A. Robb, J. R. Cheeseman, G. Scalmani, V. Barone, G. A. Petersson, H. Nakatsuji, X. Li, M. Caricato, A. V. Marenich, J. Bloino, B. G. Janesko, R. Gomperts, B. Mennucci, H. P. Hratchian, J. V. Ortiz, A. F. Izmaylov, J. L. Sonnenberg, D. Williams-Young, F. Ding, F. Lipparini, F. Egidi, J. Goings, B. Peng, A. Petrone, T. Henderson, D. Ranasinghe, V. G. Zakrzewski, J. Gao, N. Rega, G. Zheng, W. Liang, M. Hada, M. Ehara, K. Toyota, R. Fukuda, J. Hasegawa, M. Ishida, T. Nakajima, Y. Honda, O. Kitao, H. Nakai, T. Vreven, K. Throssell, J. A. Montgomery, Jr., J. E. Peralta, F. Ogliaro, M. J. Bearpark, J. J. Heyd, E. N. Brothers, K. N. Kudin, V. N. Staroverov, T. A. Keith, R. Kobayashi, J. Normand, K. Raghavachari, A. P. Rendell, J. C. Burant, S. S. Iyengar, J. Tomasi, M. Cossi, J. M. Millam, M. Klene, C. Adamo, R. Cammi, J. W. Ochterski, R. L. Martin, K. Morokuma, O. Farkas, J. B. Foresman, and D. J. Fox, Gaussian, Inc., Wallingford CT, 2016.
- (23) Becke, A. D. “Density-functional thermochemistry. III. The role of exact exchange,” *J. Chem. Phys.* **1993**, *98*, 5648–5652.
- (24) a) McLean, A. D.; Chandler, G. S. “Contracted Gaussian-basis sets for molecular calculations. 1. 2nd row atoms, Z=11-18,” *J. Chem. Phys.* **1980**, *72*, 5639–5648. b)

- Raghavachari, K.; Binkley, J. S.; Seeger, R.; Pople, J. A. "Self-Consistent Molecular Orbital Methods. 20. Basis set for correlated wave-functions," *J. Chem. Phys.* **1980**, *72*, 650–654.
- (25) GaussView, Version 6, Roy Dennington, Todd Keith, and John Millam, Semichem Inc., Shawnee Mission, KS, 2016.
- (26) Lu, T.; Chen, F. Multiwfn: A multifunctional wavefunction analyzer. *J. Comput. Chem.* **2012**, *33*, 580–592.
- (27) Humphrey, W.; Dalke, A.; Schulten, K. VMD: Visual Molecular Dynamics. *J. Molec. Graphics.* **1996**, *14*, 33–38.
- (28) Guan, Z.; Chen, S.; Huang, Y.; Yao, H. Rhodium(III)-Catalyzed Intramolecular Olefin Hydroarylation of Aromatic Aldehydes Using a Transient Directing Group. *Org. Lett.* **2019**, *21*, 3959–3962.
- (29) Cerichelli, G.; Cerritelli, S.; Chiarini, M.; De Maria, P.; Fontana, A. Alkylation of Carbonyl Compounds in Water: Formation of C-C and C-O Bonds in the Presence of Surfactants. *Chem. Eur. J.* **2002**, *8*, 5204–5210.
- (30) Stubbs, E.; Brown, M.; Steele, A.; Song, C.; Emrick, T. Designing Branched Deoxybenzoin Polyesters as Polymeric Flame Retardants. *Polym. Chem.* **2019**, *57*, 1765–1770.
- (31) Ivanov, K. L.; Vatsouro, I. M.; Bezzubov, S. I.; Melnikov, M. Y.; Budynina, E. M. Domino construction of a bullataketal core via double bond cleavage in activated dihydrofurans. *Org. Chem. Front.* **2018**, *5*, 1655–1663.
- (32) Yamane, M.; Kubota, Y.; Narasaka, K. Palladium-Catalyzed Carboacylation of Alkenes by Using Acylchromates as Acyl Donors. *Bull. Chem. Soc. Jpn.* **2005**, *78*, 331–340.
- (33) Bergonzini, G.; Cassani, C.; Lorimer-Olsson, H.; Hörberg, J.; Wallentin, C.-J. Visible-Light-Mediated Photocatalytic Difunctionalization of Olefins by Radical Acylarylation and Tandem Acylation/ Semipinacol Rearrangement. *Chem. Eur. J.* **2016**, *22*, 3292–3295.

2.8.7: Supplemental Figures

2.8.7.1: Electrochemical Measurements

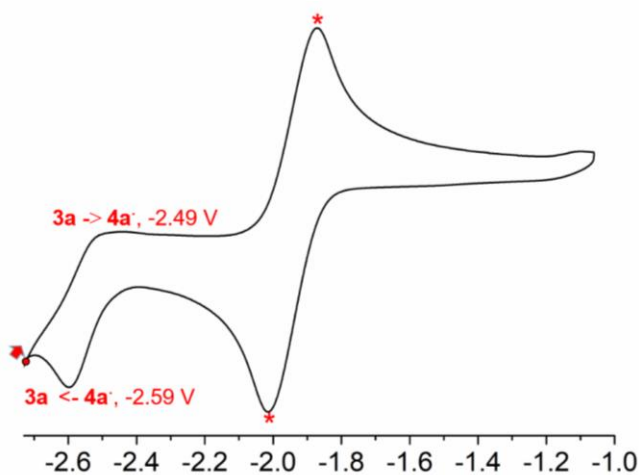


Figure 2.6: Cyclic voltammograms of **3a** (1 mM) vs Fc/Fc⁺ in THF (0.1 M nBu₄NPF₆) at room temperature (scan rate: 100 mV/s). $E_{1/2}^* = -1.98$ V.

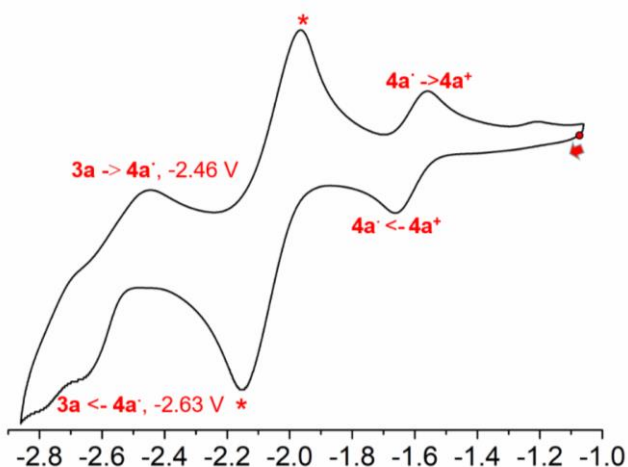


Figure 2.7: Cyclic voltammograms of **4a'** (1 mM) vs Fc/Fc⁺ in THF (0.1 M nBu₄NPF₆) at room temperature (scan rate: 100 mV/s). Cyclovoltammograms of **4a'** solutions feature the reversible peak of the [**4a'**/**4a'**⁺] couple at $E_{1/2} = -1.53$ V, $E_{1/2}^* = -2.02$ V.

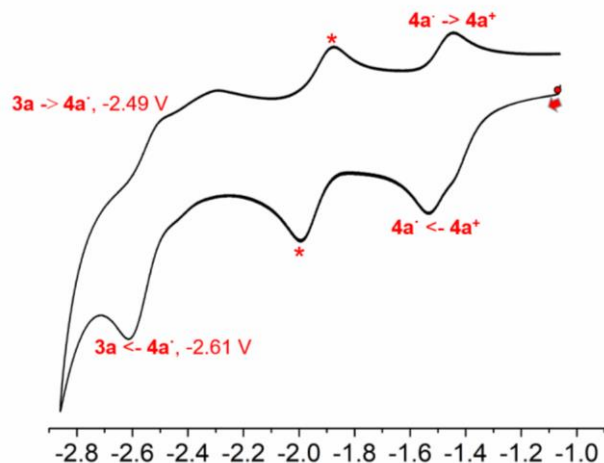


Figure 2.8: Cyclic voltammograms of $4a^+$ (0.1 mM) vs Fc/Fc⁺ in THF (0.1 M nBu₄NPF₆) at room temperature (scan rate: 100 mV/s). Cyclovoltammograms of $4a^+$ solutions feature the reversible peak of the [$4a^+/4a^+$] couple at $E_{1/2} = -1.50$ V, $E_{1/2}^* = -1.98$ V.

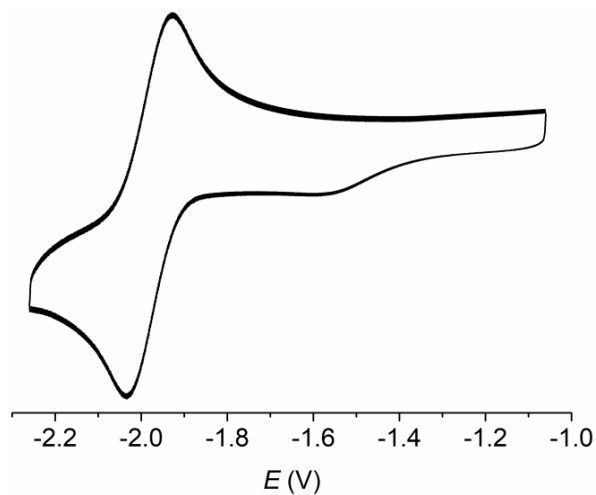


Figure 2.9: Cyclic voltammograms of $1a$ (0.1 mM) vs Fc/Fc⁺ in THF (0.1 M nBu₄NPF₆) at room temperature (scan rate: 100 mV/s). Cyclovoltammograms of $1a$ solutions feature the reversible peak at $E_{1/2} = -1.98$ V.

2.8.7.2: Computational Analysis

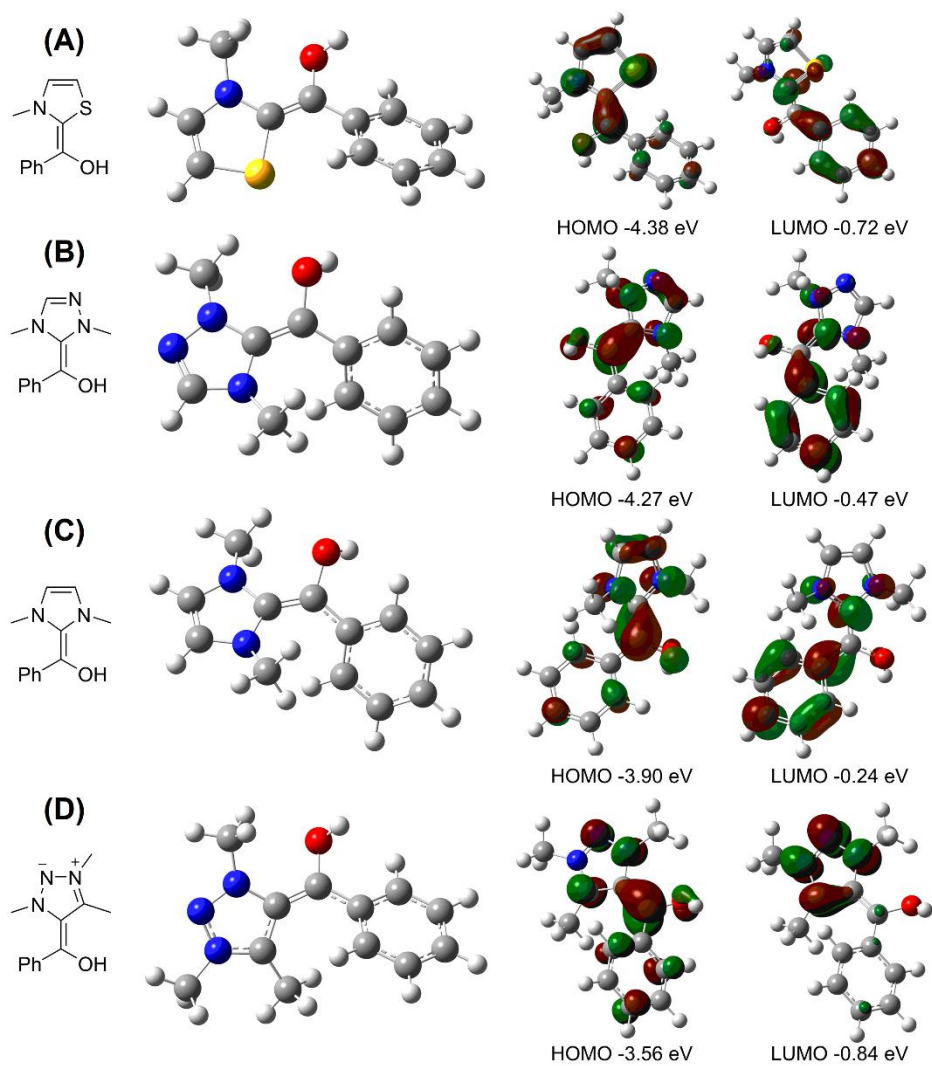


Figure 2.10: The optimized structure and HOMO and LUMO orbitals with their energy (in eV). Isovalue = 0.05.

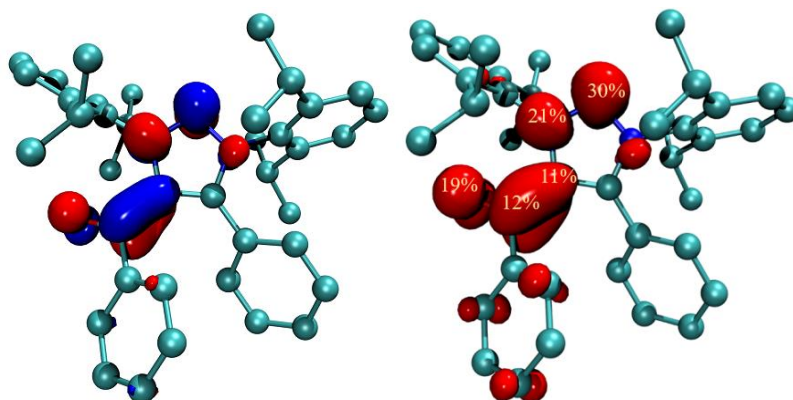


Figure 2.11: The representation of SOMO (Isovalue = 0.06) and spin density of **4a**' (Isovalue = 0.002).

CHAPTER 3:
INVESTIGATIONS OF
MESOIONIC CARBENE-
ISOCYANIDE ADDUCTS

3.1: Introduction to Carbene-Isocyanide Adducts

As discussed in chapter 1, a classical reaction of carbenes is the formation of ketenes on exposure to carbon monoxide (CO).¹ For stable carbenes to undergo this reaction they must be sufficiently electrophilic, which is demonstrated by how it proceeds well for alkyl amino carbenes, including the CAAC² and BiCAAC³, and diamido carbenes (DACs)⁴, but not for Arduengo N-heterocyclic carbenes (NHCs).^{5,6} In the latter case, only weak Van-der-Waals interactions exist between the carbene and CO. While this formation of the ketene is somewhat ubiquitous, it was only recently applied to a catalytic transformation in the form of the CAAC-catalyzed carbonylation of quinones by CO, as reported by Bertrand and co-workers in 2020.³

Isocyanides are considered stand-ins for CO due to their isolobal structure and relative ease of use, being liquids or solids at room temperature rather than gas. In this vein, carbenes react with isocyanides much like they do with CO, generating the corresponding ketenimine. Again, this reactivity is known primarily for electrophilic carbenes, such as the original phosphino-silyl carbene⁷, alkyl amino carbenes⁸, and DACs.⁹ Similarly, it was previously reported that NHCs are unreactive with isocyanides, as would be expected due to their low electrophilicity.⁸ However, this thinking was challenged by a 2019 report by Stephan and co-workers that NHCs react with cyclohexyl isocyanide to give a 3-azabutadiene derivative after a 1,3-proton shift. This discrepancy appeared to be mainly due to differences in experimental procedure, with the original report attempting the reaction at low temperature and Stephan's report demonstrating a room temperature reaction overnight.

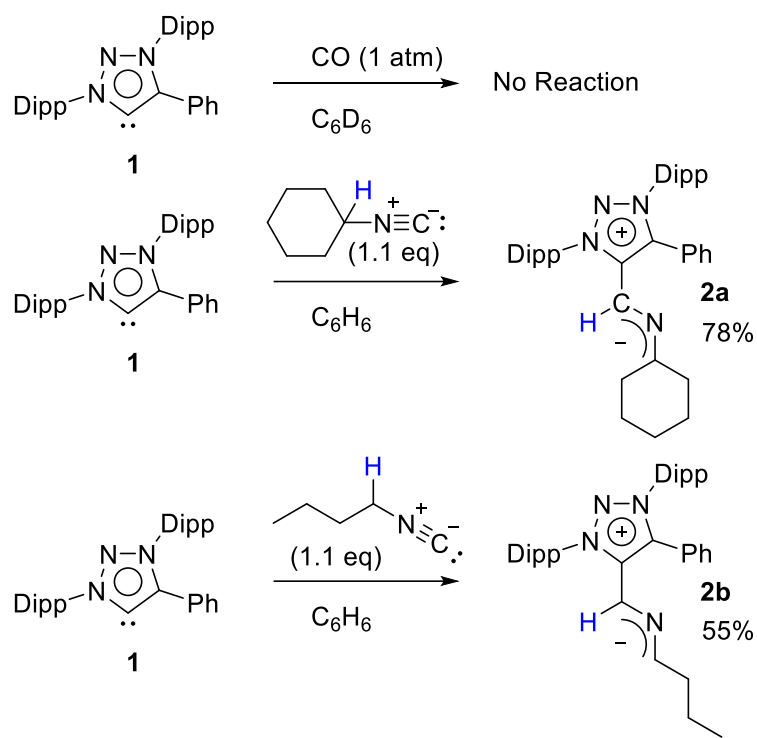
Inspired by the CAAC-catalyzed carbonylation reaction, we sought to expand carbene organocatalysis through the reactions of 1,2,3-triazolium mesoionic carbenes (MICs) with CO and isocyanides. The results of this investigation are reported in this chapter, including the

discovery of radical species from the reaction with quaternary isocyanides where a 1,3-proton shift is inaccessible.

3.2: Results and Discussion

We commenced our investigation by testing if MICs are similarly unreactive with CO as Arduengo-type NHCs are. A C₆D₆ solution of carbene **1** was placed under a CO atmosphere and monitored by NMR. No reaction was observed, validating our assumption that MICs are insufficiently electrophilic to react with CO.

We proceeded to test the reactivity of MICs with commercially available cyclohexyl isocyanide (CyNC). Following the addition of CyNC to a benzene solution of **1** at room temperature, the reaction mixture gradually became green. After the reaction mixture was stirred overnight, filtration and evaporation of the solvent in vacuum yielded **2a** as a green powder. NMR analysis showed two sets of signals in ~3:2 ratio, suggesting the existence of rotamers. **2a** crystallized out of a hexane solution, allowing structural confirmation via single crystal x-ray diffraction (XRD) analysis. The C1-C33, C33-N4, and N4-C34 bond lengths are 1.37 Å, 1.37 Å, and 1.29 Å, respectively. Furthermore, the C1-C33-N4 bond angle is 121° and the C33-N4-C34 bond angle is 123°. Taken together, these values point to a delocalized π -system along the carbene-isocyanide adduct. Similarly, addition of n-butyl isocyanide to a benzene solution of **1** gave **2b**, as indicated by NMR and mass spectrometry.



Scheme 3.1: Reactivity of MIC **1** with carbon monoxide, cyclohexyl isocyanide, and n-butyl isocyanide.

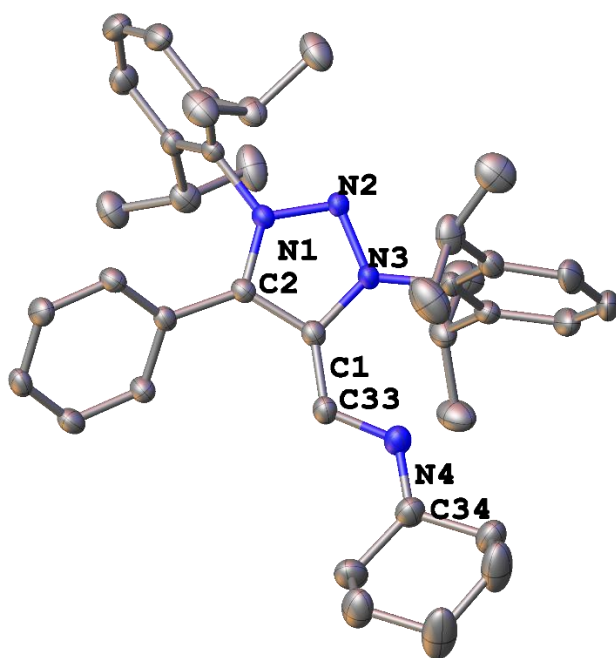
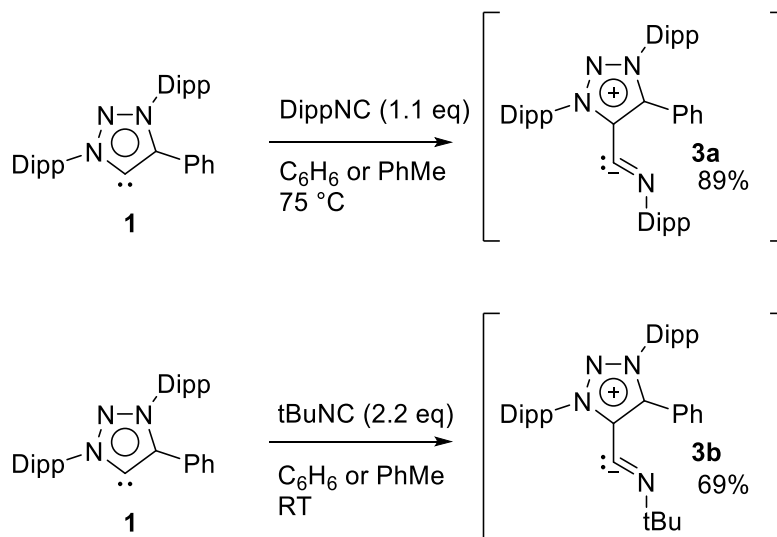


Figure 3.1: Solid state structure of **2a**

Notably, the structures of **2a-b** indicate a 1,3-proton shift from the ipso carbon of the isocyanide to the isocyanide carbon itself. This is in line with the reactivity reported by Stephan *et. al.* of IMes and SIMes NHCs with CyNC.¹⁰ The main difference here is that the mesoionic character of the 1,2,3-triazolydenes extends to the isocyanide adducts as we cannot draw a fully neutral resonance form. However, they still contain similar olefinic signals in NMR (for **2a**, ¹H: 5.78 ppm, ¹³C: 85.30, 84.84 ppm) to the CyNC adduct formed by IMes. Like Stephan, we reason that although the formation of a cumulene-like structure with isocyanides may be unfavorable for MICs, the subsequent proton shift drives the overall reaction by formation of an extended π system.

These results made us curious as to the effect of blocking the 1,3-proton shift by using a quaternary isocyanide. Addition of 2,6-diisopropylphenyl isocyanide (DippNC) to a C₆D₆ solution of **1** did not appear to give a reaction after 1 hour at room temperature. However, upon heating to 75 °C for 3 hours, the solution took on a purple color. To our surprise, NMR of this sample showed disappearance of all signals associated with the carbene, with only line-broadened signals for excess isocyanide present. This suggested to us the formation of some paramagnetic product and, indeed, EPR spectroscopy of this product showed a strong signal which was simulated to $g_{\text{iso}} = 2.0039$ with hyperfine coupling to four nitrogen atoms ($a_{\text{iso}} = 26.2$ MHz, 11.8 MHz, 7.5 MHz, 4.8 MHz) and a few hydrogen atoms. This would be in line with the formation of an adduct between **1** and the isocyanide with delocalization of the radical component. Reaction of **1** with tert-butyl isocyanide was more difficult as the product decomposed at 75 °C. However, when this reaction was repeated with an excess of the isocyanide at room temperature for one week, a similarly purple solution without carbene NMR signals was obtained. The EPR spectrum of this solution similarly revealed a strong signal which

was simulated to $g_{\text{iso}} = 2.0036$ with hyperfine coupling to four nitrogen atoms ($a_{\text{iso}} = 28.5$ MHz, 12.4 MHz, 12.2 MHz, 2.2 MHz), also suggesting the formation of an adduct with delocalization of a radical component.



Scheme 3.2: Reactivity of MIC **1** with quaternary isocyanides DippNC and tBuNC

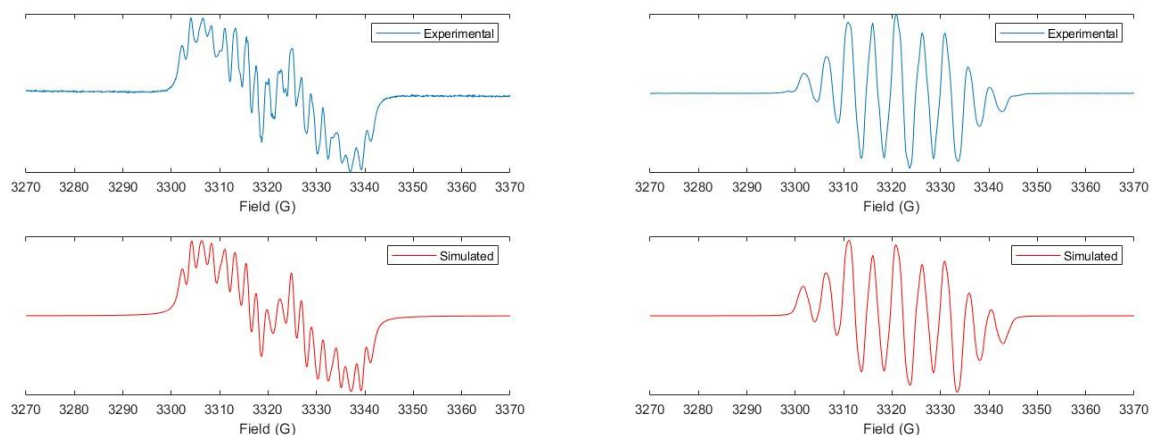
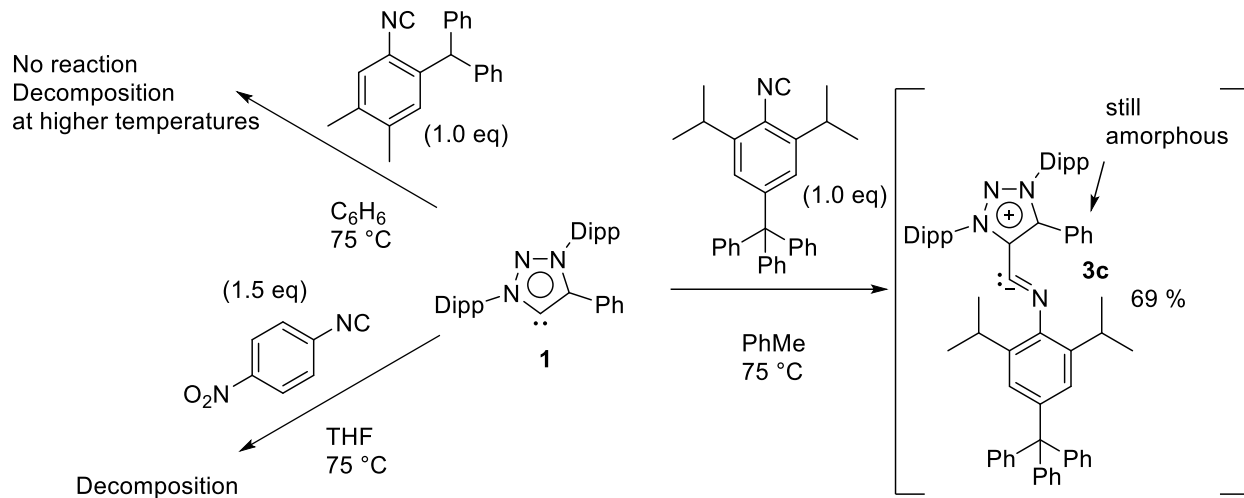


Figure 3.2: EPR spectra of **3a** (left) and **3b** (right) in benzene. Experimental data (top) is in blue with the simulation fit (bottom) in red.

We hypothesized that the products of these reactions, **3a-b**, were the direct adducts of the isocyanides to carbene **1**, much like the lithium aldimines formed by addition of organolithiums to isocyanides^{11,12}, although we could not readily explain why these structures would have

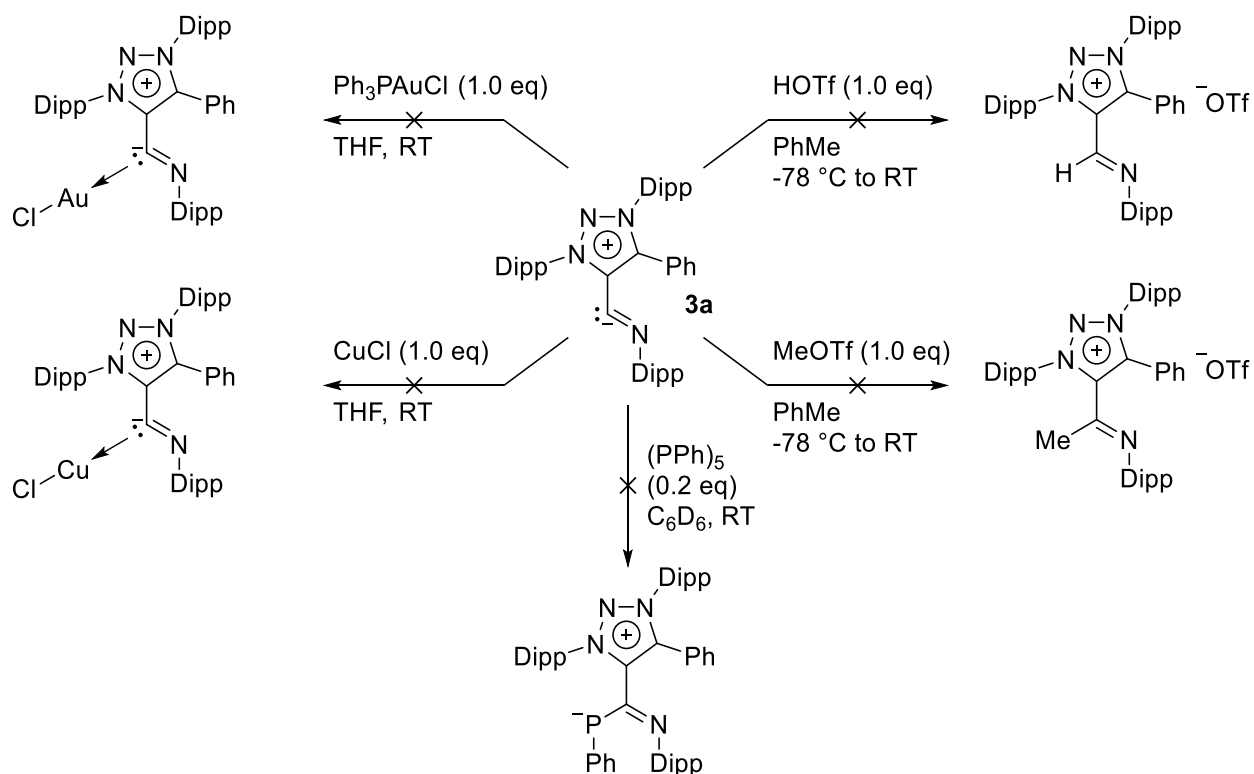
radical character. Preparatory scale synthesis of **3a-b** in toluene gave, after removal of the solvent and excess isocyanide in vacuum, glassy dark purple solids. These products were extremely soluble in polar and non-polar solvents, ranging from pentane to acetonitrile. They were even somewhat soluble in hexamethyldisiloxane, a particularly lipophilic solvent used for the crystallization of nonpolar solids. Regardless of solubility, molecules **3a-b** were completely amorphous, to the extent that there was no evidence of crystallinity in a powder XRD study of **3a**. As such, we could not directly elucidate their structure.

Several other quaternary isocyanides were reacted with **1** in the hopes that using bulky or otherwise easily-crystallizable substituents might allow us to establish the structure of these NMR-silent products by XRD. While 2,6-diisopropyl-4-tritylphenyl isocyanide did afford purple NMR-silent solid **3c**, this was similarly amorphous, and no X-ray structure could be obtained. 2-benzhydryl-4,5-dimethylphenyl isocyanide was unreactive with **1**, probably owing to its large steric bulk at the isocyanide. **1** was also reacted with 4-nitrophenyl isocyanide due to the known crystallizing ability of nitro groups, but this resulted in an intractable mixture of decomposition products, likely due to the ease of reducing nitrobenzene derivatives (see chapter 4 for reduction by free MIC).



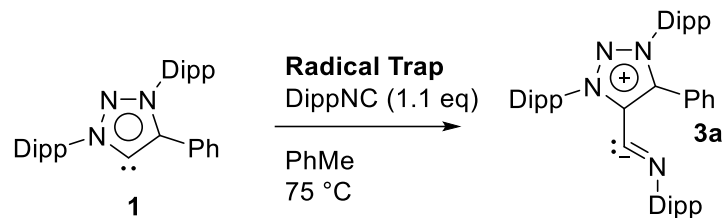
Scheme 3.3: Attempts to obtain crystalline adduct **3** by use of different isocyanides.

Having exhausted the normal methods of structural characterization, we set out to synthesize derivatives which may be characterized by NMR and/or XRD. Hypothesizing that **3a** may behave as the direct adduct as shown in scheme 3.2 despite its radical character, we attempted protonation with triflic acid to make a neutral imine. However, this yielded a complex mixture of products by NMR. Similar results were obtained upon attempted alkylation with methyl triflate or complexation with copper (I) chloride or triphenylphosphine gold (I) chloride. We also recognized that **3a** may behave similarly to a free carbene and attempted the formation of a phosphinidene adduct.¹³⁻¹⁵ However, even after allowing a mixture of **3a** and 0.2 equivalents of phenylphosphinidene pentamer (1 equivalent monomer) to sit for 11 days, no reaction was observed.

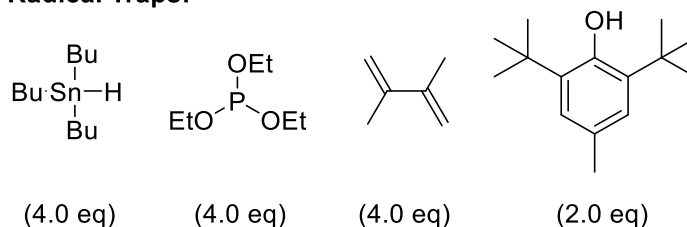


Scheme 3.4: Attempted derivatization of **3a** with electrophilic reagents.

We then considered that given **3a**'s apparent radical character, it may react with known radical trapping reagents. Specifically, we utilized tributyltin hydride, triethyl phosphite, 2,3-dimethyl-1,3-butadiene, and butylated hydroxytoluene (BHT). These reagents are not directly reactive with either carbene **1** or DippNC, so we tested the synthesis of **3a** in the presence of an excess of all these reagents to see if the reaction was inhibited or an intermediate or product would be trapped. However, the reaction of **1** with DippNC still proceeded cleanly to the same NMR-silent purple product **3a** in all cases.

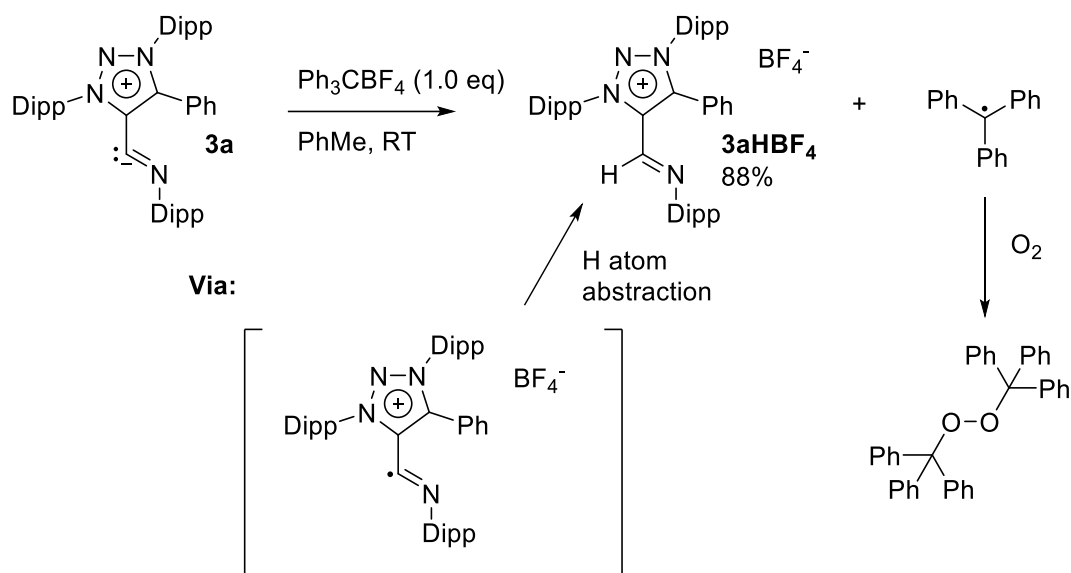


Radical Traps:



Scheme 3.5: Formation of **3a** proceeds in the presence of known radical traps.

We were therefore relieved when a reaction between **3a** and triphenylcarbenium tetrafluoroborate in toluene gave a yellow-brown solution. After washing with hexane and drying in vacuum, a powder with an NMR indicative of primarily a single product with three Dipp groups (identified by isopropyl C-H) was recovered. Single crystal XRD confirmed the structure of **3aHBF₄** as a triazolium imine salt. The C1-N1 bond length is 1.25 Å, and the C2-C1-N1 angle is 123.5°, both quite reasonable for an imine. Furthermore, the imine is approximately co-planar with the triazolium ring in the solid state, in line with extended π -conjugation.



Scheme 3.6: Synthesis of **3aH** from **3a** with postulated radical cation intermediate.

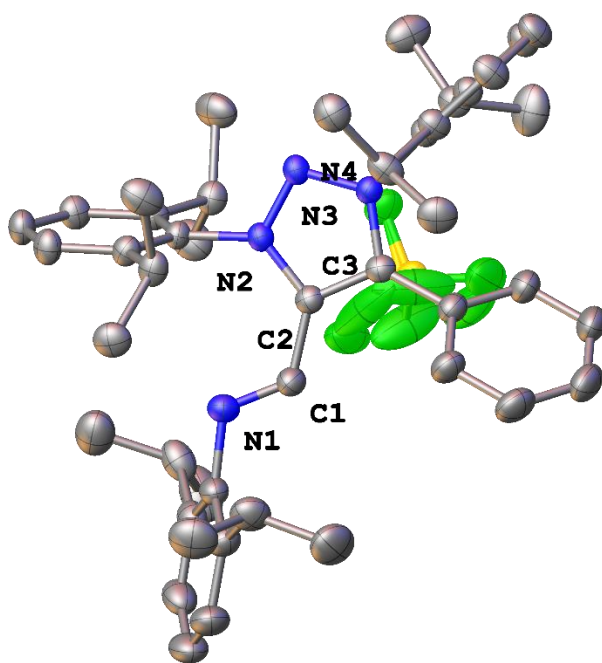


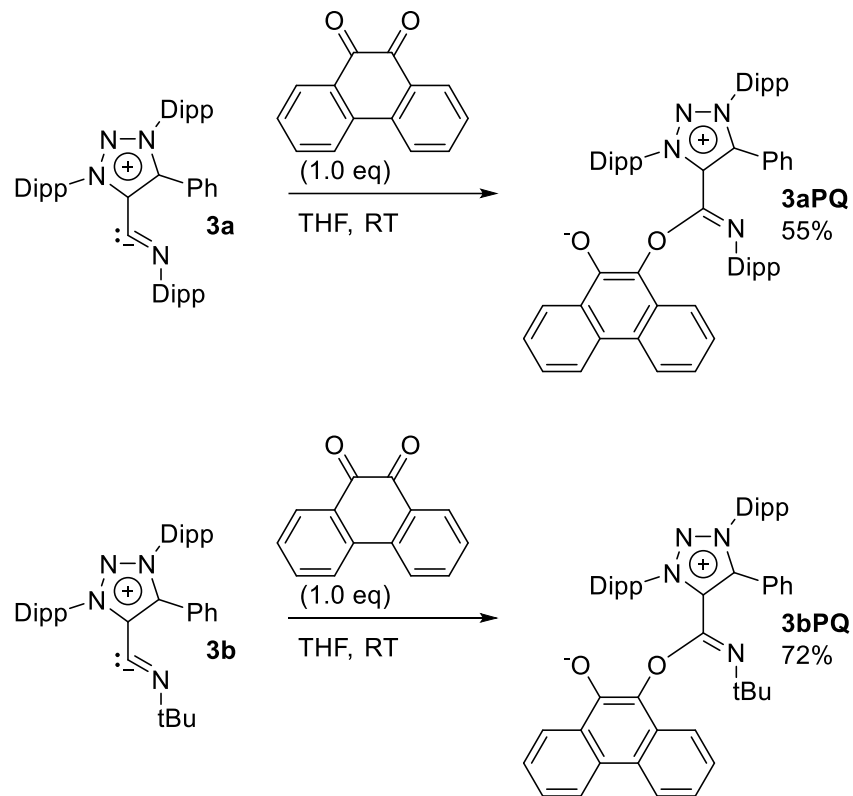
Figure 3.3: Solid state structure of **3aHBF₄**, with hydrogen atoms omitted for clarity. The tetrafluoroborate anion (background) is disordered in orientation.

We propose that the triphenylmethyl cation oxidizes **3a** by one electron to give a highly reactive sigma radical which, in turn, abstracts a hydrogen atom from solvent to give the imine.

There is precedence for similar reactivity in the oxidation of NHCs by trityl cation.¹⁶ Our

proposed mechanism is also supported by the presence of bis(triphenylmethyl)peroxide, which crystallized separately from **3aHBF₄**. This peroxide is known to result from the exposure of the Gomberg triphenylmethyl radical to oxygen¹⁷, indicating an SET process occurred. Curiously, attempting a similar oxidation with nitrosonium hexafluoroantimonate gave a complex mixture, although nitrosonium ($E^{\circ\prime} = 0.87$ V Vs. Fc/Fc⁺, acetonitrile) is a significantly stronger oxidant than trityl cation ($E^{\circ\prime} = -0.11$ V Vs. Fc/Fc⁺, acetonitrile)¹⁸, and may have overoxidized the substrate. It should also be noted that **3aHBF₄**, despite its charged structure, is soluble in aromatic hydrocarbons, reflecting on the high solubility of products **3**.

We also considered the reaction of **3a** with quinones, as these are known to be one-electron oxidants as well as classical electrophiles. When a mixture of **3a** and phenanthrenequinone was dissolved in THF, the solution rapidly changed to a lighter shade of purple from **3a**, indicating a reaction had occurred. This product was also NMR-silent but crystallized out of THF/hexane so the structure of **3aPQ** could be verified by single crystal XRD. Again, the imine (C33-N4) bond length is a reasonable 1.27 Å and the environment of C33 is roughly trigonal planar with bond angles of 122.2°, 118.9°, and 118.6°. Of note, the phenanthrenequinone ring is twisted out of the imine plane, likely due to the crowded steric environment. Phenanthrenequinone similarly reacts with **3b** to give **3bPQ**.



Scheme 3.7: Reaction of phenanthrenequinone with **3a** and **3b**, giving adducts **3aPQ** and **3bPQ**, respectively.

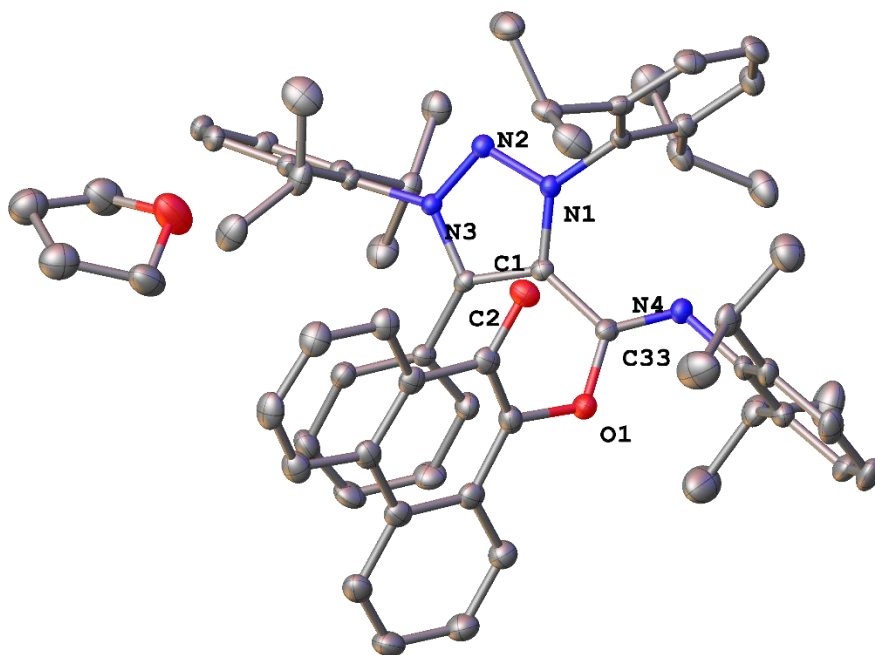


Figure 3.4: Solid state structure of **3aPQ** with hydrogen atoms omitted for clarity. One molecule of THF co-crystallized in the unit cell.

EPR measurements of **3aPQ** gave a well-defined signal which was simulated to $g_{\text{iso}} = 2.0052$ with hyperfine coupling to one nitrogen and two hydrogen atoms ($a_{\text{iso}} = 4.47$ MHz, 3.96 MHz, and 3.51 MHz respectively). Similarly, **3bPQ** gave an EPR signal simulated to $g_{\text{iso}} = 1.9916$ with hyperfine coupling to one nitrogen and two hydrogen atoms ($a_{\text{iso}} = 3.63$ MHz, 3.72 MHz, and 3.53 MHz respectively). It is not immediately clear how these structures are paramagnetic. Furthermore, the coupling to only one nitrogen suggests the radical component is not delocalized on the triazolium ring in contrast to the results for **3a** and **3b**.

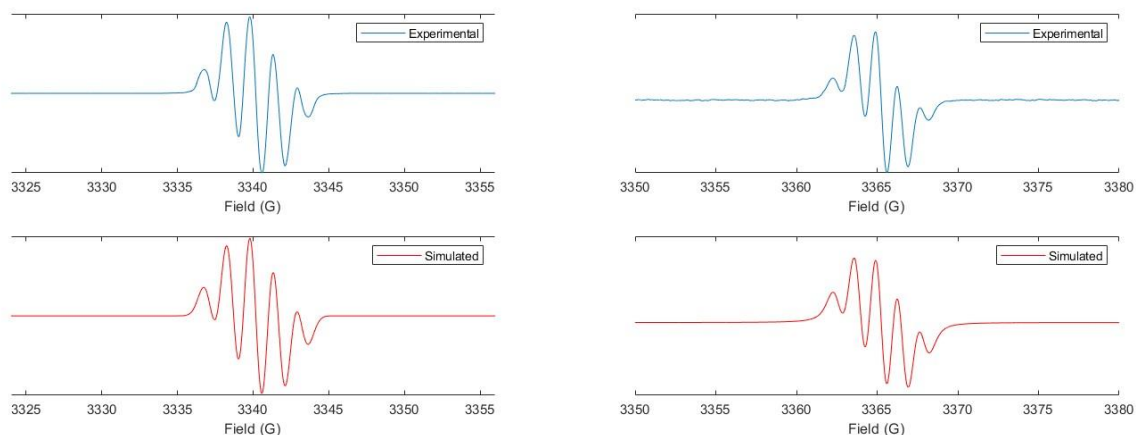
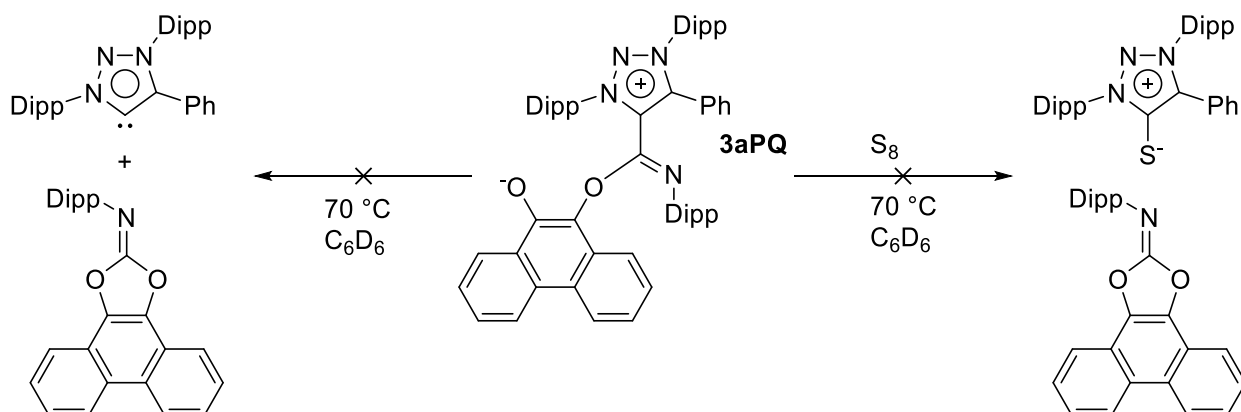


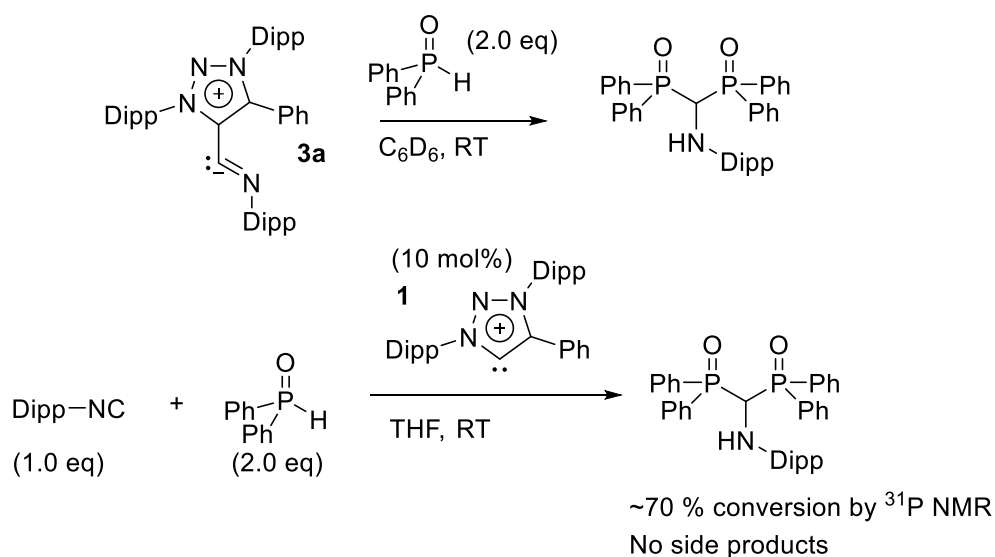
Figure 3.5: EPR spectra of **3aPQ** (left) and **3bPQ** (right) in benzene. Experimental data (top) is in blue with the simulation fit (bottom) in red.

Since the structure of **3aPQ** is similar to an intermediate in the CAAC-catalyzed carbonylation of phenanthrenequinone³, we postulated the quinone might swing closed onto the isocyanide carbon under the right conditions and extrude the free carbene to give the corresponding dioxol-2-imine (analogous to carbonate). However, heating in C₆D₆ at 70 °C overnight resulted in no change. This experiment was repeated with the addition of sulfur to trap the free carbene but this time an intractable mixture was observed by NMR with the absence of the carbene sulfur adduct and dioxol-2-imine.



Scheme 3.8: **3aPQ** does not give the dioxol-2-imine on heating, even with a trapping agent.

With the synthesis of **3a**HBF₄ and **3a**PQ in hand, we observed that compounds of type **3** appear to preferentially react by SET. Even though **3a**PQ appears to be the direct polar addition product of **3** onto phenanthrenequinone, the possibility of a one-electron mechanism could not be ignored. Classical radical traps do not react, but we wondered about other radical reagents. One such example that caught our attention was diphenylphosphine oxide.¹⁹ Indeed, when a C₆D₆ solution of **3a** and two equivalents of diphenylphosphine oxide was allowed to sit overnight, ³¹P NMR indicated the formation of a single new phosphorus product. The ¹H and ¹³C NMR were less clear but the product was confirmed as the formal double insertion of the isocyanide into the P-H bond of the phosphine oxide after checking by mass spectrometry and comparing to literature.²⁰

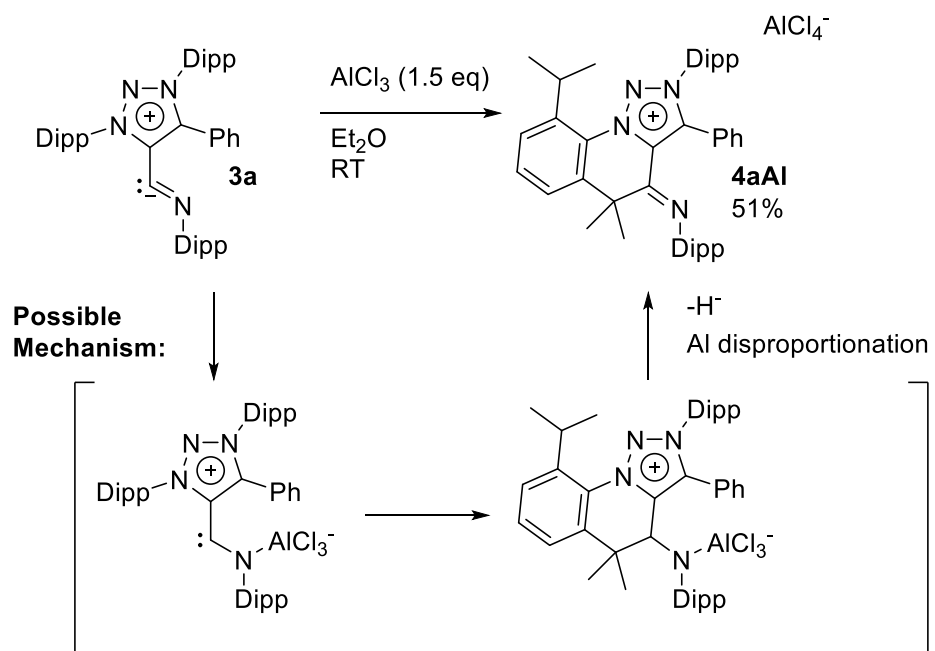


Scheme 3.9: Bisphosphonation of Dipp isocyanide stoichiometrically from **3a** (*top*) and catalytically with respect to MIC **1** (*bottom*).

Of note, the bisphosphonation of isocyanides by diphenylphosphine oxide was previously catalyzed by rhodium complexes.²⁰ This piqued our interest as we have been seeking organocatalytic applications of carbenes. We reacted DippNC with 2 equivalents of diphenylphosphine oxide in the presence of 10 mol% **1** as catalyst and tracked the reaction by ³¹P

NMR. After stirring overnight at room temperature, a ~70% conversion was observed with only trace byproducts. This appeared to be the limit of this reaction as a further 24 hours at 70 °C did not yield more product. However, while we were pursuing this investigation, a report was published which showed stoichiometric DBU effecting the bisphosphonation of isonitriles.²¹ Given the ease of this transformation with cheap, commercially-available reagents, we ceased this line of inquiry.

One other possibility we considered was that molecules of type **3** might react with a classical Lewis acid without the possibility of redox chemistry. When a diethyl ether solution of **3a** and aluminum trichloride was stirred for several hours, a yellow precipitate formed. Characterization of this precipitate by NMR and single crystal XRD gave the structure of **4aAl** as the insertion product of an isopropyl C-H from the carbene framework into the isocyanide carbon to form a polycyclic cation. The C33-N4 bond distance is 1.27 Å, in line with a carbon-nitrogen double bond. Furthermore, the bond angles around C33 are 122.2° (N4-C33-C27), 126.9° (N4-C33-C1), and 110.7° (C27-C33-C1), indicating a distorted sp² geometry at the central carbon.



Scheme 3.10: Synthesis of **3aAl** with possible mechanism.

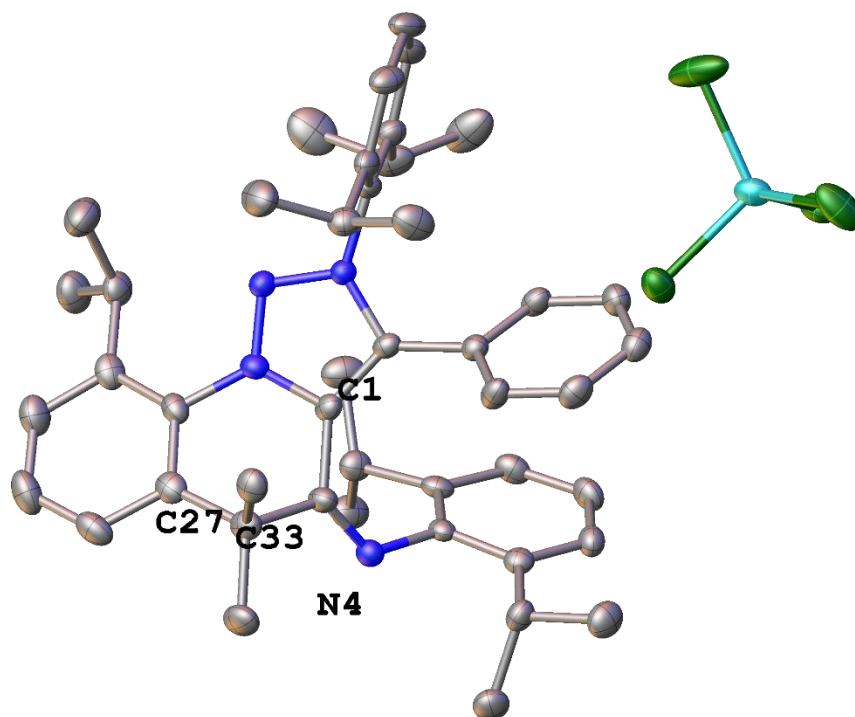


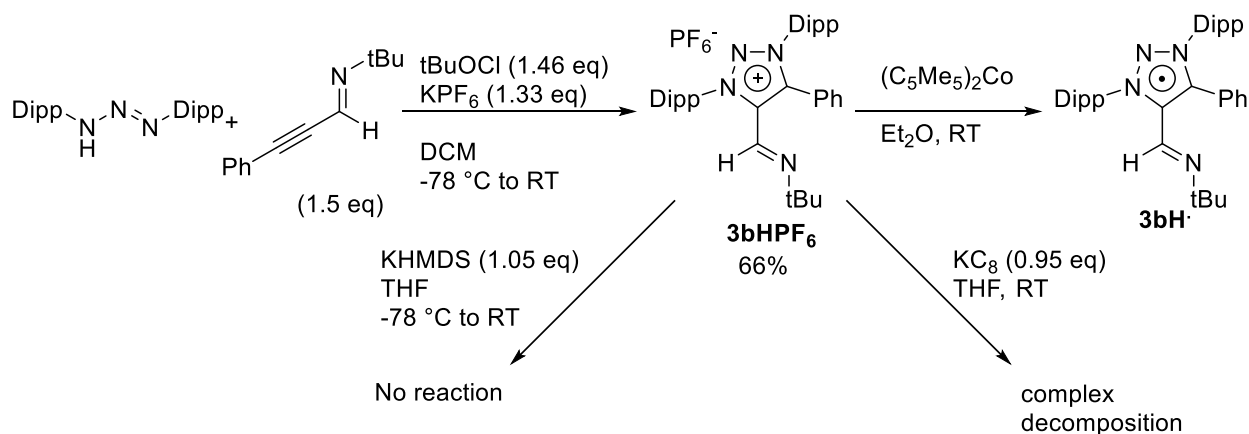
Figure 3.6: Solid state structure of **3aAl**.

Presumably, the aluminum chloride coordinated the imine nitrogen, giving a carbene-like species. Electrophilic carbenes have been known to insert benzylic C-H bonds²², and an insertion reaction followed by hydride abstraction and disproportionation of aluminum gives the final product. We expect aluminum hydride species to be formed in this reaction, although only AlCl_4^- was present in the precipitate as determined by ^{27}Al NMR. In this sense, we can think of **3a** acting as a reducing agent, albeit more in the conventional polar sense.

Overall, the reactivity pattern of molecules **3** was perplexing. They react cleanly with some oxidants but not most electrophilic reagents. Furthermore, the fact that they are NMR-silent is difficult to reconcile with their presumed structures. We had reasoned that there might be a room-temperature accessible triplet state, but variable temperature NMR of **3a** in THF- d_8 showed no signal down to $-80\text{ }^\circ\text{C}$. Density functional theory calculations at the M06-2X/6-31G**//cc-pVTZ(-f) level of theory with a Truhlar correction added more confusion by indicating **3a** possesses a singlet-triplet gap of 14.13 Kcal/mol. Similarly, the singlet-triplet gap for **3b** was calculated as 12.91 Kcal/mol. These values do not explain the lack of an NMR signal at room temperature, and we certainly would expect to see something at $-80\text{ }^\circ\text{C}$. We then wondered if there was a different structure that could match the spectroscopic and reactivity data previously taken.

One possibility we considered was the neutral radical **3aH \cdot** , which would certainly explain the synthesis of **3aHBF $_4$** by oxidation. With consideration to the ease of synthesis, we decided to build the cation by cycloaddition of the corresponding propargyl imine to (bis)Dipp triazene as is used for the synthesis of carbene **1**.²³ As the synthesis of the propargyl tert-butyl imine is already known²⁴, **3bHPF $_6$** was targeted for this investigation. This also allowed us to test if deprotonation of the imine might give **3b**. **3bHPF $_6$** was then stirred with KHMDS in THF,

but no reaction was observed. Potassium graphite proved to be too harsh of a reducing agent for **3bHPF₆**, leading only to decomposition. Cyclic voltammetry measurements of **3bHPF₆** revealed a one-electron redox at -1.69 V vs. Fc/Fc⁺, which puts the reduction within reach of decamethylcobaltocene.¹⁸ Indeed, reduction of **3bHPF₆** with decamethylcobaltocene gave a radical **3bH[•]**, which was characterized by EPR spectroscopy. However, this spectrum was visibly different from that of **3b**, so we reason these are two different structures. The EPR for **3bH[•]** is very complex but the rough fit gave $g_{\text{iso}} = 2.0040$ with coupling to four nitrogen atoms ($a_{\text{iso}} = 19.63 \text{ MHz}, 10.74 \text{ MHz}, 7.22 \text{ MHz}, 6.82 \text{ MHz}$). As of now, we can still only point to the derivative products of molecules **3** as indication of their true structure.



Scheme 3.11: Synthesis of **3bHPF₆** by cyclization of the corresponding alkyne, followed by reaction with base and reductants.

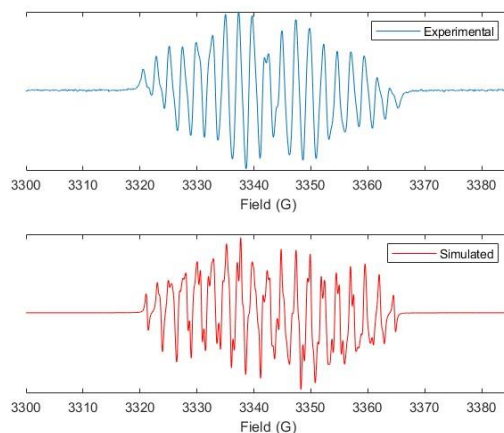


Figure 3.7: EPR spectrum of **3bH•** in benzene. Experimental data (*top*) is in blue with the simulation fit (*bottom*) in red.

3.3: Conclusions

Arduengo NHCs react with isocyanides where a 1,3-proton shift from the *ipso* C-H is accessible. We have now shown that 1,2,3-triazolium mesoionic carbenes are similarly reactive with such isocyanides and possess different reactivity with quaternary isocyanides where the proton shift is not possible. The MIC adducts thus formed are NMR-silent, EPR-active, and completely amorphous for all isocyanides tested, making structural confirmation difficult. These adducts do not cleanly react with electrophilic reagents, nor is their formation inhibited by radical trapping agents, but they do form crystalline NMR-active derivatives on exposure to oxidants. These results suggest that the reaction of MICs with quaternary isocyanides gives a direct adduct reminiscent of ketenimines derived from electrophilic carbenes. Furthermore, these adducts react with the P-H bond of a phosphine oxide to give the formal double insertion product of the isocyanide.

DFT calculations did not completely support the structure of molecules **3**, but a reasonable alternative, the reduced form of **3aH**, was ruled out by direct synthesis and comparison of EPR spectra. More investigation is needed to ascertain a definitive structure.

3.4: Acknowledgements

Chapter 3 contains material currently being prepared for submission for publication.

Vianna, A.; Melaimi, M.; Mulks, F. F.; Bertrand, G. Investigations of Mesoionic Carbene-Isocyanide Adducts. The dissertation author was the primary researcher and first author of this material.

3.5: Experimental Procedures and Data

3.5.1: Materials

Unless otherwise noted, all reagents were obtained from commercial suppliers and used directly without further purification. Anhydrous triethylamine and diisopropylamine were dried by distillation from calcium hydride. Anhydrous Et₂O, THF, pentane, and benzene were dried by distillation over sodium-benzophenone ketyl under an argon atmosphere. Anhydrous toluene was dried by distillation over sodium metal under an argon atmosphere. Anhydrous hexane, CH₂Cl₂, and CHCl₃ were dried by distillation over calcium hydride under an argon atmosphere. Anhydrous acetonitrile was dried by distillation over either phosphorus pentoxide or calcium hydride under an argon atmosphere. C₆D₆ was obtained as anhydrous grade and was stored over a potassium mirror in a Teflon-sealed Schlenk. CDCl₃ and CD₃CN were dried by distillation over calcium hydride under an argon atmosphere and stored over molecular sieves prior to use. Carbene **1**²³, 2,6-diisopropyl-4-tritylaniline²⁵, 4-nitrophenyl isocyanide²⁶, 1,3-bis(2,6-diisopropylphenyl)triazene²⁷, and N-(tert-butyl)-3-phenylprop-2-yn-1-imine²⁴ were synthesized according to literature procedures.

3.5.2: General Methods, Instrumentation, and Measurements

Air and water-sensitive manipulations were carried out in flame-dried glassware equipped with magnetic stir bars under argon using standard Schlenk techniques or in an argon glovebox.

NMR spectra were recorded on Bruker AVANCE 300 MHz, JEOL ECZ 400 MHz, JEOL ECA 500 MHz, or Varian INOVA 500 MHz spectrometers. The ^1H and ^{13}C chemical shift data for each signal are given relative to tetramethylsilane (TMS) in units of δ (ppm) where δ (TMS) = 0 and referenced to the residual solvent resonances. ^{31}P NMR is similarly reported relative to phosphoric acid where δ (H_3PO_4) = 0. ^{27}Al NMR is reported relative to Aluminum nitrate in D_2O where δ ($\text{Al}(\text{NO}_3)_3$) = 0. Splitting patterns are denoted as s (singlet), d (doublet), t (triplet), q (quartet), sept (septet), hept (heptet), m (multiplet) and br (broad).

Mass spectrometry measurements were taken by the UCSD Molecular Mass Spectrometry Facility.

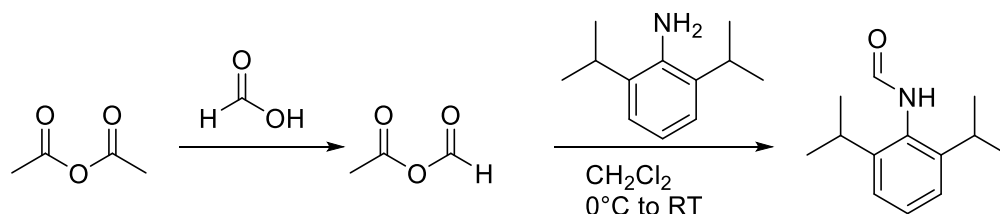
EPR spectra were recorded on a Bruker EMX spectrometer and simulated using EasySpin, a Matlab toolbox.²⁸ All spectra were fit using the garlic function assuming an isotropic fast-motion regime and using the spectrometer-reported microwave frequency for g value calculation.

Data collections for X-ray diffraction experiments were performed on a Bruker APEX-II CCD diffractometer, using graphite-monochromated Mo $\text{K}\alpha$ radiation ($\lambda = 0.71073 \text{ \AA}$) or Cu $\text{K}\alpha$ radiation ($\lambda = 1.54178 \text{ \AA}$). Structures were solved using Olex2²⁹ with the ShelXT³⁰ solution program using Intrinsic Phasing. The Structures were refined using the ShelXL³¹ package using the full-matrix least-squares method for all non-hydrogen atoms. Hydrogen atoms were then placed at calculated positions.

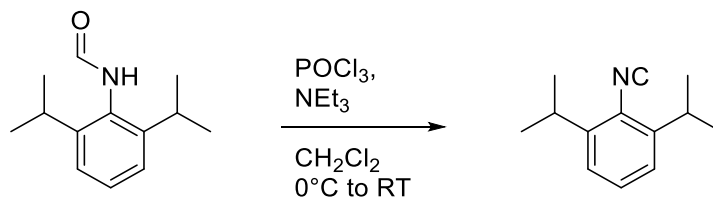
Cyclic voltammetry experiments were performed in an argon glovebox using a CH Instruments model 620E electrochemical analyzer with a glassy carbon working electrode and a platinum wire counter electrode. A Ag/AgNO_3 reference electrode was built from a silver wire

inserted into a glass tube with a Vycor frit filled with a 0.01 M acetonitrile solution of AgNO_3 . Potentials are referenced to the Fc/Fc^+ couple using ferrocene as an internal standard.

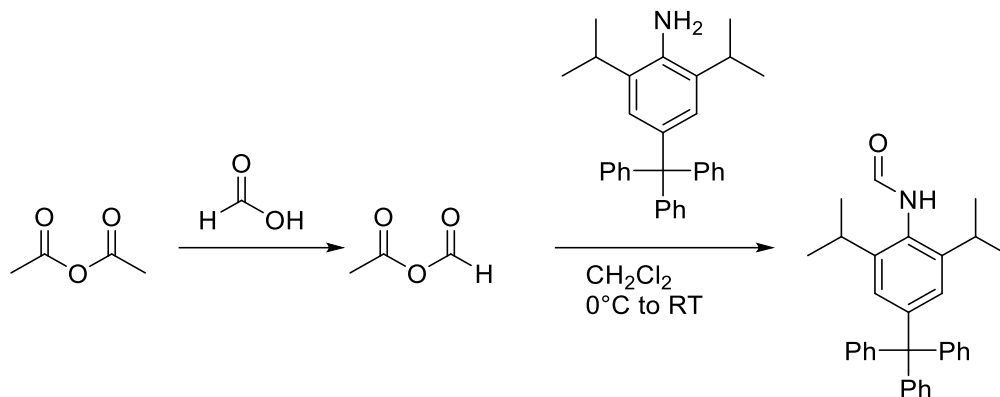
3.5.3: Synthetic and Reaction Procedures



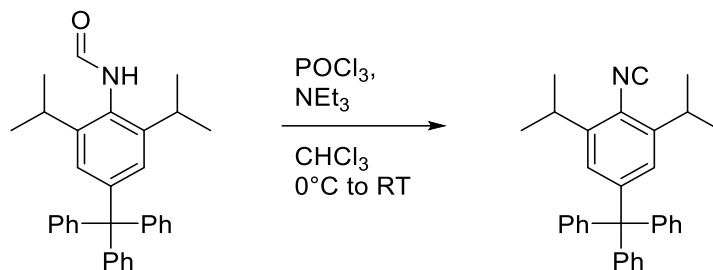
N-(2,6-diisopropylphenyl)formamide. Acetic anhydride (24 mL, 254 mmol) and formic acid (12 mL, 318 mmol) were mixed at room temperature. After stirring for 1.5 hours, the resultant mixed anhydride was added dropwise to a solution of 2,6-diisopropylaniline (32 mL, 170 mmol) in 60 mL dichloromethane at 0°C . The mixture was stirred overnight, slowly warming to room temperature. The solution was quenched by the addition of saturated aqueous sodium carbonate (100 mL, gas evolution) and water and dichloromethane were added to dissolve precipitated solids. The layers were separated, and the organic was washed with more aqueous sodium carbonate (3 X 100 mL), dried over magnesium sulfate, and filtered. The solvent was removed under reduced pressure and the product further dried in vacuum to yield a white solid (32.46 g, 93 %). Spectroscopic data indicated a mixture of rotamers (3:2 ratio). ^1H NMR (CDCl_3 , 400 MHz): δ 8.47 (d, $J = 1.5$ Hz, minor 1H), 8.03 (d, $J = 11.9$ Hz, major 1H), 7.38 – 7.28 (m, 1H), 7.24 – 7.17 (m, 1H), 3.22 (hept, $J = 6.9$ Hz, major 2H), 3.09 (tt, $J = 8.8, 4.3$ Hz, minor 2H), 1.24 – 1.18 (overlapping doublet, 12H). ^{13}C NMR (CDCl_3 , 101 MHz): δ 165.32, 160.74, 146.91, 146.25, 130.01, 129.53, 129.10, 128.97, 123.97, 123.72, 28.93, 28.53, 23.78, 23.76.



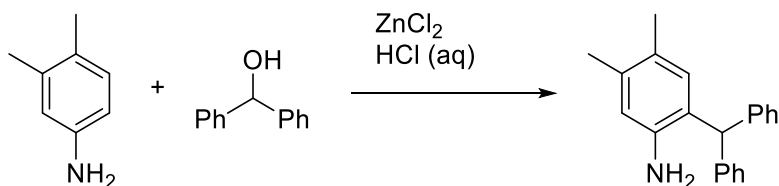
2-isocyano-1,3-diisopropylbenzene. To a solution of N-(2,6-diisopropylphenyl)formamide (9.80 g, 47.7 mmol) and triethylamine (24 mL, 172 mmol) in dry dichloromethane (200 mL) at 0°C was slowly added phosphoryl chloride (5.4 mL, 58 mmol). The mixture was stirred for 3 hours at this temperature, whereupon saturated aqueous sodium carbonate (150 mL) was carefully added (gas evolution). The mixture was stirred a further 3 days, then diluted with water to dissolve precipitated solids. The layers were separated and the aqueous was extracted again with dichloromethane (2 x 100 mL). The combined dichloromethane extracts were dried over magnesium sulfate and filtered. The solvent was removed under reduced pressure to obtain an orange oil that was further dried under vacuum (8.34 g, 93%). The oil was stored in the refrigerator prior to use. ¹H NMR (CDCl₃, 400 MHz): δ 7.33 (t, J = 7.8 Hz), 7.17 (d, J = 7.8 Hz), 3.38 (hept, J = 6.9 Hz), 1.28 (d, J = 6.9 Hz). ¹³C NMR (CDCl₃, 101 MHz): δ 168.36, 145.10, 129.46, 123.65, 123.38, 29.92, 22.74.



N-(2,6-diisopropyl-4-tritylphenyl)formamide. Acetic anhydride (6.76 mL, 71.5 mmol) and formic acid (3.10 mL, 82.2 mmol) were mixed at room temperature. After stirring for 1.5 hours, the resultant mixed anhydride was added slowly to a solution of 2,6-diisopropyl-4-tritylaniline (5.00 g, 11.9 mmol) in dichloromethane (20 mL) at 0 °C. The mixture was stirred overnight, slowly warming to room temperature. The solution was quenched with saturated aqueous sodium carbonate (gas evolution) and diluted with dichloromethane to dissolve residual solids. The layers were separated, and the organic layer was washed twice more with aqueous sodium carbonate and once with water. The dichloromethane layer was dried over magnesium sulfate, filtered, and the solvent was removed in vacuum to give the product as a colorless solid (4.38 g, 82%). ¹H NMR (500 MHz, CDCl₃) δ 8.48 (d, *J* = 1.3 Hz, 1H), 8.06 (d, *J* = 12.0 Hz, 1H), 7.39 – 7.14 (m, 13H), 7.04 (d, *J* = 6.4 Hz, 1H), 3.19 – 2.96 (m, 2H), 1.03 (dd, *J* = 6.8, 1.8 Hz, 7H). ¹³C NMR (126 MHz, CDCl₃) δ 165.09, 160.55, 147.21, 146.84, 146.82, 146.70, 146.55, 146.53, 145.14, 144.65, 131.07, 130.97, 128.33, 128.30, 128.23, 127.95, 127.91, 127.73, 127.50, 127.42, 127.28, 126.96, 126.69, 126.00, 125.88, 28.82, 28.38, 23.55, 23.51.

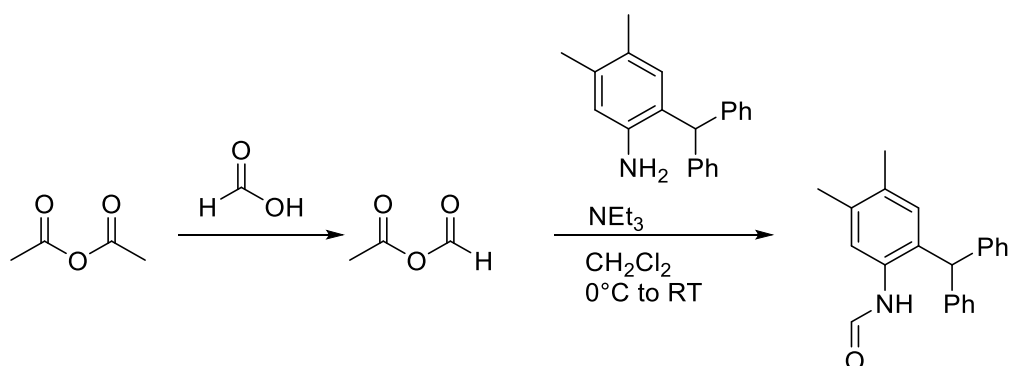


2,6-diisopropyl-4-tritylphenyl isocyanide. To a solution of N-(2,6-diisopropyl-4-tritylphenyl)formamide (1.50 g, 3.35 mmol) and triethylamine (2.10 mL, 15.1 mmol) in dry chloroform (30 mL) at 0 °C was added phosphoryl chloride (0.47 mL, 5.0 mmol) dropwise. The reaction mixture was stirred 16 hours overnight, slowing coming to room temperature and then quenched with 60 mL saturated aqueous sodium carbonate (gas evolution). After stirring for a further 5 hours, the reaction was diluted with an additional 50 mL chloroform and the layers were separated. The organic layer was washed with 60 mL additional sodium carbonate solution and then 120 mL water, adding brine as necessary to break the emulsion. After drying over magnesium sulfate, and filtration, the solvent was removed in vacuum to an oil, which was then precipitated with hexane to give a colorless solid (0.94 g, 65%). ¹H NMR (500 MHz, CDCl₃) δ 7.30 – 7.27 (m, 6H), 7.24 – 7.17 (m, 9H), 7.04 (s, 2H), 3.39 – 3.24 (m, 2H), 1.12 (d, *J* = 6.9 Hz, 12H). ¹³C NMR (126 MHz, CDCl₃) δ 167.97, 148.14, 146.35, 143.78, 131.06, 127.71, 126.49, 126.25, 65.37, 29.89, 22.65.



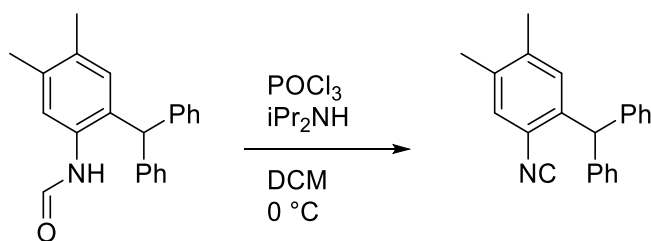
2-benzhydryl-4,5-dimethylaniline. To a mixture of 3,4-dimethylaniline (50 g, 413 mmol) and diphenylmethanol (80 g, 434 mmol) in the melt at 100 °C was added a solution of zinc chloride (56.8 g, 417 mmol) in concentrated hydrochloric acid (110 mL) dropwise over 35

minutes. After the addition was complete, the reaction was heated to 160 °C and then cooled to 130 °C. After remaining at this temperature overnight, the reaction was cooled to room temperature. 250 mL dichloromethane was added to dissolve most of the solids and the reaction was slowly quenched with 250 mL saturated aqueous sodium bicarbonate. The layers were separated, and the aqueous layer was extracted with 25 mL dichloromethane. The combined organic layers were washed with two 250 mL portions of water, using brine as necessary to break emulsions, dried over magnesium sulfate, and filtered. The solvent was removed under reduced pressure to a sludge which was subsequently triturated in 200 mL absolute ethanol. The precipitate was filtered and washed with a small amount of methanol. Additional yield was obtained by evaporating the filtrate under reduced pressure and repeating the trituration to give, over two crops, the product as a colorless solid (53.15 g, 45%). ¹H NMR (400 MHz, CDCl₃) δ 7.34 – 7.24 (m, 6H), 7.20 – 7.14 (m, 4H), 6.73 (s, 1H), 6.50 (s, 1H), 5.63 (s, 1H), 2.23 (s, 3H), 2.11 (s, 3H). ¹³C NMR (101 MHz, CDCl₃) δ 142.72, 139.38, 135.81, 131.32, 129.65, 128.61, 126.67, 119.45, 51.74, 19.50, 19.24.



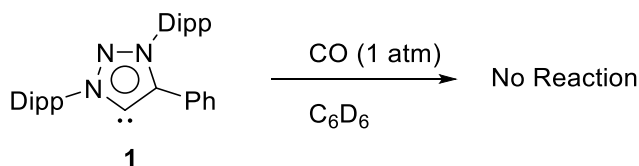
N-(2-benzhydryl-4,5-dimethylphenyl)formamide. Acetic anhydride (100 mL, 1.06 mol) and formic acid (46 mL, 1.22 mol) were mixed at room temperature. After stirring for 1.5 hours, the resultant mixed anhydride was added slowly to a solution of 2-benzhydryl-4,5-dimethylaniline (50 g, 0.174 mol) and triethylamine (25 mL, 0.18 mol) in dichloromethane (400

mL) at 0 °C. The mixture was stirred overnight, coming to room temperature. The reaction was quenched with 400 mL saturated aqueous sodium carbonate. The layers were separated, and the organic layer was washed with two addition 400 mL portions of aqueous sodium carbonate, dried over magnesium sulfate, and filtered. The solvent was removed under reduced pressure and the remaining acid removed by drying in high vacuum to give a crude product containing some residual aniline. The crude was redissolved in ca. 400 mL dichloromethane and poured into ca. 1 L hexane to precipitate. After filtration and drying under vacuum, the product was obtained as a colorless solid (36.02 g, 66%). The NMR shows a ~3:2 ratio of rotamers: ¹H NMR (400 MHz, CDCl₃) δ 8.37 (d, J = 11.4 Hz, major 1H), 8.21 (d, J = 1.7 Hz, minor 1H), 7.57 (s, minor 1H), 7.35 – 7.22 (m, overlapping 6H), 7.08 (dt, J = 8.8, 7.3 Hz, overlapping 4H), 6.98 – 6.85 (m, overlapping 1H), 6.61 (s, major 1H), 6.56 (s, minor 1H), 5.54 (s, major 1H), 5.53 (s, minor 1H), 2.25 (s, major 1H), 2.24 (s, minor 1H), 2.14 (s, major 1H), 2.12 (s, minor 1H). ¹³C NMR (101 MHz, CDCl₃) δ 163.16, 159.36, 142.25, 142.00, 136.31, 135.94, 135.02, 134.43, 134.32, 133.11, 132.14, 131.76, 131.49, 131.27, 129.54, 129.51, 128.90, 128.88, 127.10, 127.03, 126.18, 124.50, 52.11, 51.94, 19.72, 19.63, 19.61, 19.53.

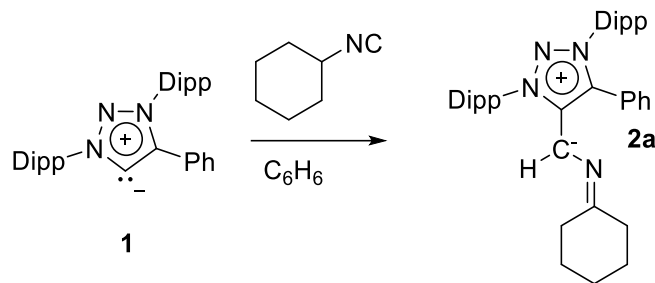


((2-isocyano-4,5-dimethylphenyl)methylene)dibenzene. To a solution of N-(2-benzhydryl-4,5-dimethylphenyl)formamide (4.00 g, 12.7 mmol) and dry diisopropylamine (6.25 mL, 44.6 mmol) in dichloromethane (30 mL) at 0 °C was added phosphoryl chloride (1.8 mL, 19.3 mmol) dropwise. After stirring for 5 hours, 40 mL saturated aqueous sodium bicarbonate

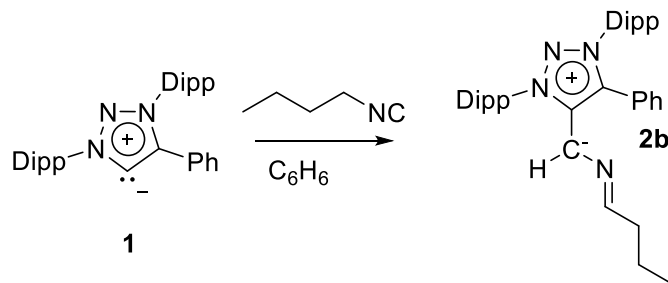
was added to quench (gas evolution). After stirring overnight, the layers were separated and the aqueous was extracted with two 30 mL portions of dichloromethane. The combined organic layers were washed with three 300 mL portions of aqueous sodium bicarbonate, dried over magnesium sulfate, and filtered. The solvent was removed in vacuum to give a light-yellow solid, which was then triturated in hexane and filtered to give the product as a colorless solid. (2.66 g, 71%). ^1H NMR (500 MHz, CDCl_3) δ 7.32 – 7.28 (m, 4H), 7.26 – 7.21 (m, 2H), 7.14 (s, 1H), 7.11 – 7.07 (m, 4H), 6.74 (s, 1H), 5.82 (s, 1H), 2.22 (s, 3H), 2.17 (s, 3H). ^{13}C NMR (126 MHz, CDCl_3) δ 165.83, 141.92, 138.42, 137.83, 136.26, 131.27, 129.57, 128.57, 127.97, 126.80, 124.10, 52.16, 20.10, 19.31. LRMS (EI) m/z Calcd for $\text{C}_{22}\text{H}_{19}\text{N}$ $[\text{M}]^+$ 297.15, found 297.1.



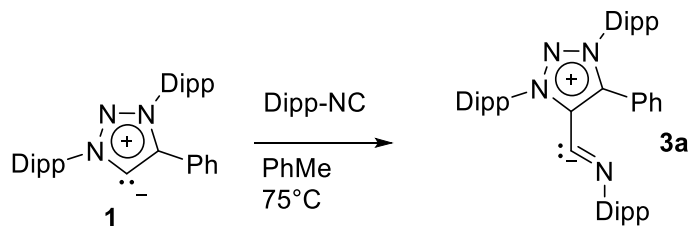
Attempted reaction of carbene 1 with CO. A sample of carbene **1** was loaded into a J-Young NMR tube under argon and dissolved in benzene- d_6 . The sample was subjected to three freeze-pump-thaw cycles in ice and then the headspace was backfilled with 1 atmosphere of CO. After sitting for two hours at room temperature, ^1H and ^{13}C NMR revealed only signals consistent with carbene **1**.



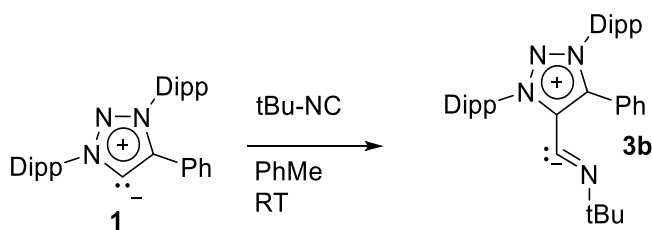
(1,3-bis(2,6-diisopropylphenyl)-5-phenyl-1H-1,2,3-triazol-3-ium-4-yl)(cyclohexylideneamino)-methanide (2a). To a solution of carbene **1** (600 mg, 1.29 mmol) in dry benzene (20 mL) was added cyclohexyl isocyanide (0.18 mL, 1.4 mmol). The reaction mixture was stirred overnight at room temperature, during which time it took on a green color, and then filtered. The solvent was removed in vacuum and the product was further dried in vacuum at 60°C to remove the excess free isocyanide, yielding **2a** as a green powder (572 mg, 78%). Crystals suitable for X-Ray analysis were obtained by the slow evaporation of a hexane solution of **2a**. *Note:* The NMR spectra show extra signals indicative of restricted rotation at the NMR timescale. ¹H NMR (500 MHz, C₆D₆) δ 7.53 (t, *J* = 8.1 Hz, 1H), 7.40 – 7.31 (m, 1H), 7.26 – 7.17 (m, 1H), 7.10 (tt, *J* = 10.3, 5.3 Hz, 1H), 7.03 – 6.96 (m, 1H), 6.96 – 6.84 (m, 2H), 6.77 (t, *J* = 7.4 Hz, 1H), 6.69 (s, 1H), 5.78 (s, 1H) 3.68 – 3.45 (m, 2H), 3.24 – 3.06 (m, 2H), 2.29 – 2.15 (m, 1H), 2.10 – 1.86 (m, 1H), 1.57 – 1.47 (m, 3H), 1.39 (ddd, *J* = 20.2, 14.6, 5.6 Hz, 5H), 1.29 – 1.16 (m, 6H), 0.90 (t, *J* = 7.2 Hz, 3H). ¹³C NMR (126 MHz, C₆D₆) δ 148.30, 147.04, 146.10, 146.07, 143.74, 143.18, 143.14, 141.09, 137.61, 131.18, 131.14, 130.84, 130.63, 130.54, 129.11, 128.61, 128.35, 127.29, 127.05, 126.76, 126.43, 124.97, 124.44, 124.31, 123.12, 121.43, 85.30, 84.84, 39.28, 38.84, 29.48, 29.27, 29.22, 29.14, 28.34, 28.26, 27.11, 27.03, 26.94, 26.83, 26.76, 26.65, 26.14, 26.05, 24.98, 24.52, 24.34, 23.77, 23.46, 22.69, 22.61.



(1,3-bis(2,6-diisopropylphenyl)-4-phenyl-1H-1,2,3-triazol-3-ium-5-yl)(butylideneamino)methanide (2b). To a solution of carbene **1** (600 mg, 1.29 mmol) in benzene was added n-butyl isocyanide (0.15 mL, 1.42 mmol). The reaction was stirred overnight at room temperature, during which time it took on a green color, and then filtered. The solvent was removed in vacuum and the product was further dried in vacuum at 60 °C to remove the excess free isocyanide, yielding **2b** as a green powder (390 mg, 55%). *Note:* The NMR spectra show extra signals indicative of restricted rotation at the NMR timescale. ¹H NMR (500 MHz, C₆D₆) δ 7.58 – 7.51 (m, 1H), 7.41 – 7.19 (m, 2H), 7.14 – 6.95 (m, 2H), 6.95 – 6.83 (m, 2H), 6.80 – 6.75 (m, 1H), 6.69 (s, 1H), 5.83 (s, 1H), 3.60 (dq, *J* = 13.1, 6.5 Hz, 1H), 3.51 – 3.40 (m, 1H), 3.18 – 3.00 (m, 2H), 2.19 – 2.11 (m, 1H), 1.98 (td, *J* = 7.4, 4.7 Hz, 1H), 1.51 (d, *J* = 6.8 Hz, 1H), 1.40 – 1.33 (m, 4H), 1.22 – 1.16 (m, 4H), 0.92 – 0.77 (m, 5H). ¹³C NMR (126 MHz, C₆D₆) δ 147.88, 146.78, 145.69, 145.65, 142.19, 139.89, 137.84, 137.76, 136.90, 136.73, 130.82, 130.76, 130.33, 129.82, 128.94, 127.17, 127.07, 126.75, 126.40, 124.53, 124.06, 123.94, 123.04, 90.82, 90.57, 37.78, 29.86, 29.08, 28.88, 28.83, 28.77, 25.75, 25.65, 24.19, 24.16, 23.96, 23.25, 23.04, 22.30, 22.23, 20.76, 20.13, 14.06, 13.98. HRMS (ESI) *m/z* Calcd for C₃₇H₄₉N₄ [M+H]⁺ 549.3952, found 549.3941.

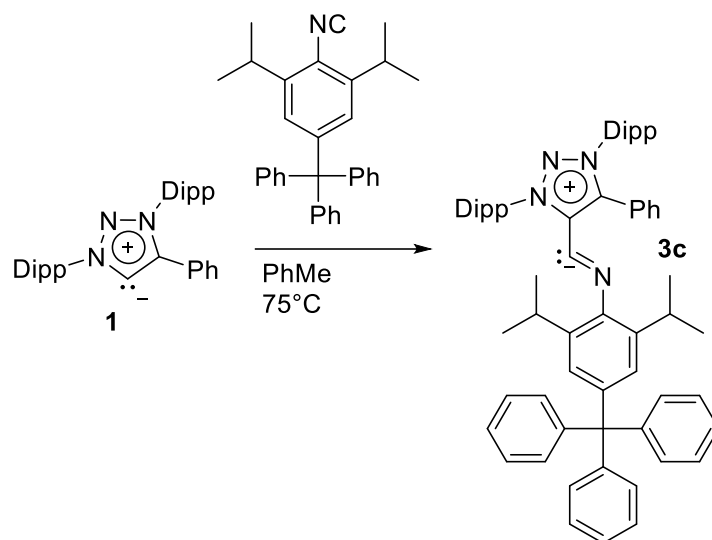


1,3-bis(2,6-diisopropylphenyl)-5-(((2,6-diisopropylphenyl)imino)methaneidyl)-4-phenyl-1H-1,2,3-triazol-3-ium (3a). To a solution of carbene **1** (1.20 g, 2.58 mmol) in dry toluene (15 mL) was added 2,6-diisopropylphenyl isocyanide (0.56 mL, 520 mg, 2.8 mmol) and the reaction mixture was heated to 75°C for 3 hours, whereupon it took on a purple color. The solvent was removed in vacuum and the product dried overnight at 40°C to give a purple, NMR silent solid (1.50 g, 89%). Powder XRD of a sample of **3a** indicated a completely amorphous compound. As such, the solid-state structure cannot be determined directly *Note: the product is amorphous and tends to form a glass on the inside of the reaction flask. Maximization of the yield by scraping the inside of the flask is not recommended as the dissertation author has cracked multiple flasks in this manner.*

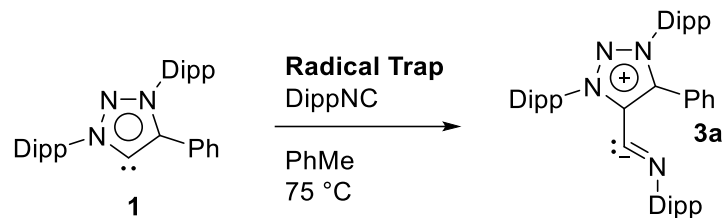


5-((tert-butylimino)methaneidyl)-1,3-bis(2,6-diisopropylphenyl)-4-phenyl-1H-1,2,3-triazol-3-ium (3b). To a solution of carbene **1** (1.20 g, 2.58 mmol) in dry toluene (20 mL) was added tert-butyl isocyanide (0.64 mL, 470 mg, 5.66 mmol) and the reaction mixture was stirred at room temperature for 9 days (1 week minimum), during which time, it took on a purple color. After filtration, the solvent was removed in vacuum to give a purple, NMR silent solid (980 mg, 69%). *Note: the product is amorphous and tends to form a glass on the inside of the reaction*

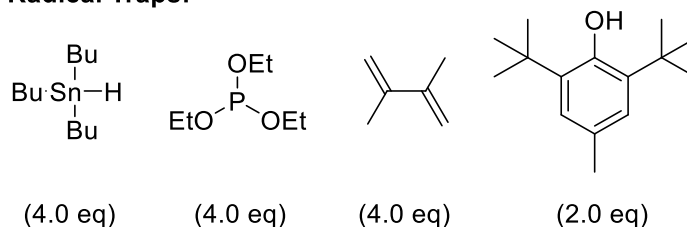
flask. Maximization of the yield by scraping the inside of the flask is not recommended as the dissertation author has cracked multiple flasks in this manner.



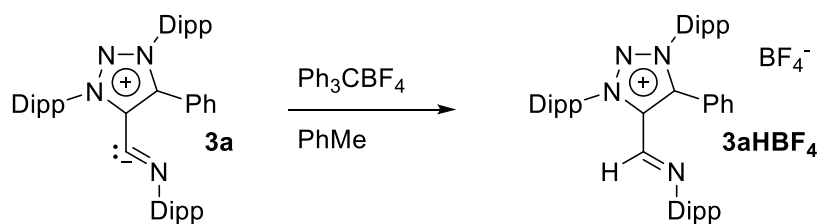
5-(((2,6-diisopropyl-4-tritylphenyl)imino)methaneidyl)-1,3-bis(2,6-diisopropylphenyl)-4-phenyl-1H-1,2,3-triazol-3-ium (3c). Carbene **1** (200 mg, 0.43 mmol) and 2,6-diisopropyl-4-tritylphenyl isocyanide (185 mg, 0.43 mmol) were dissolved in dry toluene (5 mL) and heated to 75 °C for 3 hours. After removal of the solvent in vacuum and drying overnight, **3c** was obtained as a dark purple, NMR silent, amorphous solid (265 mg, 69%) which, similarly to the other molecules **3**, could not be crystallized for XRD analysis.



Radical Traps:

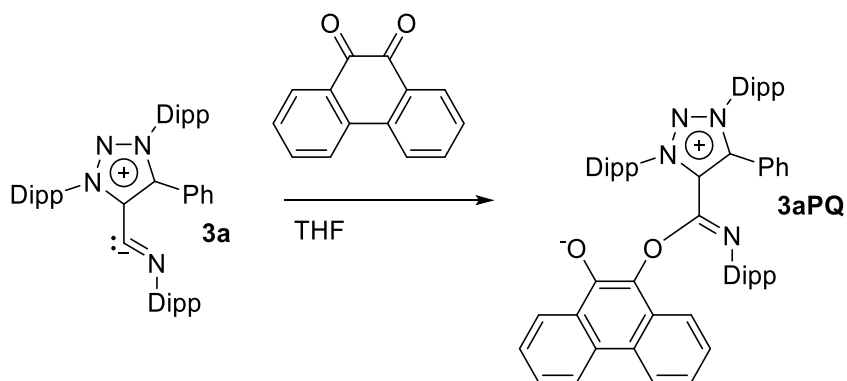


Generalized procedure for checking the formation of 3a with radical traps. To a solution of carbene **1** (300 mg, 0.64 mmol) and the corresponding radical trap (2.58 mmol, 1.29 mmol for BHT) was added 2,6-diisopropylphenyl isocyanide (0.14 mL, 0.71 mmol) and the reaction mixture was heated to 75°C for 3 hours. In all cases, the solution had turned purple. An aliquot of each solution was analyzed by ¹³C NMR (126 MHz), and ³¹P NMR (121 MHz) for triethyl phosphite, revealing only signals for unreacted radical trap.

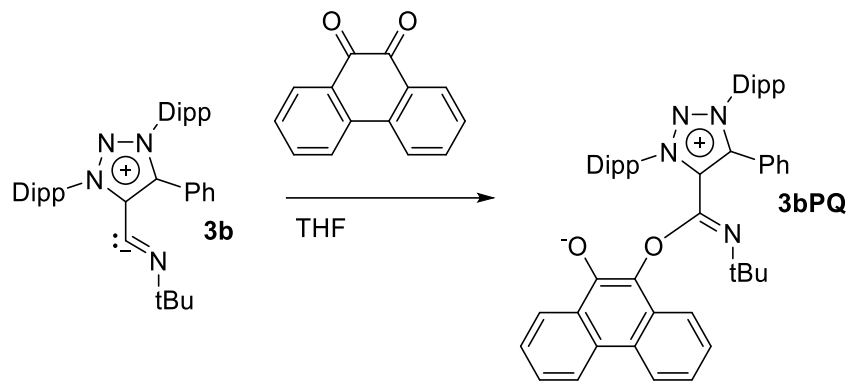


1,3-bis(2,6-diisopropylphenyl)-5-(((2,6-diisopropylphenyl)imino)methyl)-4-phenyl-1H-1,2,3-triazol-3-ium tetrafluoroborate (3aHBF₄). A mixture of **3a** (400 mg, 0.61 mmol) and triphenylcarbenium tetrafluoroborate was dissolved in dry toluene (15 mL). After stirring for 2 hours at room temperature, the solvent was removed in vacuum. The crude product was washed with 15 mL hexane followed by an additional 5 mL hexane. After drying in vacuum, **3aHBF₄** was obtained as a tan solid (398 mg, 88%). Crystals suitable for single crystal XRD analysis

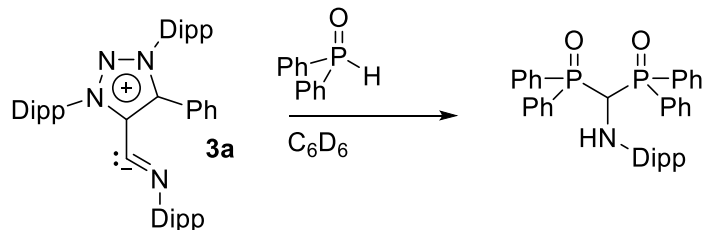
were obtained by vapor diffusion of hexane into a benzene solution of **3a**HBF₄. Analogously, the byproduct bis(triphenylmethyl)peroxide was crystallized by slow evaporation of a benzene solution of the crude product and verified by comparison of the unit cell. ¹H NMR (500 MHz, C₆D₆) δ 7.96 (d, *J* = 8.1 Hz, 1H), 7.40 – 7.27 (m, 4H), 7.11 – 6.95 (m, 14H), 3.12 – 3.03 (m, 2H), 2.92 (dt, *J* = 13.3, 6.6 Hz, 2H), 2.70 (dq, *J* = 12.9, 6.4 Hz, 2H), 1.49 – 1.43 (m, 3H), 1.29 – 0.99 (m, 33H). ¹³C NMR (126 MHz, C₆D₆) δ 148.28, 147.68, 147.21, 147.01, 146.92, 146.82, 144.41, 143.55, 143.21, 138.63, 138.17, 137.90, 133.32, 133.04, 132.15, 131.64, 131.17, 130.98, 130.23, 129.92, 129.85, 129.33, 129.32, 126.61, 126.56, 125.21, 125.10, 124.90, 123.95, 123.00, 121.19, 29.72, 29.66, 29.50, 29.43, 29.32, 28.63, 27.98, 26.21, 26.00, 24.53, 23.04, 22.93.



10-((1,3-bis(2,6-diisopropylphenyl)-4-phenyl-1H-1,2,3-triazol-3-ium-5-yl)((2,6-diisopropylphenyl)imino)methoxy)phenanthren-9-olate (3aPQ). To a mixture of **3a** (400 mg, 0.61 mmol) and phenanthrenequinone (128 mg, 0.61 mmol) was added dry tetrahydrofuran (10 mL). After stirring overnight at room temperature, the solvent was removed in vacuum. The residue was extracted with 10 mL toluene and the solvent was removed in vacuum to give **3aPQ** as a purple solid (292 mg, 55%). Crystals suitable for single crystal XRD analysis were obtained by layering hexane over a tetrahydrofuran solution of **3aPQ**.



10-((1,3-bis(2,6-diisopropylphenyl)-4-phenyl-1H-1,2,3-triazol-3-ium-5-yl)(tert-butylimino)methoxy)phenanthren-9-olate (3bPQ). To a mixture of **3b** (165 mg, 0.3 mmol) and phenanthrenequinone (62 mg, 0.3 mmol) was added dry tetrahydrofuran (8 mL). After stirring overnight at room temperature, the solvent was removed in vacuum. The residue was extracted with 10 mL toluene followed by another 5 mL toluene and the solvent was removed in vacuum to give **3bPQ** as a purple solid (164 mg, 72%).



Reaction of 3a with diphenylphosphine oxide. **3a** (25 mg, 0.038 mmol) and diphenylphosphine oxide (15 mg, 0.077 mmol) were loaded into a J-Young NMR tube under argon and dissolved in benzene-d₆. After sitting overnight at room temperature, ³¹P NMR revealed the phosphine oxide had been mostly converted to a new product. More phosphine oxide (19 mg, 0.93 mmol) was added, and the reaction was allowed to sit overnight. ³¹P NMR indicated unreacted diphenylphosphine oxide, along with some byproducts. Comparison to literature²⁰ indicated the bisphosphonation product of the isocyanide was formed, which was

confirmed by mass spectrometry analysis. ^{31}P NMR (121 MHz, C_6D_6) δ 26.87. LRMS m/z calc for $[\text{M}+\text{Na}]^+$ 614.24, found 614.23

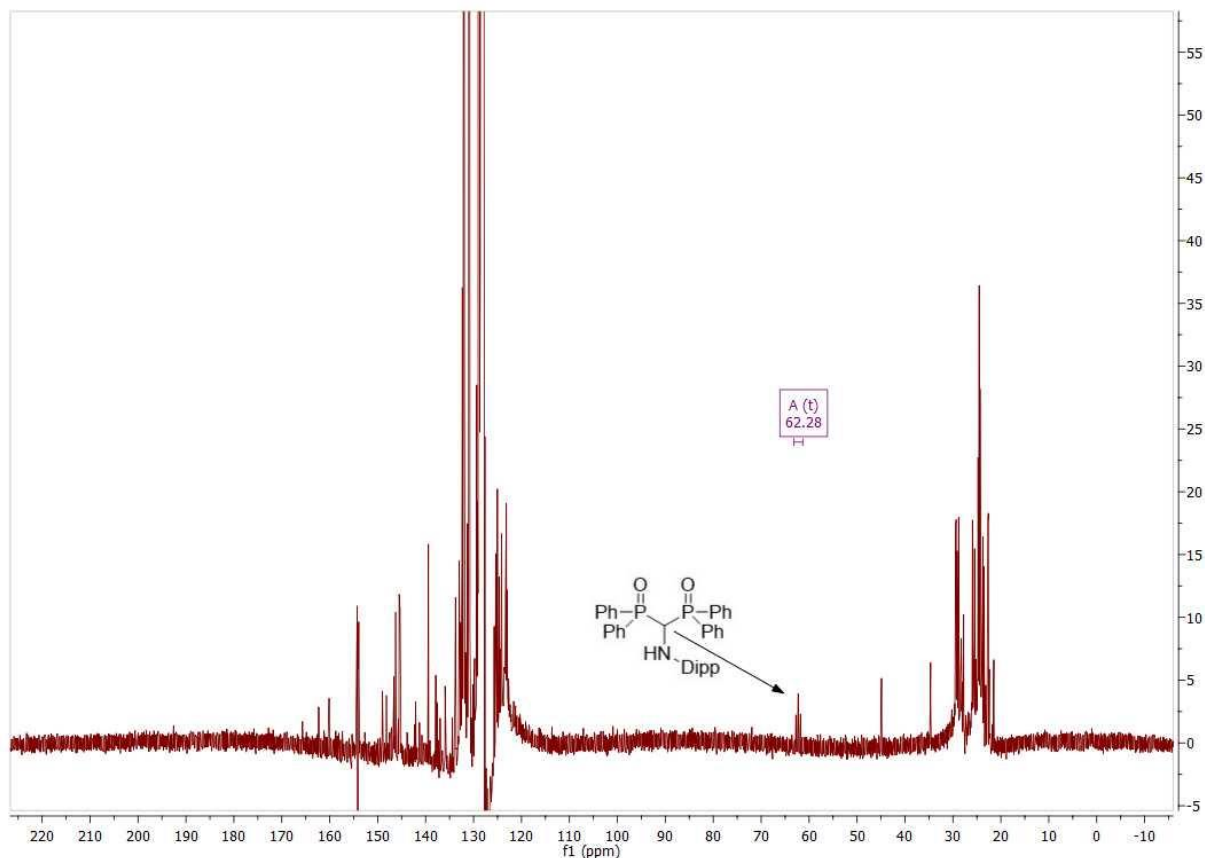
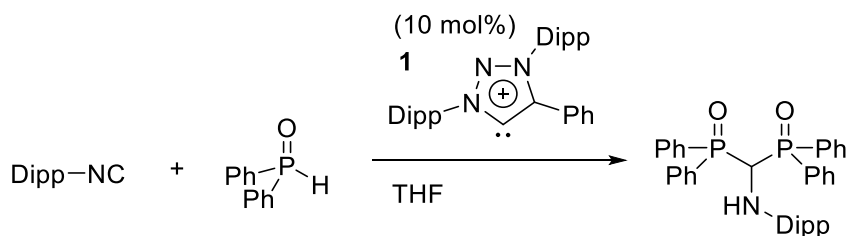


Figure 3.8: ^{13}C NMR (126 MHz, C_6D_6) of the reaction of **3a** with 2x excess diphenylphosphine oxide after sitting overnight. The highlighted signal was characteristic for the product ($J_{\text{C-P}} = 59.9$ Hz). The unphased signal at ~ 154 ppm is an unresolved artifact from the NMR instrument.



Bisphosphonation of isocyanide with diphenylphosphine oxide by MIC catalysis.

2,6-diisopropylphenyl isocyanide (27.8 mg, 0.15 mmol), diphenylphosphine oxide (60 mg, 0.30 mmol), and carbene **1** (6.9 mg, 0.015 mmol) were loaded into a J-Young NMR tube and

dissolved in 0.6 mL dry THF. After sitting overnight at room temperature, ^{31}P NMR revealed approximately 70% conversion of diphenylphosphine oxide to the bisphosphonation product, with only trace impurities. After heating the tube to 70 °C overnight, ^{31}P NMR revealed the starting material:product ratio as unchanged.

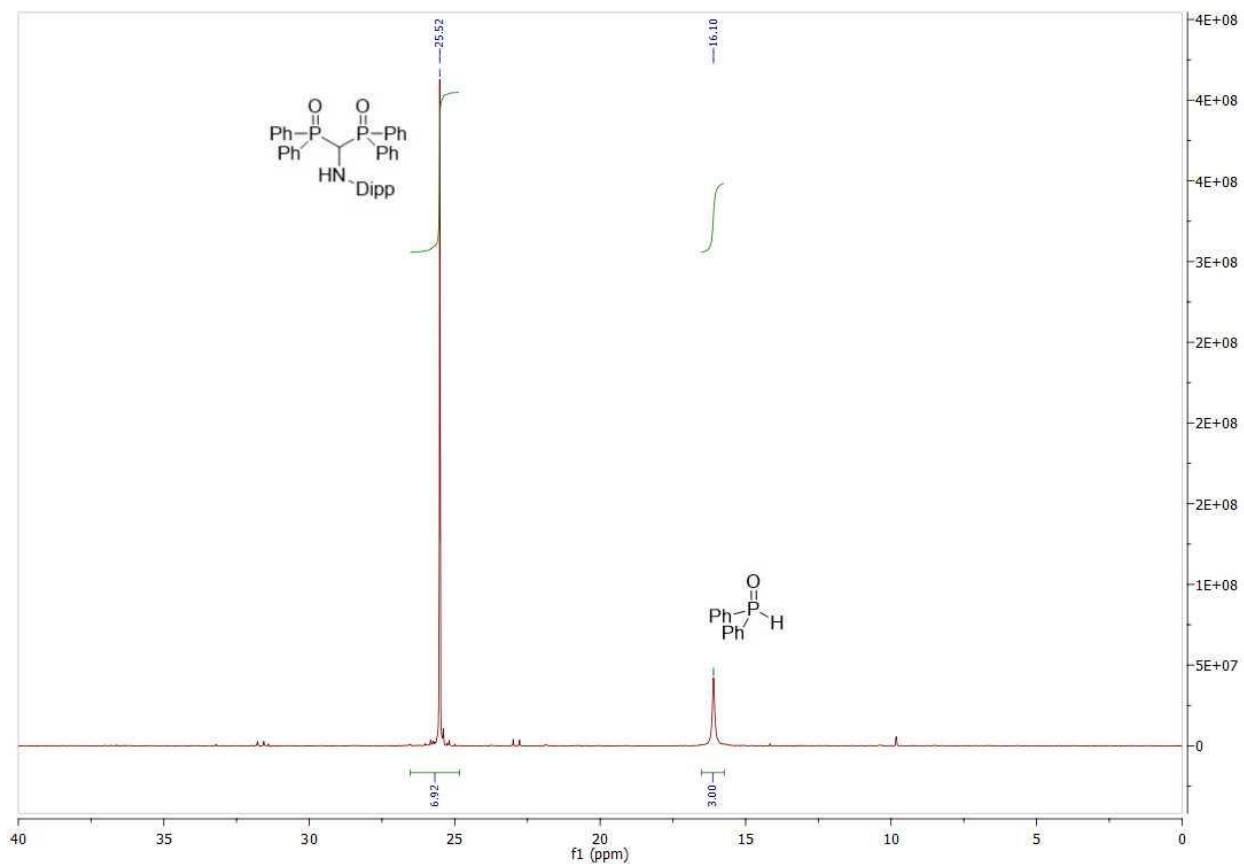
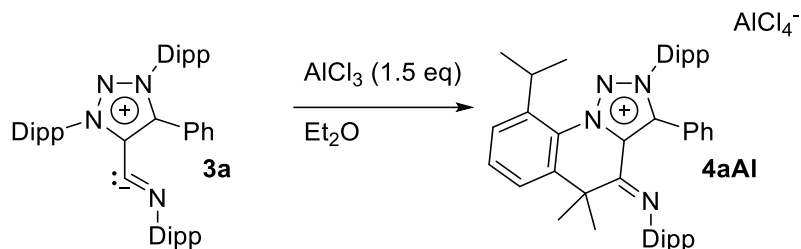
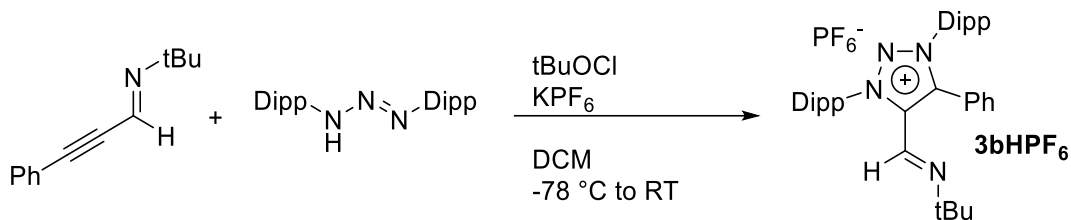


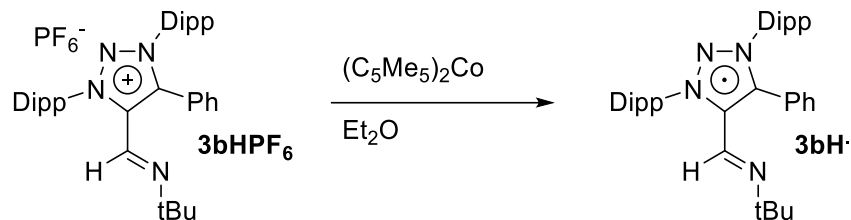
Figure 3.9: ^{31}P NMR (121 MHz, THF) of carbene **1**-catalyzed bisphosphonation of 2,6-diisopropylphenyl isocyanide after overnight at room temperature.



2-(2,6-diisopropylphenyl)-4-((2,6-diisopropylphenyl)imino)-9-isopropyl-5,5-dimethyl-3-phenyl-4,5-dihydro-2H-[1,2,3]triazolo[1,5-a]quinolin-10-ium tetrachloroaluminate (4aAl). A mixture of **3a** (196 mg, 0.30 mmol) and aluminum trichloride (60 mg, 0.45 mmol) were dissolved in diethyl ether (10 mL) at room temperature. The solution gradually became yellow orange with the formation of a precipitate. After stirring overnight, the solution was filtered and the precipitate was washed with 5 mL ether and dried in vacuum to give **4aAl** as a yellow solid (125 mg, 51%). Crystals suitable for single crystal XRD analysis were obtained by vapor diffusion of pentane into a dichloromethane solution of **4aAl**. ^1H NMR (500 MHz, CDCl_3) δ 8.15 (s, 1H), 7.87 – 7.29 (m, 7H), 7.27 – 7.16 (m, 2H), 7.13 – 6.97 (m, 1H), 6.99 – 6.78 (m, 1H), 6.70 (d, $J = 6.9$ Hz, 1H), 6.50 (d, $J = 7.3$ Hz, 1H), 6.17 (d, $J = 7.7$ Hz, 1H), 2.58 – 2.48 (m, 1H), 2.48 – 2.39 (m, 1H), 2.34 (dp, $J = 13.6, 6.9$ Hz, 1H), 2.20 – 2.09 (m, 1H), 2.02 (br, $J = 9.7$ Hz, 1H), 1.38 (d, $J = 6.8$ Hz, 3H), 1.31 (d, $J = 6.7$ Hz, 3H), 1.21 (ddd, $J = 19.4, 11.3, 5.6$ Hz, 9H), 1.13 – 1.04 (m, 6H), 0.92 (t, $J = 7.6$ Hz, 6H), 0.79 (d, $J = 6.8$ Hz, 3H). ^{13}C NMR (126 MHz, CDCl_3) δ 146.16, 145.81, 145.73, 145.68, 145.24, 143.16, 142.54, 142.34, 138.01, 137.71, 136.58, 134.13, 133.78, 133.53, 133.06, 132.40, 130.99, 130.53, 130.21, 129.97, 129.59, 128.71, 128.31, 128.04, 127.11, 126.23, 125.48, 125.11, 124.83, 123.88, 122.92, 119.75, 119.34, 45.85, 30.03, 29.91, 29.87, 29.31, 28.57, 27.97, 26.09, 25.60, 24.28, 24.12, 23.61, 23.05, 22.96, 21.97, 20.35. ^{27}Al NMR (104 MHz, CDCl_3) δ 106.36.



4-((tert-butylimino)methyl)-1,3-bis(2,6-diisopropylphenyl)-5-phenyl-1H-1,2,3-triazol-3-ium hexafluorophosphate (3bHPF₆). 1,3-bis(2,6-diisopropylphenyl)triazene (2.19 g, 6 mmol) and anhydrous potassium hexafluorophosphate (1.47 g, 8 mmol) were dissolved in dry dichloromethane (40 mL) and chilled at -78 °C. Tert-butyl hypochlorite (1.00 mL, 8.8 mmol) was added slowly and the reaction was stirred at this temperature. After 30 minutes, N-(tert-butyl)-3-phenylprop-2-yn-1-imine (1.67 g, 9 mmol) was added dropwise and the reaction was allowed to slowly come to room temperature overnight. The reaction was filtered, and the solid extracted twice with 10 mL additional dichloromethane. The solvent was removed in vacuum and the residue was triturated in 120 mL diethyl ether. Filtration and washing of the precipitate with excess diethyl ether followed by drying in vacuum gave **3bHPF₆** as a tan solid (2.77 g, 66%). ¹H NMR (400 MHz, CD₃CN) δ 8.11 (s, 1H), 7.70 (td, *J* = 7.8, 3.0 Hz, 2H), 7.61 (t, *J* = 7.4 Hz, 2H), 7.56 – 7.43 (m, 8H), 2.51 – 2.36 (m, 4H), 1.23 (d, *J* = 6.7 Hz, 6H), 1.18 – 1.12 (m, 12H), 1.03 (d, *J* = 6.7 Hz, 6H), 0/99 (s, 9H). ¹³C NMR (101 MHz, CD₃CN) δ 156.40, 146.58, 146.13, 145.51, 141.31, 137.96, 134.44, 133.59, 133.33, 131.36, 130.25, 129.54, 126.36, 125.62, 121.89, 60.79, 29.99, 29.87, 28.74, 25.88, 25.31, 23.15, 22.47.



Radical 3bH \cdot . A mixture of **3bHPF $_6$** and decamethyl cobaltocene was dissolved in dry diethyl ether (5 mL) at room temperature, whereupon the solution immediately took on a purple color. After stirring for 15 minutes, the solvent was removed in vacuum and the residue extracted with 5 mL dry toluene. After evaporation of the toluene and drying in vacuum, **3bH \cdot** was obtained as a purple solid, which was then analyzed by EPR.

3.5.4: EPR Fitting Data

Table 3.1: Full EPR fitting parameters for **3a**.

3a Fitting Parameter	Value
g	2.00388255894734
N1 coupling	26.18324800000000 MHz
N2 coupling	11.81065200000000 MHz
N3 coupling	7.518644000000000 MHz
N4 coupling	4.800236000000000 MHz
H1 coupling	5.141836000000000 MHz
H2 coupling	1.322924400000000 MHz
Gaussian linewidth	0.0699354170441811 mT
Lorentzian linewidth	0.0950000000000000mT

Table 3.2: Full EPR fitting parameters for **3b**.

3b Fitting Parameter	Value
g	2.00355158371854
N1 coupling	28.4908540265756 MHz
N2 coupling	12.4297347417166 MHz
N3 coupling	12.2014019118744 MHz
N4 coupling	2.17001689595204 MHz
H1 coupling	4.09629005662958 MHz
H2 coupling	2.74814904387236 MHz
H3 coupling	2.66627317922512 MHz
Gaussian linewidth	0.0950000000000000 mT
Lorentzian linewidth	0.0450000000000000 mT

Table 3.3: Full EPR fitting parameters for **3aPQ**.

3aPQ Fitting Parameter	Value
g	2.00520000000000
N1 coupling	4.47126098767523 MHz
H1 coupling	3.95702164981726 MHz
H2 coupling	3.50727696351760 MHz
Gaussian linewidth	0.0959093842951797 mT

Table 3.4: Full EPR fitting parameters for **3bPQ**.

3bPQ Fitting Parameter	Value
g	1.99160579378192
N1 coupling	3.62841358196700 MHz
H1 coupling	3.72003865106740 MHz
H2 coupling	3.53358914295771 MHz
Gaussian linewidth	0.0590673385967844 mT
Lorentzian linewidth	0.0470668799628923 mT

Table 3.5: Full EPR fitting parameters for **3bH**.

3bH Fitting Parameter	Value
g	2.00395365521835
N1 coupling	19.6250935499864 MHz
N2 coupling	10.7397918143066 MHz
N3 coupling	7.21499137675836 MHz
N4 coupling	6.81911220000000 MHz
H1 coupling	21.4138032931654 MHz
H2 coupling	6.19631081339986 MHz
H3 coupling	5.37331096545860 MHz
Gaussian linewidth	0.0238404431800017 mT
Lorentzian linewidth	0.0246652067406737 mT

3.5.5: Electrochemical Data

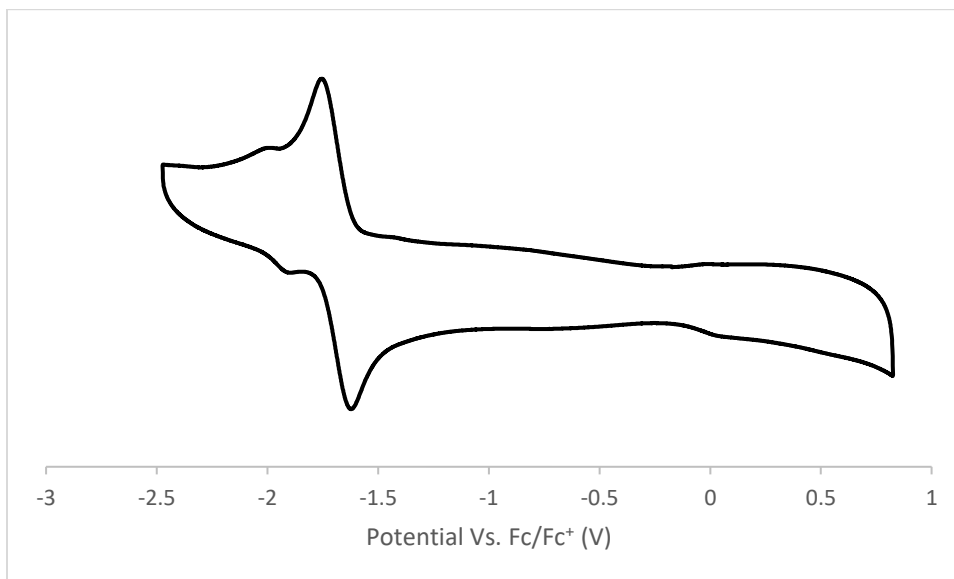


Figure 3.9: Cyclic voltammogram of **3bHPF₆** in THF (0.1 M nBu₄NPF₆) at room temperature (scan rate: 100 mV/s). The **3bHPF₆/3bH[•]** couple is at $E_{1/2} = -1.69$ V.

3.5.6: Computational Details

Computational studies were performed using density functional theory (DFT). Singlet-triplet gaps were calculated at three levels of theory: M06-2X/6-31G**//cc-pVTZ(-f) (method **1**), M06-2X/6-31G**//cc-pVTZ(-f) with the Truhlar correction applied (method **2**), and CAM-B3LYP/6-31G**//M06-2X/cc-pVTZ(-f) (method **3**). In all cases, the Poisson Boltzmann solvation model for toluene was used. Method **2** was considered the most reliable for representing the actual structure.

Table 3.6: calculated singlet-triplet gaps for **3a**, **3b**, and **3aPQ** at three different levels of theory.

Molecule	S-T gap (method 1) (kcal/mol)	S-T gap (method 2) (kcal/mol)	S-T gap (method 3) (kcal/mol)
3a	14.43	14.13	11.11
3b	16.23	12.91	16.18
3aPQ	33.71	31.65	25.89

3.5.7: X-ray Crystallographic Data

Crystal data and structure refinement for **2a**:

An X-ray-quality crystal of **2a** was obtained by slow evaporation of a hexane solution. Thermal ellipsoids were at the 50% probability level. Hydrogen atoms were omitted for clarity. Two molecules crystallized in the asymmetric unit.

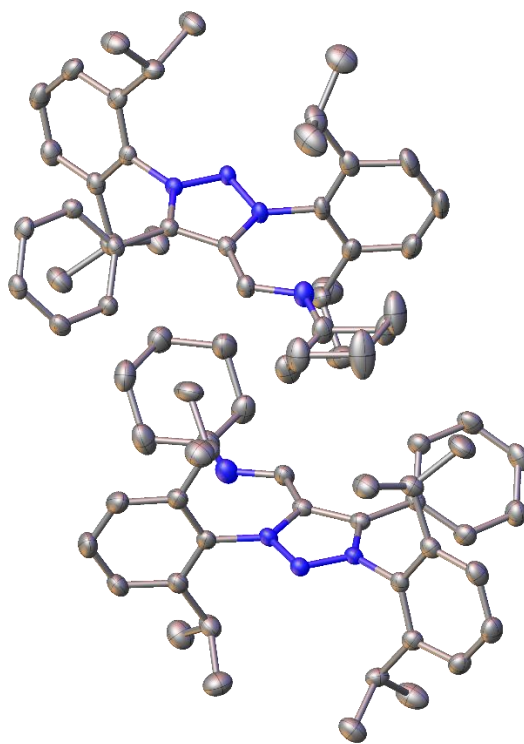


Table 3.7: Crystal Data and Structure Refinement for **2a**.

Empirical formula	C ₃₉ H ₅₀ N ₄
Formula weight	574.83
Temperature/K	100.0
Crystal system	orthorhombic
Space group	P2 ₁ 2 ₁ 2 ₁
a/Å	10.0543(2)
b/Å	24.7801(3)
c/Å	27.0664(4)
α/°	90

Table 3.7 continued: Crystal Data and Structure Refinement for **2a**.

$\beta/^\circ$	90
$\gamma/^\circ$	90
Volume/ \AA^3	6743.50(19)
Z	8
$\rho_{\text{calc}}/\text{g}/\text{cm}^3$	1.132
μ/mm^{-1}	0.502
F(000)	2496.0
Crystal size/ mm^3	$0.42 \times 0.4 \times 0.275$
Radiation	CuK α ($\lambda = 1.54178$)
2 Θ range for data collection/ $^\circ$	4.834 to 138.714
Index ranges	$-12 \leq h \leq 11, -29 \leq k \leq 30, -32 \leq l \leq 32$
Reflections collected	88952
Independent reflections	12589 [$R_{\text{int}} = 0.0313, R_{\text{sigma}} = 0.0196$]
Data/restraints/parameters	12589/0/792
Goodness-of-fit on F^2	1.043
Final R indexes [$I \geq 2\sigma(I)$]	$R_1 = 0.0408, wR_2 = 0.1099$
Final R indexes [all data]	$R_1 = 0.0428, wR_2 = 0.1118$
Largest diff. peak/hole / $e \text{\AA}^{-3}$	0.50/-0.21
Flack parameter	0.6(4)

Table 3.8: Fractional atomic coordinates ($\times 10^4$) and Equivalent Isotropic Displacement Parameters ($\text{\AA}^2 \times 10^3$) for **2a**. U_{eq} is defined as 1/3 of the trace of the orthogonalized U_{IJ} tensor.

Atom	x	y	z	$U(\text{eq})$
N1	10287.6(18)	6584.1(7)	5910.9(7)	19.5(4)
N1A	9877.2(18)	3360.2(7)	3946.2(7)	20.7(4)
N2	11501.1(18)	6369.0(7)	5928.6(7)	20.3(4)
N3	11236.9(18)	5834.6(7)	6016.1(7)	21.8(4)
N3A	8975.0(19)	4092.6(7)	3738.0(7)	22.2(4)
N2A	8688.6(19)	3586.7(7)	3913.2(7)	21.9(4)
N4	10035(2)	4784.3(8)	6271.5(8)	30.2(4)
N4A	10188(2)	5070.9(9)	3322.9(9)	34.6(5)
C3	7859(2)	6369.9(9)	5990.0(8)	20.4(4)
C2A	10912(2)	3677.9(9)	3809.7(8)	21.6(4)
C9A	9951(2)	2803.3(9)	4111.7(8)	22.3(4)
C3A	12324(2)	3526.8(9)	3838.1(8)	23.2(5)
C21A	7878(2)	4456.8(9)	3654.6(9)	24.0(5)
C1A	10336(2)	4183.9(9)	3664.2(8)	22.6(4)

Table 3.8 continued: Fractional atomic coordinates ($\times 10^4$) and Equivalent Isotropic Displacement Parameters ($\text{\AA}^2 \times 10^3$) for **2a**. U_{eq} is defined as 1/3 of the trace of the orthogonalized U_{ij} tensor.

Atom	<i>x</i>	<i>y</i>	<i>z</i>	$U(\text{eq})$
C9	10198(2)	7156.2(8)	5807.0(8)	21.1(4)
C1	9881(2)	5716.9(9)	6054.6(8)	22.1(4)
C33	9294(2)	5230.0(9)	6151.3(9)	26.0(5)
C2	9280(2)	6232.5(9)	5979.8(8)	20.7(4)
C6	5110(2)	6555.0(9)	6046.6(9)	27.4(5)
C26	12766(2)	5141.5(9)	5721.2(10)	29.1(5)
C4A	12805(2)	3014.2(10)	3719.1(10)	30.0(5)
C10	9867(2)	7313.4(9)	5328.0(9)	25.1(5)
C10A	9643(2)	2399.5(9)	3772.1(9)	25.5(5)
C4	6945(2)	6016.5(9)	5767.0(9)	25.2(5)
C14A	10382(2)	2701.2(9)	4595.4(9)	25.6(5)
C13A	10538(3)	2162.0(10)	4726.7(10)	32.4(5)
C7	5998(2)	6912.4(10)	6260.7(9)	28.4(5)
C26A	7301(2)	4467.2(9)	3186.0(10)	27.9(5)
C14	10445(2)	7516.3(9)	6191.9(9)	25.2(5)
C12A	10276(3)	1752.9(10)	4397.3(10)	35.0(6)
C15A	9139(3)	2521.9(10)	3253.4(9)	28.5(5)
C21	12355(2)	5481.6(9)	6104.3(9)	25.3(5)
C30A	7800(3)	4117.0(11)	2763.7(9)	32.8(5)
C5	5591(2)	6109.4(10)	5797.2(10)	29.0(5)
C33A	10927(2)	4639.8(9)	3482.5(9)	27.6(5)
C22A	7461(2)	4787.5(10)	4042.0(10)	28.6(5)
C8	7358(2)	6821.9(9)	6233.1(9)	24.9(5)
C15	9696(3)	6900.3(10)	4915.9(9)	30.1(5)
C11A	9821(3)	1866.5(9)	3925.0(10)	30.4(5)
C18	10805(3)	7324.9(10)	6709.6(9)	29.8(5)
C18A	10598(3)	3158.8(10)	4961.5(9)	30.1(5)
C30	12116(3)	5144.0(10)	5214.9(10)	33.2(6)
C8A	13252(2)	3918.0(10)	3982.3(10)	30.1(5)
C11	9774(3)	7865.1(10)	5239.1(10)	33.2(5)
C27A	8146(3)	4794.5(11)	4540.1(10)	33.6(6)
C6A	15053(3)	3291.4(11)	3887.9(10)	34.2(6)
C23A	6403(3)	5135.5(10)	3949.7(11)	36.3(6)
C25	13804(3)	4786.1(10)	5821.7(12)	37.3(6)

Table 3.8 continued: Fractional atomic coordinates ($\times 10^4$) and Equivalent Isotropic Displacement Parameters ($\text{\AA}^2 \times 10^3$) for **2a**. U_{eq} is defined as 1/3 of the trace of the orthogonalized U_{ij} tensor.

Atom	<i>x</i>	<i>y</i>	<i>z</i>	$U(\text{eq})$
C7A	14599(3)	3797.5(11)	4008.8(10)	35.3(6)
C13	10356(3)	8064.4(9)	6081.0(10)	32.3(5)
C5A	14152(3)	2900.5(11)	3744.6(11)	34.8(6)
C25A	6240(3)	4820.9(11)	3113.4(11)	35.6(6)
C23	13974(3)	5120.6(11)	6652.8(11)	39.5(6)
C34	9507(3)	4324.2(10)	6380.9(10)	35.1(6)
C22	12953(2)	5491.2(10)	6568.1(10)	30.7(5)
C12	10022(3)	8234.6(10)	5610.7(11)	36.8(6)
C24A	5795(3)	5152.4(11)	3492.0(12)	39.7(6)
C27	12475(3)	5864.8(12)	6977.2(10)	39.1(6)
C31A	6934(3)	3619.2(12)	2692.8(11)	43.7(7)
C34A	10712(3)	5495.8(11)	3128.1(11)	37.3(6)
C20	9925(3)	7579.8(12)	7104.7(10)	39.9(6)
C24	14388(3)	4770.1(11)	6283.8(13)	42.3(7)
C19	12271(3)	7441.1(13)	6814.5(11)	42.6(7)
C16	11043(3)	6795.1(15)	4672.6(11)	46.0(7)
C37A	11679(3)	6604.1(11)	3216.9(12)	42.6(7)
C17	8658(3)	7069.9(13)	4533.4(11)	40.6(6)
C35	10395(3)	3885.1(11)	6567.6(12)	41.3(6)
C16A	7785(3)	2255.3(12)	3168.1(11)	40.1(6)
C19A	9280(3)	3296.2(12)	5213.8(11)	40.4(6)
C20A	11673(3)	3036.5(13)	5343.0(11)	45.2(7)
C39	8048(3)	4186.3(12)	6394.4(12)	41.2(7)
C32A	7904(3)	4433.5(13)	2278.2(11)	44.4(7)
C32	11583(3)	4587.7(12)	5076.8(12)	44.4(7)
C29A	8756(3)	5355.6(13)	4636.0(12)	44.3(7)
C39A	12173(3)	5619.5(11)	3059.0(12)	41.0(7)
C38A	12548(3)	6121.9(11)	3348.9(13)	44.6(7)
C17A	10126(3)	2348.9(15)	2858.3(10)	46.9(7)
C28	13592(3)	6083.9(14)	7297.7(11)	49.0(7)
C36A	10204(3)	6468.8(12)	3272.8(11)	43.3(7)
C38	7635(3)	4012.3(13)	6908.4(13)	46.8(7)
C28A	7202(3)	4630.5(14)	4956.1(11)	47.0(7)
C29	11432(3)	5582.2(17)	7286.8(13)	57.2(9)

Table 3.8 continued: Fractional atomic coordinates ($\times 10^4$) and Equivalent Isotropic Displacement Parameters ($\text{\AA}^2 \times 10^3$) for **2a**. U_{eq} is defined as 1/3 of the trace of the orthogonalized U_{ij} tensor.

Atom	<i>x</i>	<i>y</i>	<i>z</i>	$U(\text{eq})$
C31	13071(4)	5346.7(14)	4815.4(12)	50.2(8)
C35A	9819(3)	5959.1(12)	2987.7(12)	47.2(7)
C36	10004(4)	3738.0(16)	7087.0(15)	62.6(10)
C37	8528(4)	3568.0(17)	7103.9(17)	72.0(13)

Table 3.9: Anisotropic Displacement Parameters ($\text{\AA}^2 \times 10^3$) for **2a**. The anisotropic displacement factor exponent takes the form: $-2\pi^2[h^2a^{*2}U_{11}+2hka^*b^*U_{12}+\dots]$.

Atom	U_{11}	U_{22}	U_{33}	U_{23}	U_{13}	U_{12}
N1	15.5(9)	20.9(8)	22.2(9)	-0.3(7)	0.4(7)	-0.1(7)
N1A	16.7(9)	22.0(8)	23.4(9)	-1.0(7)	-2.3(7)	-1.9(7)
N2	16.1(9)	20.3(9)	24.6(9)	2.1(7)	-0.8(7)	1.0(7)
N3	15.4(9)	20.8(9)	29.1(9)	3.7(7)	-0.4(7)	0.9(7)
N3A	17.3(9)	22.2(9)	27.2(9)	0.5(7)	-3.2(7)	-2.3(7)
N2A	18.6(9)	22.7(9)	24.5(9)	-0.5(7)	-1.3(7)	-1.4(7)
N4	25.9(10)	28.6(10)	36.2(11)	7.8(8)	2.0(9)	1.5(8)
N4A	27.7(11)	32.7(11)	43.3(12)	5.6(9)	-4.0(9)	-3.0(9)
C3	16.5(10)	22.9(10)	21.8(10)	4.4(8)	-0.9(8)	-0.5(8)
C2A	19.5(11)	22.9(10)	22.5(10)	-2.4(8)	0.9(8)	-3.3(8)
C9A	15.1(10)	23.0(10)	28.8(11)	2.7(8)	1.6(8)	-1.5(8)
C3A	18.9(11)	27.6(11)	23.1(11)	2.5(9)	0.1(8)	-1.5(9)
C21A	17.3(11)	21.5(10)	33.1(12)	-0.7(9)	-1.3(9)	-3.3(9)
C1A	20.0(11)	25.7(11)	22.2(10)	-2.5(8)	-1.7(8)	-2.7(9)
C9	14.2(10)	20.4(10)	28.7(11)	2.2(8)	3.0(9)	-1.4(8)
C1	18.9(11)	24.8(10)	22.7(10)	1.7(8)	-0.4(8)	0.2(9)
C33	19.9(11)	25.8(11)	32.2(12)	4.0(9)	0.5(9)	1.7(9)
C2	17.9(10)	22.5(10)	21.9(10)	0.3(8)	-0.1(8)	-1.6(8)
C6	16.1(11)	30.2(11)	35.7(12)	6.7(9)	1.7(9)	1.0(9)
C26	19.6(11)	21.4(11)	46.2(15)	0.4(10)	-0.1(10)	-2.2(9)
C4A	21.9(12)	31.4(12)	36.8(13)	-1.7(10)	0.4(10)	-3.9(10)
C10	17.5(10)	26.7(11)	31.0(12)	4.7(9)	0.6(9)	0.0(9)
C10A	20.1(11)	25.6(11)	30.7(12)	-0.1(9)	2.1(9)	-3.9(9)
C4	19.9(11)	24.5(11)	31.3(12)	-1.1(9)	-1.6(9)	-0.6(9)
C14A	18.2(11)	30.2(11)	28.3(11)	2.0(9)	0.3(9)	-2.6(9)

Table 3.9 continued: Anisotropic Displacement Parameters ($\text{\AA}^2 \times 10^3$) for **2a**. The anisotropic displacement factor exponent takes the form: $-2\pi^2[h^2a^{*2}U_{11}+2hka^*b^*U_{12}+\dots]$.

Atom	U_{11}	U_{22}	U_{33}	U_{23}	U_{13}	U_{12}
C13A	28.5(13)	35.7(13)	33.1(13)	9.9(10)	-3.9(10)	-2.4(11)
C7	21.8(11)	26.6(11)	36.7(13)	-0.8(10)	6.2(10)	2.7(9)
C26A	22.1(12)	26.4(11)	35.2(13)	0.3(10)	-3.9(10)	-2.6(9)
C14	16.6(11)	25.6(11)	33.4(12)	-3.0(9)	5.0(9)	-0.6(9)
C12A	32.3(14)	26.1(12)	46.7(15)	7.2(10)	0.4(12)	-0.3(10)
C15A	32.0(13)	25.9(11)	27.7(12)	-2.9(9)	-1.5(10)	-4.6(10)
C21	15.7(11)	21.6(10)	38.7(13)	8.0(9)	-0.4(9)	0.5(9)
C30A	28.4(13)	40.4(14)	29.7(12)	-1.4(11)	-5.5(10)	2.9(11)
C5	20.5(11)	29.1(11)	37.3(13)	3.2(10)	-4.4(10)	-5.0(9)
C33A	21.0(12)	26.2(11)	35.6(13)	1.4(9)	-3.5(10)	-2.1(9)
C22A	20.3(11)	26.5(11)	39.0(14)	-2.7(10)	-2.2(10)	-2.6(9)
C8	19.7(11)	25.4(11)	29.5(12)	-1.0(9)	0.3(9)	-3.4(9)
C15	30.3(13)	35.4(12)	24.6(11)	5.3(10)	-0.5(10)	-3.0(11)
C11A	28.6(12)	24.4(11)	38.3(13)	-1.1(10)	1.2(10)	-3.4(10)
C18	27.0(13)	32.6(12)	29.8(12)	-6.8(10)	-1.8(10)	-0.9(10)
C18A	27.2(12)	34.5(12)	28.6(12)	0.5(10)	-2.7(10)	-4.9(10)
C30	24.2(12)	32.4(12)	43.1(15)	-8.2(11)	-1.8(11)	2.9(10)
C8A	22.1(12)	31.1(12)	37.0(13)	-3.2(10)	-0.5(10)	-3.9(10)
C11	29.3(13)	31.9(12)	38.4(13)	11.1(10)	-0.7(11)	0.7(10)
C27A	28.6(13)	38.2(13)	34.0(13)	-11.3(11)	-3.2(10)	5.0(11)
C6A	17.6(11)	45.5(14)	39.5(14)	8.7(11)	1.5(10)	-0.1(11)
C23A	27.0(13)	31.9(13)	50.0(16)	-10.7(11)	-1.7(12)	1.7(11)
C25	24.2(12)	25.8(12)	61.8(18)	-3.7(12)	1.6(12)	1.4(10)
C7A	24.5(12)	38.4(13)	42.9(14)	3.0(11)	-4.0(11)	-10.3(11)
C13	25.5(12)	24.3(11)	47.0(15)	-6.8(10)	4.1(11)	-0.1(10)
C5A	24.8(12)	35.1(13)	44.6(15)	1.1(11)	2.5(11)	3.7(10)
C25A	26.3(13)	37.7(13)	42.8(14)	-1.1(11)	-12.3(11)	1.3(11)
C23	27.5(13)	41.3(14)	49.6(16)	17.2(13)	-10.9(12)	3.1(11)
C34	31.3(13)	29.6(12)	44.5(15)	9.9(11)	1.1(11)	0.1(11)
C22	20.9(12)	31.0(12)	40.0(14)	10.3(10)	-1.3(10)	-1.9(10)
C12	29.4(13)	23.0(11)	58.1(17)	5.5(11)	3.7(12)	0.6(10)
C24A	27.6(13)	34.7(13)	56.6(17)	-1.7(12)	-8.4(12)	7.9(11)
C27	36.7(15)	49.7(16)	30.9(13)	7.9(12)	-4.8(11)	8.9(13)
C31A	52.1(18)	40.0(15)	38.9(15)	-7.9(12)	0.4(13)	-2.8(14)
C34A	30.9(14)	33.7(13)	47.4(15)	6.2(12)	-2.4(12)	-1.6(11)

Table 3.9 continued: Anisotropic Displacement Parameters ($\text{\AA}^2 \times 10^3$) for **2a**. The anisotropic displacement factor exponent takes the form: $-2\pi^2[h^2a^{*2}U_{11}+2hka^*b^*U_{12}+\dots]$.

Atom	U_{11}	U_{22}	U_{33}	U_{23}	U_{13}	U_{12}
C20	34.6(15)	52.6(16)	32.5(13)	-13.2(12)	2.2(11)	-2.5(13)
C24	22.6(13)	29.0(12)	75(2)	10.1(13)	-6.3(13)	5.2(10)
C19	29.4(14)	56.4(17)	41.9(15)	-11.4(13)	-5.4(12)	1.6(13)
C16	34.1(15)	71(2)	33.1(14)	-9.7(14)	-4.2(12)	13.8(14)
C37A	42.5(16)	33.7(14)	51.6(17)	2.7(12)	-3.9(13)	0.3(12)
C17	31.1(14)	53.1(17)	37.7(14)	0.3(12)	-7.2(12)	0.5(13)
C35	36.6(15)	31.6(13)	55.7(17)	12.6(12)	5.9(13)	4.9(12)
C16A	29.7(14)	50.9(16)	39.9(15)	2.9(12)	-5.5(11)	-7.6(12)
C19A	35.0(15)	48.6(16)	37.5(14)	-8.1(12)	0.9(12)	1.1(12)
C20A	38.6(16)	56.9(18)	40.1(16)	-7.7(13)	-13.1(13)	1.0(14)
C39	34.2(15)	36.6(14)	52.7(17)	14.1(12)	-1.0(12)	-5.6(12)
C32A	41.6(16)	55.0(18)	36.7(15)	6.0(13)	-0.9(12)	1.7(14)
C32	39.3(16)	42.7(16)	51.2(17)	-13.6(13)	2.9(13)	-8.1(13)
C29A	36.7(15)	49.7(17)	46.5(16)	-16.0(13)	-6.3(13)	-6.7(13)
C39A	33.3(15)	31.9(13)	57.7(18)	6.5(12)	6.4(13)	-1.6(11)
C38A	37.9(16)	36.4(14)	59.5(19)	3.0(13)	-7.8(14)	-2.7(12)
C17A	38.0(16)	72(2)	30.8(14)	-4.5(13)	1.5(12)	-9.8(15)
C28	49.8(18)	63(2)	33.9(14)	4.1(13)	-0.6(13)	-5.9(16)
C36A	41.1(16)	41.5(15)	47.3(16)	7.5(12)	3.8(13)	13.1(13)
C38	34.5(15)	49.3(17)	56.6(19)	14.5(14)	12.8(14)	7.7(13)
C28A	47.1(18)	55.8(18)	38.2(16)	-3.1(13)	1.0(13)	-0.8(15)
C29	37.6(17)	89(3)	45.2(17)	1.6(17)	6.4(14)	-3.3(17)
C31	50.7(19)	52.9(18)	47.0(17)	4.0(14)	-4.2(15)	-11.3(15)
C35A	35.2(15)	48.0(16)	58.3(18)	17.4(14)	-7.6(14)	-0.4(13)
C36	49(2)	70(2)	68(2)	35.9(18)	12.6(17)	23.2(18)
C37	52(2)	76(2)	88(3)	53(2)	30(2)	19.6(19)

Table 3.10: Bond Lengths for **2a**.

Atom	Atom	Length/ \AA	Atom	Atom	Length/ \AA
N1	N2	1.332(3)	C26A	C30A	1.520(4)
N1	C9	1.448(3)	C26A	C25A	1.394(4)
N1	C2	1.350(3)	C14	C18	1.523(3)
N1A	N2A	1.323(3)	C14	C13	1.394(3)

Table 3.10 continued: Bond Lengths for 2a.

Atom	Atom	Length/Å	Atom	Atom	Length/Å
N1A	C2A	1.356(3)	C12A	C11A	1.387(4)
N1A	C9A	1.453(3)	C15A	C16A	1.531(4)
N2	N3	1.371(3)	C15A	C17A	1.521(4)
N3	C1	1.398(3)	C21	C22	1.392(4)
N3	C21	1.444(3)	C30A	C31A	1.522(4)
N3A	N2A	1.371(3)	C30A	C32A	1.534(4)
N3A	C21A	1.443(3)	C22A	C27A	1.514(4)
N3A	C1A	1.401(3)	C22A	C23A	1.392(4)
N4	C33	1.371(3)	C15	C16	1.529(4)
N4	C34	1.292(3)	C15	C17	1.528(4)
N4A	C33A	1.371(3)	C18	C20	1.525(4)
N4A	C34A	1.290(3)	C18	C19	1.529(4)
C3	C2	1.468(3)	C18A	C19A	1.529(4)
C3	C4	1.406(3)	C18A	C20A	1.525(4)
C3	C8	1.393(3)	C30	C32	1.525(4)
C2A	C3A	1.471(3)	C30	C31	1.531(4)
C2A	C1A	1.436(3)	C8A	C7A	1.388(4)
C9A	C10A	1.394(3)	C11	C12	1.383(4)
C9A	C14A	1.402(3)	C27A	C29A	1.542(4)
C3A	C4A	1.397(3)	C27A	C28A	1.528(4)
C3A	C8A	1.401(3)	C6A	C7A	1.374(4)
C21A	C26A	1.395(4)	C6A	C5A	1.382(4)
C21A	C22A	1.395(3)	C23A	C24A	1.382(4)
C1A	C33A	1.368(3)	C25	C24	1.382(4)
C9	C10	1.394(3)	C13	C12	1.382(4)
C9	C14	1.394(3)	C25A	C24A	1.387(4)
C1	C33	1.368(3)	C23	C22	1.396(4)
C1	C2	1.428(3)	C23	C24	1.388(5)
C6	C7	1.385(4)	C34	C35	1.496(4)
C6	C5	1.382(4)	C34	C39	1.506(4)
C26	C21	1.399(4)	C22	C27	1.521(4)
C26	C30	1.518(4)	C27	C28	1.519(4)
C26	C25	1.393(4)	C27	C29	1.514(4)
C4A	C5A	1.385(4)	C34A	C39A	1.512(4)
C10	C15	1.524(3)	C34A	C35A	1.506(4)

Table 3.10 continued: Bond Lengths for 2a.

Atom	Atom	Length/Å	Atom	Atom	Length/Å
C10	C11	1.391(3)	C37A	C38A	1.523(4)
C10A	C15A	1.523(3)	C37A	C36A	1.528(4)
C10A	C11A	1.395(3)	C35	C36	1.504(5)
C4	C5	1.383(3)	C39	C38	1.515(4)
C14A	C13A	1.391(3)	C39A	C38A	1.519(4)
C14A	C18A	1.521(3)	C36A	C35A	1.530(4)
C13A	C12A	1.376(4)	C38	C37	1.516(4)
C7	C8	1.388(3)	C36	C37	1.543(6)

Table 3.11: Bond Angles for 2a.

Atom	Atom	Atom	Angle/°	Atom	Atom	Atom	Angle/°
N2	N1	C9	117.10(17)	C13A	C12A	C11A	120.7(2)
N2	N1	C2	115.12(17)	C10A	C15A	C16A	110.4(2)
C2	N1	C9	127.76(18)	C17A	C15A	C10A	112.0(2)
N2A	N1A	C2A	115.34(18)	C17A	C15A	C16A	110.6(2)
N2A	N1A	C9A	118.04(18)	C26	C21	N3	118.2(2)
C2A	N1A	C9A	126.61(19)	C22	C21	N3	118.4(2)
N1	N2	N3	102.43(16)	C22	C21	C26	123.4(2)
N2	N3	C1	113.77(17)	C26A	C30A	C31A	111.6(2)
N2	N3	C21	117.56(18)	C26A	C30A	C32A	112.0(2)
C1	N3	C21	128.35(18)	C31A	C30A	C32A	110.2(2)
N2A	N3A	C21A	117.74(18)	C6	C5	C4	120.5(2)
N2A	N3A	C1A	113.72(18)	C1A	C33A	N4A	121.4(2)
C1A	N3A	C21A	128.55(19)	C21A	C22A	C27A	122.6(2)
N1A	N2A	N3A	102.80(17)	C23A	C22A	C21A	117.3(2)
C34	N4	C33	122.8(2)	C23A	C22A	C27A	120.0(2)
C34A	N4A	C33A	122.9(2)	C7	C8	C3	120.8(2)
C4	C3	C2	118.9(2)	C10	C15	C16	109.2(2)
C8	C3	C2	123.2(2)	C10	C15	C17	112.9(2)
C8	C3	C4	117.9(2)	C17	C15	C16	111.1(2)
N1A	C2A	C3A	125.4(2)	C12A	C11A	C10A	120.5(2)
N1A	C2A	C1A	105.82(19)	C14	C18	C20	112.2(2)
C1A	C2A	C3A	128.7(2)	C14	C18	C19	110.0(2)
C10A	C9A	N1A	117.8(2)	C20	C18	C19	110.6(2)

Table 3.11 continued: Bond Angles for 2a.

Atom	Atom	Atom	Angle/°	Atom	Atom	Atom	Angle/°
C10A	C9A	C14A	123.7(2)	C14A	C18A	C19A	109.5(2)
C14A	C9A	N1A	118.4(2)	C14A	C18A	C20A	113.2(2)
C4A	C3A	C2A	123.6(2)	C20A	C18A	C19A	110.8(2)
C4A	C3A	C8A	117.6(2)	C26	C30	C32	111.6(2)
C8A	C3A	C2A	118.8(2)	C26	C30	C31	111.6(2)
C26A	C21A	N3A	118.2(2)	C32	C30	C31	110.1(2)
C22A	C21A	N3A	118.6(2)	C7A	C8A	C3A	121.0(2)
C22A	C21A	C26A	123.2(2)	C12	C11	C10	120.8(2)
N3A	C1A	C2A	102.33(18)	C22A	C27A	C29A	110.0(2)
C33A	C1A	N3A	127.5(2)	C22A	C27A	C28A	111.8(2)
C33A	C1A	C2A	130.1(2)	C28A	C27A	C29A	111.3(2)
C10	C9	N1	118.0(2)	C7A	C6A	C5A	119.2(2)
C14	C9	N1	118.1(2)	C24A	C23A	C22A	121.2(2)
C14	C9	C10	124.0(2)	C24	C25	C26	120.9(3)
N3	C1	C2	102.45(18)	C6A	C7A	C8A	120.6(2)
C33	C1	N3	128.2(2)	C12	C13	C14	120.7(2)
C33	C1	C2	129.3(2)	C6A	C5A	C4A	120.8(2)
C1	C33	N4	121.4(2)	C24A	C25A	C26A	121.0(2)
N1	C2	C3	125.68(19)	C24	C23	C22	120.9(3)
N1	C2	C1	106.23(19)	N4	C34	C35	118.3(2)
C1	C2	C3	128.1(2)	N4	C34	C39	127.3(2)
C5	C6	C7	119.3(2)	C35	C34	C39	114.1(2)
C21	C26	C30	122.6(2)	C21	C22	C23	117.0(3)
C25	C26	C21	117.2(2)	C21	C22	C27	122.0(2)
C25	C26	C30	120.1(2)	C23	C22	C27	120.9(2)
C5A	C4A	C3A	120.8(2)	C13	C12	C11	120.8(2)
C9	C10	C15	121.3(2)	C23A	C24A	C25A	120.1(2)
C11	C10	C9	116.8(2)	C28	C27	C22	113.5(2)
C11	C10	C15	121.7(2)	C29	C27	C22	109.9(3)
C9A	C10A	C15A	122.6(2)	C29	C27	C28	111.2(3)
C9A	C10A	C11A	117.1(2)	N4A	C34A	C39A	127.8(3)
C11A	C10A	C15A	120.3(2)	N4A	C34A	C35A	118.8(3)
C5	C4	C3	121.0(2)	C35A	C34A	C39A	113.2(2)
C9A	C14A	C18A	121.2(2)	C25	C24	C23	120.4(2)
C13A	C14A	C9A	116.5(2)	C38A	C37A	C36A	111.2(2)

Table 3.11 continued: Bond Angles for **2a**.

Atom	Atom	Atom	Angle/°	Atom	Atom	Atom	Angle/°
C13A	C14A	C18A	122.2(2)	C34	C35	C36	109.6(3)
C12A	C13A	C14A	121.4(2)	C34	C39	C38	110.7(3)
C6	C7	C8	120.6(2)	C34A	C39A	C38A	110.1(3)
C21A	C26A	C30A	122.4(2)	C39A	C38A	C37A	112.3(3)
C25A	C26A	C21A	117.3(2)	C37A	C36A	C35A	112.1(3)
C25A	C26A	C30A	120.4(2)	C39	C38	C37	111.4(3)
C9	C14	C18	122.1(2)	C34A	C35A	C36A	110.6(2)
C9	C14	C13	116.8(2)	C35	C36	C37	110.2(3)
C13	C14	C18	121.1(2)	C38	C37	C36	111.1(3)

Table 3.12: Hydrogen Atom Coordinates ($\text{\AA} \times 10^4$) and Isotropic Displacement Parameters ($\text{\AA}^2 \times 10^3$) for **2a**.

Atom	x	y	z	U(eq)
H	8353.36	5200.04	6134.72	31
Ha	4179.23	6615.53	6070.91	33
Hb	12201.02	2740.2	3619.42	36
Hc	7261.75	5709.36	5592.93	30
Hd	10832.41	2074.66	5050.56	39
He	5673.3	7222.59	6427.98	34
Hf	10408.11	1388.46	4494.52	42
Hg	9017.3	2921.26	3225.88	34
Hh	8714.57	3990.71	2852.16	39
Hi	4988.33	5865.2	5645.51	35
Hj	11869.54	4658.08	3466.55	33
Hk	7954.65	7071.1	6381.69	30
Hl	9388.76	6554.92	5069.21	36
Hm	9628.03	1579.24	3703.83	37
Hn	10672.41	6925.24	6722.4	36
Ho	10887.03	3483.5	4770.25	36
Hp	11344.21	5398.12	5227.83	40
Hq	12955.96	4271.17	4063.19	36
Hr	9537.33	7989.6	4919.01	40
Hs	8888.33	4526.2	4529.91	40
Ht	15976.49	3211.28	3902.72	41

Table 3.12 continued: Hydrogen Atom Coordinates ($\text{\AA}\times 10^4$) and Isotropic Displacement Parameters ($\text{\AA}^2\times 10^3$) for **2a**.

Atom	x	y	z	U(eq)
Hu	6092.76	5365.36	4205.97	44
Hv	14115.49	4551.51	5569.3	45
Hw	15210.86	4067.09	4111.38	42
Hx	10526.62	8323.95	6331.48	39
Hy	14460.38	2549.36	3662.51	42
Hz	5815.24	4835.04	2800.14	43
H1	14390.59	5108.25	6967.6	47
H2	9962.13	8609.8	5542.04	44
H3	5071.84	5391.51	3436.49	48
H4	12034.18	6180.64	6815.5	47
H5	6865.21	3423.03	3006.1	66
H6	7335.18	3384.35	2442.31	66
H7	6045.34	3729.6	2584.13	66
H8	10046.59	7972.11	7102.28	60
H9	10170.27	7436.72	7429.72	60
H10	8991.05	7494.17	7036.09	60
H11	15077.47	4517.68	6349.11	51
H12	12822.95	7265.43	6563.09	64
H13	12505.99	7300.7	7141.61	64
H14	12424.58	7831.51	6806.18	64
H15	11357.56	7126.26	4512.87	69
H16	10949.34	6509.56	4424.48	69
H17	11685.34	6682.03	4924.39	69
H18	11859.26	6714.07	2871.73	51
H19	11904.17	6911.37	3435.1	51
H20	7811.14	7143.01	4699.38	61
H21	8537.47	6778.98	4292.3	61
H22	8961.66	7396.61	4363.18	61
H23	11331.32	4008.41	6562.03	50
H24	10318.43	3564.39	6351.34	50
H25	7881.61	1862.28	3186.78	60
H26	7449.16	2355.87	2840.98	60
H27	7158.53	2377.07	3421.98	60
H28	8609.43	3379.89	4962.57	61
H29	9403.58	3609.61	5429.84	61

Table 3.12 continued: Hydrogen Atom Coordinates ($\text{\AA}\times 10^4$) and Isotropic Displacement Parameters ($\text{\AA}^2\times 10^3$) for **2a**.

Atom	x	y	z	U(eq)
H30	8982.97	2987.09	5410.91	61
H31	11391.77	2731.67	5548.71	68
H32	11813.81	3354.36	5551.91	68
H33	12503.99	2944.78	5173.43	68
H34	7864.51	3891.35	6157.39	49
H35	7521.02	4505.13	6293.44	49
H36	7009.72	4512.68	2154.11	67
H37	8388.12	4217.75	2033.68	67
H38	8381.77	4772.38	2336.57	67
H39	12325.79	4333.98	5045.28	67
H40	11106.73	4610.34	4761.54	67
H41	10973.98	4461.49	5334.77	67
H42	9405.7	5438.33	4376.86	66
H43	9199.99	5356.57	4958.37	66
H44	8050.88	5628.53	4633.74	66
H45	12362.3	5676.76	2703.87	49
H46	12712.32	5309.9	3174.22	49
H47	13489.78	6212.41	3281.47	54
H48	12461.94	6046.12	3706.58	54
H49	10967.79	2541.44	2906.02	70
H50	9765.7	2434.26	2531.1	70
H51	10281.17	1959.34	2883.06	70
H52	13994.94	5787.56	7484.93	73
H53	13233.42	6352.77	7527.41	73
H54	14267.55	6252.63	7087.39	73
H55	9665.84	6775.86	3151.15	52
H56	9996.74	6416.93	3627.26	52
H57	6704.22	3882.25	6900.07	56
H58	7675.41	4326.39	7133.93	56
H59	6450.63	4882.25	4967.8	71
H60	7677.61	4639.61	5271.94	71
H61	6871.1	4264.43	4895.3	71
H62	10673.55	5484.66	7077.78	86
H63	11133.34	5823.96	7550.99	86
H64	11814.85	5254.94	7432.2	86

Table 3.12 continued: Hydrogen Atom Coordinates ($\text{\AA}\times 10^4$) and Isotropic Displacement Parameters ($\text{\AA}^2\times 10^3$) for **2a**.

Atom	x	y	z	U(eq)
H65	13354.88	5715.04	4894.79	75
H66	12619.52	5344.88	4494.63	75
H67	13851.26	5110.01	4801.22	75
H68	8883.56	5864.27	3061.5	57
H69	9893.15	6027.93	2628.42	57
H70	10146.34	4051.38	7307.6	75
H71	10567.64	3437.38	7205.72	75
H72	8401.94	3238.08	6903.04	86
H73	8275.95	3482.95	7448.81	86

Crystal data and structure refinement for **3aHBF₄**:

An X-ray-quality crystal of **3aHBF₄** was obtained by vapor diffusion of hexane into a benzene solution in the glovebox. Thermal ellipsoids were at the 50% probability level.

Hydrogen atoms were omitted for clarity.

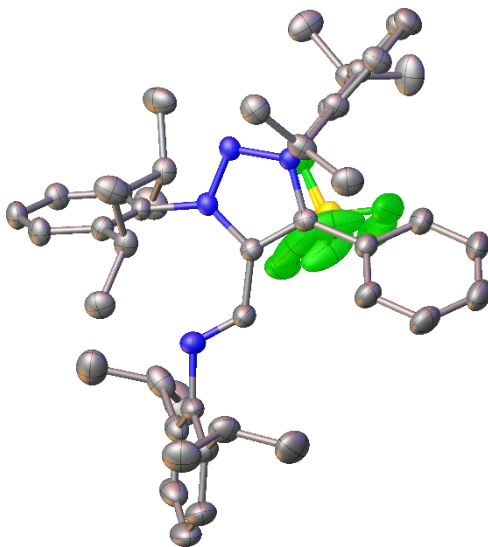


Table 3.13: Crystal Data and Structure Refinement for **3aHBF₄**.

Empirical formula	C ₄₅ H ₅₇ BF ₄ N ₄
Formula weight	740.75
Temperature/K	100.15
Crystal system	monoclinic

Table 3.13 continued: Crystal Data and Structure Refinement for **3aHBF₄**.

Space group	P2 ₁ /c
a/Å	16.2092(7)
b/Å	10.5335(4)
c/Å	25.2551(10)
α/°	90
β/°	103.525(2)
γ/°	90
Volume/Å ³	4192.5(3)
Z	4
ρ _{calc} /cm ³	1.174
μ/mm ⁻¹	0.650
F(000)	1584.0
Crystal size/mm ³	0.5 × 0.7 × 0.7
Radiation	CuKα (λ = 1.54178)
2Θ range for data collection/°	5.608 to 136.882
Index ranges	-19 ≤ h ≤ 19, 0 ≤ k ≤ 12, 0 ≤ l ≤ 30
Reflections collected	7654
Independent reflections	7654 [R _{int} = ?, R _{sigma} = 0.0456]
Data/restraints/parameters	7654/37/537
Goodness-of-fit on F ²	1.135
Final R indexes [I ≥ 2σ (I)]	R ₁ = 0.0762, wR ₂ = 0.1583
Final R indexes [all data]	R ₁ = 0.0931, wR ₂ = 0.1673
Largest diff. peak/hole / e Å ⁻³	0.34/-0.24

Table 3.14: Fractional atomic coordinates (x10⁴) and Equivalent Isotropic Displacement Parameters (Å²x10³) for **3aHBF₄**. U_{eq} is defined as 1/3 of the trace of the orthogonalized U_{ij} tensor.

Atom	x	y	z	U(eq)
F1	7962.9(10)	8262.8(17)	5269.1(7)	45.4(4)
N2	8326.1(13)	3962.1(18)	5656.7(8)	22.6(4)
N4	7861.6(12)	3985.8(18)	4808.4(8)	22.6(4)
N3	8579.9(13)	3979.5(18)	5192.5(8)	23.4(4)
N1	7237.8(14)	3612(2)	6464.3(9)	30.8(5)
C22	7879.2(16)	3876(2)	4238.5(10)	25.2(5)
C3	7158.0(16)	3968(2)	5015.4(10)	25.7(5)

Table 3.14 continued: Fractional atomic coordinates ($\times 10^4$) and Equivalent Isotropic Displacement Parameters ($\text{\AA}^2 \times 10^3$) for **3aHBF4**. U_{eq} is defined as 1/3 of the trace of the orthogonalized U_{ij} tensor.

Atom	<i>x</i>	<i>y</i>	<i>z</i>	U(eq)
C10	8974.1(15)	3902(2)	6164.2(10)	23.2(5)
C2	7460.6(15)	3960(2)	5572.5(10)	25.1(5)
C15	9394.1(16)	5021(2)	6370.6(10)	25.1(5)
C1	6955.9(17)	3957(3)	5981.6(11)	29.8(6)
C4	6285.5(16)	3848(3)	4688.0(11)	31.2(6)
C16	9193.2(17)	6299(2)	6090.4(11)	30.2(6)
C27	7957.7(16)	4980(2)	3947.4(11)	27.8(6)
C11	9148.8(16)	2706(2)	6407.3(11)	27.2(6)
C23	7773.1(17)	2656(2)	4009.7(11)	29.7(6)
C13	10219.5(18)	3747(3)	7100.0(11)	32.7(6)
C34	6663.9(17)	3626(3)	6822.1(11)	31.7(6)
C14	10021.7(17)	4904(3)	6845.9(11)	31.0(6)
C28	8084.3(17)	6283(2)	4216.7(11)	30.6(6)
C31	7704.0(19)	1469(2)	4337.0(11)	33.6(6)
C12	9780.8(17)	2659(3)	6883.4(11)	32.7(6)
C19	8706.3(17)	1500(2)	6162.1(11)	31.5(6)
C24	7739.8(19)	2575(3)	3455.1(11)	35.8(6)
C25	7811.4(19)	3648(3)	3152.2(11)	38.6(7)
C35	6708.0(19)	4673(3)	7176.2(11)	36.2(6)
C26	7925.3(18)	4835(3)	3397.9(11)	33.8(6)
C9	5781.1(18)	2880(3)	4817.6(13)	40.2(7)
C5	5962.8(18)	4655(3)	4249.8(12)	39.1(7)
C33	8484(2)	626(3)	4376.8(13)	40.2(7)
C21	9293(2)	739(3)	5889.1(13)	44.1(8)
C32	6883(2)	737(3)	4094.3(13)	41.4(7)
C20	8399.7(19)	704(3)	6585.4(12)	38.2(7)
C39	6112.5(18)	2603(3)	6822.9(12)	39.1(7)
C8	4950.7(19)	2727(3)	4513.4(14)	48.6(8)
C30	9005(2)	6691(3)	4313.6(15)	47.8(8)
C36	6177(2)	4659(3)	7538.3(13)	47.9(8)
C18	9102(2)	7338(3)	6491.1(13)	46.3(8)
C40	6034(2)	1488(3)	6429.5(13)	44.9(7)
C6	5140.7(19)	4471(4)	3944.5(13)	48.5(8)
F2	6982(5)	6769(7)	5196(4)	98(4)

Table 3.14 continued: Fractional atomic coordinates ($\times 10^4$) and Equivalent Isotropic Displacement Parameters ($\text{\AA}^2 \times 10^3$) for **3aHBF₄**. U_{eq} is defined as 1/3 of the trace of the orthogonalized U_{IJ} tensor.

Atom	<i>x</i>	<i>y</i>	<i>z</i>	U(eq)
C43	7342(2)	5735(3)	7178.0(12)	43.5(7)
C17	9877(2)	6664(3)	5794.3(14)	47.8(8)
C7	4646(2)	3522(4)	4078.0(14)	50.5(9)
C37	5631(2)	3652(4)	7548.4(14)	54.9(9)
C29	7513(2)	7292(3)	3884.5(15)	54.3(9)
C38	5601(2)	2644(4)	7199.8(14)	50.7(8)
C44	8177(2)	5419(4)	7568.0(16)	59.3(10)
B1	7188(3)	7969(6)	5385(3)	38(4)
C41	6181(3)	210(3)	6728.3(16)	59.8(10)
C42	5167(2)	1496(4)	6024.0(16)	61.7(10)
C45	7018(3)	7042(3)	7307.5(15)	67.6(12)
F4	7196(3)	7945(8)	5927.0(18)	72(3)
F3	6566(3)	8778(7)	5141(4)	99(4)
F2A	6591(3)	7851(9)	4832.8(19)	78(3)
F3A	7182(4)	6789(7)	5573(5)	118(5)
F1A	6911(4)	8836(7)	5623(4)	96(4)
B1A	7161(4)	7925(6)	5317(3)	35(3)

Table 3.15: Anisotropic Displacement Parameters ($\text{\AA}^2 \times 10^3$) for **3aHBF₄**. The anisotropic displacement factor exponent takes the form: $-2\pi^2[h^2a^{*2}U_{11}+2hka^*b^*U_{12}+\dots]$.

Atom	U₁₁	U₂₂	U₃₃	U₂₃	U₁₃	U₁₂
F1	35.0(9)	43.6(10)	57.4(11)	8.2(8)	10.8(8)	-6.3(7)
N2	26.6(11)	17.6(10)	23.1(10)	0.1(8)	4.6(9)	0.3(8)
N4	23.6(10)	18.9(10)	25.1(11)	1.6(8)	4.9(9)	-0.6(8)
N3	28.0(11)	17.5(10)	23.6(10)	-0.4(8)	3.9(9)	0.1(8)
N1	30.0(12)	32.2(12)	32.0(12)	0.6(10)	10.8(10)	-1.6(9)
C22	27.7(13)	23.8(13)	23.8(12)	0.0(10)	5.2(10)	-1.9(10)
C3	27.2(13)	20.3(12)	30.5(14)	-0.4(10)	8.8(11)	1.1(10)
C10	22.8(12)	21.8(12)	23.6(12)	0.3(10)	2.5(10)	0.2(10)
C2	26.2(13)	21.0(12)	28.3(13)	1.1(10)	6.7(11)	1.4(10)
C15	26.8(13)	21.3(12)	27.3(13)	-1.2(10)	6.4(11)	-1.2(10)
C1	26.6(13)	34.0(14)	28.6(14)	-0.6(11)	6.2(11)	0.6(11)
C4	25.7(13)	36.5(15)	30.8(14)	-1.6(11)	5.3(11)	1.6(11)

Table 3.15 continued: Anisotropic Displacement Parameters ($\text{\AA}^2 \times 10^3$) for **3aHBF₄**. The anisotropic displacement factor exponent takes the form: $-2\pi^2[h^2a^{*2}U_{11}+2hka^*b^*U_{12}+\dots]$.

Atom	U ₁₁	U ₂₂	U ₃₃	U ₂₃	U ₁₃	U ₁₂
C16	33.3(14)	21.5(13)	34.0(14)	-0.8(11)	4.0(12)	0.3(10)
C27	29.4(14)	24.2(13)	30.3(14)	3.5(10)	7.6(11)	1.0(10)
C11	27.0(13)	22.4(13)	31.3(14)	2.6(10)	4.8(11)	-0.1(10)
C23	34.6(14)	24.4(13)	31.0(14)	-1.6(11)	9.1(12)	-5.7(11)
C13	32.8(14)	32.4(15)	28.9(14)	3.8(11)	-0.4(11)	0.2(11)
C34	28.1(13)	39.3(16)	28.8(14)	4.0(12)	8.5(11)	4.5(11)
C14	35.0(15)	25.2(13)	31.2(14)	-2.5(11)	4.5(12)	-3.8(11)
C28	37.4(15)	22.4(13)	33.3(14)	1.2(11)	11.1(12)	0.6(11)
C31	48.5(17)	22.2(13)	32.5(14)	-1.4(11)	14.2(13)	-7.5(12)
C12	35.1(15)	26.5(14)	33.1(15)	5.6(11)	0.8(12)	0.5(11)
C19	33.0(14)	21.6(13)	36.8(15)	3.6(11)	1.7(12)	-2.4(11)
C24	46.3(17)	29.1(14)	32.4(15)	-5.8(12)	10.4(13)	-8.7(12)
C25	46.9(17)	43.2(17)	25.9(14)	-0.8(12)	9.1(13)	-5.7(13)
C35	38.7(16)	39.3(16)	30.2(14)	2.9(12)	7.2(12)	10.4(12)
C26	39.5(16)	31.4(15)	30.1(14)	4.8(11)	7.4(12)	-1.7(12)
C9	27.4(14)	46.8(18)	46.0(17)	4.2(14)	7.5(13)	-3.2(12)
C5	28.8(15)	48.3(18)	38.8(16)	6.6(13)	5.2(13)	4.1(13)
C33	48.7(18)	27.8(15)	43.9(17)	1.0(12)	10.2(14)	-2.4(13)
C21	60(2)	30.0(15)	45.5(18)	-6.2(13)	19.2(16)	-10.9(14)
C32	46.8(18)	27.2(15)	51.7(18)	-0.4(13)	14.6(15)	-9.6(13)
C20	43.6(17)	25.1(14)	47.6(17)	3.5(12)	14.2(14)	-4.7(12)
C39	30.0(15)	46.5(18)	42.0(17)	6.5(13)	10.8(13)	-0.1(13)
C8	28.5(15)	58(2)	59(2)	-3.7(16)	9.6(15)	-8.8(14)
C30	42.5(18)	38.7(17)	63(2)	-18.0(15)	14.5(16)	-8.4(14)
C36	51.1(19)	60(2)	34.6(17)	2.8(15)	14.5(15)	17.1(16)
C18	67(2)	25.5(15)	48.6(19)	-2.1(13)	18.1(17)	4.7(14)
C40	42.7(17)	44.0(18)	50.3(18)	1.2(14)	15.3(15)	-13.1(14)
C6	31.2(16)	72(2)	39.4(17)	7.3(16)	1.8(14)	9.1(15)
F2	106(6)	63(5)	157(8)	-72(6)	96(6)	-55(5)
C43	64(2)	31.2(16)	34.0(16)	1.4(12)	9.0(15)	3.1(14)
C17	58(2)	36.4(17)	54(2)	15.5(15)	25.0(16)	6.6(15)
C7	29.1(16)	73(2)	44.7(18)	-5.2(17)	-0.9(14)	1.2(15)
C37	45.0(19)	79(3)	46.7(19)	9.3(18)	23.6(16)	13.2(18)
C29	62(2)	24.4(15)	68(2)	5.8(15)	-3.7(18)	2.8(14)
C38	37.0(17)	69(2)	51(2)	8.5(17)	19.2(15)	-1.8(16)

Table 3.15 continued: Anisotropic Displacement Parameters ($\text{\AA}^2 \times 10^3$) for **3aHBF₄**. The anisotropic displacement factor exponent takes the form: $-2\pi^2[h^2a^{*2}U_{11}+2hka^*b^*U_{12}+\dots]$.

Atom	U ₁₁	U ₂₂	U ₃₃	U ₂₃	U ₁₃	U ₁₂
C44	55(2)	55(2)	63(2)	14.4(18)	4.8(18)	-10.3(17)
B1	26(5)	45(10)	41(5)	-6(6)	7(4)	7(5)
C41	68(2)	43(2)	73(3)	4.8(18)	26(2)	-14.5(17)
C42	45(2)	75(3)	63(2)	-4.2(19)	7.9(17)	-23.7(18)
C45	109(3)	41(2)	48(2)	-12.4(16)	8(2)	14(2)
F4	48(3)	118(7)	52(3)	-6(3)	19(2)	-23(3)
F3	49(3)	95(6)	160(10)	83(7)	36(4)	26(3)
F2A	43(3)	136(7)	51(3)	1(3)	3.7(19)	-25(3)
F3A	40(3)	69(6)	247(13)	100(8)	37(6)	13(3)
F1A	58(4)	96(6)	142(9)	-83(7)	37(5)	-14(4)
B1A	33(4)	21(8)	49(4)	7(5)	5(3)	-5(5)

Table 3.16: Bond Lengths for **3aHBF₄**.

Atom	Atom	Length/ \AA	Atom	Atom	Length/ \AA
F1	B1	1.389(6)	C34	C35	1.411(4)
F1	B1A	1.380(6)	C34	C39	1.401(4)
N2	N3	1.330(3)	C28	C30	1.517(4)
N2	C10	1.456(3)	C28	C29	1.526(4)
N2	C2	1.369(3)	C31	C33	1.529(4)
N4	N3	1.330(3)	C31	C32	1.536(4)
N4	C22	1.451(3)	C19	C21	1.527(4)
N4	C3	1.361(3)	C19	C20	1.531(4)
N1	C1	1.252(3)	C24	C25	1.385(4)
N1	C34	1.441(3)	C25	C26	1.389(4)
C22	C27	1.398(3)	C35	C36	1.395(4)
C22	C23	1.403(4)	C35	C43	1.518(4)
C3	C2	1.378(4)	C9	C8	1.394(4)
C3	C4	1.467(4)	C5	C6	1.388(4)
C10	C15	1.399(3)	C39	C40	1.524(4)
C10	C11	1.401(3)	C39	C38	1.401(4)
C2	C1	1.460(4)	C8	C7	1.378(5)
C15	C16	1.520(3)	C36	C37	1.386(5)
C15	C14	1.386(4)	C40	C41	1.535(5)

Table 3.16 *continued*: Bond Lengths for 3aHBF₄.

Atom	Atom	Length/Å	Atom	Atom	Length/Å
C4	C9	1.394(4)	C40	C42	1.533(5)
C4	C5	1.397(4)	C6	C7	1.372(5)
C16	C18	1.521(4)	F2	B1	1.365(6)
C16	C17	1.524(4)	C43	C44	1.513(5)
C27	C28	1.524(4)	C43	C45	1.536(4)
C27	C26	1.385(4)	C37	C38	1.372(5)
C11	C12	1.386(4)	B1	F4	1.366(6)
C11	C19	1.517(4)	B1	F3	1.354(6)
C23	C31	1.518(4)	F2A	B1A	1.351(6)
C23	C24	1.392(4)	F3A	B1A	1.357(6)
C13	C14	1.380(4)	F1A	B1A	1.352(6)
C13	C12	1.392(4)			

Table 3.17: Bond Angles for 3aHBF₄.

Atom	Atom	Atom	Angle/°	Atom	Atom	Atom	Angle/°
N3	N2	C10	117.91(19)	C30	C28	C27	110.6(2)
N3	N2	C2	112.35(19)	C30	C28	C29	109.8(3)
C2	N2	C10	129.7(2)	C23	C31	C33	110.4(2)
N3	N4	C22	120.41(19)	C23	C31	C32	111.3(2)
N3	N4	C3	112.9(2)	C33	C31	C32	111.1(2)
C3	N4	C22	126.3(2)	C11	C12	C13	121.2(2)
N4	N3	N2	104.14(19)	C11	C19	C21	109.8(2)
C1	N1	C34	117.8(2)	C11	C19	C20	111.9(2)
C27	C22	N4	118.7(2)	C21	C19	C20	111.4(2)
C27	C22	C23	124.3(2)	C25	C24	C23	121.2(3)
C23	C22	N4	116.9(2)	C24	C25	C26	120.5(3)
N4	C3	C2	105.2(2)	C34	C35	C43	120.8(3)
N4	C3	C4	124.6(2)	C36	C35	C34	117.3(3)
C2	C3	C4	129.9(2)	C36	C35	C43	121.8(3)
C15	C10	N2	118.6(2)	C27	C26	C25	121.1(3)
C15	C10	C11	124.3(2)	C4	C9	C8	119.9(3)
C11	C10	N2	117.1(2)	C6	C5	C4	119.2(3)
N2	C2	C3	105.4(2)	C34	C39	C40	123.2(3)
N2	C2	C1	127.9(2)	C34	C39	C38	117.1(3)

Table 3.17 continued: Bond Angles for **3aHBF₄**.

Atom	Atom	Atom	Angle/°	Atom	Atom	Atom	Angle/°
C3	C2	C1	126.7(2)	C38	C39	C40	119.6(3)
C10	C15	C16	122.7(2)	C7	C8	C9	119.3(3)
C14	C15	C10	116.3(2)	C37	C36	C35	121.0(3)
C14	C15	C16	121.1(2)	C39	C40	C41	112.1(3)
N1	C1	C2	123.5(2)	C39	C40	C42	110.8(3)
C9	C4	C3	118.1(2)	C42	C40	C41	110.2(3)
C9	C4	C5	120.0(3)	C7	C6	C5	120.4(3)
C5	C4	C3	121.8(3)	C35	C43	C45	113.3(3)
C15	C16	C18	111.8(2)	C44	C43	C35	110.0(3)
C15	C16	C17	110.5(2)	C44	C43	C45	110.9(3)
C18	C16	C17	109.9(2)	C6	C7	C8	121.2(3)
C22	C27	C28	122.3(2)	C38	C37	C36	120.4(3)
C26	C27	C22	116.7(2)	C37	C38	C39	121.5(3)
C26	C27	C28	121.1(2)	F2	B1	F1	107.0(5)
C10	C11	C19	123.1(2)	F2	B1	F4	106.1(6)
C12	C11	C10	116.4(2)	F4	B1	F1	114.7(5)
C12	C11	C19	120.5(2)	F3	B1	F1	112.2(5)
C22	C23	C31	123.2(2)	F3	B1	F2	109.1(7)
C24	C23	C22	116.3(2)	F3	B1	F4	107.4(6)
C24	C23	C31	120.5(2)	F2A	B1A	F1	113.2(5)
C14	C13	C12	120.2(2)	F2A	B1A	F3A	108.4(6)
C35	C34	N1	117.5(2)	F2A	B1A	F1A	109.0(6)
C39	C34	N1	119.9(3)	F3A	B1A	F1	110.5(5)
C39	C34	C35	122.6(3)	F1A	B1A	F1	106.3(5)
C13	C14	C15	121.7(2)	F1A	B1A	F3A	109.3(8)
C27	C28	C29	112.4(2)				

Table 3.18: Hydrogen Atom Coordinates ($\text{\AA} \times 10^4$) and Isotropic Displacement Parameters ($\text{\AA}^2 \times 10^3$) for **3aHBF₄**.

Atom	<i>x</i>	<i>y</i>	<i>z</i>	U(eq)
H1	6382.65	4231.83	5875.65	36
H16	8641.77	6222.51	5814.37	36
H13	10656.28	3693.16	7423.85	39
H14	10323.51	5639.18	7000.77	37
H28	7937.31	6215.86	4578.8	37

Table 3.18 continued: Hydrogen Atom Coordinates ($\text{\AA}\times 10^4$) and Isotropic Displacement Parameters ($\text{\AA}^2\times 10^3$) for **3aHBF₄**.

Atom	<i>x</i>	<i>y</i>	<i>z</i>	U(eq)
H31	7687.16	1736.77	4714.12	40
H12	9917	1869.67	7064.94	39
H19	8197.13	1751.96	5873.93	38
H24	7666.65	1769.61	3281.24	43
H25	7782.35	3571.64	2773.45	46
H26	7982.04	5560.09	3185.42	41
H9	6002.68	2324.1	5112.92	48
H5	6301.66	5322.79	4161.61	47
H33A	8511.65	343.26	4011.56	60
H33B	8443.57	-115.43	4603.94	60
H33C	8997.13	1108.72	4540.31	60
H21A	9464.62	1265.41	5613.42	66
H21B	8993.79	-15.8	5714.98	66
H21C	9797.79	477.08	6163.63	66
H32A	6396.62	1311.53	4052.23	62
H32B	6820.66	38.12	4338.21	62
H32C	6908.24	393.85	3737.73	62
H20A	8890.04	342.08	6843.92	57
H20B	8035.05	16.22	6401.88	57
H20C	8077.77	1242.68	6781.32	57
H8	4598.65	2082.69	4605.35	58
H30A	9368.02	6048.76	4533.77	72
H30B	9081.24	7505.71	4506.55	72
H30C	9160.48	6783.15	3963.23	72
H36	6189.72	5349.65	7781.79	58
H18A	8711.45	7055.2	6710.33	69
H18B	8878.34	8107.98	6290.54	69
H18C	9658.38	7519.82	6730.76	69
H40	6480.37	1587.93	6217.98	54
H6	4919.37	5004.36	3641.41	58
H43	7448.43	5781.53	6804.14	52
H17A	10422.87	6749.29	6058.61	72
H17B	9727.37	7473.57	5605.05	72
H17C	9920.25	6003.4	5528.87	72
H7	4083.64	3410.15	3866.51	61

Table 3.18 continued: Hydrogen Atom Coordinates ($\text{\AA}\times 10^4$) and Isotropic Displacement Parameters ($\text{\AA}^2\times 10^3$) for **3aHBF₄**.

Atom	<i>x</i>	<i>y</i>	<i>z</i>	U(eq)
H37	5274.37	3658.32	7798.31	66
H29A	7710.56	7483.58	3555.13	82
H29B	7531.92	8064.33	4103.15	82
H29C	6928.57	6974.76	3781.8	82
H38	5225.89	1959.72	7214.37	61
H44A	8094.92	5370.74	7939.74	89
H44B	8593.68	6081.78	7549.07	89
H44C	8384.12	4600.01	7467.75	89
H41A	6740.35	210.85	6981.6	90
H41B	6154.2	-476.08	6462.73	90
H41C	5741.46	78.75	6931.48	90
H42A	4717.77	1410.93	6222.14	93
H42B	5135.6	784.36	5769.82	93
H42C	5094.93	2296.25	5820.72	93
H45A	6468.14	7212.76	7058.51	101
H45B	7425.82	7696.59	7262.86	101
H45C	6953.62	7049.4	7683.76	101

Table 3.19: Atomic Occupancy for **3aHBF₄**.

Atom	Occupancy	Atom	Occupancy	Atom	Occupancy
F2	0.508(11)	B1	0.508(11)	F4	0.508(11)
F3	0.508(11)	F2A	0.492(11)	F3A	0.492(11)
F1A	0.492(11)	B1A	0.492(11)		

Crystal data and structure refinement for 3aPQ:

An X-ray-quality crystal of **3aPQ** was obtained by layering hexane over a THF solution in the glovebox. Thermal ellipsoids were at the 50% probability level. Hydrogen atoms were omitted for clarity.

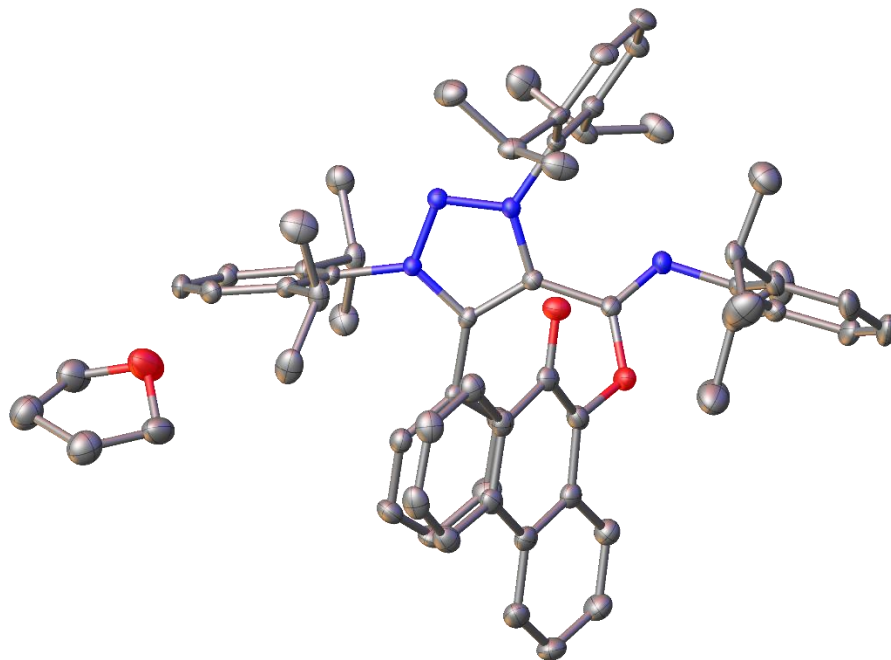


Table 3.20: Crystal Data and Structure Refinement for **3aPQ**.

Empirical formula	C ₆₃ H ₇₂ N ₄ O ₃
Formula weight	933.24
Temperature/K	100.0
Crystal system	triclinic
Space group	P-1
a/Å	10.8127(4)
b/Å	14.4784(7)
c/Å	17.5063(7)
α/°	85.708(2)
β/°	81.2270(10)
γ/°	73.0180(10)
Volume/Å ³	2589.13(19)
Z	2
ρ _{calc} /cm ³	1.197

Table 3.20 continued: Crystal Data and Structure Refinement for **3aPQ**.

μ/mm^{-1}	0.073
F(000)	1004.0
Crystal size/ mm^3	$0.41 \times 0.35 \times 0.2$
Radiation	MoK α ($\lambda = 0.71073$)
2 Θ range for data collection/ $^\circ$	2.942 to 51.362
Index ranges	$-13 \leq h \leq 13, -17 \leq k \leq 17, -21 \leq l \leq 17$
Reflections collected	22097
Independent reflections	9834 [$R_{\text{int}} = 0.0384, R_{\text{sigma}} = 0.0538$]
Data/restraints/parameters	9834/0/643
Goodness-of-fit on F^2	1.037
Final R indexes [$I \geq 2\sigma(I)$]	$R_1 = 0.0481, wR_2 = 0.1060$
Final R indexes [all data]	$R_1 = 0.0723, wR_2 = 0.1194$
Largest diff. peak/hole / $e \text{ \AA}^{-3}$	0.26/-0.27

Table 3.21: Fractional atomic coordinates ($\times 10^4$) and Equivalent Isotropic Displacement Parameters ($\text{\AA}^2 \times 10^3$) for **3aPQ**. U_{eq} is defined as 1/3 of the trace of the orthogonalized U_{IJ} tensor.

Atom	x	y	z	U(eq)
O1	7876.7(12)	1679.7(9)	6987.6(7)	22.3(3)
O2	5557.2(12)	2300.6(10)	7972.5(7)	24.0(3)
N1	7243.4(13)	3270.0(10)	8628.8(8)	14.2(3)
N2	6710.9(13)	4217.4(10)	8674.9(8)	15.1(3)
N3	6713.4(13)	4533.1(10)	7942.9(8)	13.5(3)
N4	8938.6(14)	1396.7(11)	8059.7(8)	17.8(3)
C1	7565.9(16)	2979.0(13)	7879.2(10)	14.6(4)
C2	7243.7(16)	3811.3(12)	7427.8(10)	13.7(4)
C3	7484.5(17)	3981.2(13)	6587.5(10)	16.1(4)
C4	8721.5(17)	3560.7(13)	6197.7(11)	20.9(4)
C5	8984.4(19)	3720.3(15)	5406.0(11)	27.7(5)
C6	8020(2)	4294.1(15)	5002.3(11)	28.9(5)
C7	6784.1(19)	4707.8(14)	5386.8(11)	26.0(5)
C8	6516.1(18)	4557.5(13)	6175.2(11)	20.5(4)
C9	6222.4(16)	5569.5(12)	7787.5(10)	14.5(4)
C10	7130.7(17)	6098.8(13)	7637.4(10)	16.7(4)
C11	6631.9(18)	7093.9(13)	7515.4(10)	20.0(4)
C12	5302.3(18)	7521.1(13)	7550.4(10)	21.5(4)

Table 3.21 continued: Fractional atomic coordinates ($\times 10^4$) and Equivalent Isotropic Displacement Parameters ($\text{\AA}^2 \times 10^3$) for **3aPQ**. U_{eq} is defined as 1/3 of the trace of the orthogonalized U_{ij} tensor.

Atom	<i>x</i>	<i>y</i>	<i>z</i>	<i>U</i> (eq)
C13	4436.2(18)	6970.2(13)	7696.4(10)	20.3(4)
C14	4874.8(17)	5972.3(13)	7810.3(10)	17.3(4)
C15	8596.4(17)	5648.7(13)	7606.6(11)	20.3(4)
C16	9324.1(19)	5879.4(16)	6829.7(12)	30.4(5)
C17	9098.2(19)	5980.2(15)	8278.0(12)	28.3(5)
C18	3907.3(17)	5374.3(14)	7950.6(12)	24.3(4)
C19	2998.7(19)	5595.9(15)	7325.0(13)	31.8(5)
C20	3105(2)	5557.4(18)	8749.2(13)	39.0(6)
C21	7423.2(17)	2706.7(12)	9354.3(10)	15.7(4)
C22	8681.7(18)	2420.6(13)	9563.1(10)	19.5(4)
C23	8848.6(19)	1874.4(14)	10248.1(11)	24.6(4)
C24	7816.7(19)	1632.4(14)	10695.4(11)	26.3(5)
C25	6583.8(19)	1950.6(14)	10478.4(10)	23.6(4)
C26	6340.0(17)	2509.5(13)	9803.5(10)	18.0(4)
C27	9815.3(18)	2724.5(14)	9104.9(11)	24.3(4)
C28	11084.7(19)	1899.4(16)	9054.4(12)	32.0(5)
C29	9966(2)	3613.8(17)	9457.5(14)	40.2(6)
C30	4945.7(17)	2918.0(14)	9626.4(10)	21.2(4)
C31	4255(2)	2129.7(17)	9652.8(12)	33.7(5)
C32	4201(2)	3693.1(16)	10204.8(12)	32.6(5)
C33	8139.0(17)	1957.9(13)	7655.1(10)	16.4(4)
C34	9447.7(18)	403.3(13)	7863.5(10)	19.5(4)
C35	10726.2(18)	81.5(14)	7475.6(11)	23.1(4)
C36	11216(2)	-893.6(14)	7308.1(12)	28.3(5)
C37	10485(2)	-1528.1(15)	7521.3(13)	32.5(5)
C38	9237(2)	-1197.6(14)	7919.3(12)	29.9(5)
C39	8685.2(18)	-232.9(13)	8097.0(11)	23.1(4)
C40	11533.5(19)	772.3(15)	7205.8(12)	28.4(5)
C41	12954(2)	390.1(17)	7384.5(16)	44.1(6)
C42	11516(3)	1017.5(18)	6344.8(13)	46.2(6)
C43	7321.4(18)	106.7(14)	8543.0(11)	25.1(4)
C44	7339(2)	-252.1(17)	9381.7(13)	38.9(6)
C45	6311(2)	-200.2(19)	8180.1(15)	46.2(6)
C46	6663.9(18)	2117.8(13)	6711.6(11)	21.2(4)

Table 3.21 continued: Fractional atomic coordinates ($\times 10^4$) and Equivalent Isotropic Displacement Parameters ($\text{\AA}^2 \times 10^3$) for **3aPQ**. U_{eq} is defined as 1/3 of the trace of the orthogonalized U_{IJ} tensor.

Atom	<i>x</i>	<i>y</i>	<i>z</i>	<i>U</i> (eq)
C47	5546.2(18)	2377.4(13)	7243.7(11)	20.3(4)
C48	4325.5(18)	2782.9(13)	6909.9(11)	20.3(4)
C49	3152.2(18)	3045.4(14)	7417.3(12)	24.9(4)
C50	1977.1(19)	3431.2(15)	7142.1(12)	29.1(5)
C51	1964.8(19)	3572.2(15)	6344.3(12)	28.6(5)
C52	3091.8(19)	3305.8(14)	5839.1(12)	26.8(5)
C53	4312.5(18)	2896.1(13)	6099.4(11)	22.0(4)
C54	5531.1(18)	2588.1(13)	5575.4(11)	22.1(4)
C55	5594(2)	2683.3(14)	4764.5(11)	27.7(5)
C56	6756(2)	2361.6(15)	4289.3(12)	31.5(5)
C57	7909(2)	1923.9(15)	4605.4(12)	31.0(5)
C58	7889.1(19)	1837.0(14)	5391.4(11)	25.7(4)
C59	6709.7(18)	2176.5(13)	5896.1(11)	21.6(4)
O3	8070.1(17)	8422.0(12)	6213.6(9)	48.2(4)
C60	7426(2)	8107.6(17)	5675.6(13)	38.4(6)
C61	6233(2)	8933.5(17)	5568.8(14)	41.0(6)
C62	6607(2)	9826.3(17)	5755.9(14)	42.2(6)
C63	7970(2)	9409.1(17)	5987.6(14)	42.7(6)

Table 3.22: Anisotropic Displacement Parameters ($\text{\AA}^2 \times 10^3$) for **3aPQ**. The anisotropic displacement factor exponent takes the form: $-2\pi^2[h^2a^{*2}U_{11}+2hka^*b^*U_{12}+\dots]$.

Atom	U_{11}	U_{22}	U_{33}	U_{23}	U_{13}	U_{12}
O1	23.9(7)	19.9(7)	20.4(7)	-2.3(6)	-4.8(5)	-1.0(6)
O2	26.5(7)	27.4(8)	19.9(7)	0.5(6)	-4.2(6)	-10.2(6)
N1	14.7(7)	12.7(8)	15.3(8)	0.6(6)	-2.3(6)	-4.1(6)
N2	14.8(7)	14.7(8)	15.4(8)	-0.1(6)	-1.0(6)	-4.3(6)
N3	14.0(7)	12.6(8)	13.5(7)	-0.1(6)	-1.2(6)	-3.4(6)
N4	19.5(8)	14.5(8)	18.6(8)	0.7(6)	-2.8(6)	-3.7(6)
C1	13.4(9)	15.4(9)	14.9(9)	-1.2(7)	-0.9(7)	-4.4(7)
C2	11.3(8)	13.0(9)	16.7(9)	-2.6(7)	-1.1(7)	-3.1(7)
C3	20.3(9)	13.7(9)	15.0(9)	-0.5(7)	-1.2(7)	-6.6(7)
C4	19.2(10)	20.2(10)	21.3(10)	0.8(8)	-3.1(8)	-2.7(8)
C5	27.1(11)	31.2(12)	21.9(11)	-2.7(9)	4.9(8)	-7.3(9)

Table 3.22 continued: Anisotropic Displacement Parameters ($\text{\AA}^2 \times 10^3$) for **3aPQ**. The anisotropic displacement factor exponent takes the form: $-2\pi^2[h^2a^{*2}U_{11}+2hka^*b^*U_{12}+\dots]$.

Atom	U ₁₁	U ₂₂	U ₃₃	U ₂₃	U ₁₃	U ₁₂
C6	40.0(12)	31.4(12)	15.3(10)	3.8(9)	-2.2(9)	-12.1(10)
C7	31.6(11)	24.9(11)	21.3(10)	4.9(9)	-9.0(9)	-6.6(9)
C8	20.4(10)	18.2(10)	22.1(10)	-1.9(8)	-3.3(8)	-3.9(8)
C9	17.8(9)	10.3(9)	13.8(9)	-1.7(7)	-2.4(7)	-1.2(7)
C10	19.1(9)	16.4(9)	14.0(9)	-1.1(7)	-1.2(7)	-4.4(7)
C11	23.4(10)	15.9(10)	21.4(10)	-1.7(8)	-0.7(8)	-7.5(8)
C12	27.6(10)	13.7(10)	21.2(10)	-0.9(8)	-4.6(8)	-2.2(8)
C13	18.4(9)	19.1(10)	20.7(10)	-1.4(8)	-5.7(8)	0.2(8)
C14	18.2(9)	16.9(10)	16.7(9)	-2.2(8)	-3.6(7)	-4.0(7)
C15	17.2(9)	15.6(10)	28.3(11)	0.4(8)	-1.8(8)	-5.9(7)
C16	22.7(11)	31.7(12)	33.8(12)	0.5(10)	2.2(9)	-6.6(9)
C17	24.0(11)	28.7(12)	33.5(12)	0.7(9)	-7.5(9)	-8.1(9)
C18	18.1(10)	16.9(10)	38.4(12)	-0.3(9)	-7.1(9)	-4.1(8)
C19	20.9(10)	28.7(12)	48.0(14)	-6.5(10)	-10.6(10)	-6.4(9)
C20	34.3(12)	49.4(15)	38.7(13)	4.6(11)	-0.8(10)	-23.8(11)
C21	23.2(10)	12.1(9)	11.8(9)	1.0(7)	-2.8(7)	-5.0(7)
C22	23.7(10)	17.2(10)	18.1(9)	-1.0(8)	-4.0(8)	-6.0(8)
C23	25.0(10)	24.5(11)	23.6(10)	3.0(9)	-8.6(8)	-4.4(8)
C24	37.3(12)	25.5(11)	15.8(10)	5.7(8)	-6.8(9)	-8.7(9)
C25	31.0(11)	25.9(11)	15.2(9)	0.5(8)	2.0(8)	-13.2(9)
C26	24.0(10)	16.3(10)	15.0(9)	-4.5(8)	-0.9(8)	-7.8(8)
C27	21.9(10)	30.2(11)	23.0(10)	7.9(9)	-8.7(8)	-10.0(8)
C28	22.2(11)	42.6(14)	30.8(12)	8.7(10)	-6.5(9)	-9.4(9)
C29	43.5(14)	38.9(14)	45.8(14)	3.9(11)	-9.3(11)	-23.4(11)
C30	21.6(10)	28.7(11)	15.0(9)	-1.2(8)	0.5(8)	-11.5(8)
C31	34.7(12)	45.7(14)	28.9(12)	4.5(10)	-6.1(9)	-24.6(11)
C32	27.5(11)	41.6(14)	25.2(11)	-6.0(10)	-0.6(9)	-4.6(10)
C33	19.9(9)	14.6(9)	14.2(9)	0.8(7)	0.1(7)	-5.7(7)
C34	25.4(10)	13.8(9)	17.9(9)	0.7(8)	-8.8(8)	-0.8(8)
C35	25.9(10)	20.7(10)	19.0(10)	-1.2(8)	-6.2(8)	0.7(8)
C36	28.8(11)	22.0(11)	28.1(11)	-6.6(9)	-6.6(9)	5.0(9)
C37	35.6(12)	17.0(11)	41.0(13)	-7.0(9)	-13.5(10)	4.2(9)
C38	36.8(12)	15.7(10)	39.5(12)	2.9(9)	-15.5(10)	-6.8(9)
C39	28.5(11)	15.9(10)	24.9(10)	2.2(8)	-10.7(8)	-3.3(8)
C40	25.1(11)	23.7(11)	30.9(11)	-1.1(9)	0.9(9)	-0.5(9)

Table 3.22 continued: Anisotropic Displacement Parameters ($\text{\AA}^2 \times 10^3$) for **3aPQ**. The anisotropic displacement factor exponent takes the form: $-2\pi^2[h^2a^{*2}U_{11}+2hka^*b^*U_{12}+\dots]$.

Atom	U ₁₁	U ₂₂	U ₃₃	U ₂₃	U ₁₃	U ₁₂
C41	27.3(12)	33.3(14)	67.6(17)	3.1(12)	-4.4(11)	-4.4(10)
C42	60.6(16)	36.1(14)	35.6(14)	4.4(11)	4.9(12)	-11.2(12)
C43	29.7(11)	15.5(10)	31.3(11)	4.0(9)	-6.0(9)	-8.5(8)
C44	40.2(13)	39.0(14)	36.2(13)	6.5(11)	-4.9(10)	-11.5(11)
C45	34.0(13)	56.6(17)	52.2(16)	-13.9(13)	-11.0(11)	-14.1(12)
C46	23.4(10)	17.9(10)	23.0(10)	1.1(8)	-7.9(8)	-4.9(8)
C47	26.1(10)	15.3(10)	21.5(10)	1.9(8)	-3.2(8)	-10.0(8)
C48	22.5(10)	14.8(10)	25.8(10)	-1.7(8)	-4.0(8)	-7.9(8)
C49	25.8(11)	21.9(11)	29.1(11)	1.2(9)	-4.3(9)	-10.0(8)
C50	24.3(11)	28.1(12)	35.9(12)	1.2(9)	-2.0(9)	-10.5(9)
C51	21.4(10)	25.7(11)	41.5(13)	2.6(10)	-11.9(9)	-8.1(9)
C52	29.4(11)	26.0(11)	28.4(11)	2.5(9)	-10.2(9)	-11.1(9)
C53	27.1(10)	16.7(10)	25.3(10)	0.4(8)	-6.9(8)	-9.5(8)
C54	28.8(11)	17.0(10)	22.5(10)	-1.7(8)	-4.7(8)	-9.0(8)
C55	35.9(12)	23.4(11)	25.9(11)	-2.4(9)	-10.6(9)	-7.9(9)
C56	43.6(13)	30.7(12)	18.7(10)	-3.8(9)	-4.2(9)	-7.7(10)
C57	34.8(12)	29.7(12)	25.5(11)	-5.8(9)	-0.5(9)	-5.0(9)
C58	27.6(11)	24.0(11)	24.0(11)	-1.2(9)	-2.4(9)	-5.4(9)
C59	27.2(10)	15.3(10)	22.8(10)	-0.9(8)	-3.1(8)	-7.0(8)
O3	71.5(12)	39.7(10)	44.5(10)	8.3(8)	-25.3(9)	-26.7(9)
C60	57.7(15)	34.1(13)	28.9(12)	0.4(10)	-12.6(11)	-18.6(11)
C61	45.5(14)	40.0(14)	41.0(14)	-2.7(11)	-2.9(11)	-19.0(11)
C62	47.6(14)	37.4(14)	43.6(14)	-5.6(11)	-5.3(11)	-14.8(11)
C63	59.2(16)	36.3(14)	40.1(14)	1.9(11)	-11.5(12)	-23.3(12)

Table 3.23: Bond Lengths for **3aPQ**.

Atom	Atom	Length/ \AA	Atom	Atom	Length/ \AA
O1	C33	1.359(2)	C26	C30	1.521(3)
O1	C46	1.420(2)	C27	C28	1.530(3)
O2	C47	1.274(2)	C27	C29	1.529(3)
N1	N2	1.3269(19)	C30	C31	1.530(3)
N1	C1	1.371(2)	C30	C32	1.525(3)
N1	C21	1.464(2)	C34	C35	1.405(3)
N2	N3	1.3279(19)	C34	C39	1.407(3)

Table 3.23 continued: Bond Lengths for **3aPQ**.

Atom	Atom	Length/Å	Atom	Atom	Length/Å
N3	C2	1.367(2)	C35	C36	1.392(3)
N3	C9	1.458(2)	C35	C40	1.516(3)
N4	C33	1.265(2)	C36	C37	1.375(3)
N4	C34	1.430(2)	C37	C38	1.385(3)
C1	C2	1.376(2)	C38	C39	1.388(3)
C1	C33	1.484(2)	C39	C43	1.519(3)
C2	C3	1.469(2)	C40	C41	1.546(3)
C3	C4	1.390(2)	C40	C42	1.524(3)
C3	C8	1.394(2)	C43	C44	1.521(3)
C4	C5	1.388(3)	C43	C45	1.528(3)
C5	C6	1.382(3)	C46	C47	1.383(3)
C6	C7	1.384(3)	C46	C59	1.418(3)
C7	C8	1.381(3)	C47	C48	1.470(3)
C9	C10	1.397(2)	C48	C49	1.403(3)
C9	C14	1.398(2)	C48	C53	1.418(3)
C10	C11	1.396(2)	C49	C50	1.375(3)
C10	C15	1.522(2)	C50	C51	1.398(3)
C11	C12	1.383(3)	C51	C52	1.365(3)
C12	C13	1.382(3)	C52	C53	1.410(3)
C13	C14	1.392(2)	C53	C54	1.458(3)
C14	C18	1.524(2)	C54	C55	1.409(3)
C15	C16	1.530(3)	C54	C59	1.421(3)
C15	C17	1.529(3)	C55	C56	1.373(3)
C18	C19	1.536(3)	C56	C57	1.399(3)
C18	C20	1.526(3)	C57	C58	1.370(3)
C21	C22	1.399(2)	C58	C59	1.416(3)
C21	C26	1.397(2)	O3	C60	1.424(3)
C22	C23	1.392(3)	O3	C63	1.431(3)
C22	C27	1.517(3)	C60	C61	1.506(3)
C23	C24	1.379(3)	C61	C62	1.533(3)
C24	C25	1.380(3)	C62	C63	1.525(3)
C25	C26	1.395(3)			

Table 3.24: Bond Angles for 3aPQ.

Atom	Atom	Atom	Angle/°	Atom	Atom	Atom	Angle/°
C33	O1	C46	121.10(14)	C26	C30	C31	111.77(16)
N2	N1	C1	112.36(14)	C26	C30	C32	108.97(15)
N2	N1	C21	117.49(14)	C32	C30	C31	110.38(16)
C1	N1	C21	130.14(14)	O1	C33	C1	118.93(15)
N1	N2	N3	104.12(13)	N4	C33	O1	122.18(16)
N2	N3	C2	113.10(14)	N4	C33	C1	118.63(16)
N2	N3	C9	118.17(13)	C35	C34	N4	118.69(16)
C2	N3	C9	128.67(14)	C35	C34	C39	121.87(17)
C33	N4	C34	118.62(15)	C39	C34	N4	119.36(16)
N1	C1	C2	105.61(15)	C34	C35	C40	121.79(17)
N1	C1	C33	124.09(15)	C36	C35	C34	117.81(18)
C2	C1	C33	130.30(16)	C36	C35	C40	120.32(18)
N3	C2	C1	104.76(15)	C37	C36	C35	121.44(19)
N3	C2	C3	123.71(15)	C36	C37	C38	119.67(19)
C1	C2	C3	131.29(16)	C37	C38	C39	121.80(19)
C4	C3	C2	118.64(15)	C34	C39	C43	121.96(17)
C4	C3	C8	119.41(16)	C38	C39	C34	117.38(18)
C8	C3	C2	121.94(16)	C38	C39	C43	120.65(18)
C5	C4	C3	119.98(17)	C35	C40	C41	113.16(17)
C6	C5	C4	120.22(18)	C35	C40	C42	110.55(18)
C5	C6	C7	120.00(18)	C42	C40	C41	110.31(19)
C8	C7	C6	120.16(18)	C39	C43	C44	109.85(16)
C7	C8	C3	120.23(17)	C39	C43	C45	112.68(17)
C10	C9	N3	117.71(15)	C44	C43	C45	110.93(18)
C10	C9	C14	124.22(16)	C47	C46	O1	118.54(16)
C14	C9	N3	118.07(15)	C47	C46	C59	125.77(17)
C9	C10	C15	123.63(16)	C59	C46	O1	115.49(16)
C11	C10	C9	116.57(16)	O2	C47	C46	123.31(17)
C11	C10	C15	119.80(16)	O2	C47	C48	121.51(17)
C12	C11	C10	120.84(17)	C46	C47	C48	115.16(17)
C13	C12	C11	120.76(17)	C49	C48	C47	118.11(17)
C12	C13	C14	121.11(17)	C49	C48	C53	120.16(17)
C9	C14	C18	123.19(16)	C53	C48	C47	121.72(17)
C13	C14	C9	116.46(16)	C50	C49	C48	120.98(19)
C13	C14	C18	120.34(16)	C49	C50	C51	119.00(19)

Table 3.24 continued: Bond Angles for **3aPQ**.

Atom	Atom	Atom	Angle/°	Atom	Atom	Atom	Angle/°
C10	C15	C16	111.08(15)	C52	C51	C50	121.02(18)
C10	C15	C17	110.72(15)	C51	C52	C53	121.56(19)
C17	C15	C16	111.03(15)	C48	C53	C54	119.81(17)
C14	C18	C19	111.19(16)	C52	C53	C48	117.23(18)
C14	C18	C20	110.60(16)	C52	C53	C54	122.95(18)
C20	C18	C19	110.07(16)	C55	C54	C53	122.96(17)
C22	C21	N1	117.06(15)	C55	C54	C59	118.45(18)
C26	C21	N1	118.88(15)	C59	C54	C53	118.59(17)
C26	C21	C22	124.03(16)	C56	C55	C54	121.26(19)
C21	C22	C27	123.06(16)	C55	C56	C57	120.21(19)
C23	C22	C21	116.73(17)	C58	C57	C56	120.1(2)
C23	C22	C27	120.12(16)	C57	C58	C59	120.94(19)
C24	C23	C22	121.18(17)	C46	C59	C54	118.85(17)
C23	C24	C25	120.21(17)	C58	C59	C46	122.22(17)
C24	C25	C26	121.79(18)	C58	C59	C54	118.94(17)
C21	C26	C30	124.13(16)	C60	O3	C63	104.45(16)
C25	C26	C21	115.98(16)	O3	C60	C61	105.83(18)
C25	C26	C30	119.76(16)	C60	C61	C62	103.84(19)
C22	C27	C28	111.77(16)	C63	C62	C61	103.75(19)
C22	C27	C29	109.95(17)	O3	C63	C62	105.49(18)
C29	C27	C28	111.23(17)				

Table 3.25: Hydrogen Atom Coordinates ($\text{\AA} \times 10^4$) and Isotropic Displacement Parameters ($\text{\AA}^2 \times 10^3$) for **3aPQ**.

Atom	x	y	z	U(eq)
H4	9386.42	3164.18	6473.3	25
H5	9830.74	3434.14	5140.65	33
H6	8204.25	4404.69	4460.77	35
H7	6118.71	5096.1	5107.57	31
H8	5668.97	4847.79	6437.68	25
H11	7213.08	7482.91	7406.83	24
H12	4980.32	8200.91	7473.29	26
H13	3526.35	7277.88	7719.28	24
H15	8766.9	4931.54	7661.38	24

Table 3.25 continued: Hydrogen Atom Coordinates ($\text{\AA}\times 10^4$) and Isotropic Displacement Parameters ($\text{\AA}^2\times 10^3$) for **3aPQ**.

Atom	x	y	z	U(eq)
H16A	8995.44	5651.02	6409.9	46
H16B	10259.59	5555.79	6814.93	46
H16C	9183.42	6579.26	6766.5	46
H17A	8964.86	6680.04	8228.42	42
H17B	10031.21	5650.46	8267.65	42
H17C	8620.1	5822.51	8768.34	42
H18	4411.38	4675.25	7929.78	29
H19A	2426.87	6258.84	7374.11	48
H19B	2466.85	5144.03	7389.04	48
H19C	3522.55	5526.25	6812.81	48
H20A	3691.47	5394.44	9145.24	59
H20B	2505.44	5155.03	8834.61	59
H20C	2603.74	6240.21	8780.58	59
H23	9688.47	1664.43	10410.46	29
H24	7955.23	1245.28	11154.41	32
H25	5881.65	1784.76	10797.1	28
H27	9606.71	2908.33	8567.21	29
H28A	11387.11	1777.44	9562.34	48
H28B	11750.55	2077.96	8676.61	48
H28C	10929.63	1314.34	8891.76	48
H29A	9151.11	4138.38	9463.55	60
H29B	10678.54	3820.07	9147.45	60
H29C	10164.02	3453.06	9987.57	60
H30	4968.38	3225.01	9095.38	25
H31A	4726.58	1649.16	9266.06	51
H31B	3359.47	2419.58	9540.92	51
H31C	4236.81	1815.44	10168.41	51
H32A	4197.47	3407.13	10730.26	49
H32B	3300.89	3959.87	10094.63	49
H32C	4626.64	4210.39	10161.22	49
H36	12074.55	-1125.88	7040.54	34
H37	10833.14	-2189.58	7396.44	39
H38	8746.79	-1643.72	8074.66	36
H40	11114.89	1385.08	7488.65	34
H41A	13421.68	-169.73	7068.73	66

Table 3.25 continued: Hydrogen Atom Coordinates ($\text{\AA}\times 10^4$) and Isotropic Displacement Parameters ($\text{\AA}^2\times 10^3$) for **3aPQ**.

Atom	x	y	z	U(eq)
H41B	12952.07	198.03	7933.42	66
H41C	13390.64	899.53	7264.68	66
H42A	11997.47	1493.99	6186.96	69
H42B	10611.53	1285.68	6243.03	69
H42C	11928.69	430.38	6050.74	69
H43	7058.97	828.96	8537.08	30
H44A	6466.02	-5.68	9671.76	58
H44B	7964.17	-21.55	9609.07	58
H44C	7598.35	-960.07	9404.53	58
H45A	6528.08	-906.98	8194.29	69
H45B	6312.28	42.56	7642.23	69
H45C	5443.14	66.79	8470.82	69
H49	3169.9	2955.22	7959.11	30
H50	1185.5	3599.4	7488.99	35
H51	1159.67	3857.92	6150.71	34
H52	3052.46	3398.67	5299.39	32
H55	4817.72	2975.59	4542.41	33
H56	6777.84	2436.45	3744.07	38
H57	8706.74	1686.44	4274.29	37
H58	8678.13	1544.76	5600.69	31
H60A	7174.78	7522.2	5879.94	46
H60B	8003.56	7957.12	5177.52	46
H61A	5464.29	8858.16	5926.81	49
H61B	6036.74	8977.16	5030.98	49
H62A	6620.7	10269.81	5298.01	51
H62B	5988.96	10179.65	6186.06	51
H63A	8645.77	9450.59	5546.51	51
H63B	8079.03	9764.01	6423	51

Crystal data and structure refinement for **3aAl**:

An X-ray-quality crystal of **3aAl** was obtained by vapor diffusion of pentane into a dichloromethane solution in the glovebox. Thermal ellipsoids were at the 50% probability level. Hydrogen atoms were omitted for clarity.

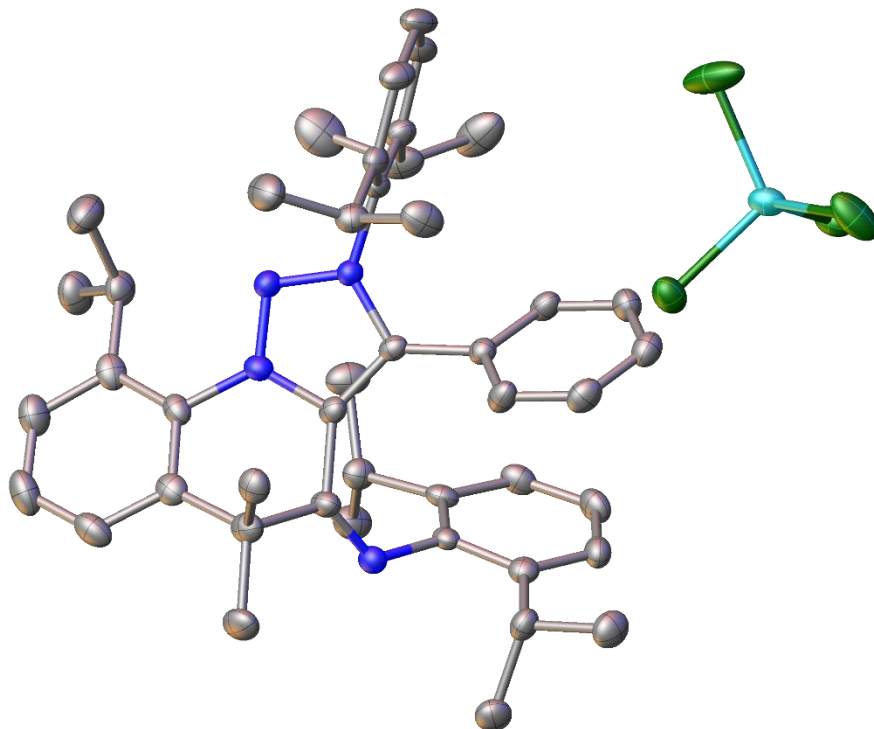


Table 3.26: Crystal Data and Structure Refinement for **3aAl**.

Empirical formula	C ₄₅ H ₅₅ AlCl ₄ N ₄
Formula weight	820.71
Temperature/K	273.15
Crystal system	monoclinic
Space group	P2 ₁
a/Å	12.2300(5)
b/Å	15.1447(6)
c/Å	13.1596(6)
α/°	90

Table 3.26 continued: Crystal Data and Structure Refinement for **3aAl**.

$\beta/^\circ$	115.0380(10)
$\gamma/^\circ$	90
Volume/ \AA^3	2208.37(16)
Z	2
$\rho_{\text{calc}}/\text{cm}^3$	1.234
μ/mm^{-1}	0.323
F(000)	868.0
Crystal size/ mm^3	$0.5 \times 0.4 \times 0.35$
Radiation	MoK α ($\lambda = 0.71073$)
2 Θ range for data collection/ $^\circ$	3.814 to 50.826
Index ranges	$-14 \leq h \leq 14, -18 \leq k \leq 18, -15 \leq l \leq 15$
Reflections collected	48319
Independent reflections	8142 [$R_{\text{int}} = 0.0545, R_{\text{sigma}} = 0.0357$]
Data/restraints/parameters	8142/1/499
Goodness-of-fit on F^2	1.169
Final R indexes [$I \geq 2\sigma(I)$]	$R_1 = 0.0350, wR_2 = 0.0913$
Final R indexes [all data]	$R_1 = 0.0434, wR_2 = 0.1059$
Largest diff. peak/hole / $e \text{\AA}^{-3}$	0.41/-0.67
Flack parameter	-0.03(2)

Table 3.27: Fractional atomic coordinates ($\times 10^4$) and Equivalent Isotropic Displacement Parameters ($\text{\AA}^2 \times 10^3$) for **3aAl**. U_{eq} is defined as 1/3 of the trace of the orthogonalized U_{II} tensor.

Atom	x	y	z	U(eq)
C11	-1383.4(9)	1503.1(6)	7928.0(8)	32.1(2)
C12	450.9(8)	2905.4(7)	7244.2(8)	33.7(2)
C14	-2646.5(10)	3279.9(9)	6145.1(11)	51.9(3)
Al1	-1099.1(11)	2845.6(8)	7587.2(9)	29.2(3)
C13	-863.1(16)	3672.1(8)	8965.3(11)	67.3(5)
N4	4461(3)	4358(2)	5273(2)	22.2(6)
N3	3622(2)	5999.8(19)	7740(2)	18.8(6)
N2	4806(3)	6149.0(19)	8250(2)	20.9(6)
N1	5223(3)	5795.4(19)	7565(2)	21.2(6)
C40	2427(3)	3977(3)	3311(3)	26.2(8)
C10	2434(3)	7261(2)	7800(3)	23.3(8)
C15	2617(3)	7705(2)	6856(3)	26.7(8)

Table 3.27 continued: Fractional atomic coordinates ($\times 10^4$) and Equivalent Isotropic Displacement Parameters ($\text{\AA}^2 \times 10^3$) for **3aAl**. U_{eq} is defined as 1/3 of the trace of the orthogonalized U_{ij} tensor.

Atom	<i>x</i>	<i>y</i>	<i>z</i>	U(eq)
C8	1223(3)	5000(2)	6346(3)	25.2(8)
C34	3645(3)	3750(2)	5409(3)	19.1(7)
C3	2004(3)	5409(2)	5980(3)	20.6(7)
C11	1787(3)	7690(3)	8308(3)	30.3(9)
C37	1989(3)	2557(3)	5512(3)	29.8(8)
C35	2604(3)	3553(2)	4425(3)	22.2(7)
C4	1575(3)	5733(3)	4885(3)	27.6(8)
C5	369(4)	5657(3)	4180(3)	30.2(9)
C6	-418(4)	5261(3)	4554(3)	29.6(9)
C12	1612(4)	7306(3)	9174(3)	35.1(10)
C41	1124(4)	3969(3)	2425(3)	35.2(9)
C9	2885(3)	6427(2)	8222(3)	21.3(7)
C2	3282(3)	5559(2)	6742(3)	19.7(7)
C30	7224(3)	5838(3)	9907(3)	30.2(9)
C33	4720(3)	5094(2)	5773(3)	24.1(8)
C7	17(3)	4932(3)	5637(3)	29.1(8)
C14	2710(3)	6009(3)	9086(3)	26.3(8)
C38	3037(3)	2719(3)	6444(3)	27.4(8)
C36	1778(3)	2965(3)	4496(3)	26.6(8)
C21	6478(3)	5846(2)	7754(3)	23.4(7)
C32	8204(4)	5276(3)	10798(4)	41.6(11)
C42	3242(4)	3513(3)	2849(3)	33.4(9)
C13	2062(3)	6481(3)	9558(3)	33.4(9)
C26	7407(3)	5907(3)	8830(3)	27.1(8)
C43	5112(3)	3369(3)	7456(3)	26.0(8)
C39	3907(3)	3301(2)	6425(3)	22.2(7)
C27	5589(3)	5743(2)	5616(3)	27.3(8)
C45	5741(4)	2474(3)	7713(3)	35.0(9)
C17	3465(4)	8493(3)	7287(4)	42.7(11)
C28	4951(4)	6651(3)	5254(3)	29.3(8)
C22	6650(3)	5837(2)	6766(3)	25.9(8)
C16	1410(4)	7970(3)	5922(3)	38.9(10)
C1	4339(3)	5419(2)	6637(3)	21.2(7)
C31	7175(4)	6759(3)	10363(4)	45.6(11)

Table 3.27 continued: Fractional atomic coordinates ($\times 10^4$) and Equivalent Isotropic Displacement Parameters ($\text{\AA}^2 \times 10^3$) for **3aAl**. U_{eq} is defined as 1/3 of the trace of the orthogonalized U_{IJ} tensor.

Atom	<i>x</i>	<i>y</i>	<i>z</i>	$U(\text{eq})$
C29	5965(4)	5410(3)	4716(4)	35.3(10)
C18	3216(4)	5108(3)	9532(3)	39.0(10)
C44	5003(4)	3698(3)	8506(3)	36.9(10)
C25	8561(4)	6025(3)	8893(4)	35.0(9)
C23	7832(4)	5942(3)	6894(4)	33.0(9)
C19	2305(5)	4511(3)	9695(4)	54.0(13)
C24	8768(4)	6050(3)	7938(4)	38.4(10)
C20	4356(5)	5200(4)	10618(4)	54.0(13)

Table 3.28: Anisotropic Displacement Parameters ($\text{\AA}^2 \times 10^3$) for **3aAl**. The anisotropic displacement factor exponent takes the form: $-2\pi^2[h^2a^{*2}U_{11}+2hka^*b^*U_{12}+\dots]$.

Atom	U_{11}	U_{22}	U_{33}	U_{23}	U_{13}	U_{12}
C11	39.8(5)	26.6(5)	38.4(5)	4.2(4)	24.9(4)	5.7(4)
C12	29.0(5)	43.2(5)	30.2(5)	6.1(4)	13.8(4)	0.4(4)
C14	38.6(6)	65.0(8)	59.2(7)	32.4(6)	27.5(6)	22.9(5)
Al1	38.1(6)	27.4(6)	28.8(6)	2.4(5)	20.7(5)	2.9(5)
Cl3	134.4(13)	39.5(6)	62.6(8)	-18.3(6)	75.2(9)	-27.6(7)
N4	23.6(15)	22.1(16)	23.2(15)	-0.8(13)	12.2(13)	-1.9(12)
N3	19.4(14)	19.2(15)	17.9(14)	-0.7(12)	8.0(12)	-0.4(12)
N2	21.2(15)	20.8(15)	20.2(14)	-1.7(12)	8.4(12)	-0.9(11)
N1	23.4(15)	19.4(15)	23.9(15)	-1.1(12)	12.9(13)	0.9(12)
C40	26.9(19)	27.5(19)	20.7(18)	-2.2(15)	6.6(16)	-5.2(15)
C10	17.9(18)	27(2)	21.6(18)	-3.1(15)	5.6(15)	0.0(14)
C15	31(2)	23(2)	26.7(18)	0.0(15)	13.6(16)	2.9(15)
C8	31(2)	25.6(19)	19.0(17)	-2.7(15)	10.3(16)	-5.5(15)
C34	20.9(17)	17.1(17)	23.4(17)	-2.6(14)	13.5(14)	0.3(13)
C3	22.4(18)	18.6(17)	20.9(17)	-2.2(14)	9.4(15)	-1.7(14)
C11	30(2)	32(2)	26.3(19)	-4.8(16)	9.3(17)	8.6(16)
C37	29(2)	28(2)	39(2)	2.2(17)	20.7(18)	-4.4(16)
C35	24.9(18)	18.3(18)	25.1(17)	-0.8(14)	12.1(15)	2.7(14)
C4	32(2)	31(2)	20.6(18)	-2.6(15)	11.9(16)	-11.4(16)
C5	36(2)	29(2)	20.5(18)	1.7(15)	7.6(17)	-1.2(17)
C6	27(2)	27(2)	29(2)	-3.1(16)	6.3(17)	-1.0(15)

Table 3.28 continued: Anisotropic Displacement Parameters ($\text{\AA}^2 \times 10^3$) for **3aAl**. The anisotropic displacement factor exponent takes the form: $-2\pi^2[h^2a^{*2}U_{11}+2hka^*b^*U_{12}+\dots]$.

Atom	U ₁₁	U ₂₂	U ₃₃	U ₂₃	U ₁₃	U ₁₂
C12	30(2)	51(3)	27(2)	-9.2(18)	14.1(18)	7.6(19)
C41	33(2)	38(2)	28(2)	0.6(17)	5.8(18)	3.2(17)
C9	17.7(16)	27.4(19)	18.1(16)	-6.5(14)	7.0(14)	-0.6(14)
C2	25.9(18)	16.6(16)	17.8(16)	-0.9(13)	10.2(14)	-2.4(13)
C30	22.2(19)	34(2)	29(2)	0.5(17)	5.8(16)	1.6(16)
C33	28(2)	22.8(19)	26.7(19)	-3.4(15)	17.1(16)	-3.4(15)
C7	25(2)	32(2)	31(2)	-2.3(17)	13.1(17)	-4.8(16)
C14	31(2)	28(2)	20.6(17)	-3.3(15)	11.4(15)	-3.0(16)
C38	31(2)	28(2)	28.4(19)	7.7(15)	18.0(17)	4.6(16)
C36	21.7(18)	25.4(19)	31.9(19)	-4.9(16)	10.7(16)	-3.6(15)
C21	21.1(18)	18.6(17)	32.5(19)	1.2(15)	13.2(16)	0.2(14)
C32	30(2)	54(3)	35(2)	7(2)	7.6(19)	1(2)
C42	37(2)	41(2)	23.1(19)	-0.1(17)	13.8(17)	-0.9(18)
C13	32(2)	50(3)	23.7(19)	-8.9(18)	16.9(17)	-5.7(19)
C26	23.3(18)	21.0(18)	35(2)	6.3(16)	9.9(16)	3.7(15)
C43	26.1(19)	27.8(19)	22.3(18)	3.0(15)	8.4(16)	3.7(15)
C39	27.0(18)	21.7(17)	24.1(18)	1.5(14)	16.9(15)	5.0(14)
C27	34(2)	22.4(19)	31(2)	-0.6(15)	19.4(17)	-5.5(15)
C45	31(2)	41(2)	30(2)	2.9(18)	9.9(18)	10.5(18)
C17	48(3)	34(2)	54(3)	-10(2)	29(2)	-11(2)
C28	31(2)	29(2)	29.1(19)	3.9(16)	13.8(17)	-5.3(16)
C22	30.0(19)	17.0(17)	33(2)	2.2(15)	15.9(17)	-0.3(15)
C16	40(2)	47(3)	30(2)	12(2)	15.7(19)	12(2)
C1	25.5(19)	18.4(18)	21.2(17)	-2.0(14)	11.2(15)	-5.2(14)
C31	40(3)	45(3)	45(3)	-13(2)	12(2)	-3(2)
C29	43(2)	37(2)	38(2)	-3.0(18)	29(2)	-10.2(19)
C18	60(3)	34(2)	30(2)	4.0(18)	26(2)	2(2)
C44	48(3)	35(2)	28(2)	4.7(18)	16.0(19)	11.9(19)
C25	26(2)	35(2)	40(2)	5.8(19)	10.0(18)	-0.6(17)
C23	35(2)	29(2)	45(2)	6.9(18)	27(2)	3.2(17)
C19	87(4)	43(3)	34(2)	1(2)	27(3)	-19(3)
C24	25(2)	38(2)	52(3)	11(2)	16(2)	-2.0(17)
C20	54(3)	50(3)	58(3)	25(2)	24(3)	21(2)

Table 3.29: Bond Lengths for **3aAl**.

Atom	Atom	Length/Å	Atom	Atom	Length/Å
C11	Al1	2.1420(15)	C35	C36	1.379(5)
C12	Al1	2.1283(14)	C4	C5	1.375(5)
C14	Al1	2.1390(16)	C5	C6	1.389(6)
Al1	Cl3	2.1204(16)	C6	C7	1.385(6)
N4	C34	1.424(5)	C12	C13	1.373(6)
N4	C33	1.264(5)	C9	C14	1.394(5)
N3	N2	1.333(4)	C2	C1	1.374(5)
N3	C9	1.455(4)	C30	C32	1.531(6)
N3	C2	1.372(4)	C30	C26	1.529(5)
N2	N1	1.322(4)	C30	C31	1.530(6)
N1	C21	1.449(4)	C33	C27	1.525(5)
N1	C1	1.367(5)	C33	C1	1.483(5)
C40	C35	1.530(5)	C14	C13	1.392(6)
C40	C41	1.525(5)	C14	C18	1.511(6)
C40	C42	1.539(6)	C38	C39	1.391(5)
C10	C15	1.511(5)	C21	C26	1.393(5)
C10	C11	1.394(5)	C21	C22	1.403(5)
C10	C9	1.396(5)	C26	C25	1.390(5)
C15	C17	1.524(6)	C43	C39	1.526(5)
C15	C16	1.521(5)	C43	C45	1.525(5)
C8	C3	1.385(5)	C43	C44	1.527(5)
C8	C7	1.375(5)	C27	C28	1.554(5)
C34	C35	1.411(5)	C27	C22	1.528(5)
C34	C39	1.411(5)	C27	C29	1.526(5)
C3	C4	1.398(5)	C22	C23	1.392(5)
C3	C2	1.473(5)	C18	C19	1.519(7)
C11	C12	1.375(6)	C18	C20	1.522(7)
C37	C38	1.370(5)	C25	C24	1.383(6)
C37	C36	1.394(6)	C23	C24	1.376(6)

Table 3.30: Bond Angles for **3aAl**.

Atom	Atom	Atom	Angle/°	Atom	Atom	Atom	Angle/°
C12	A11	C11	108.84(6)	C1	C2	C3	132.9(3)
C12	A11	C14	109.38(6)	C26	C30	C32	112.0(3)
C14	A11	C11	108.46(7)	C26	C30	C31	110.3(4)
C13	A11	C11	110.89(6)	C31	C30	C32	110.7(3)
C13	A11	C12	110.19(7)	N4	C33	C27	122.2(3)
C13	A11	C14	109.05(8)	N4	C33	C1	127.0(3)
C33	N4	C34	122.6(3)	C1	C33	C27	110.7(3)
N2	N3	C9	116.5(3)	C8	C7	C6	120.4(4)
N2	N3	C2	112.9(3)	C9	C14	C18	123.2(3)
C2	N3	C9	129.9(3)	C13	C14	C9	116.3(4)
N1	N2	N3	103.8(3)	C13	C14	C18	120.5(4)
N2	N1	C21	123.2(3)	C37	C38	C39	122.0(3)
N2	N1	C1	113.0(3)	C35	C36	C37	120.6(3)
C1	N1	C21	123.7(3)	C26	C21	N1	121.8(3)
C35	C40	C42	109.5(3)	C26	C21	C22	124.4(3)
C41	C40	C35	114.0(3)	C22	C21	N1	113.8(3)
C41	C40	C42	109.7(3)	C12	C13	C14	121.2(4)
C11	C10	C15	119.9(3)	C21	C26	C30	124.1(3)
C11	C10	C9	116.1(3)	C25	C26	C30	119.7(3)
C9	C10	C15	124.0(3)	C25	C26	C21	116.1(4)
C10	C15	C17	110.9(3)	C39	C43	C44	113.9(3)
C10	C15	C16	110.6(3)	C45	C43	C39	110.1(3)
C16	C15	C17	111.7(3)	C45	C43	C44	108.5(3)
C7	C8	C3	119.8(3)	C34	C39	C43	123.8(3)
C35	C34	N4	115.4(3)	C38	C39	C34	117.0(3)
C39	C34	N4	122.7(3)	C38	C39	C43	119.0(3)
C39	C34	C35	121.5(3)	C33	C27	C28	108.9(3)
C8	C3	C4	120.1(3)	C33	C27	C22	105.9(3)
C8	C3	C2	121.4(3)	C33	C27	C29	110.4(3)
C4	C3	C2	118.3(3)	C22	C27	C28	109.0(3)
C12	C11	C10	121.3(4)	C29	C27	C28	109.4(3)
C38	C37	C36	120.1(3)	C29	C27	C22	113.1(3)
C34	C35	C40	119.8(3)	C21	C22	C27	121.5(3)
C36	C35	C40	121.7(3)	C23	C22	C21	116.3(3)
C36	C35	C34	118.4(3)	C23	C22	C27	122.2(3)

Table 3.30 continued: Bond Angles for **3aAl**.

Atom	Atom	Atom	Angle/°	Atom	Atom	Atom	Angle/°
C5	C4	C3	119.5(3)	N1	C1	C2	105.5(3)
C4	C5	C6	120.3(4)	N1	C1	C33	116.0(3)
C7	C6	C5	119.8(4)	C2	C1	C33	137.9(3)
C13	C12	C11	120.7(4)	C14	C18	C19	112.9(4)
C10	C9	N3	116.2(3)	C14	C18	C20	110.1(4)
C14	C9	N3	119.4(3)	C19	C18	C20	110.9(4)
C14	C9	C10	124.3(3)	C24	C25	C26	121.4(4)
N3	C2	C3	122.0(3)	C24	C23	C22	121.1(4)
N3	C2	C1	104.7(3)	C23	C24	C25	120.6(4)

Table 3.31: Hydrogen Atom Coordinates ($\text{\AA} \times 10^4$) and Isotropic Displacement Parameters ($\text{\AA}^2 \times 10^3$) for **3aAl**.

Atom	<i>x</i>	<i>y</i>	<i>z</i>	U(eq)
H40	2686.76	4594.4	3459.81	31
H15	2994.8	7276.55	6546.43	32
H8	1512.94	4771.2	7068.34	30
H11	1468.01	8247.18	8056.5	36
H37	1416.49	2173.22	5556.66	36
H4	2102.15	5997.52	4633.71	33
H5	78.97	5872.28	3451.06	36
H6	-1235.42	5217.18	4079.45	36
H12	1183.4	7608.43	9503.79	42
H41A	872.63	3370.33	2211.74	53
H41B	1066.96	4295.4	1779.28	53
H41C	612.9	4235.05	2726.81	53
H30	6444.98	5550.09	9721.51	36
H7	-509.1	4664.32	5885.7	35
H38	3170.16	2430.58	7110.79	33
H36	1075.18	2840.32	3861.9	32
H32A	8276.39	4723.77	10474.12	62
H32B	7989.85	5168.78	11409.58	62
H32C	8960.49	5584.56	11068.73	62
H42A	4066.06	3539.52	3397.35	50
H42B	3168.62	3802.15	2174.45	50
H42C	3000.63	2906.61	2688.84	50

Table 3.31 continued: Hydrogen Atom Coordinates ($\text{\AA}\times 10^4$) and Isotropic Displacement Parameters ($\text{\AA}^2\times 10^3$) for **3aAl**.

Atom	<i>x</i>	<i>y</i>	<i>z</i>	U(eq)
H13	1931.94	6231.73	10143.1	40
H43	5625.08	3784.07	7283.75	31
H45A	5284.81	2068.31	7943.39	53
H45B	6536.37	2537.45	8305.12	53
H45C	5796.13	2250.91	7053.81	53
H17A	3108.33	8927.7	7584.03	64
H17B	3602.57	8745.26	6682.12	64
H17C	4219.49	8301.07	7867.1	64
H28A	4223.93	6581.05	4579.59	44
H28B	5478.68	7057.44	5121.06	44
H28C	4754.99	6877.07	5838.77	44
H16A	907.21	7457.6	5657.14	58
H16B	1539.95	8228.67	5316.24	58
H16C	1021.46	8392.41	6204.56	58
H31A	7042.04	6706.89	11029.15	68
H31B	6528	7089.36	9808.12	68
H31C	7925.7	7058.39	10538.93	68
H29A	6399.11	4865.14	4956.92	53
H29B	6473.75	5841.37	4595.19	53
H29C	5259.56	5315.61	4029.47	53
H18	3444.08	4827.06	8978.78	47
H44A	4625.44	4268.08	8362.2	55
H44B	5792.71	3741.05	9113.23	55
H44C	4523.51	3290.43	8704.04	55
H25	9207.38	6089.13	9592.25	42
H23	7992.64	5938.45	6263.43	40
H19A	2115.73	4744.51	10279.26	81
H19B	2640.92	3929.56	9899.36	81
H19C	1583.65	4480.06	9008.94	81
H24	9546.53	6140.97	8002.86	46
H20A	4913.85	5584.77	10498.02	81
H20B	4718.73	4629.96	10851.05	81
H20C	4152.7	5443.72	11189.61	81

3.6: Chapter 3 References

- (1) Sander, Wolfram.; Bucher, Goetz.; Wierlacher, Stefan. Carbenes in Matrixes: Spectroscopy, Structure, and Reactivity. *Chem. Rev.* **1993**, *93* (4), 1583–1621. <https://doi.org/10.1021/cr00020a009>.
- (2) Lavallo, V.; Canac, Y.; Donnadiu, B.; Schoeller, W. W.; Bertrand, G. CO Fixation to Stable Acyclic and Cyclic Alkyl Amino Carbenes: Stable Amino Ketenes with a Small HOMO–LUMO Gap. *Angewandte Chemie International Edition* **2006**, *45* (21), 3488–3491. <https://doi.org/10.1002/anie.200600987>.
- (3) Peltier, J. L.; Tomás-Mendivil, E.; Tolentino, D. R.; Hansmann, M. M.; Jazzar, R.; Bertrand, G. Realizing Metal-Free Carbene-Catalyzed Carbonylation Reactions with CO. *J. Am. Chem. Soc.* **2020**, *142* (43), 18336–18340. <https://doi.org/10.1021/jacs.0c09938>.
- (4) Hudnall, T. W.; Bielawski, C. W. An N,N'-Diamidocarbene: Studies in C–H Insertion, Reversible Carbonylation, and Transition-Metal Coordination Chemistry. *J. Am. Chem. Soc.* **2009**, *131* (44), 16039–16041. <https://doi.org/10.1021/ja907481w>.
- (5) Dixon, D. A.; Arduengo, A. J.; Dobbs, K. D.; Khasnis, D. V. On the Proposed Existence of a Ketene Derived from Carbon Monoxide and 1,3-Di-1-Adamantylimidazol-2-Ylidene. *Tetrahedron Letters* **1995**, *36* (5), 645–648. [https://doi.org/10.1016/0040-4039\(94\)02341-8](https://doi.org/10.1016/0040-4039(94)02341-8).
- (6) Goedecke, C.; Leibold, M.; Siemeling, U.; Frenking, G. When Does Carbonylation of Carbenes Yield Ketenes? A Theoretical Study with Implications for Synthesis. *J. Am. Chem. Soc.* **2011**, *133* (10), 3557–3569. <https://doi.org/10.1021/ja109812r>.
- (7) Igau, A.; Baceiredo, A.; Trinquier, G.; Bertrand, G. [Bis(Diisopropylamino)Phosphino]Trimethylsilylcarbene: A Stable Nucleophilic Carbene. *Angewandte Chemie International Edition in English* **1989**, *28* (5), 621–622. <https://doi.org/10.1002/anie.198906211>.
- (8) Martin, D.; Canac, Y.; Lavallo, V.; Bertrand, G. Comparative Reactivity of Different Types of Stable Cyclic and Acyclic Mono- and Diamino Carbenes with Simple Organic Substrates. *J. Am. Chem. Soc.* **2014**, *136* (13), 5023–5030. <https://doi.org/10.1021/ja412981x>.
- (9) Hudnall, T. W.; Moorhead, E. J.; Gusev, D. G.; Bielawski, C. W. N,N'-Diamidoketenimines via Coupling of Isocyanides to an N-Heterocyclic Carbene. *J. Org. Chem.* **2010**, *75* (8), 2763–2766. <https://doi.org/10.1021/jo100427g>.
- (10) Kim, Y.; Liu, L. L.; Stephan, D. W. N-Heterocyclic Carbene Derived 3-Azabutadiene as a π -Base in Classic and Frustrated Lewis Pair Chemistry. *Chem. Eur. J.* **2019**, *25* (29), 7110–7113. <https://doi.org/10.1002/chem.201901609>.
- (11) Walborsky, H. M.; Niznik, G. E. Lithium Aldimines. A New Synthetic Intermediate. *J. Am. Chem. Soc.* **1969**, *91* (27), 7778–7778. <https://doi.org/10.1021/ja50001a064>.

- (12) Niznik, G. E.; Morrison, W. H.; Walborsky, H. M. Metallo Aldimines. Masked Acyl Carbanion. *J. Org. Chem.* **1974**, *39* (5), 600–604. <https://doi.org/10.1021/jo00919a004>.
- (13) Arduengo, I., Anthony J.; Dias, H. V. R.; Calabrese, J. C. A Carbene•Phosphinidene Adduct: “Phosphaalkene.” *Chem. Lett.* **1997**, *26* (2), 143–144. <https://doi.org/10.1246/cl.1997.143>.
- (14) Arduengo, A. J.; Calabrese, J. C.; Cowley, A. H.; Dias, H. V. R.; Goerlich, J. R.; Marshall, W. J.; Riegel, B. Carbene–Pnictinidene Adducts. *Inorg. Chem.* **1997**, *36* (10), 2151–2158. <https://doi.org/10.1021/ic970174q>.
- (15) Back, O.; Henry-Ellinger, M.; Martin, C. D.; Martin, D.; Bertrand, G. 31P NMR Chemical Shifts of Carbene–Phosphinidene Adducts as an Indicator of the π -Accepting Properties of Carbenes. *Angewandte Chemie International Edition* **2013**, *52* (10), 2939–2943. <https://doi.org/10.1002/anie.201209109>.
- (16) Dong, Z.; Pezzato, C.; Sienkiewicz, A.; Scopelliti, R.; Fadaei-Tirani, F.; Severin, K. SET Processes in Lewis Acid–Base Reactions: The Tritylation of N-Heterocyclic Carbenes. *Chem. Sci.* **2020**, *11* (29), 7615–7618. <https://doi.org/10.1039/D0SC01278E>.
- (17) Tao, X.; Daniliuc, C. G.; Janka, O.; Pöttgen, R.; Knitsch, R.; Hansen, M. R.; Eckert, H.; Lübbsmeyer, M.; Studer, A.; Kehr, G.; Erker, G. Reduction of Dioxygen by Radical/B(p-C6F4X)3 Pairs to Give Isolable Bis(Borane)Superoxide Compounds. *Angewandte Chemie International Edition* **2017**, *56* (52), 16641–16644. <https://doi.org/10.1002/anie.201709309>.
- (18) Connelly, N. G.; Geiger, W. E. Chemical Redox Agents for Organometallic Chemistry. *Chem. Rev.* **1996**, *96* (2), 877–910. <https://doi.org/10.1021/cr940053x>.
- (19) Saunders, J. O.; Wang, Z.; Ding, K. Diphenylphosphine Oxide. In *Encyclopedia of Reagents for Organic Synthesis*; John Wiley & Sons, Ltd, 2007. <https://doi.org/10.1002/047084289X.rd428.pub2>.
- (20) Hirai, T.; Han, L.-B. Palladium-Catalyzed Insertion of Isocyanides into P(O)–H Bonds: Selective Formation of Phosphinoyl Imines and Bisphosphinoylaminomethanes. *J. Am. Chem. Soc.* **2006**, *128* (23), 7422–7423. <https://doi.org/10.1021/ja060984d>.
- (21) Yuan, Q.; Liu, H.-W.; Cai, Z.-J.; Ji, S.-J. Direct 1,1-Bisphosphonation of Isocyanides: Atom- and Step-Economical Access to Bisphosphinoylaminomethanes. *ACS Omega* **2021**, *6* (12), 8495–8501. <https://doi.org/10.1021/acsomega.1c00160>.
- (22) Moerdyk, J. P.; Schilter, D.; Bielawski, C. W. N,N'-Diamidocarbenes: Isolable Divalent Carbons with Bona Fide Carbene Reactivity. *Accounts of Chemical Research* **2016**, *49* (8), 1458–1468. <https://doi.org/10.1021/acs.accounts.6b00080>.
- (23) Bouffard, J.; Keitz, B. K.; Tonner, R.; Guisado-Barrios, G.; Frenking, G.; Grubbs, R. H.; Bertrand, G. Synthesis of Highly Stable 1,3-Diaryl-1 H -1,2,3-Triazol-5-Ylidenes and

- Their Applications in Ruthenium-Catalyzed Olefin Metathesis. *Organometallics* **2011**, *30* (9), 2617–2627. <https://doi.org/10.1021/om200272m>.
- (24) Said, S. B.; Młochowski, J.; Skarzewski, J. Synthesis of 2-Alkyl-3-Vinyloxaziridines as Potential Antitumor Agents. *Liebigs Annalen der Chemie* **1990**, *1990* (5), 461–464. <https://doi.org/10.1002/jlac.199019900187>.
- (25) Semba, K.; Shinomiya, M.; Fujihara, T.; Terao, J.; Tsuji, Y. Highly Selective Copper-Catalyzed Hydroboration of Allenes and 1,3-Dienes. *Chemistry – A European Journal* **2013**, *19* (22), 7125–7132. <https://doi.org/10.1002/chem.201300443>.
- (26) Škoch, K.; Císařová, I.; Štěpnička, P. Selective Gold-Catalysed Synthesis of Cyanamides and 1-Substituted 1H-Tetrazol-5-Amines from Isocyanides. *Chemistry – A European Journal* **2018**, *24* (52), 13788–13791. <https://doi.org/10.1002/chem.201803252>.
- (27) Barrett, A. G. M.; Crimmin, M. R.; Hill, M. S.; Hitchcock, P. B.; Kociok-Köhn, G.; Procopiou, P. A. Triazenide Complexes of the Heavier Alkaline Earths: Synthesis, Characterization, And Suitability for Hydroamination Catalysis. *Inorg. Chem.* **2008**, *47* (16), 7366–7376. <https://doi.org/10.1021/ic800789x>.
- (28) Stoll, S.; Schweiger, A. EasySpin, a Comprehensive Software Package for Spectral Simulation and Analysis in EPR. *Journal of Magnetic Resonance* **2006**, *178* (1), 42–55. <https://doi.org/10.1016/j.jmr.2005.08.013>.
- (29) Dolomanov, O. V.; Bourhis, L. J.; Gildea, R. J.; Howard, J. a. K.; Puschmann, H. OLEX2: A Complete Structure Solution, Refinement and Analysis Program. *J Appl Cryst* **2009**, *42* (2), 339–341. <https://doi.org/10.1107/S0021889808042726>.
- (30) Sheldrick, G. M. SHELXT – Integrated Space-Group and Crystal-Structure Determination. *Acta Cryst A* **2015**, *71* (1), 3–8. <https://doi.org/10.1107/S2053273314026370>.
- (31) Sheldrick, G. M. Crystal Structure Refinement with SHELXL. *Acta Cryst C* **2015**, *71* (1), 3–8. <https://doi.org/10.1107/S2053229614024218>.

CHAPTER 4: SINGLE
ELECTRON TRANSFER
REACTIONS OF FREE
MESOIONIC CARBENES

4.1: Introduction

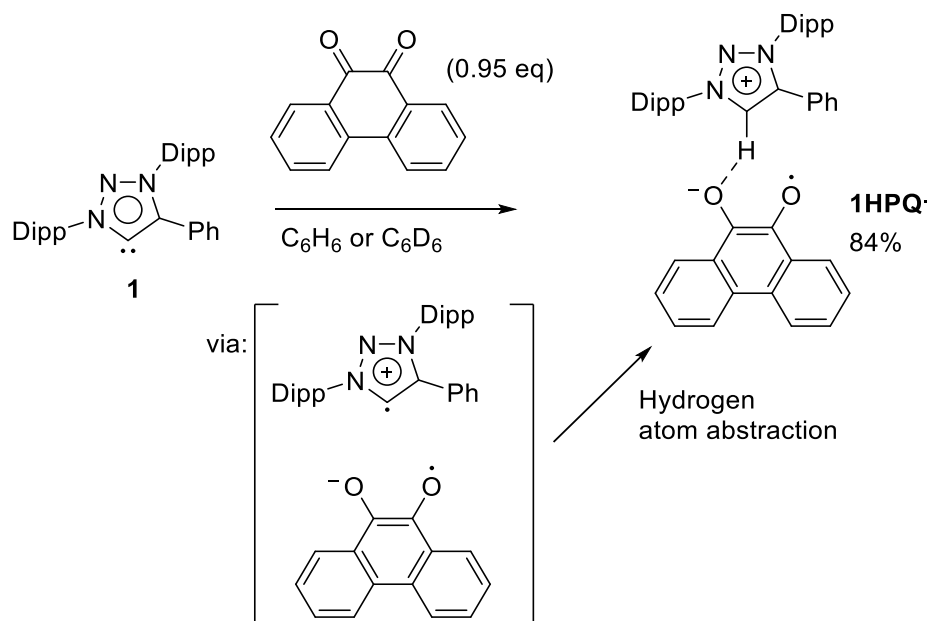
While single electron transfer (SET) is normally the purview of metallic elements (i.e. sodium, magnesium, etc.), this reactivity is also accessible to a number of organic molecules. A relatively common example is tetrakis(dimethylamino)ethylene, or TDAE, which can undergo two successive single electron oxidations to a resonance-stabilized dication.^{1,2} This resonance stability is a common feature of many organic electron donors, as exemplified by bis-imidazolium and bis-benzimidazolium electron donors (see chapter 1).³⁻⁸ Naturally, organic electron donors are tempting reagents as they do not have the same sustainability issues as metal elements do.

As in chapter 3, we were curious as to the possibility of expanding on the carbene-catalyzed carbonylation of quinones with carbon monoxide⁹ by using different carbenes. In that report, it was found that the carbene used was critical, as a smaller dimethyl substituted CAAC or the BiCAAC would react directly with phenanthrenequinone to form a spirocyclic dioxolane or a lactone insertion product, respectively. Naturally, we wanted to check if mesoionic carbenes would react directly with phenanthrenequinone and, in the process, we made a serendipitous discovery of SET reactivity of the MIC.

4.2: Results and Discussion

To our surprise, upon dissolving a 1:1 mixture of MIC **1** and phenanthrenequinone in C₆D₆, the solution immediately took on a purple color. Curiously, this sample proved to be NMR silent. However, we were excited to find that this unknown product crystallized spontaneously out of the benzene solution allowing an XRD study. The solid-state structure was determined to be **1HPQ**, the salt of a cationic protonated triazolium with the phenanthrenequinone radical anion (semiquinone). A single electron transfer from the carbene to the quinone must have

occurred, but that necessarily implies the formation of a carbene radical cation, a species which hitherto has never been isolated.



Scheme 4.1: Reduction of phenanthrenequinone by free MIC 1.

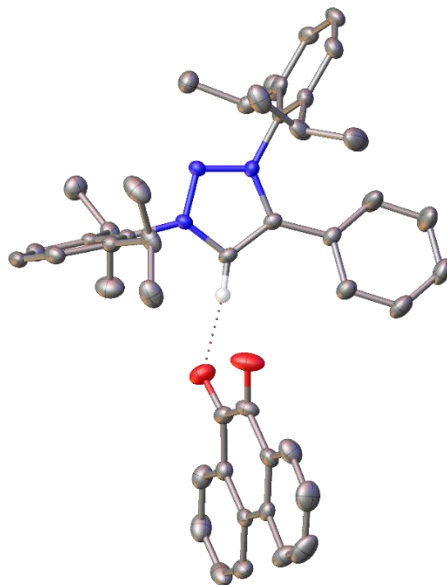


Figure 4.1: Solid state structure of 1HPQ.

Hydrogen atoms are not readily identified in single-crystal XRD, but the relative position of the carbene to the semiquinone suggested a hydrogen-bonding interaction between the two. Furthermore, an EPR study of **1HPQ** indicated a single radical species with $g_{\text{iso}} = 2.0042$ and poorly resolved hyperfine coupling which we reason is the semiquinone. Thus, we propose that carbene **1** reduces phenanthrenequinone by one electron to generate the transient carbene radical cation and this, in turn, rapidly undergoes hydrogen atom abstraction to make the protonated triazolium salt.

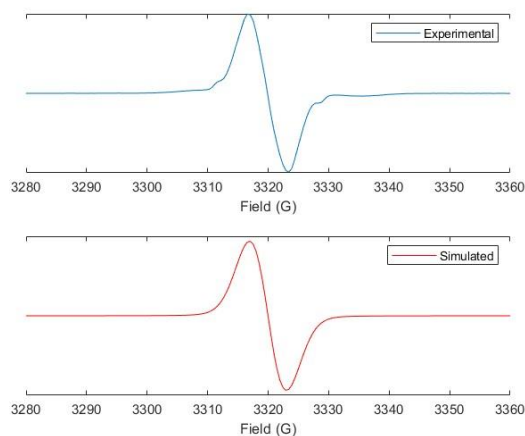
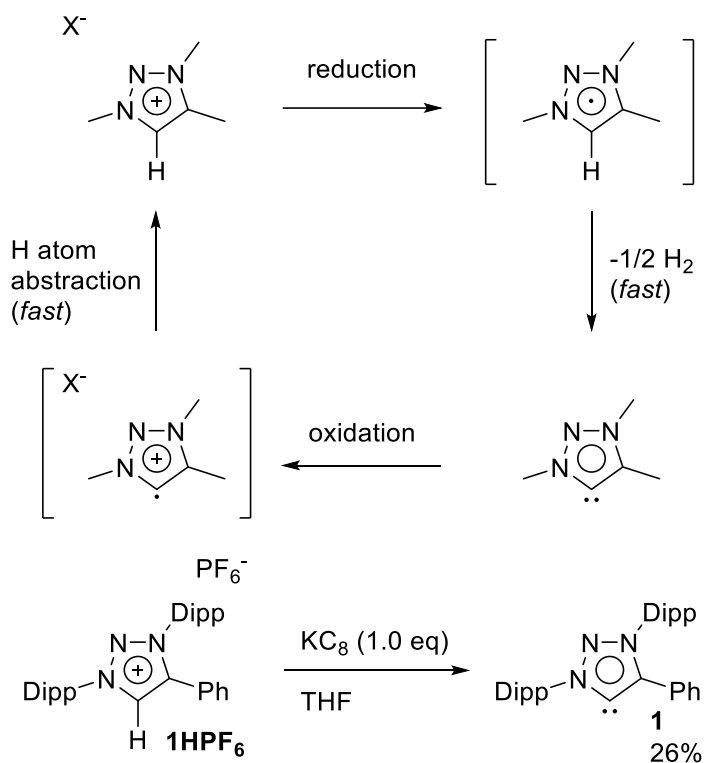


Figure 4.2: EPR spectrum of **1HPQ** with experimental data in blue (*top*) and simulated fit in red (*bottom*).

There had been some reports up to this point of free NHCs in SET reactions, although only one example showed hydrogen atom abstraction to give the protonated imidazolium salt.^{10–12} Furthermore, the radical cation could not be observed, even transiently, hinting at its rapid reactivity. Recently, CAACs were also demonstrated to undergo SET reactivity and the radical cation could be observed by EPR prior to hydrogen abstraction, but only at low temperature.¹³

Naturally, we wondered what the redox potential of the carbene might be, as that would guide our continued investigation. Cyclic voltammetry (CV) measurements of carbene **1** in THF revealed a one-electron redox couple at -1.86 vs. the ferrocene/ferrocenium (Fc/Fc⁺) couple.

However, we noted that CV of the protonated salt **1HPF₆** in THF also showed a redox couple at -1.86 V vs. Fc/Fc⁺. We reason that at room temperature, the oxidation of the free carbene is coupled with the hydrogen atom abstraction and, likewise, the reduction of the triazolium salt is coupled with loss of hydrogen (as H₂) to form the free carbene, which would obfuscate the actual reducing potential of the carbene. Indeed, when **1HPF₆** was reacted with potassium graphite in THF, carbene **1** was isolated in 26% yield.



Scheme 4.2: General reactions of triazolium/MICs under cyclic voltammetry (*top*) and the formation of carbene **1** by reduction of **1HPF₆** with KC₈ (*bottom*).

This odd behavior under cyclovoltammetry is not limited to MICs. CAAC was previously reported to have a redox couple in CV of +0.4-0.5 V vs. Fc/Fc⁺, yet it could reduce cations with redox couples as negative as -1.3 V.¹³ In the same vein, the phenanthrenequinone to semiquinone redox couple is reported at -1.13 V vs Fc/Fc⁺ in dichloromethane with 0.1M

tetrabutylammonium hexafluorophosphate electrolyte.¹⁴ The rapid reactivity of **1** with phenanthrenequinone suggests that **1** has a redox potential more negative than -1.13 V.

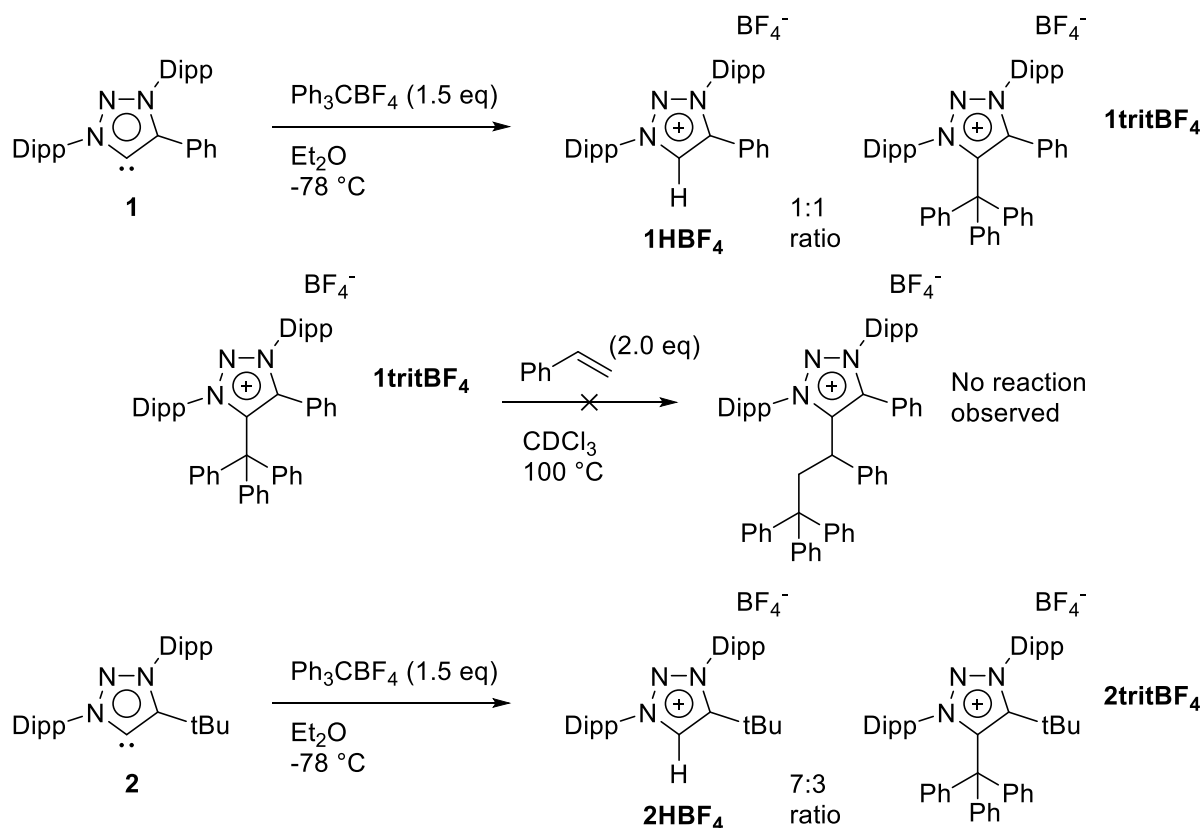
Despite the difficulty in measuring their redox potential, we wondered what other SET chemistry the MIC could do. We noticed that following our original reaction to form **1HPQ**, Severin and co-workers disclosed further proof of the SET reactivity of NHCs by reacting the IPr carbene with a triphenylmethyl radical to form the end-on adduct reminiscent of the Gomberg dimer.¹⁵ We were curious if the MIC might show similar reactivity as well.

Reaction of carbene **1** with triphenylcarbenium tetrafluoroborate at -78 °C in diethyl ether gave a 1:1 mixture of **1HBF₄** and a carbene-trityl adduct. The presence of the former suggested an SET process where the carbene radical cation underwent hydrogen atom abstraction. The product mixture could be separated by reaction with potassium tert-butoxide followed by extraction of free carbene **1** to leave just the trityl adduct, which was subsequently identified as **1tritBF₄** by NMR spectroscopy.

Given the large steric environment of the triphenylmethyl group, we wondered if **1tritBF₄** might act like a carbon-carbon frustrated Lewis pair. To that end, a sample was heated with styrene in deuterated chloroform to see if the alkene might be inserted into the triazolium-trityl C-C bond. However, even after two days at 100 °C, no reaction was observed.

Another point we considered was that although the carbene-trityl adduct was attached at the center triphenylmethyl carbon, that did not necessarily imply that its formation was a polar (two electron process). Indeed, Severin had reported that the reaction of triphenylmethyl cation with less sterically encumbered mesityl-substituted NHC gave the same type of adduct as we had observed. Thinking that a bulkier steric environment might change the MIC's reactivity, we redid the reaction using the bulky tert-butyl-substituted carbene **2**. In this case, a mixture of the

protonated triazolium (**2HBF₄**) and the centrally tethered adduct (**2tritBF₄**) was still observed, but now in a ~7:3 ratio.

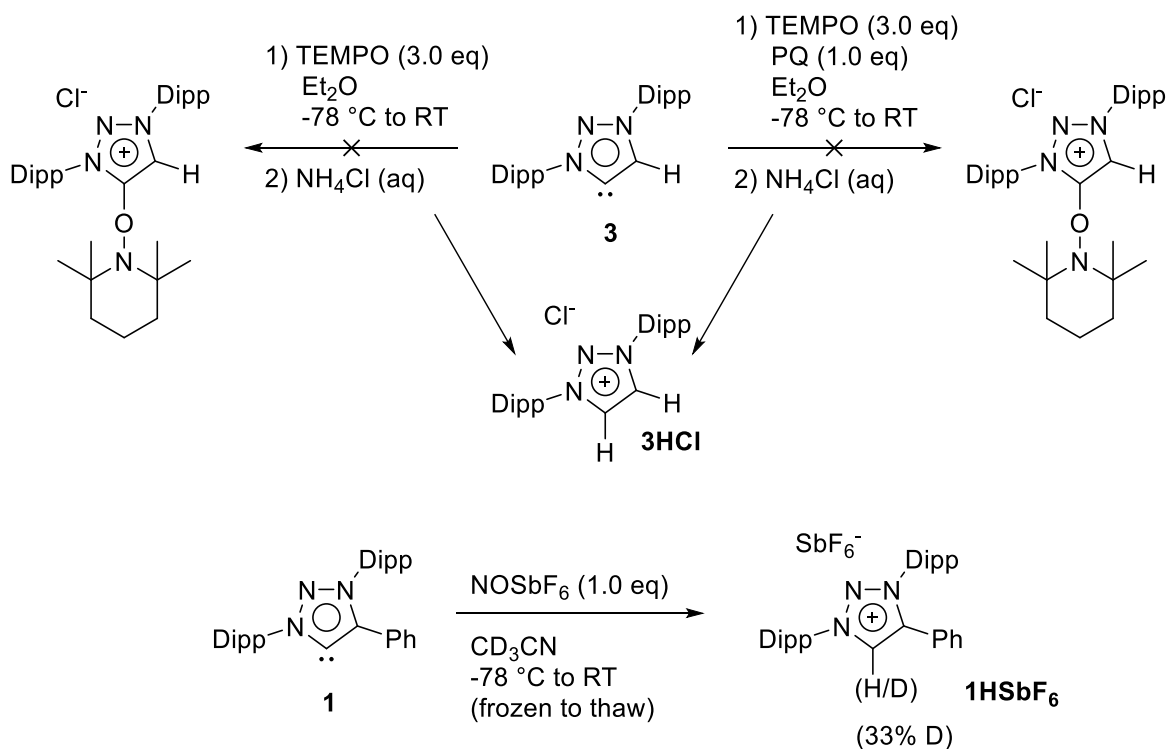


Scheme 4.3: Reactions of carbenes **1** and **2** with trityl cation.

These results prompted us to consider that radical cations derived from mesoionic carbenes might undergo hydrogen abstraction faster than other carbenes. Indeed, in the case of analogous Arduengo-type NHCs, no EPR signal for the radical cation could be observed even at low temperature. Regardless, we wondered if it might be possible to use a radical trapping reagent to unambiguously prove the formation of the MIC radical cation. The sterically unencumbered MIC **3** was chosen for this purpose to maximize the chance that the radical would react with the trap rather than abstract a hydrogen atom.

Carbene **3** was reacted with an excess of TEMPO in diethyl ether at -78°C but, after workup with ammonium chloride, only **3HCl** was obtained. This reaction was repeated with the

addition of one equivalent of phenanthrenequinone in case TEMPO alone is insufficiently oxidizing but, again, only **3HCl** was obtained after workup. Throughout these experiments, we reasoned that the most likely source of the hydrogen atom was the solvent. However, none of the previous reports verified this theory. As such, we reacted carbene **1** with nitrosonium hexafluoroantimonate in deuterated acetonitrile by layering frozen solutions of each and allowing them to slowly thaw. To further reduce the presence of hydrogen atoms, the glassware used was silanized by chlorotrimethylsilane. While ^1H NMR showed all signals consistent with **1HSbF₆**, a ^2H NMR study showed some deuterium enrichment at the triazolium C-H. By comparison of the peak integrations in the ^1H NMR, deuterium enrichment was estimated at ~33%. Presumably, protons are preferentially abstracted over deuterium atoms due to the kinetic isotope effect, explaining the partial isotopic enrichment, although there may be other mechanisms at work too.

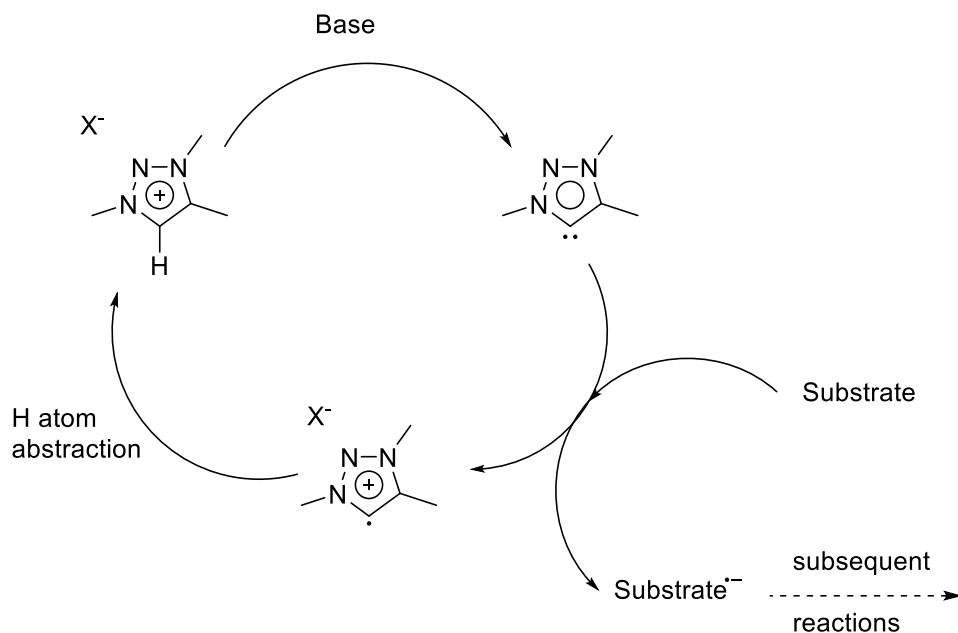


Scheme 4.4: MIC radical cation trapping experiments with TEMPO and deuterated acetonitrile. PQ = phenanthrenequinone.

Having investigated the nature of stoichiometric SET from MICs, we considered the possible applications of this process. We found ourselves inspired by some recent reports showing NHC-catalyzed metal-free Heck-type cyclization reactions via an SET process.^{16,17} The proposed mechanism showed a thiazole-derived NHC reducing an α -bromo carbonyl compound by one electron to make the corresponding alpha radical and this, in turn effected a radical addition to a tethered arene. The final step of the proposed cycle involved SET back to the carbene radical cation, regenerating the neutral carbene. We thought this was unlikely as we would expect the carbene radical cation to undergo rapid hydrogen atom abstraction, especially at the high temperatures used (100 °C to 110 °C).

However, we reasoned this may not be a limitation because after hydrogen atom abstraction, the carbene precursor is regenerated. In the presence of excess base, this would

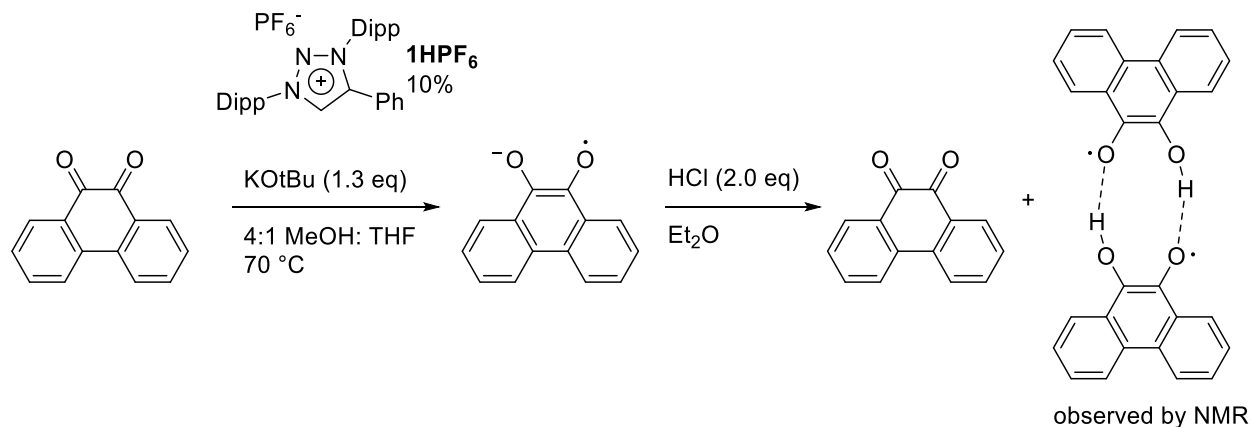
simply be deprotonated to reform the free carbene. As such, we envisaged a catalytic cycle where our protonated MIC precursor would be deprotonated in situ, reduce a substrate by SET, and undergo hydrogen atom abstraction to regenerate the protonated MIC. The necessary stoichiometric component is the base, and this need not be a reducing agent itself. We only know of two examples of a catalytic reducing agent acting by SET and both are regenerated by boron hydrides, which are classical organic reducing agents.^{18–20}



Scheme 4.5: General hypothetical catalytic cycle for the MIC as a reducing agent. X^- could be the reduced substrate, or a fragmentation product thereof, in addition to the counterion of the carbene precursor.

We turned back to phenanthrenequinone as we knew this substrate was reactive with the MIC. Reaction of phenanthrenequinone with 10 % of the catalyst **1HPF**₆ in the presence of excess potassium tert-butoxide in 4:1 methanol:THF led to a dark red solution with the disappearance of the insoluble orange phenanthrenequinone. We had hoped that by using a protic solvent, the semiquinone anion might be protonated to the neutral radical, which has been known to dimerize to an NMR-active adduct which we could characterize.²¹ However, this solution was

instead found to be NMR silent and EPR active. Upon quenching with hydrogen chloride in diethyl ether and evaporation of the solvent, NMR showed primarily regeneration of the phenanthrenequinone but with some ^{13}C signals matching the phenanthrenequinhydrone dimer (see experimental section). Given the poor solubility and air-instability of the dimer, we did not determine the % conversion.

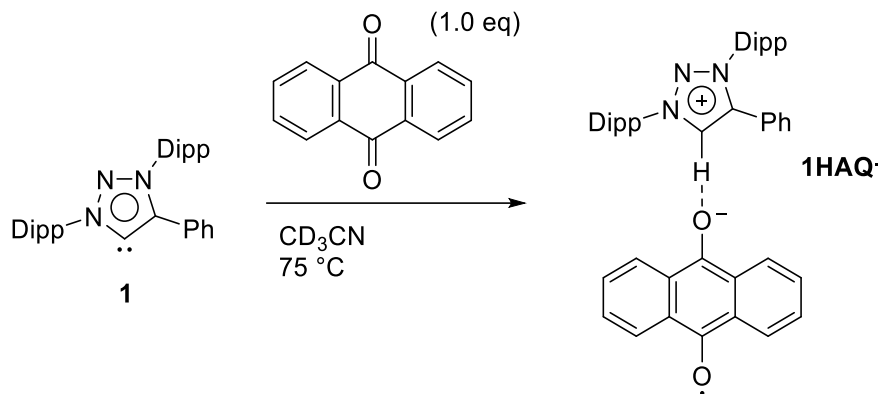


Scheme 4.6: Catalytic reduction of phenanthrenequinone by **1HPF₆** with quenching to phenanthrenequinhydrone dimer.

We recognized that if MICs could reduce phenanthrenequinone, they would likely also reduce the isomeric anthraquinone. Industrially, the reduction of anthraquinone is one half of the anthraquinone process to generate hydrogen peroxide.²² A 2-substituted anthraquinone is reduced by hydrogen over a palladium catalyst to the corresponding hydroquinone. The hydroquinone is then oxidized back to anthraquinone by oxygen gas, giving hydrogen peroxide. Given the well-known expense and sustainability issues with using transition metal catalysts, we wondered if our system might act a substitute for the first step of the industrial process.

The direct reaction of carbene **1** with anthraquinone is slow, likely due to the latter's poor solubility in all solvents and its more negative redox potential (compared to phenanthrenequinone) for the quinone/semiquinone couple of -1.49 V vs. Fc/Fc⁺.¹⁴ Ultimately, heating a 1:1 mixture in deuterated acetonitrile gave a purple solution with clear decrease in

NMR signal intensity and broadened peaks suggestive of a paramagnetic component. Upon cooling, purple crystals formed out of the solution, allowing a single crystal XRD study to confirm the structure of **1HAQ**. Furthermore, EPR spectroscopy of **1HAQ** in benzene revealed a signal with $g_{\text{iso}} = 2.0052$ and hyperfine coupling to several groups of hydrogen atoms in agreement with the presence of a semiquinone.



Scheme 4.7: Stoichiometric reduction of anthraquinone with carbene **1**

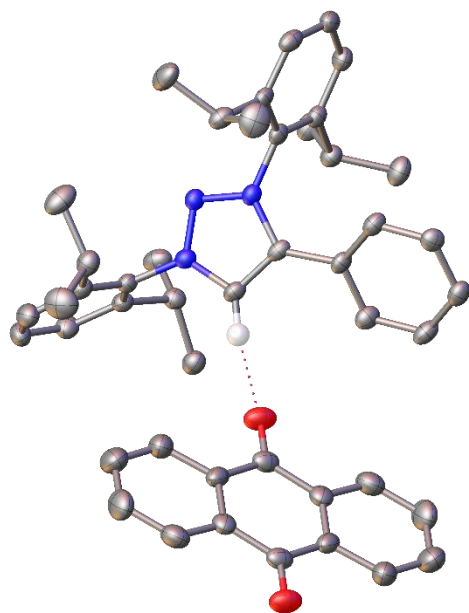


Figure 4.3: Solid state structure of **1HAQ**.

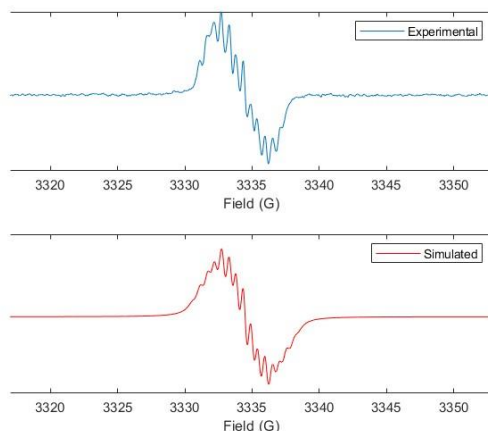
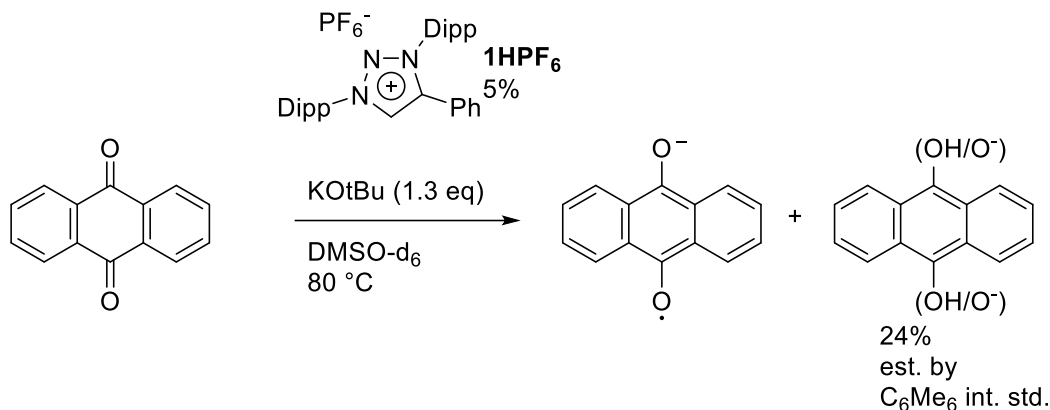
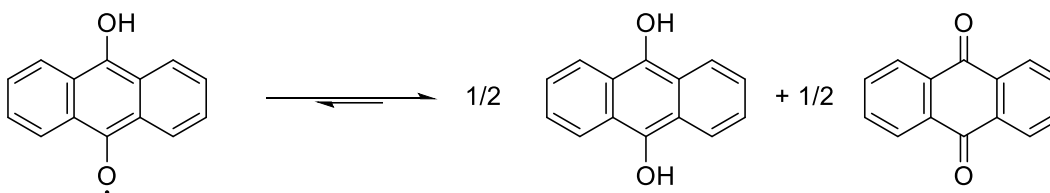


Figure 4.4: EPR spectrum of **1HAQ** with experimental data in blue (*top*) and simulated fit in red (*bottom*).

We then attempted the catalytic reduction of anthraquinone with 5% of catalyst **1HPF₆** and potassium tert-butoxide as base in deuterated dimethylsulfoxide (for solubility). The reaction solution immediately turned red and was heated to 80 °C overnight. All NMR signals corresponding to the starting material had disappeared but, to our surprise, we observed signals consistent with dihydroxyanthracene (**AQH₂**) according to literature values for the aromatic hydrogen atoms²³, although it may not have been the protonated form. By comparison to a hexamethylbenzene internal standard, the yield of the **AQH₂** was estimated at 24 % with, presumably, the remainder of the starting material converted to the NMR-silent semiquinone. It is known that semiquinones disproportionate into the corresponding quinone and hydroquinone upon protonation²⁴, but the results with the phenanthrenequinone in methanol suggested this will not simply occur in protic solvent. Regardless, this was an encouraging result.



Semiquinone Equilibrium:

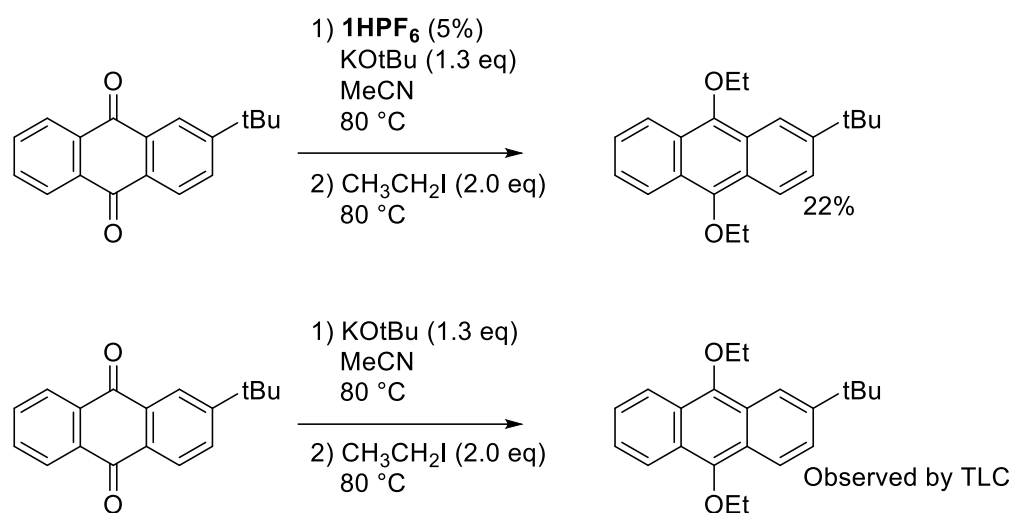


Scheme 4.8: Catalytic reduction of anthraquinone by **1HFP₆** in DMSO-d_6 (*above*) with the semiquinone equilibrium (*below*).

Given the instability of anthrahydroquinones in air, we sought a surrogate for their formation that would be easier to characterize. We reasoned that if the semiquinone were reacted with a small alkyl electrophile, it might still disproportionate into the dialkoxyanthracene and anthraquinone by SET. This would result in a maximum 50 % yield of the dialkoxyanthracene if no **AQH₂** is formed prior to the addition of the electrophile but could still be a proof of concept for the MIC as a catalytic reducing agent.

For improved solubility, 2-tert-butylanthraquinone was chosen as the substrate and was reacted with 5% **1HFP₆** in acetonitrile with potassium tert-butoxide as the base. After heating at 80°C to generate the semiquinone, an excess of ethyl iodide was added, and the reaction was heated until the purple color of the semiquinone had disappeared. 2-(tert-butyl)-9,10-

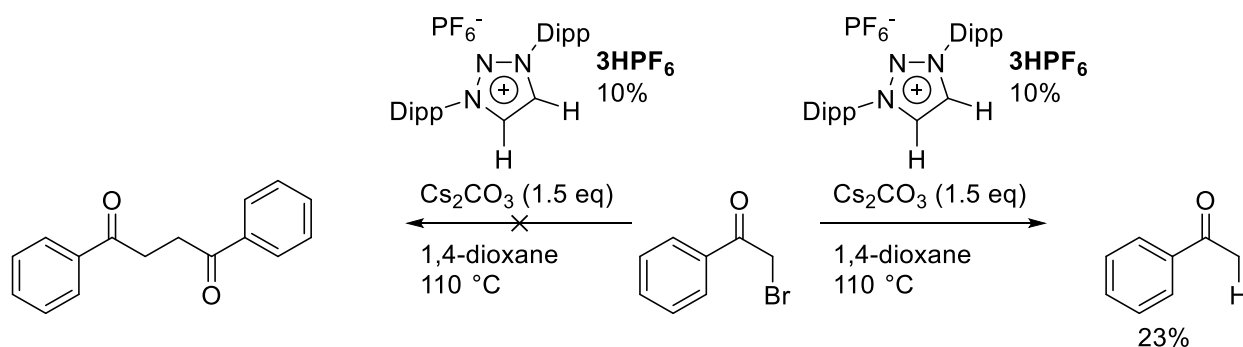
diethoxyanthracene was isolated after workup in 22 % yield. However, a control experiment without the carbene precursor present also showed the presence of this product.



Scheme 4.9: Reduction of 2-tert-butylanthraquinone followed by ethylation gives 2-(tert-butyl)-9,10-diethoxyanthracene with or without carbene catalyst.

Potassium tert-butoxide is known to form a charge transfer complex with anthraquinone²⁵, although the full reduction and functionalization of the quinone was unexpected. There is also one report of anthraquinone being reduced in a similar manner by LDA.²⁶ We considered that by using a non-reducing base, we might demonstrate the catalytic reducing power of the MIC. However, when the same reaction was run using cesium carbonate instead of potassium tert-butoxide, no product was observed. Even using the oxophilic chlorotriisopropylsilane as the electrophile gave no disiloxanthracene product. Curiously, it has been reported that hydroxide can reduce anthraquinone to the semiquinone in aprotic solvents²⁷ and this will necessarily be present when carbonate is used as a reagent. Taken together, these results and known reports suggested that anthraquinones are not the best model for MICs as catalytic reducing agents. Furthermore, the SET reactivity of tert-butoxide also makes it a poor choice of base so we subsequently avoided its use.²⁸

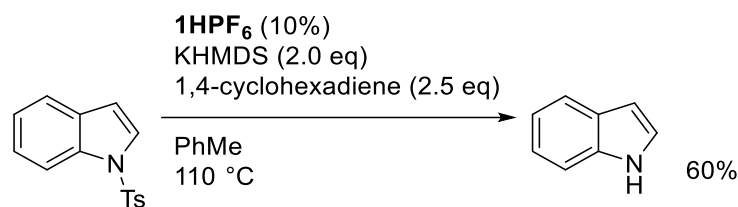
Since NHCs are known to reduce α -bromo carbonyl compounds^{16,17} to the corresponding radicals, we chose 2-bromoacetophenone as a possible model. In the absence of any other substrate, we expected the reduction product to be the homocoupled diketone (1,4-diphenylbutane-1,4-dione). Reaction with 10 % of catalyst **3HPF₆** and cesium carbonate as the base in dioxane at 110 °C did not give this product, but acetophenone was observed instead. Presumably, this is the result of the α -radical undergoing hydrogen abstraction rather than dimerizing. After purification, acetophenone was isolated in 23 % yield, demonstrating a weakly catalytic reduction. However, all the starting 2-bromoacetophenone was used up in this reaction with no other clear product, suggesting other side reactions which we could not identify.



Scheme 4.10: Catalytic reduction of 2-bromoacetophenone with MIC gives acetophenone rather than the diketone.

Another model we considered came from the work of Murphy and co-workers on organic electron donors in which they showed that sulfonamides could be reductively cleaved by SET.^{8,29} N-toluenesulfonylindole is a tempting model as it is relatively easy (compared to other sulfonamides) to cleave the N-S bond to the amide and a sulfinyl radical. In line with their reduction procedure where KHMDS was used to generate the electron donor in-situ, we reacted N-tosylindole with 10 % **1HPF₆** using KHMDS as the base in toluene at 110 °C. An excess of 1,4-cyclohexadiene, a known hydrogen atom donor, was also added to quench any formed

radicals. After heating overnight, indole was recovered in 60% yield, again demonstrating catalytic reduction with the MIC.



Scheme 4.11: Catalytic reduction of N-tosylindole (Ts = 4-toluenesulfonyl) by MIC to indole.

4.3: Conclusion

Mesoionic carbenes can behave as single electron transfer reagents where the resultant radical cation rapidly abstracts a hydrogen atom to form the protonated triazolium salt. At a minimum, some of the hydrogen abstraction appears to come from solvent. Stoichiometric MIC can reduce phenanthrenequinone and anthraquinones to the corresponding semiquinone. Recognizing that the triazolium salt is simply the MIC precursor, we envisaged the use of the MIC as a catalytic reducing agent. Through representative reductions of 2-bromoacetophenone and N-tosylindole, we have demonstrated some catalytic activity and further investigation is ongoing in our lab.

4.4: Acknowledgements

Chapter 4 contains material currently being prepared for submission for publication. Vianna, A.; Melaimi, M.; Bertrand, G. Single-Electron Transfer Reactions of Free Mesoionic Carbenes. The dissertation author was the primary researcher and first author of this material.

4.5: Experimental Procedures

4.5.1: Materials

Unless otherwise noted, all reagents were obtained from commercial suppliers and used directly without further purification. Cesium carbonate was dried under vacuum at 120 °C overnight and stored in a glovebox prior to use. TEMPO was purified by sublimation and stored

in a -36 °C freezer in a glovebox prior to use. Anhydrous 1,4-dioxane was procured from Sigma Aldrich in Sure/Seal™ packaging. Anhydrous Et₂O, THF, pentane, and benzene were dried by distillation over sodium-benzophenone ketyl under an argon atmosphere. Anhydrous toluene was dried by distillation over sodium metal under an argon atmosphere. Anhydrous hexane, CH₂Cl₂, and CHCl₃ were dried by distillation over calcium hydride under an argon atmosphere. Anhydrous acetonitrile was dried by distillation over either phosphorus pentoxide or calcium hydride under an argon atmosphere. C₆D₆ was obtained as anhydrous grade and was stored over a potassium mirror in a Teflon-sealed Schlenk. CDCl₃ and CD₃CN were dried by distillation over calcium hydride under an argon atmosphere and stored over molecular sieves prior to use. DMSO-d₆ was dried and stored over molecular sieves under an argon atmosphere. Carbenes **1**³⁰, **2**³⁰, and **3**³¹, as well as their protonated hexafluorophosphate salts³⁰, and N-toluenesulfonylindole³² were synthesized according to literature procedures.

4.5.2: General Methods, Instrumentation, and Measurements

Air and water-sensitive manipulations were carried out in flame-dried glassware equipped with magnetic stir bars under argon using standard Schlenk techniques or in an argon glovebox.

NMR spectra were recorded on Bruker AVANCE 300 MHz, JEOL ECZ 400 MHz, JEOL ECA 500 MHz, or Varian INOVA 500 MHz spectrometers. The ¹H and ¹³C chemical shift data for each signal are given relative to tetramethylsilane (TMS) in units of δ (ppm) where δ (TMS) = 0 and referenced to the residual solvent resonances. Splitting patterns are denoted as s (singlet), d (doublet), t (triplet), q (quartet), sept (septet), hept (heptet), m (multiplet) and br (broad).

Mass spectrometry measurements were taken by the UCSD Molecular Mass Spectrometry Facility.

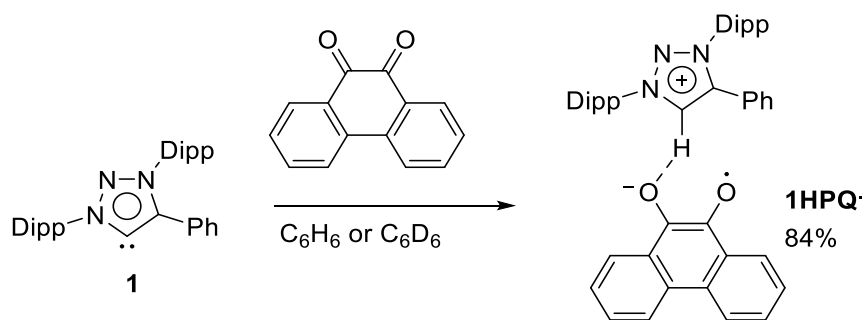
EPR spectra were recorded on a Bruker EMX spectrometer.

Data collections for X-ray diffraction experiments were performed on a 'Bruker APEX-II CCD' diffractometer, using graphite-monochromated Mo K α radiation ($\lambda = 0.71073 \text{ \AA}$). Structures were solved using Olex2³³ with the ShelXT³⁴ solution program using Intrinsic Phasing. The Structures were refined using the ShelXL³⁵ package using the full-matrix least-squares method for all non-hydrogen atoms. Hydrogen atoms were then placed at calculated positions.

Cyclic voltammetry experiments were performed in an argon glovebox using a CH Instruments model 620E electrochemical analyzer with a glassy carbon working electrode and a platinum wire counter electrode. A Ag/AgNO₃ reference electrode was built from a silver wire inserted into a glass tube with a Vycor frit filled with a 0.01 M acetonitrile solution of AgNO₃. Potentials are referenced to the Fc/Fc⁺ couple using ferrocene as an external standard.

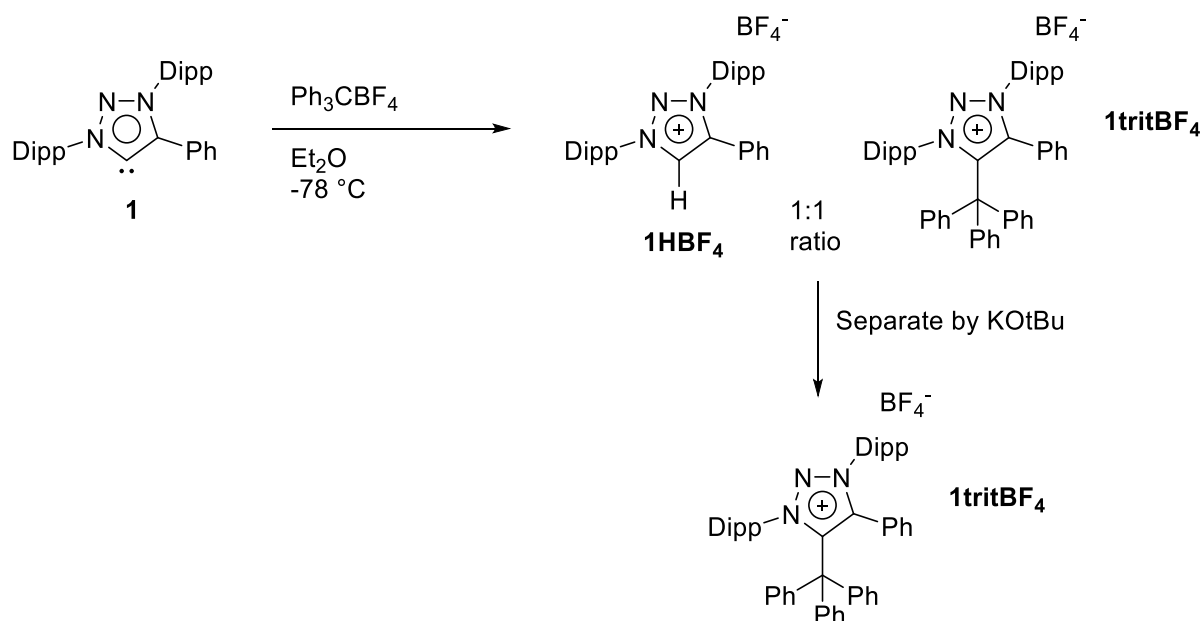
Thin layer chromatography was performed on aluminum-backed silica plates using ultraviolet visualization. Column chromatography was performed on a Buchi Reveleris X2 Flash Chromatography System using pre-packed silica columns with an ultraviolet detector.

4.5.3: Synthetic and Reaction Procedures



1HPQ: A mixture of carbene **1** (352 mg, 0.76 mmol) and phenanthrenequinone (150 mg, 0.72 mmol) was dissolved in dry benzene (10 mL) at room temperature. The solution immediately turned purple and was stirred for 1 hour, during which time a precipitate formed. The solvent was removed in vacuum and the residue was washed with 10 mL dry hexane and

dried in vacuum to give **1HPQ** as a purple powder (408 mg, 84%). Crystals suitable for X-Ray analysis were obtained by spontaneous crystallization out of an NMR-scale reaction in C₆D₆ in a J-Young NMR tube.



Reaction of carbene 1 with Ph₃CBF₄: formation of 1,3-bis(2,6-diisopropylphenyl)-4-phenyl-5-trityl-1H-1,2,3-triazol-3-ium tetrafluoroborate (1tritBF₄). A mixture of **1** (300 mg, 0.64 mmol) and triphenylcarbenium tetrafluoroborate (319 mg, 0.97 mmol) was dissolved in dry diethyl ether (10 mL) at -78 °C. After stirring at this temperature for 30 minutes, the reaction was warmed to room temperature and stirred overnight. The solution was filtered, and the precipitate washed with 10 mL hexane and dried in vacuum to give a 1:1 molar mixture of **1HBF₄** and **1tritBF₄**. To separate **1tritBF₄**, the product mixture (300 mg) and potassium tert-butoxide (42 mg, 0.38 mmol) were dissolved in 10 mL dry diethyl ether at 0 °C. After stirring for 15 minutes, the suspension was warmed to room temperature and stirred for 30 minutes. The suspension was filtered, and the insoluble solids were washed with 10 mL dry toluene. The solid was then taken up in dichloromethane, filtered, dried over magnesium sulfate, and filtered again. The solvent was removed in vacuum to an oil, which was precipitated with hexane. After further drying in

vacuum, **1tritBF₄** was obtained as a colorless solid. ¹H NMR (500 MHz, CDCl₃) δ 7.50 – 7.40 (m, 2H), 7.22 – 7.18 (m, 3H), 7.18 – 7.08 (m, 5H), 7.08 – 7.00 (m, 5H), 7.00 – 6.87 (m, 5H), 6.85 (t, *J* = 7.9 Hz, 4H), 6.62 (d, *J* = 7.6 Hz, 2H), 2.61 – 2.45 (m, 4H), 1.30 (d, *J* = 6.7 Hz, 6H), 1.25 (d, *J* = 6.7 Hz, 6H), 1.19 – 1.13 (m, 12H). ¹³C NMR (125 MHz, CDCl₃) δ 148.24, 147.27, 145.78, 145.37, 133.30, 133.23, 131.90, 131.20, 130.00, 128.75, 128.26, 127.97, 125.12, 124.63, 122.54, 62.63, 30.20, 29.94, 27.70, 27.07, 22.73, 21.71. LRMS (ESI) *m/z* Calcd for C₅₁H₅₄N₃ [M]⁺ 708.43, found 708.55.

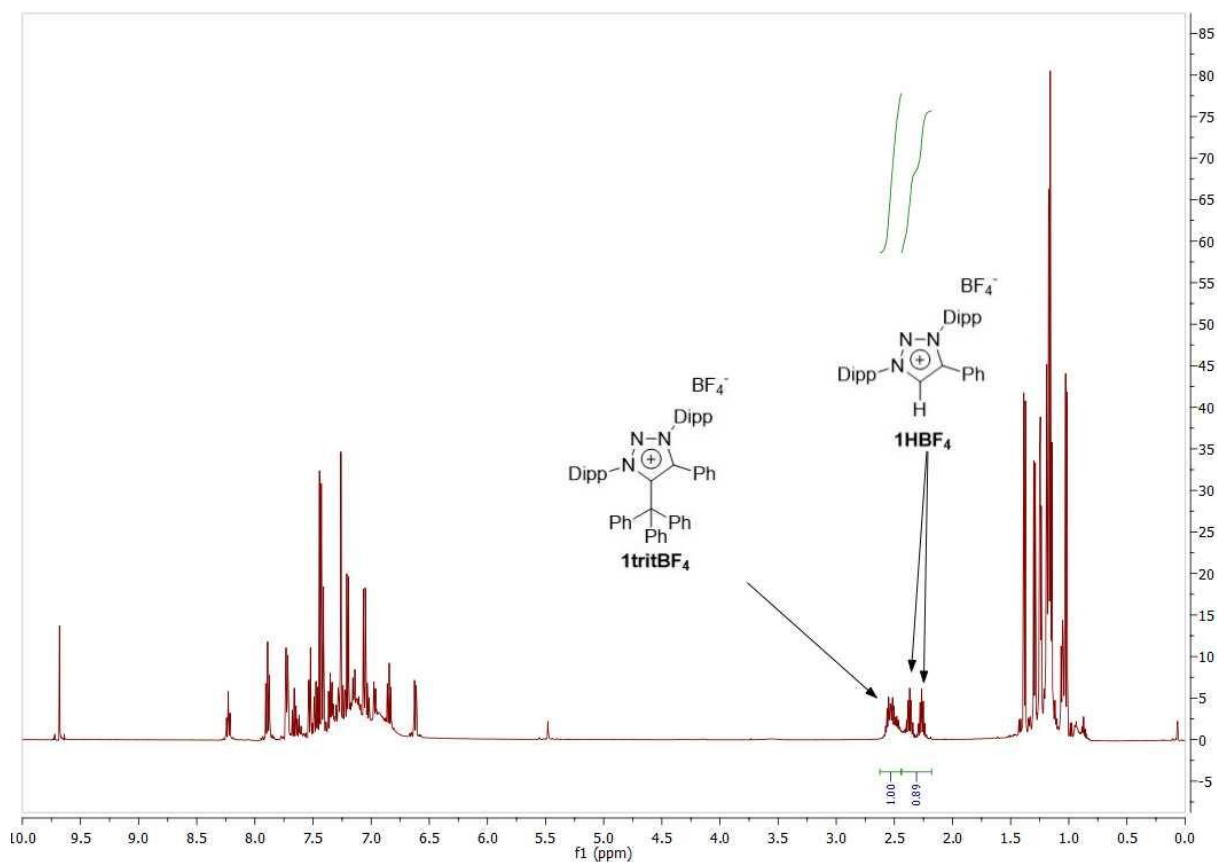
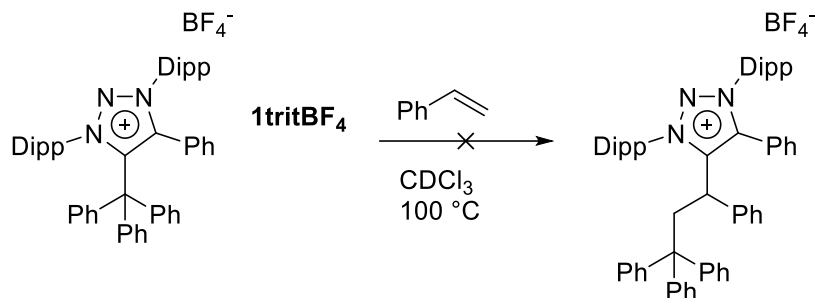
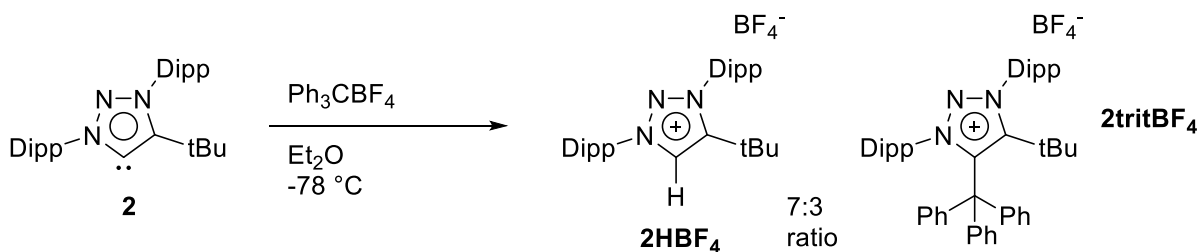


Figure 4.5: **1tritBF₄** and **1HBF₄** product mixture with characteristic isopropyl C-H highlighted.



Attempted reaction of 1tritBF₄ with styrene. A J-young NMR tube was charged with 1tritBF₄ (30 mg, 0.038 mmol) and styrene (0.01 mL, 0.075 mmol) and the reagents were dissolved in CDCl₃. No reaction was observed by ¹H NMR after 3 days at 80 °C or 2 days at 100 °C.



Reaction of carbene 2 with Ph₃CBF₄: formation of 5-(tert-butyl)-1,3-bis(2,6-diisopropylphenyl)-4-trityl-1H-1,2,3-triazol-3-ium tetrafluoroborate (2tritBF₄). A mixture of 2 (300 mg, 0.67 mmol) and triphenylcarbenium tetrafluoroborate (333 mg, 1.01 mmol) was dissolved in dry diethyl ether (10 mL) at -78 °C. After stirring at this temperature for 30 minutes, the reaction was slowly warmed to room temperature and stirred for 4 hours. After filtration, the yellow precipitate was dried in vacuum to give a 7:3 molar mixture of 2HBF₄ and 2tritBF₄ by ¹H NMR.

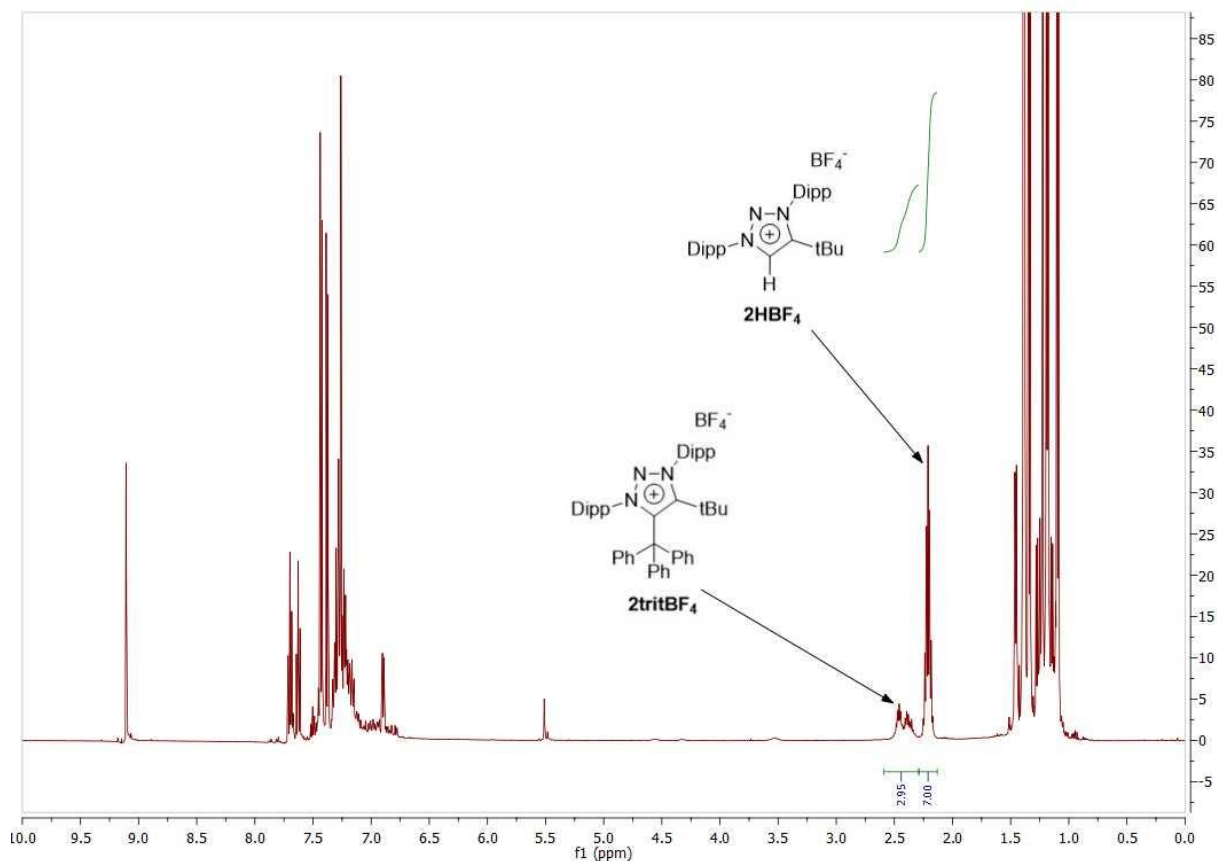
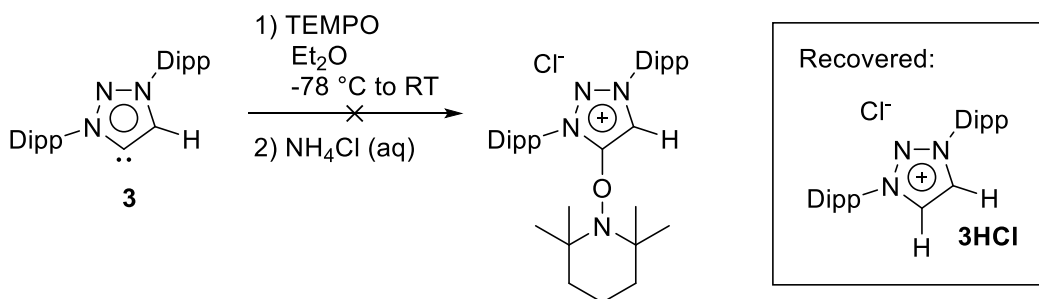
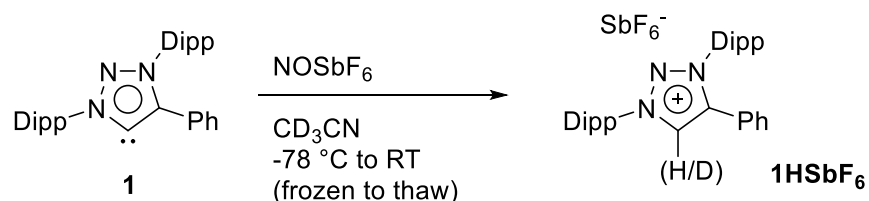


Figure 4.6: 2tritBF_4 and 2HBF_4 product mixture with characteristic isopropyl C-H highlighted.



Attempted oxidation and trapping of carbene 3 with TEMPO. A mixture of **3** (300 mg, 0.77 mmol) and TEMPO (361 mg, 2.31 mmol) were dissolved in dry diethyl ether (10 mL) at $-78\text{ }^\circ\text{C}$. After stirring for 30 minutes at this temperature, the reaction was warmed to room temperature and stirred for 30 minutes. 5 mL saturated aqueous ammonium chloride and 20 mL dichloromethane were added, and the layers were separated. The organic layer was evaporated under reduced pressure to an oil, which was precipitated with diethyl ether. After filtration, only

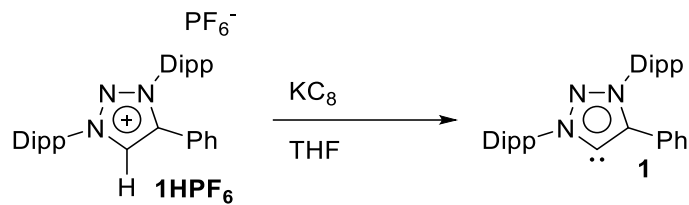
3HCl was recovered as a colorless solid. NMR (400 MHz, CDCl₃) δ 9.87 (s, 2H), 7.65 (t, $J = 7.8$ Hz, 2H), 7.39 (d, $J = 7.8$ Hz, 4H), 2.22 (m, 4H), 1.29 (d, $J = 6.6$ Hz, 12H), 1.13 (d, $J = 6.6$ Hz, 12H). NMR (100 MHz, CDCl₃) δ 145.07, 136.98, 133.34, 130.46, 124.92, 29.33, 24.68, 23.72.



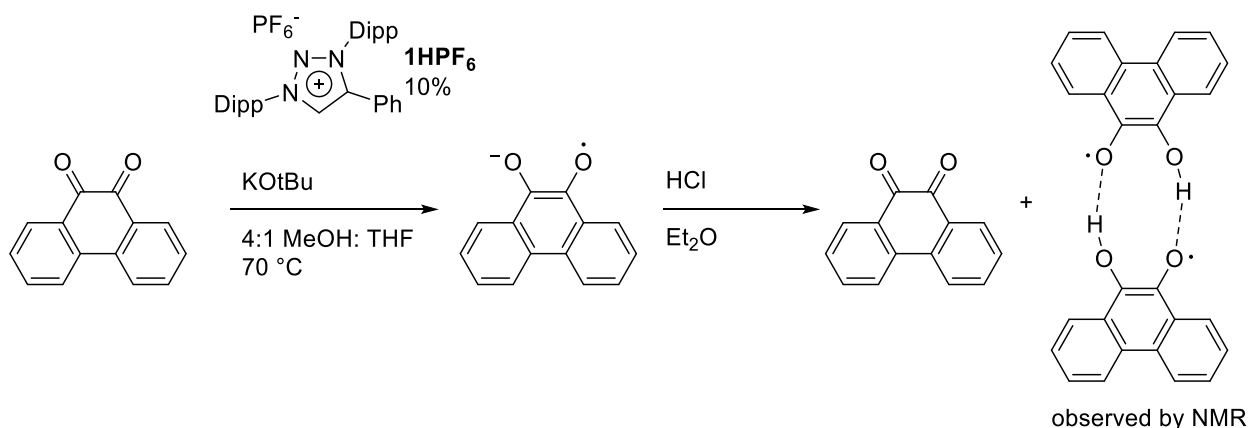
Oxidation of **1** with NOSbF₆ in deuterated acetonitrile (partial deuterium

incorporation). All glassware for this reaction was pre-treated with a 5% chlorotrimethylsilane solution in toluene to minimize the influence of free hydroxyl groups on the glass surface. The glassware was subsequently rinsed with hexane and flamed-dried under vacuum prior to use. A solution of carbene **1** (93 mg, 0.20 mmol) in dry deuterated acetonitrile (2 mL) was frozen at -78 °C. Separately, a solution of nitrosonium hexafluoroantimonate (53 mg, 0.20 mmol) in dry deuterated acetonitrile (2 mL) was chilled to just above freezing. The nitrosonium solution was carefully layered on top of the carbene **1** solution and frozen. The combined solution was then allowed to slowly thaw to room temperature overnight. The solvent was removed in vacuum to give a yellow-orange solid, which was washed with 5 mL dry benzene and dried in vacuum to give **1HSbF₆** as a colorless solid. Deuterium incorporation was estimated at 33% by ¹H NMR.

¹H NMR (400 MHz, CD₃CN) δ 9.13 (s, 1H), 7.73 (t, $J = 7.8$ Hz, 2H), 7.62 – 7.43 (m, 7H), 7.42 – 7.32 (m, 2H), 2.51 – 2.27 (m, 4H), 1.28 (d, $J = 6.7$ Hz, 6H), 1.16 (d, $J = 6.8$ Hz, 6H), 1.11 (d, $J = 7.0$ Hz, 6H), 0.99 (d, $J = 6.7$ Hz, 6H). ²H NMR (61 MHz, CH₃CN) δ 9.11. ¹³C NMR (100 MHz, CD₃CN) δ 146.40, 134.55, 134.36, 133.43, 132.63, 130.47, 130.17, 129.66, 126.60, 126.03, 122.64, 30.03, 29.80, 25.36, 24.80, 23.86, 22.49.



Reduction of 1HPF₆ with potassium graphite. In a glovebox, **1HPF₆** (300 mg, 0.49 mmol) and potassium graphite (66 mg, 0.49 mmol) were dissolved in 5 mL dry tetrahydrofuran at room temperature. The reaction was stirred for 15 minutes, and the solvent was removed in vacuum. The residue was extracted with two 5 mL portions of dry toluene and the extracts were evaporated and dried in vacuum to give carbene **1** (60 mg, 26%) with spectroscopic data matching literature.³⁰



Reduction of phenanthrenequinone with catalytic 1HPF₆. A mixture of phenanthrenequinone (200 mg, 0.96 mmol), potassium tert-butoxide (140 mg 1.25 mmol), and **1HPF₆** (59 mg, 0.096 mmol) was dissolved in a 4:1 mixture of methanol/tetrahydrofuran. After heating to 70 °C for 1 hour, the orange color of the phenanthrenequinone had disappeared. The solution was filtered, and the insoluble solids were washed with 5 mL diethyl ether. Another 4 mL diethyl ether was added, followed by hydrogen chloride in diethyl ether (2.0 M, 0.86 mL, 1.92 mmol). The reaction mixture quickly became a yellow-orange suspension and the solvent

was removed in vacuum to give a residue which NMR identified as primarily phenanthrenequinone, with a small amount of phenanthrenequinhydrone by literature values.²¹

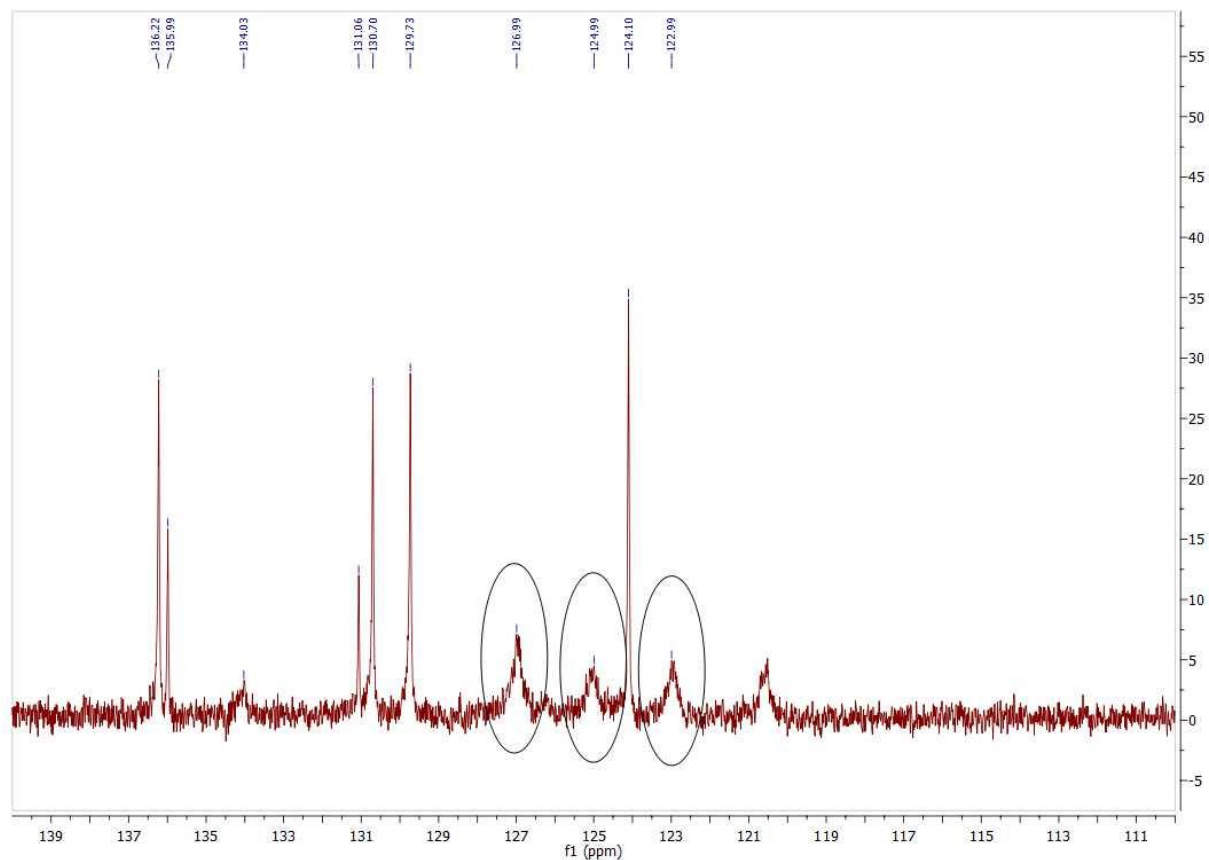
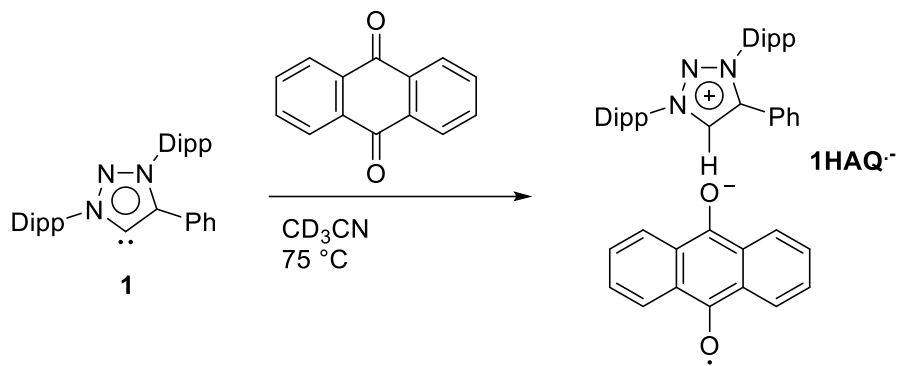
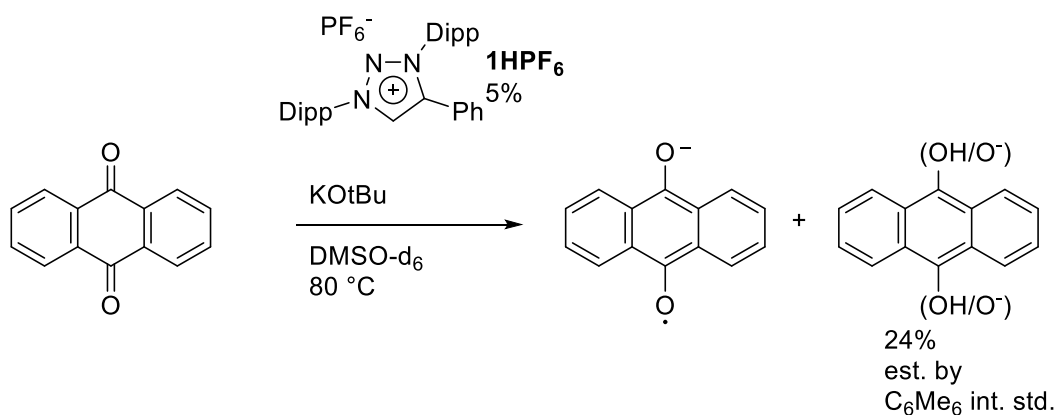


Figure 4.7: Expanded view of ¹³C NMR (125 MHz, CDCl₃) of the catalytic reduction of phenanthrenequinone after quenching with acid. Signals matching phenanthrenequinhydrone are circled.



Stoichiometric reduction of anthraquinone with carbene **1.** A mixture of carbene **1** (30 mg, 0.06 mmol) and anthraquinone (13 mg, 0.06 mmol) in a J-Young NMR tube were dissolved in deuterated acetonitrile. After heating at 75 °C overnight, the solution turned purple with NMR showing broadened, decreased intensity peaks. Upon cooling, crystals of **1HAQ** suitable for X-Ray analysis formed from the solution.



NMR-scale reduction of anthraquinone with **1HPF₆.** A mixture of anthraquinone (20 mg, 0.096 mmol), potassium tert-butoxide (14 mg, 0.13 mmol), **1HPF**₆ (3.2 mg, 0.0052 mmol), and hexamethylbenzene internal standard (3.0 mg, 0.018 mmol) in a J-Young NMR tube were dissolved in deuterated dimethyl sulfoxide (0.7 mL). After heating at 80 °C overnight, NMR analysis showed an estimated 24 % yield of the reduced anthracene product by comparison to literature NMR²³ with no observed starting anthraquinone.

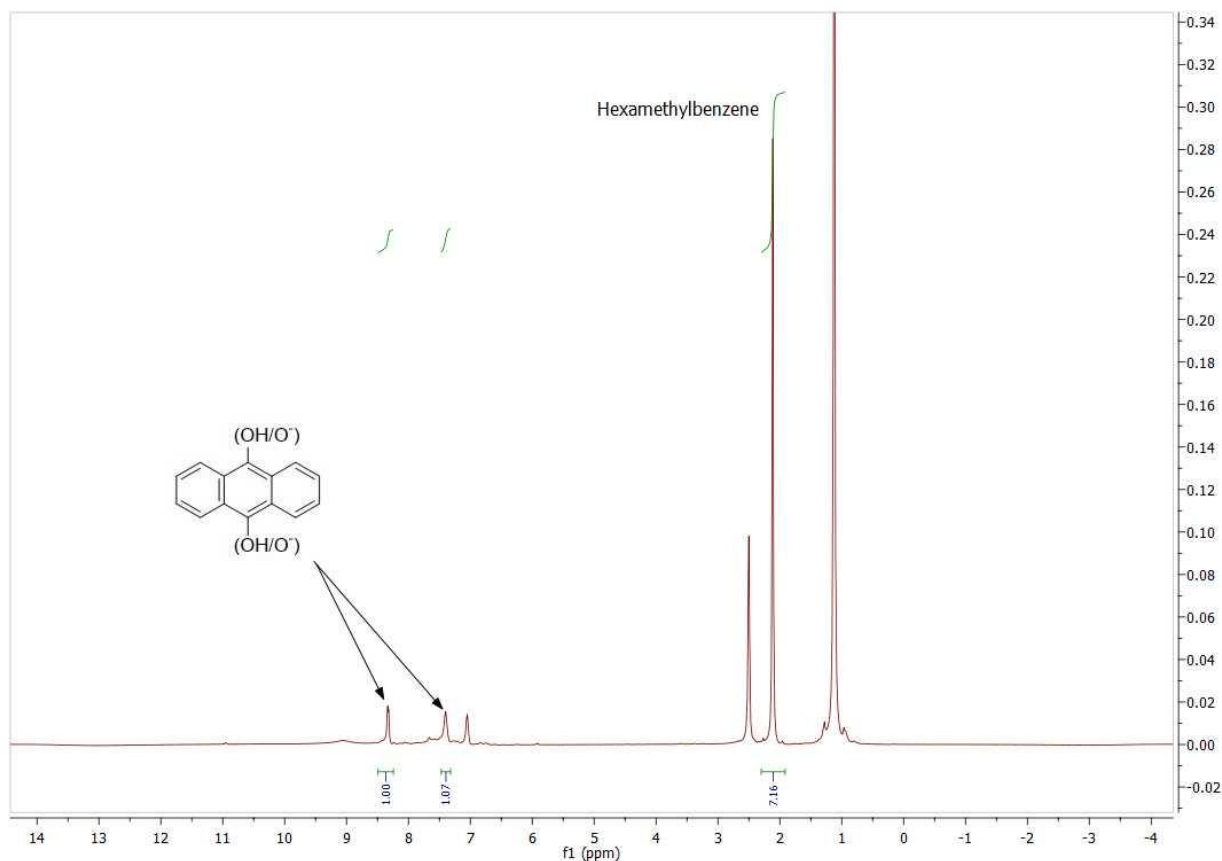
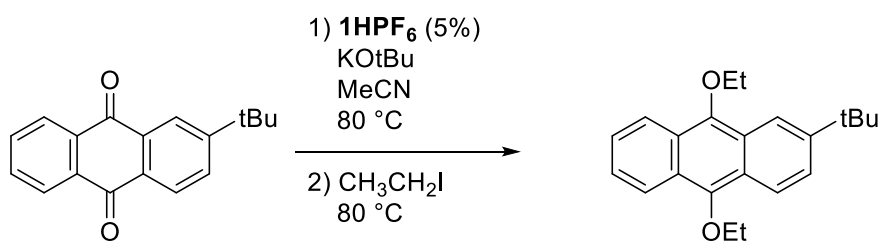
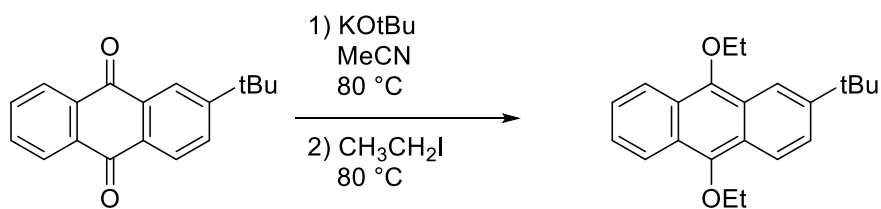


Figure 4.8: ^1H NMR (400 MHz, DMSO-d_6) of the catalytic reduction of anthraquinone after overnight heating. Signals for reduced anthracene are highlighted.

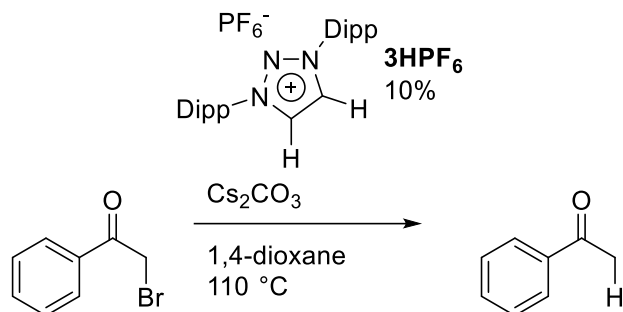


2-(tert-butyl)-9,10-diethoxyanthracene with catalytic 1HPF_6 . A mixture of 2-tert-butylanthraquinone (264 mg, 1.00 mmol), potassium tert-butoxide (146 mg, 1.3 mmol), and 1HPF_6 (31 mg, 0.05 mmol) were dissolved in dry acetonitrile (5 mL). After heating to 80 °C for 1.25 hours, the solution was cooled to room temperature. Iodoethane (0.16 mL, 2.0 mmol) was added, and the reaction heated for another 20 minutes. After cooling to room temperature, the solution was filtered, and the residue was extracted with dichloromethane. The solvent was

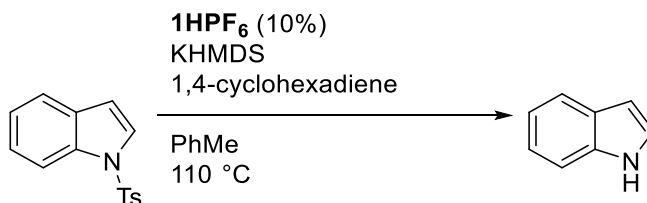
removed in vacuum and the crude product purified by column chromatography on a Combiflash system (95:5 hexanes:ethyl acetate) to give 2-(tert-butyl)-9,10-diethoxyanthracene as a slightly yellow fluorescent solid (70 mg, 22%). ^1H NMR (400 MHz, CDCl_3) δ 8.32 – 8.14 (m, 4H), 7.58 (dd, $J = 9.2, 1.9$ Hz, 1H), 7.51 – 7.38 (m, 2H), 4.25 (qd, $J = 7.0, 4.8$ Hz, 4H), 1.63 (td, $J = 7.0, 5.5$ Hz, 6H), 1.46 (s, 9H). ^{13}C NMR (100 MHz, CDCl_3) δ 147.73, 147.36, 125.47, 125.30, 125.09, 124.93, 124.86, 123.92, 122.87, 122.84, 122.81, 122.73, 120.51, 116.86, 71.70, 71.54, 35.26, 31.10, 16.30, 16.24.



2-(tert-butyl)-9,10-diethoxyanthracene without catalyst. Reduction and alkylation were performed as above in the absence of **1HPF₆**. After cooling to room temperature, the crude mixture was checked by TLC (95:5 hexanes:ethyl acetate), which indicated the formation of 2-(tert-butyl)-9,10-diethoxyanthracene. *Dihydroxyanthracene derivatives show a strong blue fluorescence under ultraviolet light and is easily resolved on visualization of the TLC.*



Reduction of 2-bromoacetophenone by catalytic 3HPF₆. A mixture of 2-bromoacetophenone (398 mg, 2.00 mmol), 3HPF₆ (107 mg, 0.20 mmol), and cesium carbonate (977 mg, 3.00 mmol) was dispersed in 1,4-dioxane (4 mL) and heated to 110 °C overnight. After cooling to room temperature, 25 mL diethyl ether was added, and the suspension was filtered. The filter cake was washed with three 5 mL portions of diethyl ether. The combined organic filtrate was washed with five 25 mL portions of water, 25 mL brine, dried over magnesium sulfate, and filtered. The solvent was removed under reduced pressure to a brown residue. The crude product was purified by column chromatography on a Combiflash system (4:1 hexanes:ethyl acetate) to give acetophenone (55 mg, 23%) with spectroscopic data matching that of a commercial sample. Repetition of the reaction with 1,4-cyclohexadiene (0.24 mL, 2.5 mmol) as a hydrogen atom source did not change the result.



Reduction of N-toluenesulfonylindole by catalytic 1HPF₆. A mixture of N-tosylindole (543 mg, 2.00 mmol), 1HPF₆ (122 mg, 0.20 mmol), and potassium bis(hexamethyldisilazide) (798 mg, 4.00 mmol) was dispersed in dry toluene (5 mL). 1,4-cyclohexadiene (0.24 mL, 2.5 mmol) was added and the reaction was heated to 110 °C for 21 hours. After cooling to room

temperature, the reaction was quenched by the addition of 10 mL saturated aqueous ammonium chloride followed by 30 mL water. The aqueous was extracted with four 20 mL portions of diethyl ether. The combined organic layers were washed with 60 mL water and then 60 mL brine, dried over magnesium sulfate, and filtered. The solvent was removed by vacuum to give, after extensive drying, indole (140 mg, 60%) with spectroscopic data matching that of a commercial sample.

4.5.4: EPR Fitting Data

Table 4.1: Full EPR fitting parameters for **1HPQ**.

1HPQ Fitting Parameter	Value
g	2.00419505688155
H1 coupling	3.00632860905450 MHz
H2 coupling	2.32754215213542 MHz
Gaussian linewidth	0.563676904777536 mT
Lorentzian linewidth	0.0564369950253122 mT

Table 4.2: Full EPR fitting parameters for **1HAQ**.

1HAQ Fitting Parameter	Value
g	2.00520273437500
H1 coupling (2 nuclei)	4.46404525957761 MHz
H2 coupling (2 nuclei)	2.84355246924962 MHz
H3 coupling (2 nuclei)	1.70634330335589 MHz
H4 coupling (2 nuclei)	1.55023968082340 MHz
Gaussian linewidth	0.0081908000000000 mT
Lorentzian linewidth	0.0520210211785799 mT

4.5.5: Electrochemical Data

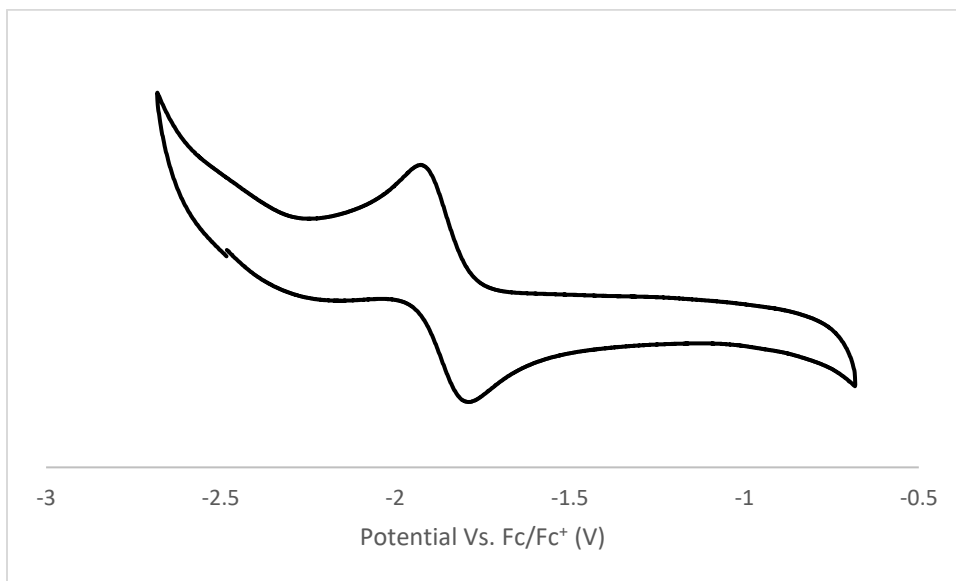


Figure 4.8: Cyclic Voltammogram of carbene **1** in THF (0.1 M nBu₄NPF₆) at room temperature (scan rate: 100 mV/s). The redox couple is at $E_{1/2} = -1.86$ V.

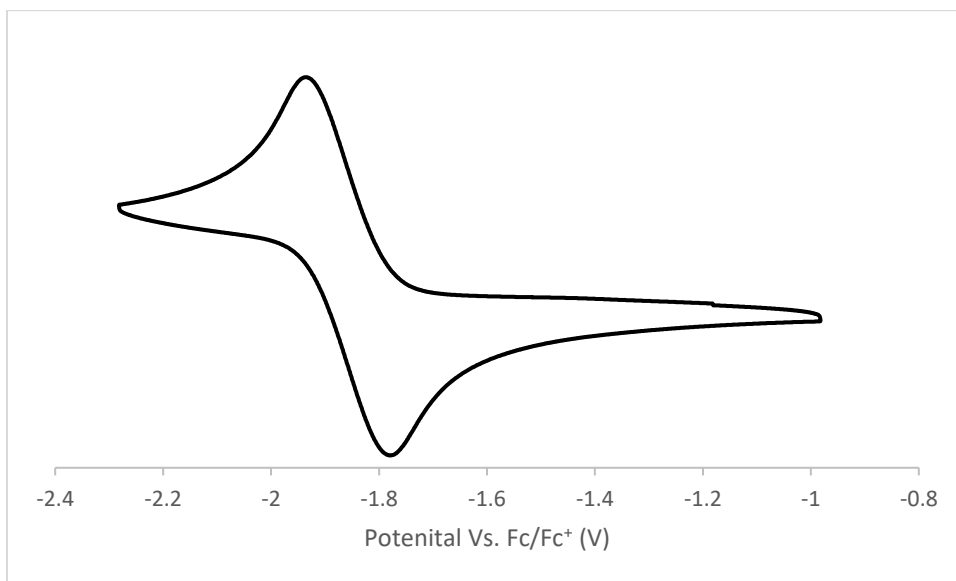


Figure 4.9: Cyclic voltammogram of **1HPF₆** in THF (0.1 M nBu₄NPF₆) at room temperature (scan rate: 100 mV/s). The redox couple is at $E_{1/2} = -1.86$ V.

4.5.6: X-ray Crystallographic Data

Crystal data and structure refinement for **1HPQ**:

An X-ray-quality crystal of **1HPQ** was obtained from a C₆D₆ reaction solution of **1** with phenanthrenequinone. Thermal ellipsoids were at the 50% probability level. Hydrogen atoms were omitted for clarity. Two molecules of **1HPQ** crystallized in the asymmetric unit, along with two molecules of benzene.

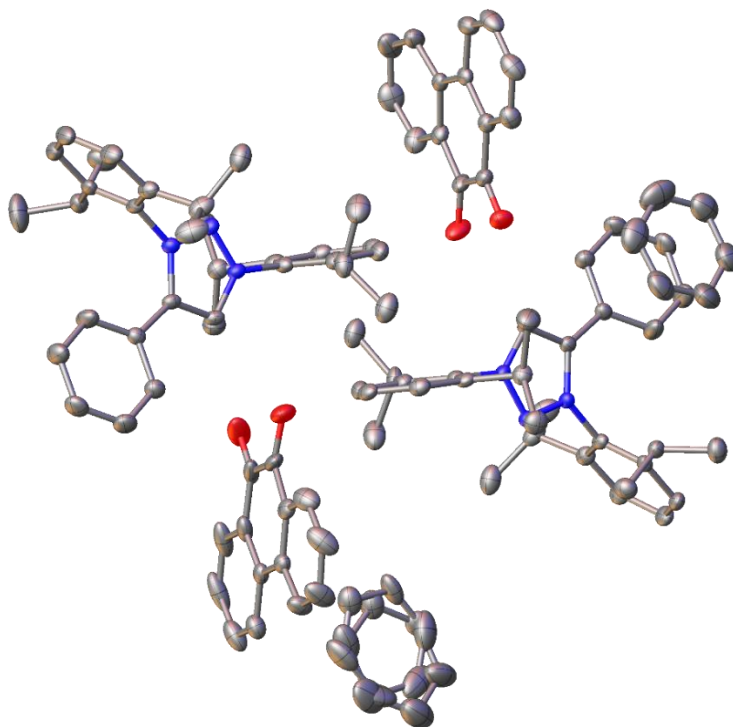


Table 4.3: Crystal Data and Structure Refinement for **1HPQ**.

Empirical formula	C ₅₂ H ₅₄ N ₃ O ₂
Formula weight	751.97
Temperature/K	100.0
Crystal system	triclinic
Space group	P-1

Table 4.3 continued: Crystal Data and Structure Refinement for **1HPQ**.

$a/\text{\AA}$	15.5048(5)
$b/\text{\AA}$	15.6824(7)
$c/\text{\AA}$	19.6974(8)
$\alpha/^\circ$	69.8200(10)
$\beta/^\circ$	75.7240(10)
$\gamma/^\circ$	71.7740(10)
Volume/ \AA^3	4217.9(3)
Z	4
$\rho_{\text{calc}}/\text{g/cm}^3$	1.184
μ/mm^{-1}	0.072
F(000)	1608.0
Crystal size/ mm^3	$0.034 \times 0.027 \times 0.02$
Radiation	MoK α ($\lambda = 0.71073$)
2 Θ range for data collection/ $^\circ$	2.8 to 53.504
Index ranges	$-18 \leq h \leq 19, -19 \leq k \leq 19, -24 \leq l \leq 24$
Reflections collected	54352
Independent reflections	17911 [$R_{\text{int}} = 0.0455, R_{\text{sigma}} = 0.0645$]
Data/restraints/parameters	17911/84/1097
Goodness-of-fit on F^2	1.010
Final R indexes [$I \geq 2\sigma(I)$]	$R_1 = 0.0580, wR_2 = 0.1321$
Final R indexes [all data]	$R_1 = 0.1154, wR_2 = 0.1569$
Largest diff. peak/hole / $e \text{\AA}^{-3}$	0.42/-0.25

Table 4.4: Fractional atomic coordinates ($\times 10^4$) and Equivalent Isotropic Displacement Parameters ($\text{\AA}^2 \times 10^3$) for **1HPQ**. U_{eq} is defined as 1/3 of the trace of the orthogonalized U_{II} tensor.

Atom	x	y	z	$U(\text{eq})$
N1	4008.5(10)	4611.1(10)	6946.0(8)	18.0(3)
O1	4122.6(10)	2876.1(10)	8885.6(8)	35.7(4)
N3	4690.4(10)	5674.7(10)	6639.9(8)	18.5(3)
N3A	406.2(10)	-578.1(10)	8343.1(8)	19.5(4)
O2	2782.6(10)	4466.4(10)	8992.9(8)	43.4(4)
N2	4303.4(10)	5247.9(10)	6361.8(8)	18.5(3)
N1A	1121.9(10)	454.5(10)	8060.8(8)	20.1(4)
N2A	791.5(10)	-165.9(10)	8634.7(8)	20.2(4)

Table 4.4 continued: Fractional atomic coordinates ($\times 10^4$) and Equivalent Isotropic Displacement Parameters ($\text{\AA}^2 \times 10^3$) for **1HPQ**. U_{eq} is defined as 1/3 of the trace of the orthogonalized U_{ij} tensor.

Atom	x	y	z	$U(\text{eq})$
O1A	2272.5(11)	835.6(13)	6050.9(9)	55.4(5)
O2A	938.1(11)	2457.5(15)	6051.5(9)	64.3(6)
C21	3528.1(12)	4017.9(12)	6838.2(10)	19.5(4)
C9A	-1.4(13)	-1328.0(13)	8835.7(10)	21.9(4)
C9	5059.2(13)	6450.3(13)	6132.7(10)	20.6(4)
C22	4058.0(13)	3181.7(13)	6684.3(10)	21.5(4)
C21A	1611.6(13)	1026.1(13)	8187.7(10)	22.4(4)
C2	4634.8(12)	5326.9(13)	7388.2(10)	19.3(4)
C26A	1086.2(13)	1857.9(13)	8350.5(10)	23.4(4)
C2A	494.0(12)	-231.7(13)	7593.6(10)	20.6(4)
C3A	216.1(13)	-579.1(13)	7092.2(10)	21.2(4)
C1	4195.5(12)	4622.1(14)	7579.3(11)	19.7(4)
C10	4491.8(13)	7352.2(13)	6065.6(11)	24.1(4)
C26	2579.1(13)	4338.5(13)	6860.5(10)	23.1(4)
C10A	-913.8(13)	-1086.7(14)	9172.6(10)	24.9(5)
C38	3266.5(13)	2187.2(13)	10857.7(11)	22.1(4)
C44	3656.1(13)	2935.9(14)	9500.6(11)	25.8(5)
C25A	1572.3(14)	2371.6(14)	8495.3(11)	27.0(5)
C24A	2512.7(14)	2064.2(14)	8487.2(11)	28.8(5)
C24	2640.4(14)	2939.4(14)	6567.5(11)	27.2(5)
C22A	2560.3(13)	693.4(13)	8159.4(11)	25.6(5)
C3	4915.2(12)	5702.0(13)	7871.7(10)	21.1(4)
C43	3812.9(13)	2156.8(13)	10170.7(11)	23.2(4)
C14	5949.9(13)	6238.4(13)	5753.0(10)	22.2(4)
C30A	60.7(13)	2200.3(13)	8343.3(11)	26.0(5)
C37	2525.8(13)	3024.8(13)	10908.7(11)	22.5(4)
C14A	544.8(14)	-2243.5(13)	8927.0(11)	26.4(5)
C23	3578.9(14)	2648.0(13)	6554.6(11)	25.7(5)
C1A	952.5(13)	456.7(13)	7419.0(10)	21.6(4)
C45	2940.6(13)	3780.5(14)	9555.8(11)	26.6(5)
C46	2397.6(13)	3802.2(13)	10272.4(11)	24.8(5)
C18	6510.5(13)	5235.5(14)	5809.9(11)	24.1(4)
C43A	2525.6(14)	1263.2(14)	4753.2(11)	27.6(5)
C38A	2374.8(13)	1954.0(13)	4077.5(11)	23.5(4)

Table 4.4 continued: Fractional atomic coordinates ($\times 10^4$) and Equivalent Isotropic Displacement Parameters ($\text{\AA}^2 \times 10^3$) for **1HPQ**. U_{eq} is defined as 1/3 of the trace of the orthogonalized U_{ij} tensor.

Atom	<i>x</i>	<i>y</i>	<i>z</i>	<i>U</i> (eq)
C13	6286.6(14)	7006.9(14)	5291.6(11)	26.9(5)
C4	4493.7(13)	5498.5(14)	8599.9(11)	27.1(5)
C12	5755.4(14)	7913.3(14)	5219.0(11)	29.6(5)
C27	5090.9(13)	2853.5(13)	6663.0(11)	25.1(5)
C25	2145.4(14)	3777.4(13)	6713.6(11)	26.2(5)
C4A	612.7(13)	-321.3(14)	6360.9(11)	28.1(5)
C11	4876.1(14)	8087.6(14)	5599.2(11)	28.8(5)
C37A	1691.5(13)	2840.4(14)	4073.9(11)	24.5(5)
C23A	2998.5(14)	1235.2(14)	8323.2(11)	29.3(5)
C42	4517.9(14)	1348.8(14)	10121.8(12)	31.2(5)
C15	3499.6(14)	7537.5(14)	6439.4(12)	30.0(5)
C13A	114.7(15)	-2954.4(15)	9369.4(11)	32.6(5)
C15A	-1453.6(13)	-73.0(15)	9094.8(11)	30.0(5)
C30	2021.8(13)	5253.4(14)	7031.7(12)	29.7(5)
C46A	1186.4(14)	2991.2(16)	4742.6(12)	33.2(5)
C11A	-1291.4(15)	-1832.5(15)	9614.6(11)	31.9(5)
C39	3456.7(14)	1403.5(14)	11465.1(12)	30.6(5)
C27A	3105.3(14)	-212.1(14)	7968.8(12)	31.8(5)
C12A	-783.6(15)	-2751.4(16)	9703.6(12)	36.6(6)
C36A	1513.2(14)	3556.7(14)	3421.1(13)	32.4(5)
C18A	1556.5(14)	-2463.9(14)	8609.0(12)	32.4(5)
C19	6324.1(14)	4896.3(14)	5232.7(12)	32.3(5)
C8	5557.6(15)	6232.5(17)	7644.2(12)	39.1(6)
C28	5587.2(14)	2641.5(15)	5944.5(12)	34.2(5)
C32A	-144.6(15)	3051.3(15)	7674.9(12)	36.5(5)
C33	1685.9(14)	4605.5(14)	10322.1(13)	35.5(5)
C6A	-198.4(15)	-1191.4(15)	6066.4(12)	34.6(5)
C42A	3175.5(16)	407.7(15)	4757.2(13)	40.1(6)
C36	1913.7(14)	3084.2(16)	11554.4(12)	33.8(5)
C8A	-391.9(15)	-1147.3(15)	7302.8(12)	35.5(5)
C40	4150.1(16)	619.2(15)	11403.6(13)	37.2(6)
C39A	2911.1(14)	1747.2(15)	3441.0(12)	34.7(5)
C44A	2059.3(15)	1433.4(17)	5452.6(12)	36.9(6)
C5A	404.5(15)	-622.2(16)	5853.3(12)	35.9(5)

Table 4.4 continued: Fractional atomic coordinates ($\times 10^4$) and Equivalent Isotropic Displacement Parameters ($\text{\AA}^2 \times 10^3$) for **1HPQ**. U_{eq} is defined as 1/3 of the trace of the orthogonalized U_{ij} tensor.

Atom	<i>x</i>	<i>y</i>	<i>z</i>	<i>U</i> (eq)
C6	5344.6(15)	6365.1(16)	8858.6(12)	36.0(5)
C7A	-594.0(16)	-1449.8(16)	6790.0(12)	37.7(6)
C20	7542.8(13)	5122.4(16)	5726.2(13)	36.7(5)
C41	4681.9(16)	593.2(15)	10729.3(13)	37.3(6)
C29	5329.1(15)	2010.1(15)	7328.2(12)	40.3(6)
C5	4712.9(15)	5830.7(15)	9087.2(12)	34.5(5)
C34	1101.5(16)	4646.8(16)	10962.6(14)	43.1(6)
C31A	-471.9(15)	2424.9(16)	9049.4(12)	37.7(5)
C32	1279.4(14)	5067.6(15)	7698.9(13)	38.6(6)
C45A	1363.1(14)	2302.1(18)	5454.7(12)	38.9(6)
C16	2860.1(14)	7821.2(15)	5872.1(13)	39.5(6)
C20A	1808.3(18)	-3178.2(15)	8178.1(13)	46.4(6)
C29A	3891.4(15)	-41.9(15)	7339.6(13)	41.2(6)
C19A	2138.9(14)	-2810.9(15)	9224.7(13)	38.9(6)
C17	3263.6(16)	8270.2(15)	6850.1(13)	42.6(6)
C31	1616.5(15)	5967.0(15)	6359.4(14)	43.3(6)
C40A	3554.2(16)	901.6(17)	3463.9(14)	47.2(7)
C7	5762.6(16)	6564.4(18)	8140.7(13)	45.5(6)
C35A	861.2(16)	4382.9(16)	3425.8(15)	45.4(7)
C41A	3678.0(18)	224.7(16)	4128.9(15)	49.1(7)
C35	1210.1(15)	3877.2(18)	11584.8(13)	44.5(6)
C33A	518.4(15)	3844.7(19)	4729.6(16)	48.3(7)
C28A	3439.1(16)	-978.1(15)	8647.4(14)	46.0(6)
C16A	-1380.4(17)	220.7(17)	9735.3(13)	46.9(6)
C49	6879.2(17)	3921(2)	9017.4(16)	55.8(7)
C34A	359.3(16)	4526.1(18)	4081.4(18)	54.1(8)
C50	7313.0(18)	4250(2)	8338.4(16)	59.0(8)
C17A	-2454.4(15)	99.1(19)	9030.9(17)	62.4(8)
C52	6729.3(18)	3379(2)	7877.0(16)	57.1(8)
C47	6270.5(18)	3020(2)	8557.4(19)	62.2(8)
C51A	1958(7)	8874(7)	3930(5)	69(2)
C51	7251.8(19)	3978(2)	7769.0(16)	67.7(9)
C48	6356(2)	3294(2)	9144.9(18)	71.5(9)
C52A	1548(3)	8211(3)	4458(2)	46.3(11)

Table 4.4 continued: Fractional atomic coordinates ($\times 10^4$) and Equivalent Isotropic Displacement Parameters ($\text{\AA}^2 \times 10^3$) for **1HPQ**. U_{eq} is defined as 1/3 of the trace of the orthogonalized U_{ij} tensor.

Atom	<i>x</i>	<i>y</i>	<i>z</i>	U(eq)
C48A	1196(6)	7778(5)	3511(3)	57.3(18)
C49A	1635(8)	8425(7)	3002(4)	73(2)
C47A	1149(2)	7667(3)	4259(2)	44.1(10)
C50A	1985(4)	8969(4)	3224(4)	66.2(15)
C48B	1560(20)	8290(20)	2980(13)	76(7)
C47B	1159(15)	7891(17)	3705(11)	61(5)
C52B	1300(8)	8187(10)	4257(7)	44.1(10)
C51B	1841(19)	8818(17)	4034(8)	36(4)
C50B	2251(12)	9146(14)	3332(8)	72(4)
C49B	2160(10)	8858(13)	2770(8)	81(5)

Table 4.5: Anisotropic Displacement Parameters ($\text{\AA}^2 \times 10^3$) for **1HPQ**. The anisotropic displacement factor exponent takes the form: $-2\pi^2[h^2a^{*2}U_{11}+2hka^*b^*U_{12}+\dots]$.

Atom	U_{11}	U_{22}	U_{33}	U_{23}	U_{13}	U_{12}
N1	17.5(8)	18.3(8)	17.1(9)	-3.1(7)	-0.3(7)	-7.3(7)
O1	33.8(9)	47.7(10)	22.5(9)	-9.6(7)	0.3(7)	-10.2(7)
N3	19.2(9)	22.9(8)	16.6(9)	-6.6(7)	-2.1(7)	-9.1(7)
N3A	23.2(9)	20.0(8)	16.4(9)	-5.7(7)	-2.1(7)	-7.3(7)
O2	34.1(9)	39.0(9)	35.3(10)	10.7(7)	-1.6(7)	-6.4(7)
N2	19.4(8)	18.7(8)	17.5(9)	-3.2(7)	-1.5(7)	-8.1(7)
N1A	22.1(9)	20.0(8)	16.3(9)	-3.2(7)	-0.7(7)	-7.0(7)
N2A	23.0(9)	20.3(8)	18.9(9)	-4.5(7)	-2.0(7)	-10.0(7)
O1A	47.0(11)	86.3(13)	24.4(9)	3.9(9)	-0.4(8)	-31.6(10)
O2A	31.9(10)	138.3(18)	38.9(11)	-53.0(12)	8.0(8)	-23.7(11)
C21	22.8(11)	21.9(10)	14.7(10)	-2.4(8)	-2.0(8)	-10.7(8)
C9A	31.1(12)	25.4(11)	14.1(10)	-2.8(8)	-3.8(9)	-17.0(9)
C9	25.7(11)	24.7(10)	16.1(10)	-4.6(8)	-2.9(8)	-14.7(9)
C22	27.2(11)	19.7(10)	15.5(10)	-0.5(8)	-0.9(8)	-10.1(8)
C21A	31.4(12)	21.5(10)	17.2(11)	-2.3(8)	-4.4(9)	-13.7(9)
C2	16.4(10)	23.2(10)	17.1(10)	-6.2(8)	-0.8(8)	-4.3(8)
C26A	30.6(12)	22.7(10)	16.1(11)	-1.7(8)	-0.2(9)	-12.5(9)
C2A	22.3(11)	21.9(10)	14.8(10)	-4.2(8)	-0.6(8)	-4.5(8)

Table 4.5 continued: Anisotropic Displacement Parameters ($\text{\AA}^2 \times 10^3$) for **1HPQ**. The anisotropic displacement factor exponent takes the form: $-2\pi^2[h^2a^{*2}U_{11}+2hka^*b^*U_{12}+\dots]$.

Atom	U ₁₁	U ₂₂	U ₃₃	U ₂₃	U ₁₃	U ₁₂
C3A	21.5(10)	21.7(10)	19.7(11)	-6.9(8)	-4.3(8)	-2.8(8)
C1	19.0(10)	25.3(11)	13.3(10)	-5.0(8)	-0.8(8)	-5.4(8)
C10	28.6(12)	24.8(11)	23.5(11)	-9.2(9)	-2.9(9)	-11.4(9)
C26	24.7(11)	24.5(11)	19.4(11)	-2.7(8)	-2.3(9)	-10.1(9)
C10A	25.6(12)	38.8(12)	15.6(10)	-6.0(9)	-5.4(9)	-16.0(10)
C38	24.1(11)	23.4(10)	23.2(11)	-5.3(9)	-6.1(9)	-11.8(9)
C44	25.3(11)	34.0(12)	20.7(11)	-6.3(9)	-1.7(9)	-14.6(9)
C25A	38.3(13)	23.1(11)	20.9(11)	-5.8(9)	1.0(9)	-14.4(9)
C24A	40.2(13)	30.8(12)	21.7(12)	-5.4(9)	-3.2(10)	-21.5(10)
C24	36.2(13)	30.0(11)	19.4(11)	-2.3(9)	-1.7(9)	-20.9(10)
C22A	28.8(12)	23.2(11)	22.6(11)	-0.7(9)	-2.8(9)	-11.0(9)
C3	19.1(10)	27.4(11)	17.9(10)	-9.3(8)	-2.4(8)	-4.5(8)
C43	23.2(11)	25.1(11)	24.0(11)	-8.5(9)	-4.0(9)	-8.0(9)
C14	21.6(11)	32.2(11)	18.0(11)	-8.2(9)	-4.4(8)	-11.9(9)
C30A	29.5(12)	22.7(10)	27.4(12)	-9.2(9)	-2.4(9)	-7.9(9)
C37	21.4(11)	29.4(11)	21.8(11)	-10.5(9)	-2.2(9)	-10.8(9)
C14A	37.0(13)	26.6(11)	20.9(11)	-6.3(9)	-4.3(9)	-16.0(10)
C23	32.8(12)	21.8(10)	22.7(11)	-4.8(9)	-2.3(9)	-10.5(9)
C1A	25.9(11)	21.7(10)	14.8(10)	-4.1(8)	-1.1(8)	-5.8(8)
C45	22.6(11)	25.9(11)	25.6(12)	3.0(9)	-2.9(9)	-10.6(9)
C46	24.4(11)	23.9(11)	27.9(12)	-5.5(9)	-2.7(9)	-11.7(9)
C18	20.3(11)	32.3(11)	20.1(11)	-6.2(9)	-1.9(8)	-9.5(9)
C43A	29.1(12)	31.0(12)	28.3(12)	-7.3(9)	-2.7(9)	-17.9(10)
C38A	23.1(11)	29.0(11)	23.5(11)	-9.3(9)	-3.4(9)	-11.4(9)
C13	24.4(11)	38.4(12)	21.1(11)	-4.7(9)	-1.8(9)	-18.1(10)
C4	26.5(11)	34.6(12)	21.3(11)	-10.1(9)	-1.1(9)	-8.9(9)
C12	33.0(13)	31.3(12)	28.4(12)	-1.3(9)	-6.6(10)	-20.2(10)
C27	26.1(11)	19.8(10)	28.7(12)	-6.2(9)	-4.1(9)	-5.8(9)
C25	24.3(11)	30.6(11)	24.0(12)	-2.0(9)	-4.1(9)	-13.3(9)
C4A	28.1(12)	33.9(12)	23.1(12)	-9.6(9)	-3.1(9)	-8.0(9)
C11	33.4(12)	24.1(11)	32.4(13)	-7.1(9)	-5.9(10)	-12.7(9)
C37A	20.4(11)	32.9(12)	26.5(12)	-13.6(9)	-2.6(9)	-10.8(9)
C23A	29.6(12)	31.8(12)	27.3(12)	-1.8(9)	-5.0(9)	-16.1(10)
C42	29.6(12)	34.3(12)	32.5(13)	-15.5(10)	-6.1(10)	-4.3(10)
C15	30.9(12)	20.7(11)	35.5(13)	-10.4(9)	6.5(10)	-9.1(9)

Table 4.5 continued: Anisotropic Displacement Parameters ($\text{\AA}^2 \times 10^3$) for **1HPQ**. The anisotropic displacement factor exponent takes the form: $-2\pi^2[h^2a^{*2}U_{11}+2hka^*b^*U_{12}+\dots]$.

Atom	U ₁₁	U ₂₂	U ₃₃	U ₂₃	U ₁₃	U ₁₂
C13A	46.2(14)	29.0(12)	28.3(13)	-1.6(10)	-10.6(11)	-20.8(10)
C15A	24.9(12)	42.4(13)	24.7(12)	-8.4(10)	-4.5(9)	-12.1(10)
C30	19.0(11)	26.1(11)	45.5(14)	-9.9(10)	-5.6(10)	-7.8(9)
C46A	19.8(11)	52.7(14)	39.1(14)	-28.1(12)	-3.2(10)	-10.0(10)
C11A	29.7(12)	46.7(14)	23.3(12)	-3.8(10)	-4.9(9)	-21.7(11)
C39	37.0(13)	33.5(12)	24.0(12)	-3.1(9)	-9.5(10)	-14.9(10)
C27A	24.9(12)	25.5(11)	46.2(15)	-10.5(10)	-7.1(10)	-6.8(9)
C12A	43.9(15)	45.2(14)	27.9(13)	2.7(10)	-11.8(11)	-31.0(12)
C36A	28.4(12)	33.0(12)	39.3(14)	-12.3(10)	-11.0(10)	-6.2(10)
C18A	41.5(14)	19.2(11)	32.4(13)	-7.4(9)	4.4(10)	-9.8(10)
C19	37.6(13)	33.1(12)	29.4(13)	-11.0(10)	-6.4(10)	-10.2(10)
C8	41.1(14)	66.6(17)	22.3(12)	-16.0(11)	3.1(10)	-33.5(13)
C28	31.4(13)	34.5(12)	35.8(14)	-17.0(10)	0.1(10)	-3.7(10)
C32A	34.2(13)	38.6(13)	31.8(13)	-3.0(10)	-6.7(10)	-9.3(10)
C33	33.0(13)	25.0(12)	47.3(15)	-10.6(10)	-5.1(11)	-6.4(10)
C6A	40.1(14)	45.0(14)	25.3(13)	-18.3(11)	-7.4(10)	-9.1(11)
C42A	58.0(16)	27.0(12)	39.4(15)	-3.4(10)	-17.1(12)	-16.2(11)
C36	26.6(12)	50.4(14)	23.7(12)	-11.6(11)	-2.9(10)	-8.7(11)
C8A	46.8(14)	48.8(14)	20.7(12)	-11.1(10)	-1.9(10)	-26.8(12)
C40	48.4(15)	24.8(12)	40.6(15)	2.7(10)	-24.8(12)	-11.9(11)
C39A	35.9(13)	43.0(13)	22.8(12)	-12.2(10)	-6.7(10)	-2.0(11)
C44A	33.2(13)	62.5(16)	18.5(12)	-4.2(11)	2.9(10)	-30.5(12)
C5A	36.2(13)	51.4(14)	20.9(12)	-14.1(11)	0.8(10)	-12.1(11)
C6	37.6(13)	50.1(14)	31.8(13)	-22.2(11)	-8.5(11)	-12.6(11)
C7A	47.0(15)	49.3(14)	28.4(13)	-12.0(11)	-6.0(11)	-27.0(12)
C20	25.9(12)	44.9(14)	42.6(15)	-16.5(11)	-4.9(10)	-9.5(10)
C41	40.1(14)	26.8(12)	48.7(16)	-15.2(11)	-20.3(12)	1.5(10)
C29	36.2(14)	38.8(13)	36.1(14)	2.2(11)	-10.8(11)	-6.9(11)
C5	35.9(13)	47.6(14)	22.2(12)	-16.5(10)	-3.1(10)	-7.6(11)
C34	37.0(14)	38.4(14)	56.1(18)	-27.5(13)	-6.1(13)	2.3(11)
C31A	35.8(13)	42.1(13)	27.3(13)	-9.9(11)	-0.8(10)	-2.5(11)
C32	26.2(12)	36.4(13)	54.0(16)	-19.5(12)	2.1(11)	-8.4(10)
C45A	20.8(12)	79.0(18)	30.5(14)	-30.5(13)	4.1(10)	-20.9(12)
C16	27.7(13)	33.7(13)	59.0(17)	-19.4(12)	-1.0(11)	-8.1(10)
C20A	69.1(18)	25.9(12)	39.0(15)	-10.7(11)	3.4(13)	-12.6(12)

Table 4.5 continued: Anisotropic Displacement Parameters ($\text{\AA}^2 \times 10^3$) for **1HPQ**. The anisotropic displacement factor exponent takes the form: $-2\pi^2[h^2a^{*2}U_{11}+2hka^*b^*U_{12}+\dots]$.

Atom	U ₁₁	U ₂₂	U ₃₃	U ₂₃	U ₁₃	U ₁₂
C29A	34.5(14)	34.7(13)	56.9(17)	-19.5(12)	2.0(12)	-12.0(11)
C19A	31.4(13)	33.3(13)	52.3(16)	-14.4(11)	-1.5(11)	-10.4(10)
C17	54.9(16)	29.9(12)	40.6(15)	-15.2(11)	7.8(12)	-13.4(11)
C31	34.1(14)	27.7(12)	63.1(18)	-1.7(12)	-15.3(12)	-7.7(10)
C40A	45.2(15)	58.3(16)	36.2(15)	-29.6(13)	-11.0(12)	10.9(12)
C7	48.7(15)	74.4(18)	32.3(14)	-21.3(13)	-0.6(12)	-39.0(14)
C35A	41.5(15)	37.6(14)	67.1(19)	-20.2(13)	-30.0(14)	-1.4(11)
C41A	63.1(18)	34.1(14)	55.1(18)	-21.2(13)	-30.3(15)	6.4(12)
C35	29.8(13)	72.0(18)	34.6(15)	-31.1(14)	0.8(11)	-3.8(12)
C33A	22.7(13)	75.0(19)	70(2)	-55.7(17)	-9.3(13)	-2.1(12)
C28A	42.3(15)	27.8(12)	61.7(18)	-1.5(12)	-12.3(13)	-10.0(11)
C16A	59.2(17)	49.5(15)	34.2(15)	-17.3(12)	-9.4(12)	-9.4(13)
C49	37.8(16)	74(2)	51.2(19)	-27.6(16)	-7.0(14)	1.9(14)
C34A	31.2(14)	53.4(17)	99(2)	-51.4(17)	-33.7(16)	11.9(12)
C50	38.2(16)	78(2)	58(2)	-11.8(16)	-18.5(14)	-10.7(14)
C17A	29.0(14)	62.9(18)	101(3)	-27.7(17)	-21.5(15)	-6.9(13)
C52	38.6(16)	74(2)	58(2)	-21.9(16)	-21.4(14)	2.0(14)
C47	37.5(16)	54.5(18)	85(3)	-21.5(17)	-3.2(16)	-1.2(13)
C51A	34(4)	67(5)	110(5)	-30(4)	-16(4)	-9(3)
C51	46.2(18)	106(3)	44.5(18)	-6.4(17)	-19.5(14)	-18.1(17)
C48	56(2)	71(2)	61(2)	-19.7(17)	19.8(16)	-2.4(17)
C52A	32(2)	68(3)	55(2)	-43(2)	-16.0(17)	0.1(18)
C48A	63(4)	62(3)	62(4)	-39(3)	-34(3)	7(3)
C49A	75(6)	73(4)	42(3)	-3(3)	-27(3)	18(4)
C47A	37.0(19)	51(2)	52(2)	-28(2)	-5.0(16)	-8.4(16)
C50A	31(3)	46(3)	84(4)	8(3)	0(3)	6(2)
C48B	34(10)	107(15)	73(8)	-42(10)	-9(7)	19(10)
C47B	36(7)	88(11)	75(8)	-58(9)	-8(7)	1(6)
C52B	37.0(19)	51(2)	52(2)	-28(2)	-5.0(16)	-8.4(16)
C51B	37(9)	38(8)	36(6)	-24(5)	-1(5)	-1(7)
C50B	51(10)	112(12)	36(6)	-18(5)	-4(5)	-2(7)
C49B	52(8)	129(12)	54(7)	-35(8)	-12(6)	1(8)

Table 4.6: Bond Lengths for 1HPQ.

Atom	Atom	Length/Å	Atom	Atom	Length/Å
N1	N2	1.328(2)	C18	C20	1.527(3)
N1	C21	1.454(2)	C43A	C38A	1.414(3)
N1	C1	1.355(2)	C43A	C42A	1.402(3)
O1	C44	1.266(2)	C43A	C44A	1.461(3)
N3	N2	1.3319(19)	C38A	C37A	1.460(3)
N3	C9	1.456(2)	C38A	C39A	1.402(3)
N3	C2	1.375(2)	C13	C12	1.380(3)
N3A	N2A	1.3311(19)	C4	C5	1.387(3)
N3A	C9A	1.449(2)	C12	C11	1.378(3)
N3A	C2A	1.374(2)	C27	C28	1.528(3)
O2	C45	1.262(2)	C27	C29	1.530(3)
N1A	N2A	1.324(2)	C4A	C5A	1.381(3)
N1A	C21A	1.455(2)	C37A	C46A	1.412(3)
N1A	C1A	1.352(2)	C37A	C36A	1.406(3)
O1A	C44A	1.270(3)	C42	C41	1.373(3)
O2A	C45A	1.261(2)	C15	C16	1.535(3)
C21	C22	1.402(3)	C15	C17	1.530(3)
C21	C26	1.393(3)	C13A	C12A	1.375(3)
C9A	C10A	1.400(3)	C15A	C16A	1.523(3)
C9A	C14A	1.395(3)	C15A	C17A	1.519(3)
C9	C10	1.393(3)	C30	C32	1.529(3)
C9	C14	1.397(3)	C30	C31	1.533(3)
C22	C23	1.396(2)	C46A	C45A	1.473(3)
C22	C27	1.516(3)	C46A	C33A	1.410(3)
C21A	C26A	1.401(3)	C11A	C12A	1.383(3)
C21A	C22A	1.392(3)	C39	C40	1.376(3)
C2	C1	1.373(3)	C27A	C29A	1.524(3)
C2	C3	1.481(2)	C27A	C28A	1.530(3)
C26A	C25A	1.394(3)	C36A	C35A	1.373(3)
C26A	C30A	1.513(3)	C18A	C20A	1.532(3)
C2A	C3A	1.479(2)	C18A	C19A	1.536(3)
C2A	C1A	1.376(2)	C8	C7	1.392(3)
C3A	C4A	1.390(3)	C33	C34	1.369(3)
C3A	C8A	1.390(3)	C6A	C5A	1.384(3)
C10	C11	1.399(3)	C6A	C7A	1.378(3)

Table 4.6 continued: Bond Lengths for **1HPQ**.

Atom	Atom	Length/Å	Atom	Atom	Length/Å
C10	C15	1.518(3)	C42A	C41A	1.360(3)
C26	C25	1.397(3)	C36	C35	1.382(3)
C26	C30	1.528(3)	C8A	C7A	1.387(3)
C10A	C15A	1.521(3)	C40	C41	1.386(3)
C10A	C11A	1.394(3)	C39A	C40A	1.381(3)
C38	C43	1.416(3)	C44A	C45A	1.450(3)
C38	C37	1.464(3)	C6	C5	1.378(3)
C38	C39	1.400(3)	C6	C7	1.374(3)
C44	C43	1.468(3)	C34	C35	1.393(3)
C44	C45	1.455(3)	C40A	C41A	1.385(3)
C25A	C24A	1.383(3)	C35A	C34A	1.385(4)
C24A	C23A	1.385(3)	C33A	C34A	1.372(4)
C24	C23	1.379(3)	C49	C50	1.344(4)
C24	C25	1.386(3)	C49	C48	1.384(4)
C22A	C23A	1.395(3)	C50	C51	1.363(4)
C22A	C27A	1.527(3)	C52	C47	1.371(4)
C3	C4	1.392(3)	C52	C51	1.355(4)
C3	C8	1.388(3)	C47	C48	1.413(4)
C43	C42	1.406(3)	C51A	C52A	1.382(7)
C14	C18	1.521(3)	C51A	C50A	1.337(8)
C14	C13	1.398(3)	C52A	C47A	1.394(5)
C30A	C32A	1.531(3)	C48A	C49A	1.375(9)
C30A	C31A	1.526(3)	C48A	C47A	1.410(6)
C37	C46	1.419(3)	C49A	C50A	1.370(9)
C37	C36	1.399(3)	C48B	C47B	1.418(19)
C14A	C13A	1.398(3)	C48B	C49B	1.380(19)
C14A	C18A	1.516(3)	C47B	C52B	1.404(14)
C45	C46	1.460(3)	C52B	C51B	1.383(14)
C46	C33	1.406(3)	C51B	C50B	1.366(14)
C18	C19	1.528(3)	C50B	C49B	1.383(15)

Table 4.7: Bond Angles for 1HPQ.

Atom	Atom	Atom	Angle/°	Atom	Atom	Atom	Angle/°
N2	N1	C21	118.04(14)	C14	C18	C20	113.01(16)
N2	N1	C1	113.27(15)	C20	C18	C19	109.22(17)
C1	N1	C21	128.67(15)	C38A	C43A	C44A	121.8(2)
N2	N3	C9	117.21(14)	C42A	C43A	C38A	119.4(2)
N2	N3	C2	112.95(14)	C42A	C43A	C44A	118.7(2)
C2	N3	C9	129.76(14)	C43A	C38A	C37A	119.28(18)
N2A	N3A	C9A	117.53(14)	C39A	C38A	C43A	117.26(19)
N2A	N3A	C2A	112.72(14)	C39A	C38A	C37A	123.45(19)
C2A	N3A	C9A	129.71(15)	C12	C13	C14	121.07(19)
N1	N2	N3	103.41(14)	C5	C4	C3	119.99(19)
N2A	N1A	C21A	118.09(14)	C11	C12	C13	120.92(19)
N2A	N1A	C1A	113.24(15)	C22	C27	C28	111.84(16)
C1A	N1A	C21A	128.67(16)	C22	C27	C29	110.06(16)
N1A	N2A	N3A	103.71(14)	C28	C27	C29	111.91(17)
C22	C21	N1	117.63(16)	C24	C25	C26	121.12(18)
C26	C21	N1	117.92(16)	C5A	C4A	C3A	120.61(19)
C26	C21	C22	124.38(16)	C12	C11	C10	121.10(19)
C10A	C9A	N3A	118.05(17)	C46A	C37A	C38A	119.62(19)
C14A	C9A	N3A	117.10(17)	C36A	C37A	C38A	122.02(19)
C14A	C9A	C10A	124.83(18)	C36A	C37A	C46A	118.4(2)
C10	C9	N3	117.06(17)	C24A	C23A	C22A	121.40(19)
C10	C9	C14	124.99(17)	C41	C42	C43	120.9(2)
C14	C9	N3	117.95(16)	C10	C15	C16	109.36(17)
C21	C22	C27	123.06(16)	C10	C15	C17	112.97(17)
C23	C22	C21	116.12(17)	C17	C15	C16	111.29(17)
C23	C22	C27	120.81(17)	C12A	C13A	C14A	121.4(2)
C26A	C21A	N1A	117.26(17)	C10A	C15A	C16A	109.74(17)
C22A	C21A	N1A	117.70(17)	C17A	C15A	C10A	113.09(18)
C22A	C21A	C26A	125.01(17)	C17A	C15A	C16A	110.58(19)
N3	C2	C3	126.58(16)	C26	C30	C32	110.63(16)
C1	C2	N3	104.55(15)	C26	C30	C31	110.56(18)
C1	C2	C3	128.65(17)	C32	C30	C31	111.96(17)
C21A	C26A	C30A	122.41(16)	C37A	C46A	C45A	122.1(2)
C25A	C26A	C21A	115.81(18)	C33A	C46A	C37A	119.0(2)
C25A	C26A	C30A	121.74(18)	C33A	C46A	C45A	118.9(2)

Table 4.7 continued: Bond Angles for **1HPQ**.

Atom	Atom	Atom	Angle/°	Atom	Atom	Atom	Angle/°
N3A	C2A	C3A	127.03(16)	C12A	C11A	C10A	121.0(2)
N3A	C2A	C1A	104.50(15)	C40	C39	C38	121.6(2)
C1A	C2A	C3A	128.32(17)	C22A	C27A	C28A	110.69(18)
C4A	C3A	C2A	116.41(17)	C29A	C27A	C22A	111.33(17)
C8A	C3A	C2A	124.83(18)	C29A	C27A	C28A	112.19(18)
C8A	C3A	C4A	118.75(17)	C13A	C12A	C11A	120.8(2)
N1	C1	C2	105.81(17)	C35A	C36A	C37A	121.4(2)
C9	C10	C11	115.97(18)	C14A	C18A	C20A	112.65(18)
C9	C10	C15	122.72(17)	C14A	C18A	C19A	109.64(17)
C11	C10	C15	121.24(18)	C20A	C18A	C19A	110.69(18)
C21	C26	C25	116.48(18)	C3	C8	C7	119.9(2)
C21	C26	C30	123.03(16)	C34	C33	C46	121.7(2)
C25	C26	C30	120.49(17)	C7A	C6A	C5A	119.31(19)
C9A	C10A	C15A	122.42(17)	C41A	C42A	C43A	121.9(2)
C11A	C10A	C9A	116.07(19)	C35	C36	C37	121.7(2)
C11A	C10A	C15A	121.44(19)	C7A	C8A	C3A	120.3(2)
C43	C38	C37	119.37(17)	C39	C40	C41	120.0(2)
C39	C38	C43	118.12(19)	C40A	C39A	C38A	122.0(2)
C39	C38	C37	122.51(19)	O1A	C44A	C43A	120.4(2)
O1	C44	C43	121.15(19)	O1A	C44A	C45A	120.4(2)
O1	C44	C45	120.40(19)	C45A	C44A	C43A	119.2(2)
C45	C44	C43	118.45(18)	C4A	C5A	C6A	120.4(2)
C24A	C25A	C26A	121.51(19)	C7	C6	C5	119.35(19)
C25A	C24A	C23A	120.26(18)	C6A	C7A	C8A	120.7(2)
C23	C24	C25	120.36(18)	C42	C41	C40	120.1(2)
C21A	C22A	C23A	115.99(18)	C6	C5	C4	120.7(2)
C21A	C22A	C27A	123.10(17)	C33	C34	C35	119.6(2)
C23A	C22A	C27A	120.91(18)	O2A	C45A	C46A	121.8(2)
C4	C3	C2	116.40(17)	O2A	C45A	C44A	120.4(2)
C8	C3	C2	124.37(18)	C44A	C45A	C46A	117.80(19)
C8	C3	C4	119.23(17)	C39A	C40A	C41A	120.0(2)
C38	C43	C44	122.15(18)	C6	C7	C8	120.9(2)
C42	C43	C38	119.27(19)	C36A	C35A	C34A	120.2(2)
C42	C43	C44	118.57(19)	C42A	C41A	C40A	119.5(2)
C9	C14	C18	122.46(17)	C36	C35	C34	119.9(2)

Table 4.7 continued: Bond Angles for **1HPQ**.

Atom	Atom	Atom	Angle/°	Atom	Atom	Atom	Angle/°
C9	C14	C13	115.92(18)	C34A	C33A	C46A	121.1(2)
C13	C14	C18	121.57(18)	C50	C49	C48	119.6(3)
C26A	C30A	C32A	109.97(16)	C33A	C34A	C35A	120.0(2)
C26A	C30A	C31A	112.46(17)	C49	C50	C51	121.4(3)
C31A	C30A	C32A	111.03(17)	C51	C52	C47	121.2(3)
C46	C37	C38	119.03(18)	C52	C47	C48	118.0(3)
C36	C37	C38	122.88(19)	C50A	C51A	C52A	118.8(6)
C36	C37	C46	118.05(19)	C52	C51	C50	120.1(3)
C9A	C14A	C13A	115.77(19)	C49	C48	C47	119.7(3)
C9A	C14A	C18A	122.73(17)	C51A	C52A	C47A	120.5(5)
C13A	C14A	C18A	121.40(18)	C49A	C48A	C47A	118.4(5)
C24	C23	C22	121.53(18)	C50A	C49A	C48A	120.1(6)
N1A	C1A	C2A	105.81(16)	C52A	C47A	C48A	119.3(4)
O2	C45	C44	120.49(19)	C51A	C50A	C49A	122.7(6)
O2	C45	C46	121.13(19)	C49B	C48B	C47B	126.4(19)
C44	C45	C46	118.37(18)	C52B	C47B	C48B	116.8(16)
C37	C46	C45	122.51(18)	C51B	C52B	C47B	116.2(12)
C33	C46	C37	119.0(2)	C50B	C51B	C52B	124.8(13)
C33	C46	C45	118.41(19)	C51B	C50B	C49B	121.6(14)
C14	C18	C19	110.14(16)	C48B	C49B	C50B	113.6(15)

Table 4.8: Hydrogen Atom Coordinates ($\text{\AA} \times 10^4$) and Isotropic Displacement Parameters ($\text{\AA}^2 \times 10^3$) for **1HPQ**.

Atom	x	y	z	U(eq)
H00Q	1250.28	2946.1	8601.92	32
H00R	2826.73	2422.99	8594.52	35
H00S	2331.31	2563.57	6475.67	33
H00X	-150.9	1686.41	8294.97	31
H010	3907.02	2070.42	6455.23	31
H011	1116.2	852.09	6945.17	26
H014	6309.79	4826.73	6303.97	29
H017	6890.7	6903.42	5023.6	32
H018	4056.17	5132.15	8763.01	33

Table 4.8 continued: Hydrogen Atom Coordinates ($\text{\AA}\times 10^4$) and Isotropic Displacement Parameters ($\text{\AA}^2\times 10^3$) for **1HPQ**:

Atom	<i>x</i>	<i>y</i>	<i>z</i>	U(eq)
H019	5999.46	8424.24	4902.54	36
H01A	5302.73	3375.51	6697.47	30
H01B	1500.29	3973.72	6713.81	31
H01L	1030.66	65.49	6209.06	34
H01D	4525.03	8717.42	5543.75	35
H01M	3643.7	1031.37	8322.23	35
H01Y	4886.1	1325.38	9661.96	37
H01H	3402.56	6935.5	6805.87	36
H01N	450.55	-3591.28	9440.57	39
H01O	-1163.14	329.1	8636.49	36
H01K	2449.97	5521.76	7154.3	36
H01P	-1907.2	-1707.48	9858.41	38
H01Z	3098.59	1413.42	11930.52	37
H01Q	2677.63	-433.15	7801	38
H01R	-1058.9	-3248.92	9999.48	44
H6AA	1850.82	3467.23	2967.28	39
H01S	1699.15	-1868.13	8264.51	39
H01C	5665.35	4942.2	5298.1	48
H01E	6669.59	4241.94	5286.61	48
H01F	6517.67	5287.29	4743.09	48
H01T	5856.74	6368.81	7150.49	47
H01G	5428.1	2100.4	5912.36	51
H01I	6252.76	2499.57	5928	51
H01J	5398.97	3188.38	5532.02	51
H01U	206.25	2890.42	7229.61	55
H01V	31.65	3575.98	7718.68	55
H01W	-803.13	3232.14	7648.59	55
H01	1608.74	5133.18	9900.14	43
H01X	-337.8	-1401.58	5717.33	41
H7AA	3267.62	-57.75	5211.98	48
H3AA	1983.43	2565.69	11983.22	41
H020	-670.14	-1329.1	7799.98	43
H021	4264.38	95.54	11823.51	45
H022	2829.83	2202.27	2980.18	42
H024	676.72	-437.5	5354.6	43

Table 4.8 continued: Hydrogen Atom Coordinates ($\text{\AA}\times 10^4$) and Isotropic Displacement Parameters ($\text{\AA}^2\times 10^3$) for **1HPQ**:

Atom	<i>x</i>	<i>y</i>	<i>z</i>	U(eq)
H025	5489.51	6593.3	9194.29	43
H026	-1009.28	-1839.03	6939.18	45
H02A	7771	5444.15	5221.4	55
H02B	7860.02	4454.04	5840.99	55
H02C	7659.85	5396.28	6062.41	55
H028	5160.48	51.67	10687.69	45
H02D	5003.49	2175.19	7777.32	60
H02E	5993.31	1834.08	7330.54	60
H02F	5143.09	1480.63	7303.01	60
H02G	4424.48	5688.41	9583.71	41
H4AA	624.77	5196.86	10982.84	52
H02U	-307.84	2955.84	9094.28	57
H02V	-316.88	1875.82	9469.2	57
H02W	-1133.11	2587.16	9037.9	57
H02H	872.54	4766.64	7604.3	58
H02I	920.41	5663.05	7793.53	58
H02J	1569.4	4653.84	8126.77	58
H02K	2937.46	8413.24	5506.82	59
H02L	2220.76	7900.85	6117.96	59
H02M	3014.06	7330.43	5629.41	59
H02X	1439.85	-2938.45	7781.73	70
H02Y	1683.82	-3773.02	8506.37	70
H	2462.43	-3280.2	7970.54	70
H02Z	4300.86	218.43	7474.43	62
HA	3641.57	402.03	6901.69	62
HB	4237.12	-636.62	7238.04	62
H02	2018.35	-3400.9	9566.31	58
HC	1977.8	-2338.96	9486.59	58
HD	2792.01	-2914.19	9014.1	58
H02N	3659.6	8054.81	7225.69	64
H02O	2618.71	8358.01	7083.07	64
H02P	3361.19	8866.96	6504.58	64
H02Q	2114.05	6078.95	5948.14	65
H02R	1283.81	6557.79	6472.13	65
H02S	1192.63	5720.49	6227.9	65

Table 4.8 continued: Hydrogen Atom Coordinates ($\text{\AA}\times 10^4$) and Isotropic Displacement Parameters ($\text{\AA}^2\times 10^3$) for **1HPQ**:

Atom	<i>x</i>	<i>y</i>	<i>z</i>	U(eq)
H8AA	3911.38	784.63	3023.39	57
H02T	6197.37	6933.59	7981.08	55
H9AA	753.89	4858.01	2977.9	54
H0BA	4110.26	-362.77	4146.38	59
H5AA	801.13	3897.43	12029.28	53
H1BA	172.89	3949.71	5176.87	58
H0AA	2910.89	-1081.8	9030.4	69
HE	3860.21	-781.52	8826.48	69
HF	3760.09	-1561.62	8519.69	69
H1AA	-732.14	142.5	9749.41	70
HG	-1650.03	-171.62	10193.89	70
HH	-1711.93	880.08	9674.64	70
H3BA	6931.61	4116.86	9407.92	67
H2BA	-95.24	5096.36	4082.13	65
H4BA	7669.77	4681.75	8253.32	71
H2AA	-2765.72	-258.81	9485.87	94
HI	-2488.5	-102.33	8621.42	94
HJ	-2754.49	769.55	8944.06	94
H5BA	6680.19	3204.91	7474	69
H6BA	5905.9	2598.94	8631.74	75
H7BA	2217.19	9254.84	4065.02	83
H030	7576	4208.07	7295.7	81
H031	6055.42	3050.14	9624.97	86
H032	1536.84	8125.27	4961.7	56
H033	929.68	7415.36	3361.73	69
H034	1696.01	8494.46	2494.8	87
H035	849.33	7226.94	4623.74	53
H036	2257.73	9432.51	2861.73	79
H0	1405.2	8147.05	2600.45	91
H1	810.47	7445.16	3813.48	73
H2	1037.99	7967.37	4754.32	53
H02{	1933.51	9038.77	4396.56	43
H3	2608.75	9582.99	3226.18	86
H4	2477.81	9035.84	2285.01	97
H00K	4003(11)	4192(12)	8034(10)	15(7)

Table 4.9: Atomic Occupancy for **1HPQ**.

Atom	Occupancy	Atom	Occupancy	Atom	Occupancy
C51A	0.744(6)	H7BA	0.744(6)	C52A	0.744(6)
H032	0.744(6)	C48A	0.744(6)	H033	0.744(6)
C49A	0.744(6)	H034	0.744(6)	C47A	0.744(6)
H035	0.744(6)	C50A	0.744(6)	H036	0.744(6)
C48B	0.256(6)	H0	0.256(6)	C47B	0.256(6)
H1	0.256(6)	C52B	0.256(6)	H2	0.256(6)
C51B	0.256(6)	H02{	0.256(6)	C50B	0.256(6)
H3	0.256(6)	C49B	0.256(6)	H4	0.256(6)
H00K	1.01(4)				

Crystal data and structure refinement for 1HAQ:

An X-ray-quality crystal of **1HAQ** was obtained from a CD₃CN reaction solution of **1** with anthraquinone. Thermal ellipsoids were at the 50% probability level. Hydrogen atoms were omitted for clarity.

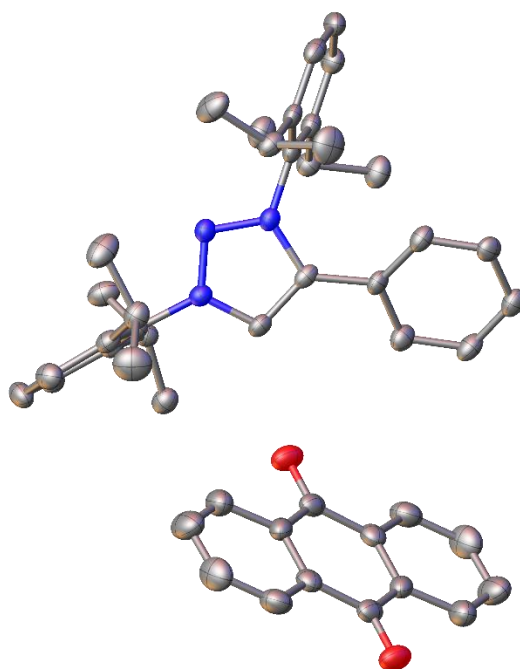


Table 4.10: Crystal Data and Structure Refinement for **1HAQ**.

Empirical formula	C ₄₆ H ₄₈ N ₃ O ₂
Formula weight	674.87
Temperature/K	100.0
Crystal system	monoclinic
Space group	C2/c
a/Å	21.2635(14)
b/Å	19.6573(13)
c/Å	19.7809(13)
α/°	90

Table 4.10 continued: Crystal Data and Structure Refinement for **1HAQ**.

$\beta/^\circ$	116.958(2)
$\gamma/^\circ$	90
Volume/ \AA^3	7369.7(8)
Z	8
$\rho_{\text{calc}}/\text{g/cm}^3$	1.217
μ/mm^{-1}	0.074
F(000)	2888.0
Crystal size/ mm^3	$0.21 \times 0.2 \times 0.08$
Radiation	MoK α ($\lambda = 0.71073$)
2Θ range for data collection/ $^\circ$	2.984 to 50.092
Index ranges	$-25 \leq h \leq 25, -23 \leq k \leq 23, -23 \leq l \leq 20$
Reflections collected	30565
Independent reflections	6526 [$R_{\text{int}} = 0.0722, R_{\text{sigma}} = 0.0739$]
Data/restraints/parameters	6526/0/468
Goodness-of-fit on F^2	1.029
Final R indexes [$I \geq 2\sigma(I)$]	$R_1 = 0.0550, wR_2 = 0.1187$
Final R indexes [all data]	$R_1 = 0.1187, wR_2 = 0.1438$
Largest diff. peak/hole / $e \text{\AA}^{-3}$	0.35/-0.30

Table 4.11: Fractional atomic coordinates ($\times 10^4$) and Equivalent Isotropic Displacement Parameters ($\text{\AA}^2 \times 10^3$) for **1HAQ**. U_{eq} is defined as 1/3 of the trace of the orthogonalized U_{ij} tensor.

Atom	x	y	z	U(eq)
O2	9192.6(10)	5873.0(10)	10362.4(11)	35.8(5)
N1	6312.9(10)	5264.0(10)	6951.1(11)	21.1(5)
O1	7352.5(11)	7924.5(10)	3619.6(11)	43.0(5)
N3	6288.2(10)	6324.5(10)	6988.4(11)	21.9(5)
N2	6068.9(10)	5776.2(10)	7204.8(11)	22.3(5)
C2	6690.4(12)	5483.5(13)	6582.9(13)	21.7(6)
C1	6666.2(13)	6177.3(13)	6610.9(13)	23.0(6)
C15	6208.8(13)	4573.8(13)	7148.7(14)	22.2(6)
C3	6122.0(13)	7000.2(13)	7152.7(14)	23.2(6)
C16	6782.5(13)	4262.7(13)	7750.9(14)	24.1(6)
C27	7049.7(13)	5065.7(13)	6249.4(14)	22.9(6)
C4	6640.4(13)	7336.9(13)	7775.3(15)	24.2(6)

Table 4.11 continued: Fractional atomic coordinates ($\times 10^4$) and Equivalent Isotropic Displacement Parameters ($\text{\AA}^2 \times 10^3$) for **1HAQ**. U_{eq} is defined as 1/3 of the trace of the orthogonalized U_{IJ} tensor.

Atom	x	y	z	U(eq)
C9	7361.9(13)	7036.2(13)	8285.0(14)	25.5(6)
C20	5549.6(13)	4269.7(13)	6734.6(14)	23.9(6)
C31	7185.6(14)	4066.7(14)	5627.4(14)	27.0(6)
C30	7775.0(14)	4347.4(14)	5608.4(15)	29.0(7)
C28	7632.0(14)	5356.0(14)	6207.8(15)	28.9(7)
C46	9930.0(13)	4991.4(13)	9245.6(15)	26.4(6)
C40	9566.4(14)	5466.3(13)	10197.3(16)	27.9(6)
C21	7489.0(13)	4606.9(14)	8202.2(14)	25.9(6)
C24	4934.1(13)	4617.5(14)	6091.1(14)	27.3(6)
C17	6675.1(14)	3603.5(14)	7926.5(16)	29.7(7)
C41	9508.3(13)	5437.5(13)	9436.2(15)	26.8(6)
C32	6827.4(14)	4421.2(13)	5950.9(14)	27.0(6)
C19	5480.0(14)	3606.7(14)	6942.0(15)	28.1(7)
C8	5468.6(14)	7279.5(14)	6654.7(15)	27.1(7)
C6	5836.4(14)	8291.4(14)	7423.2(16)	32.9(7)
C5	6472.9(14)	7990.9(13)	7904.9(16)	29.7(7)
C45	9845.2(14)	4995.6(14)	8493.5(16)	32.4(7)
C10	7930.8(14)	7447.5(14)	8202.0(16)	30.6(7)
C7	5343.3(15)	7940.9(14)	6804.7(16)	32.6(7)
C29	7990.8(14)	4993.9(15)	5890.4(15)	30.8(7)
C39	6968.8(15)	7655.8(14)	5221.8(17)	32.1(7)
C42	9024.9(14)	5867.8(14)	8865.2(16)	33.9(7)
C12	4908.3(14)	6865.8(14)	6022.0(15)	30.7(7)
C33	7420.6(16)	7724.1(13)	4264.5(16)	31.7(7)
C34	6886.6(15)	7871.0(13)	4500.0(16)	31.1(7)
C18	6036.7(15)	3280.8(14)	7527.2(16)	31.7(7)
C11	7499.2(15)	6996.8(15)	9113.7(15)	34.9(7)
C22	8069.7(14)	4227.2(15)	8106.1(16)	36.0(7)
C43	8955.1(15)	5863.0(15)	8140.5(16)	36.9(7)
C23	7658.9(15)	4675.1(15)	9036.0(15)	36.3(7)
C44	9372.1(15)	5419.4(15)	7954.3(17)	37.2(7)
C35	6271.9(16)	8237.3(14)	4020.3(18)	42.6(8)
C26	4302.9(15)	4692.8(17)	6259.4(18)	44.3(8)
C25	4714.7(16)	4237.6(17)	5345.1(16)	47.2(8)

Table 4.11 continued: Fractional atomic coordinates ($\times 10^4$) and Equivalent Isotropic Displacement Parameters ($\text{\AA}^2 \times 10^3$) for **1HAQ**. U_{eq} is defined as 1/3 of the trace of the orthogonalized U_{ij} tensor.

Atom	x	y	z	U(eq)
C38	6448.2(16)	7841.1(14)	5445.5(19)	42.8(8)
C14	4407.5(15)	6563.5(17)	6301.0(17)	44.9(8)
C13	4506.9(17)	7263.1(17)	5292.5(18)	51.4(9)
C36	5774.8(16)	8403.2(16)	4263(2)	49.7(9)
C37	5874.4(18)	8210.6(17)	4983(2)	53.5(9)

Table 4.12: Anisotropic Displacement Parameters ($\text{\AA}^2 \times 10^3$) for **1HAQ**. The anisotropic displacement factor exponent takes the form: $-2\pi^2[h^2a^{*2}U_{11}+2hka^*b^*U_{12}+\dots]$.

Atom	U ₁₁	U ₂₂	U ₃₃	U ₂₃	U ₁₃	U ₁₂
O2	31.2(11)	37.9(12)	41.0(12)	-3.8(9)	18.7(10)	2.9(9)
N1	19.2(11)	25.4(12)	18.6(12)	-1.3(10)	8.6(10)	0.8(10)
O1	58.0(14)	43.2(13)	35.7(13)	-0.9(10)	28.1(11)	-11.3(11)
N3	20.1(11)	24.6(12)	20.9(12)	1.0(10)	9.2(10)	-1.3(10)
N2	21.5(12)	24.3(12)	21.3(12)	-2.2(10)	9.9(10)	0.0(10)
C2	15.3(13)	33.7(16)	14.9(13)	-0.9(12)	5.9(11)	-2.9(12)
C1	21.8(14)	30.4(17)	18.8(14)	0.0(12)	10.8(12)	-2.0(12)
C15	23.8(15)	26.0(15)	20.7(14)	-4.2(12)	13.5(13)	-0.2(12)
C3	24.4(15)	23.2(15)	26.3(15)	0.9(12)	15.4(13)	0.7(12)
C16	22.8(14)	28.5(16)	24.3(15)	-3.7(12)	13.6(13)	0.1(13)
C27	21.6(14)	31.5(16)	17.7(14)	-2.0(12)	10.8(12)	0.0(12)
C4	23.2(15)	25.3(15)	26.0(16)	1.0(12)	13.0(13)	-1.8(12)
C9	25.0(15)	24.7(15)	25.0(15)	-0.2(12)	9.8(13)	-1.9(12)
C20	23.5(14)	29.9(16)	23.7(15)	-4.2(12)	15.4(13)	-0.4(13)
C31	31.1(16)	30.4(16)	19.6(15)	-0.8(12)	11.6(13)	-0.5(13)
C30	27.0(15)	39.0(18)	23.6(15)	-0.2(13)	13.7(13)	3.4(13)
C28	28.3(15)	35.2(17)	24.5(15)	-4.5(13)	13.3(13)	-3.9(13)
C46	20.4(14)	28.8(15)	31.4(16)	-3.4(12)	13.0(13)	-3.5(12)
C40	22.8(15)	28.2(15)	35.3(17)	-4.9(13)	15.5(14)	-5.0(13)
C21	21.9(14)	29.9(16)	25.3(15)	0.0(12)	10.2(12)	-0.4(12)
C24	22.9(14)	37.3(17)	22.3(15)	-1.8(13)	10.8(13)	-5.0(13)
C17	24.8(15)	31.3(17)	35.1(17)	0.7(13)	15.3(14)	3.3(13)
C41	21.0(14)	27.9(15)	32.2(16)	-2.8(13)	12.6(13)	-6.1(13)
C32	22.7(15)	37.3(17)	23.6(15)	-1.9(13)	12.7(13)	-1.0(13)

Table 4.12 continued: Anisotropic Displacement Parameters ($\text{\AA}^2 \times 10^3$) for **1HAQ**. The anisotropic displacement factor exponent takes the form: $-2\pi^2[h^2a^{*2}U_{11}+2hka^*b^*U_{12}+\dots]$.

Atom	U ₁₁	U ₂₂	U ₃₃	U ₂₃	U ₁₃	U ₁₂
C19	27.7(15)	33.1(17)	29.3(16)	-9.9(13)	18.1(14)	-8.8(13)
C8	24.1(15)	32.4(17)	28.3(16)	4.0(13)	14.9(13)	0.6(13)
C6	30.9(17)	23.5(16)	47.3(19)	-0.8(14)	20.5(15)	1.6(13)
C5	27.2(16)	28.6(16)	33.6(17)	-3.6(13)	14.0(14)	-3.9(13)
C45	28.0(16)	37.5(18)	33.4(17)	-3.0(14)	15.5(14)	-4.6(14)
C10	27.6(16)	35.6(17)	29.5(16)	3.6(13)	13.8(14)	2.7(13)
C7	25.7(16)	32.4(17)	39.9(18)	5.0(14)	15.0(15)	3.2(13)
C29	23.8(15)	44.7(19)	27.3(16)	-2.6(14)	14.5(13)	-4.1(14)
C39	39.5(18)	24.2(16)	44.3(19)	-4.1(14)	29.2(16)	-5.5(13)
C42	27.6(16)	34.3(17)	40.3(18)	1.4(14)	15.7(14)	2.2(14)
C12	25.6(15)	37.4(17)	27.9(16)	0.7(13)	11.0(14)	2.7(13)
C33	44.2(18)	24.1(15)	30.4(17)	-5.4(13)	20.3(15)	-8.3(14)
C34	32.6(16)	21.2(15)	41.6(18)	-2.5(13)	18.6(15)	-5.2(13)
C18	37.1(18)	25.0(16)	43.4(19)	1.1(14)	27.5(16)	3.1(14)
C11	28.1(16)	44.5(18)	29.9(17)	9.0(14)	11.2(14)	-2.3(14)
C22	24.6(15)	48.7(19)	33.6(17)	-3.3(15)	12.2(14)	4.0(14)
C43	32.2(17)	42.4(19)	32.1(17)	6.0(14)	11.0(14)	3.4(15)
C23	28.8(16)	49.9(19)	28.4(17)	-7.0(14)	11.5(14)	-2.9(14)
C44	34.6(17)	46.3(19)	30.3(17)	0.6(15)	14.4(15)	-4.2(16)
C35	48(2)	31.4(17)	50(2)	7.7(15)	23.1(18)	-1.4(15)
C26	28.4(17)	62(2)	48(2)	16.6(17)	21.6(16)	11.3(16)
C25	41.6(19)	63(2)	26.5(17)	-9.3(16)	6.5(15)	-0.9(17)
C38	48(2)	33.0(18)	60(2)	5.4(16)	35.3(19)	3.6(16)
C14	30.4(17)	66(2)	39.6(19)	-11.5(16)	17.2(15)	-12.8(16)
C13	40(2)	60(2)	40(2)	8.8(17)	5.7(17)	0.8(17)
C36	31.6(18)	48(2)	68(2)	7.2(18)	20.7(18)	8.5(16)
C37	50(2)	50(2)	76(3)	13.1(19)	42(2)	4.8(18)

Table 4.13: Bond Lengths for **1HAQ**.

Atom	Atom	Length/ \AA	Atom	Atom	Length/ \AA
O2	C40	1.270(3)	C46	C40 ¹	1.449(4)
N1	N2	1.331(3)	C46	C41	1.422(4)
N1	C2	1.375(3)	C46	C45	1.415(4)
N1	C15	1.456(3)	C40	C41	1.455(4)

Table 4.13 continued: Bond Lengths for **1HAQ**.

Atom	Atom	Length/Å	Atom	Atom	Length/Å
O1	C33	1.279(3)	C21	C22	1.527(3)
N3	N2	1.320(3)	C21	C23	1.526(4)
N3	C1	1.353(3)	C24	C26	1.529(3)
N3	C3	1.449(3)	C24	C25	1.526(4)
C2	C1	1.367(3)	C17	C18	1.377(4)
C2	C27	1.467(3)	C41	C42	1.413(4)
C15	C16	1.401(3)	C19	C18	1.382(4)
C15	C20	1.397(3)	C8	C7	1.386(4)
C3	C4	1.392(4)	C8	C12	1.515(4)
C3	C8	1.400(4)	C6	C5	1.385(4)
C16	C21	1.515(3)	C6	C7	1.381(4)
C16	C17	1.387(4)	C45	C44	1.368(4)
C27	C28	1.399(3)	C39	C33 ²	1.442(4)
C27	C32	1.387(3)	C39	C34	1.422(4)
C4	C9	1.522(4)	C39	C38	1.413(4)
C4	C5	1.389(4)	C42	C43	1.373(4)
C9	C10	1.525(4)	C12	C14	1.524(4)
C9	C11	1.531(4)	C12	C13	1.518(4)
C20	C24	1.513(4)	C33	C34	1.439(4)
C20	C19	1.394(4)	C34	C35	1.415(4)
C31	C30	1.385(4)	C43	C44	1.406(4)
C31	C32	1.385(3)	C35	C36	1.383(4)
C30	C29	1.380(4)	C38	C37	1.357(4)
C28	C29	1.385(4)	C36	C37	1.394(5)

¹2-X,1-Y,2-Z; ²3/2-X,3/2-Y,1-Z**Table 4.14:** Bond Angles for **1HAQ**.

Atom	Atom	Atom	Angle/°	Atom	Atom	Atom	Angle/°
N2	N1	C2	112.5(2)	C16	C21	C22	110.5(2)
N2	N1	C15	118.09(19)	C16	C21	C23	111.2(2)
C2	N1	C15	129.1(2)	C23	C21	C22	111.6(2)
N2	N3	C1	112.9(2)	C20	C24	C26	111.7(2)
N2	N3	C3	121.18(19)	C20	C24	C25	111.2(2)
C1	N3	C3	125.9(2)	C25	C24	C26	110.1(2)

Table 4.14 continued: Bond Angles for **1HAQ**.

Atom	Atom	Atom	Angle/°	Atom	Atom	Atom	Angle/°
N3	N2	N1	103.88(18)	C18	C17	C16	121.2(3)
N1	C2	C27	127.7(2)	C46	C41	C40	122.0(2)
C1	C2	N1	104.5(2)	C42	C41	C46	118.4(2)
C1	C2	C27	127.9(2)	C42	C41	C40	119.6(2)
N3	C1	C2	106.2(2)	C31	C32	C27	120.2(2)
C16	C15	N1	117.1(2)	C18	C19	C20	121.0(2)
C20	C15	N1	118.4(2)	C3	C8	C12	121.9(2)
C20	C15	C16	124.5(2)	C7	C8	C3	116.3(2)
C4	C3	N3	117.3(2)	C7	C8	C12	121.7(2)
C4	C3	C8	124.8(2)	C7	C6	C5	120.6(3)
C8	C3	N3	117.8(2)	C6	C5	C4	121.3(3)
C15	C16	C21	123.7(2)	C44	C45	C46	121.4(3)
C17	C16	C15	116.2(2)	C6	C7	C8	121.0(3)
C17	C16	C21	120.1(2)	C30	C29	C28	120.4(3)
C28	C27	C2	117.0(2)	C34	C39	C33 ²	121.5(2)
C32	C27	C2	123.8(2)	C38	C39	C33 ²	119.7(3)
C32	C27	C28	119.2(2)	C38	C39	C34	118.7(3)
C3	C4	C9	123.9(2)	C43	C42	C41	121.7(3)
C5	C4	C3	115.9(2)	C8	C12	C14	109.1(2)
C5	C4	C9	120.2(2)	C8	C12	C13	113.7(2)
C4	C9	C10	109.5(2)	C13	C12	C14	111.1(2)
C4	C9	C11	112.0(2)	O1	C33	C39 ²	121.4(3)
C10	C9	C11	111.5(2)	O1	C33	C34	120.8(3)
C15	C20	C24	123.7(2)	C34	C33	C39 ²	117.8(2)
C19	C20	C15	116.1(2)	C39	C34	C33	120.6(3)
C19	C20	C24	120.2(2)	C35	C34	C39	118.7(3)
C32	C31	C30	120.4(3)	C35	C34	C33	120.6(3)
C29	C30	C31	119.7(2)	C17	C18	C19	120.9(3)
C29	C28	C27	120.1(3)	C42	C43	C44	119.7(3)
C41	C46	C40 ¹	121.2(2)	C45	C44	C43	120.1(3)
C45	C46	C40 ¹	120.1(2)	C36	C35	C34	120.4(3)
C45	C46	C41	118.7(2)	C37	C38	C39	121.3(3)
O2	C40	C46 ¹	121.9(2)	C35	C36	C37	120.3(3)
O2	C40	C41	121.4(2)	C38	C37	C36	120.6(3)
C46 ¹	C40	C41	116.7(2)				

¹2-X,1-Y,2-Z; ²3/2-X,3/2-Y,1-Z

Table 4.15: Hydrogen Atom Coordinates ($\text{\AA}\times 10^4$) and Isotropic Displacement Parameters ($\text{\AA}^2\times 10^3$) for **1HAQ**.

Atom	<i>x</i>	<i>y</i>	<i>z</i>	U(eq)
H1	6873.02	6492.73	6406.55	28
H9	7373.98	6562.59	8106.84	31
H31	7026.29	3628.36	5417.17	32
H30	8029.38	4096.19	5402.29	35
H28	7781.38	5802.11	6397.53	35
H21	7457.42	5075.72	7992.94	31
H24	5089.78	5083.99	6031.5	33
H17	7048.74	3370.31	8329.44	36
H32	6427.89	4222.31	5968.57	32
H19	5043.26	3375.44	6676.93	34
H6	5738.24	8742.67	7519.09	39
H5	6801.44	8237.33	8332.65	36
H45	10122.84	4697.62	8360.19	39
H10A	7849.96	7431.02	7673.57	46
H10B	8395.39	7255.01	8531.67	46
H10C	7912.66	7920.98	8347.44	46
H7	4911.7	8156.4	6477.19	39
H29	8387.96	5191.63	5866.7	37
H42	8740.55	6168.37	8985.89	41
H12	5150.71	6479.1	5907.89	37
H18	5978.28	2827.68	7656.03	38
H11A	7479.35	7454.86	9298.58	52
H11B	7966.93	6800.21	9421.98	52
H11C	7139.22	6709.94	9151.01	52
H22A	8525.71	4443.82	8419.1	54
H22B	7972.68	4241.16	7572.37	54
H22C	8083.57	3752.99	8265.08	54
H43	8626.75	6157.87	7766.5	44
H23A	7687.55	4221.75	9254.29	54
H23B	7286.62	4937.98	9078.02	54
H23C	8111.85	4909.28	9311.25	54
H44	9325.05	5414.07	7453.29	45
H35	6200.3	8370.04	3528.78	51
H26A	4138.3	4241.2	6317.65	66
H26B	3921.24	4932.95	5839.42	66

Table 4.15 continued: Hydrogen Atom Coordinates ($\text{\AA}\times 10^4$) and Isotropic Displacement Parameters ($\text{\AA}^2\times 10^3$) for **1HAQ**.

Atom	<i>x</i>	<i>y</i>	<i>z</i>	U(eq)
H26C	4444.8	4952.51	6728.99	66
H25A	5122.85	4191.35	5243.24	71
H25B	4341.71	4492.49	4931.9	71
H25C	4538.84	3785.08	5381.04	71
H38	6501.02	7704.42	5929.04	51
H14A	4169.17	6931.59	6428.75	67
H14B	4675.99	6285.01	6752.23	67
H14C	4055.43	6279.62	5901.22	67
H13A	4171.73	6960.88	4900.94	77
H13B	4840	7447.48	5123.09	77
H13C	4249.9	7637.63	5382.47	77
H36	5363.79	8649.33	3936.97	60
H37	5537.81	8339.08	5150.68	64

4.6: Chapter 4 References

- (1) Pruet, R. L.; Barr, J. T.; Rapp, K. E.; Bahner, C. T.; Gibson, J. D.; Lafferty, R. H. Reactions of Polyfluoro Olefins. II.1 Reactions with Primary and Secondary Amines. *J. Am. Chem. Soc.* **1950**, 72 (8), 3646–3650. <https://doi.org/10.1021/ja01164a090>.
- (2) Burkholder, C.; Dolbier, W. R.; Médebielle, M. Tetrakis(Dimethylamino)Ethylene as a Useful Reductant of Some Bromodifluoromethyl Heterocycles. Application to the Synthesis of New *Gem*-Difluorinated Heteroarylated Compounds. *J. Org. Chem.* **1998**, 63 (16), 5385–5394. <https://doi.org/10.1021/jo980201+>.
- (3) Thummel, R. P.; Gouille, V.; Chen, B. Bridged Derivatives of 2,2'-Biimidazole. *J. Org. Chem.* **1989**, 54 (13), 3057–3061. <https://doi.org/10.1021/jo00274a019>.
- (4) Ames, J. R.; Houghtaling, M. A.; Terrian, D. L.; Mitchell, T. P. Annulated Derivatives of 2,2'-Biimidazole, 2-(2'-Imidazolyl)Benzimidazole, and 2,2'-Bibenzimidazole. *Can. J. Chem.* **1997**, 75 (1), 28–36. <https://doi.org/10.1139/v97-004>.
- (5) Taton, T. A.; Chen, P. A Stable Tetraazafulvalene. *Angewandte Chemie International Edition in English* **1996**, 35 (9), 1011–1013. <https://doi.org/10.1002/anie.199610111>.
- (6) Murphy, J. A.; Khan, T. A.; Zhou, S.; Thomson, D. W.; Mahesh, M. Highly Efficient Reduction of Unactivated Aryl and Alkyl Iodides by a Ground-State Neutral Organic

- Electron Donor. *Angew. Chem. Int. Ed.* **2005**, *44* (9), 1356–1360.
<https://doi.org/10.1002/anie.200462038>.
- (7) Murphy, J. A.; Zhou, S.; Thomson, D. W.; Schoenebeck, F.; Mahesh, M.; Park, S. R.; Tuttle, T.; Berlouis, L. E. A. The Generation of Aryl Anions by Double Electron Transfer to Aryl Iodides from a Neutral Ground-State Organic Super-Electron Donor. *Angewandte Chemie International Edition* **2007**, *46* (27), 5178–5183.
<https://doi.org/10.1002/anie.200700554>.
- (8) Schoenebeck, F.; Murphy, J. A.; Zhou, S.; Uenoyama, Y.; Miclo, Y.; Tuttle, T. Reductive Cleavage of Sulfones and Sulfonamides by a Neutral Organic Super-Electron-Donor (S.E.D.) Reagent. *J. Am. Chem. Soc.* **2007**, *129* (44), 13368–13369.
<https://doi.org/10.1021/ja074417h>.
- (9) Peltier, J. L.; Tomás-Mendivil, E.; Tolentino, D. R.; Hansmann, M. M.; Jazzar, R.; Bertrand, G. Realizing Metal-Free Carbene-Catalyzed Carbonylation Reactions with CO. *J. Am. Chem. Soc.* **2020**, *142* (43), 18336–18340. <https://doi.org/10.1021/jacs.0c09938>.
- (10) Dutton, J. L.; Tabeshi, R.; Jennings, M. C.; Lough, A. J.; Ragogna, P. J. Redox Reactions between Phosphines (R₃P; R = NBU, Ph) or Carbene (IPr₂IM) and Chalcogen Tetrahalides ChX₄ (IPr₂IM = 2,5-Diisopropylimidazole-2-Ylidene; Ch = Se, Te; X = Cl, Br). *Inorg. Chem.* **2007**, *46* (21), 8594–8602. <https://doi.org/10.1021/ic700627f>.
- (11) Pell, T. P.; Couchman, S. A.; Ibrahim, S.; Wilson, D. J. D.; Smith, B. J.; Barnard, P. J.; Dutton, J. L. Diverse Reactions of PhI(OTf)₂ with Common 2-Electron Ligands: Complex Formation, Oxidation, and Oxidative Coupling. *Inorg. Chem.* **2012**, *51* (23), 13034–13040. <https://doi.org/10.1021/ic302176f>.
- (12) Ramnial, T.; McKenzie, I.; Gorodetsky, B.; Tsang, E. M. W.; Clyburne, J. A. C. Reactions of N-Heterocyclic Carbenes (NHCs) with One-Electron Oxidants: Possible Formation of a Carbene Cation Radical. *Chem. Commun.* **2004**, No. 9, 1054–1055.
<https://doi.org/10.1039/B314110A>.
- (13) Maiti, A.; Elvers, B. J.; Bera, S.; Lindl, F.; Krummenacher, I.; Ghosh, P.; Braunschweig, H.; Yildiz, C. B.; Schulzke, C.; Jana, A. Disclosing Cyclic(Alkyl)(Amino)Carbenes as One-Electron Reductants: Synthesis of Acyclic(Amino)(Aryl)Carbene-Based Kekulé Diradicaloids. *Chemistry – A European Journal* *n/a* (n/a), e202104567.
<https://doi.org/10.1002/chem.202104567>.
- (14) Tao, X.; G. Daniliuc, C.; Knitsch, R.; Ryan Hansen, M.; Eckert, H.; Lübbesmeyer, M.; Studer, A.; Kehr, G.; Erker, G. The Special Role of B(C₆F₅)₃ in the Single Electron Reduction of Quinones by Radicals. *Chemical Science* **2018**, *9* (41), 8011–8018.
<https://doi.org/10.1039/C8SC03005G>.
- (15) Dong, Z.; Pezzato, C.; Sienkiewicz, A.; Scopelliti, R.; Fadaei-Tirani, F.; Severin, K. SET Processes in Lewis Acid–Base Reactions: The Tritylation of N-Heterocyclic Carbenes. *Chem. Sci.* **2020**, *11* (29), 7615–7618. <https://doi.org/10.1039/D0SC01278E>.

- (16) Wang, C.; Liu, L. NHC-Catalyzed Oxindole Synthesis via Single Electron Transfer. *Org. Chem. Front.* **2021**, *8* (7), 1454–1460. <https://doi.org/10.1039/D0QO01508C>.
- (17) Su, L.; Sun, H.; Liu, J.; Wang, C. Construction of Quaternary Carbon Center via NHC Catalysis Initiated by an Intermolecular Heck-Type Alkyl Radical Addition. *Org. Lett.* **2021**, *23* (12), 4662–4666. <https://doi.org/10.1021/acs.orglett.1c01400>.
- (18) Zhang, J.; Yang, J.-D.; Cheng, J.-P. Exploiting the Radical Reactivity of Diazaphosphinanes in Hydrodehalogenations and Cascade Cyclizations. *Chem. Sci.* **2020**, *11* (18), 4786–4790. <https://doi.org/10.1039/D0SC01352H>.
- (19) Zhang, J.; Yang, J.-D.; Cheng, J.-P. Diazaphosphinyl Radical-Catalyzed Deoxygenation of α -Carboxy Ketones: A New Protocol for Chemo-Selective C–O Bond Scission via Mechanism Regulation. *Chem. Sci.* **2020**, *11* (32), 8476–8481. <https://doi.org/10.1039/D0SC03220D>.
- (20) Rohrbach, S.; Shah, R. S.; Tuttle, T.; Murphy, J. A. Neutral Organic Super Electron Donors Made Catalytic. *Angewandte Chemie International Edition* **2019**, *58* (33), 11454–11458. <https://doi.org/10.1002/anie.201905814>.
- (21) Calderazzo, F.; Forte, C.; Marchetti, F.; Pampaloni, G.; Pieretti, L. Reaction of Phenanthrene-9,10-Dione with Phenanthrene-9,10-Diol: Synthesis and Characterization of the First Ortho-Quinhydrone Derivative. *Helvetica Chimica Acta* **2004**, *87* (4), 781–789. <https://doi.org/10.1002/hlca.200490076>.
- (22) Campos-Martin, J. M.; Blanco-Brieva, G.; Fierro, J. L. G. Hydrogen Peroxide Synthesis: An Outlook beyond the Anthraquinone Process. *Angewandte Chemie International Edition* **2006**, *45* (42), 6962–6984. <https://doi.org/10.1002/anie.200503779>.
- (23) Bauch, M.; Klaper, M.; Linker, T. Intermediates in the Cleavage of Endoperoxides. *Journal of Physical Organic Chemistry* **2017**, *30* (4), e3607. <https://doi.org/10.1002/poc.3607>.
- (24) Alegría, A. E.; López, M.; Guevara, N. Thermodynamics of Semiquinone Disproportionation in Aqueous Buffer. *J. Chem. Soc., Faraday Trans.* **1996**, *92* (24), 4965–4968. <https://doi.org/10.1039/FT9969204965>.
- (25) Huang, G.; Li, J.; Deng, Z.; Li, J.; Sun, S.; Xu, L.; Dang, L.; Li, M.-D. Room-Temperature Stable Noncovalent Charge-Transfer Dianion Biradical to Produce Singlet Oxygen by Visible or Near-Infrared Light Photoexcitation. *J. Phys. Chem. Lett.* **2021**, *12* (17), 4306–4312. <https://doi.org/10.1021/acs.jpcllett.1c00759>.
- (26) Thorley, K. J.; Song, Y.; Parkin, S. R.; Anthony, J. E. In Situ Reduction and Functionalization of Polycyclic Quinones. *Org. Lett.* **2020**, *22* (18), 7193–7196. <https://doi.org/10.1021/acs.orglett.0c02529>.

- (27) Roberts, J. L.; Sugimoto, H.; Barrette, W. C.; Sawyer, D. T. One-Electron Reduction of Anthraquinone by Hydroxide Ion in Aprotic Media. *J. Am. Chem. Soc.* **1985**, *107* (15), 4556–4557. <https://doi.org/10.1021/ja00301a036>.
- (28) Barham, J. P.; Coulthard, G.; Emery, K. J.; Doni, E.; Cumine, F.; Nocera, G.; John, M. P.; Berlouis, L. E. A.; McGuire, T.; Tuttle, T.; Murphy, J. A. KO *t* Bu: A Privileged Reagent for Electron Transfer Reactions? *J. Am. Chem. Soc.* **2016**, *138* (23), 7402–7410. <https://doi.org/10.1021/jacs.6b03282>.
- (29) Hanson, S. S.; Doni, E.; Traboulose, K. T.; Coulthard, G.; Murphy, J. A.; Dyker, C. A. Pushing the Limits of Neutral Organic Electron Donors: A Tetra(Iminophosphorano)-Substituted Bispyridinylidene. *Angewandte Chemie International Edition* **2015**, *54* (38), 11236–11239. <https://doi.org/10.1002/anie.201505378>.
- (30) Bouffard, J.; Keitz, B. K.; Tonner, R.; Guisado-Barrios, G.; Frenking, G.; Grubbs, R. H.; Bertrand, G. Synthesis of Highly Stable 1,3-Diaryl-1 H -1,2,3-Triazol-5-Ylidenes and Their Applications in Ruthenium-Catalyzed Olefin Metathesis. *Organometallics* **2011**, *30* (9), 2617–2627. <https://doi.org/10.1021/om200272m>.
- (31) Keitz, B. K.; Bouffard, J.; Bertrand, G.; Grubbs, R. H. Protonolysis of a Ruthenium–Carbene Bond and Applications in Olefin Metathesis. *J. Am. Chem. Soc.* **2011**, *133* (22), 8498–8501. <https://doi.org/10.1021/ja203070r>.
- (32) Ji, X.; Guo, J.; Liu, Y.; Lu, A.; Wang, Z.; Li, Y.; Yang, S.; Wang, Q. Marine-Natural-Product Development: First Discovery of Nortopsentin Alkaloids as Novel Antiviral, Anti-Phytopathogenic-Fungus, and Insecticidal Agents. *J. Agric. Food Chem.* **2018**, *66* (16), 4062–4072. <https://doi.org/10.1021/acs.jafc.8b00507>.
- (33) Dolomanov, O. V.; Bourhis, L. J.; Gildea, R. J.; Howard, J. a. K.; Puschmann, H. OLEX2: A Complete Structure Solution, Refinement and Analysis Program. *J Appl Cryst* **2009**, *42* (2), 339–341. <https://doi.org/10.1107/S0021889808042726>.
- (34) Sheldrick, G. M. SHELXT – Integrated Space-Group and Crystal-Structure Determination. *Acta Cryst A* **2015**, *71* (1), 3–8. <https://doi.org/10.1107/S2053273314026370>.
- (35) Sheldrick, G. M. Crystal Structure Refinement with SHELXL. *Acta Cryst C* **2015**, *71* (1), 3–8. <https://doi.org/10.1107/S2053229614024218>.